Duality and Dynamics of Supersymmetric Field Theories from D-branes on Singularities

by

Sebastián Federico Franco

Submitted to the Department of Physics
in partial fulfillment of the requirements for the degree of

Doctor of Philosophy
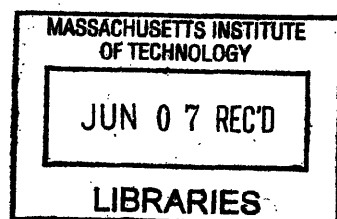
at the

MASSACHUSETTS INSTITUTE OF TECHNOLOGY

May 2005
[June 2005]

Author ....
Department of Physics
May 9, 2005

Certified by...
Amihay Hanany
Associate Professor
Thesis Supervisor

Accepted by ....
Thomas J. Greytak
Chairman, Department Committee on Graduate Students

Duality and Dynamics of Supersymmetric Field Theories from D-branes on Singularities

by

Sebastián Federico Franco

Submitted to the Department of Physics
on May 9, 2005, in partial fulfillment of the
requirements for the degree of
Doctor of Philosophy

Abstract

We carry out various investigations regarding gauge theories on the worldvolume of D-branes probing toric singularities.

We first study the connection that arises in Toric Duality between different dual gauge theory phases and the multiplicity of fields in the gauged linear sigma models associated with the probed geometries.

We introduce a straightforward procedure for the determination of toric dual theories and partial resolutions based on the (p, q) web description of toric singularities.

We study the non-conformal theories that arise in the presence of fractional branes. We introduce a systematic procedure to study the resulting cascading RG flows, including the effect of anomalous dimensions on beta functions. Supergravity solutions dual to logarithmic RG flows are constructed, validating the field theory analysis of the cascades. We systematically study the IR dynamics of cascading gauge theories. We show how the deformation in the dual geometries is encoded in a quantum modification of the moduli space.

We construct an infinite family of superconformal quiver gauge theories which are AdS/CFT dual to Sasaki-Einstein horizons with explicit metrics. The gauge theory and geometric computations of R-charges and central charges are shown to agree.

We introduce new Type IIB brane constructions denoted brane tilings which are dual to D3-branes probing arbitrary toric singularities. Brane tilings encode both the quiver and superpotential of the gauge theories on the D-brane probes. They give a connection with the statistical model of dimers. They provide the simplest known method for computing toric moduli spaces of gauge theories, which reduces to finding the determinant of the Kasteleyn matrix of a bipartite graph.

Thesis Supervisor: Amihay Hanany
Title: Associate Professor

Acknowledgments

Agradecimientos

Este es un momento emotivo para mi. El viaje que inicie varios años atrás llega a su fin. Estoy profundamente feliz. Muchas personas han contribuido para hacer este sueño realidad.

Primero, quisiera dar gracias a mi advisor, el Prof. Amihay Hanany, por su paciencia, por guiarme y por sus innumerables enseñanzas. Espero heredar al menos una pequeã porción de su sabiduría física.

Quisiera agradecer a mis colaboradores: Gerardo Aldázabal, Sergio Benvenuti, Alan Dunn, Luis Ibañez, Pavlos Kazakopoulos, Kris Kennaway, Francis Lam, Dario Martelli, Raúl Rabadán, Fouad Saad, James Sparks, David Vegh, Johannes Walcher y Brian Wecht, por la agradable experiencia de trabajar juntos y por todo lo que aprendí de ellos.

Un agradecimiento especial va para mis amigos Bo Feng, Yang-Hui He, Chris Herzog y Angel Uranga, quienes han contribuido profundamente a mi entendimiento de la Física.

Quisiera agradecer a Carlos Nuñez y Martín Schvellinger por numerosas discusiones, tanto sobre Física como sobre la vida.

También estoy profundamente agradecido a Marcelo Solimano y Gerardo Aldazábal, quienes son los responsables de mis primeros pasos, en etapas muy diferentes de mi viaje por la Física.

Gracias a todo el personal del Junior Lab. Especialmente a: el Prof. Ulrich Becker, el Prof. Jay Kirsch, Scott Sewell y el Prof. Dick. Yamamoto. Todos ellos son grandes seres humanos. He sido muy afortunado de poder contar con su apoyo durante mis años en el MIT.

Desearía también agradecer a todos en el Center for Theoretical Physics, en particular a Joyce Berggren y Scott Morley. También estoy en deuda con el Prof. Barton Zwiebach, por su ayuda y consejos.

Quiero agradecer a mi mamá y mi papá con todo mi corazón. Su amor y apoyo me han acompañado toda la vida. A ellos les debo quien soy y quien quiero ser. No

puedo imaginar dos mejores padres en este mundo. Gracias también a mi hermana Sandri, a Sandro y a Floppy, a quienes siempre llevo en mi corazón.

Finalmente, quisiera dar gracias a Carli. Ella es un ángel en mi vida. Su amor, respaldo y comprensión llenan mi existencia de alegría. No puedo esperar a nuestro matrimonio, en dos meses, que dará inicio de uno de los capítulos mas maravillosos de nuestras vidas.

Contents

List of Figures

15

19

26

List of Tables

Chapter 1

Introduction

String Theory [73, 147, 131, 111, 170] was born in an attempt to provide an alternative to field theories capable of handling the abundance of strongly interacting particles, hadrons, that was experimentally observed in the 1960s. Later on, it was realized that String Theory fails to describe the parton behavior of high energy scattering correctly and an ordinary Yang-Mills theory, Quantum Chromodynamics (QCD), emerged as the correct description of strong interactions.

In order for a string theory to be consistent, it has to live in ten spacetime dimensions and be supersymmetric. There are different approaches to make contact with four-dimensional physics. One possible avenue is by means of Kaluza-Klein's old idea of compactifying extra dimensions. In addition, every string theory has a massless spin-2 particle in its spectrum. This feature was unacceptable when trying to use String Theory to describe strong interactions. Later, this was reinterpreted as a virtue by changing the string scale from the original value of approximately 1GeV to the typical scale of a relativistic quantum theory of gravity, the Planck scale $\sqrt{\hbar c/G} \simeq 10^{19}$GeV. This massless particle is then interpreted as the graviton, and String Theory re-emerges as a serious candidate for fulfilling the long standing quest for a quantum theory that unifies all known interactions, including gravity.

There are five different ways in which String Theory can be quantized, giving rise to the five known string theories: Type IIA, Type IIB, Type I, Heterotic $SO(32)$ and Heterotic $E_8 \times E_8$. These five theories are connected by duality transformations, i.e.

it is possible to express the degrees of freedom of any of them in terms of the degrees of freedom of the others. The five string theories can be regarded as expansions around different corners in moduli space of an underlying eleven dimensional theory called M-theory. A full formulation of M-theory is unknown, but its field theory limit corresponds to eleven dimensional supergravity.

In 1995, Polchinski's discovery of the importance of D-branes [148] as the source of Ramond-Ramond fields in String Theory marked what is now known as the "Second Superstring Revolution". D-branes are non-perturbative extended objects that are defined by imposing Dirichlet boundary conditions on fundamental strings. All string theories contain D-branes in their spectrum. In addition, all but Type I string theory have another type of brane, the NS5-brane. Similar extended objects exist in M-theory. They are 2 and 5-dimensional and are respectively called M2 and M5-branes. The low energy dynamics of D-branes is described by ordinary gauge theories confined to their world-volumes.

The discovery of D-branes led to fascinating developments, connecting String Theory with black holes and supersymmetric field theories. D-branes also have a profound influence in phenomenological constructions based in String Theory. The application of the brane-world paradigm to the construction of Standard Model like theories has been a very fruitful direction of research.

This thesis will focus on the study of supersymmetric field theories and their engineering in String Theory. There are several reasons why supersymmetric field theories are of interest. On one hand, supersymmetry is crucial for the consistency of String Theory. If we believe that String Theory is the fundamental theory of nature, it is natural to expect that the connection with our non-supersymmetric world involves some supersymmetric theory at high energies. Supersymmetry would be then finally broken at low energies. Another merit of supersymmetry is that it provides an elegant solution to the hierarchy problem, stabilizing the large ratio between the Planck and electroweak scales. Finally, there is yet another motivation for the study of supersymmetric field theories that is not based on considering supersymmetry as key ingredient in a fundamental description of the universe. A standard approach

in Physics research is to start by considering a simplified version of the system of interest, usually with a high amount of symmetry. Once the symmetric problem is understood, we can approach the realistic model by progressively reducing the amount of symmetry. Along this line of thought, we can regard supersymmetric field theories as highly symmetric "toy models". We then expect that the conclusions we derive for them can be extended, at least to some extent, to more conventional field theories.

One of the most fascinating features of quantum field theories is Duality. It is often the case that more than one apparently different field theories are in fact equivalent. This is very useful, since usually phenomena that are complicated to analyze in one description become straightforward in a dual one. An outstanding example of such a correspondence is given by Seiberg duality [156], which is an equivalence between the low energy limit of $\mathcal{N} = 1$ supersymmetric field theories in 3+1 dimensions. Seiberg dual theories might have different gauge groups, matter content and interactions but their long distance physics is identical. One of the main topics we will investigate is the geometric origin of $\mathcal{N} = 1$ four dimensional dualities when gauge theories are constructed using D-branes over Calabi-Yau singularities.

D-branes are useful probes of backgrounds in String Theory. At weak string coupling, they are much heavier than fundamental strings and hence are sensitive to shorter length scales. The probed geometry determines the amount of supersymmetry, spectrum and interactions of the gauge theory living on the world-volume of the branes. One of the goals of this thesis is to find efficient ways to determine gauge theories on D-branes over singularities. We will mainly focus on the case in which the singularities are toric. The use of D-brane probes is one of the alternative approaches to engineer interesting gauge theories in String Theory. We will explore two directions that are necessary in order to obtain realistic theories: the construction of field theories with reduced supersymmetry ($\mathcal{N} = 1$ is the maximum amount of SUSY consistent with a chiral theory) and breaking of conformal invariance (with subsequent Renormalization Group flows).

Outline

In the first chapters of this thesis we review some background concepts that are important for understanding our work: Chapter 2 reviews the five consistent ten-dimensional string theories as well as eleven-dimensional supergravity and discusses their brane content, Chapter 3 gives a brief introduction to Toric Geometry and Chapter 4 explains the main approaches to the engineering of gauge theories in String Theory.

The non-uniqueness of the gauge theories on D-branes probing a given toric singularity leads to the concept of Toric Duality [45]. This is a generalization of Seiberg duality to theories with toric moduli space. The motive of Chapter 5 is a detailed study of Toric Duality, and the relation between different dual phases of the gauge theories and multiplicities of fields in the gauged linear sigma model description of the geometry. Chapter 6 exploits the (p, q) description of toric singularities to develop a method that considerably simplifies the derivation of toric dual theories and the computation of gauge theories via partial resolution. At the same time, we establish a connection between Seiberg duality in four dimensions and crossing of curves of marginal stability in five-dimensional field theories.

We then investigate the Renormalization Group (RG) flows that are induced by fractional branes. In Chapter 7 we develop a general methodology for the treatment of duality cascades. We study previously unknown logarithmic flows as well as cascades with a qualitatively different UV behavior, Duality Walls. In Chapter 8 we continue our study of cascading RG flows, performing an analytical study of duality walls and exploring the chaotic behavior of some duality cascades. The most important achievement of this chapter is the construction of supergravity duals of cascading solutions for cones over del Pezzo surfaces. This construction is easily generalized to more general toric geometries and puts the field theory analysis of such RG flows on a firm footing. In Chapter 9 we initiate a systematic study of the infrared limit of cascades. We show how the deformation of the dual geometries emerges in the field theory as a quantum modified moduli space. Of particular interest, due to their

phenomenological applications, are the cascades with several scales of strong dynamics introduced in this chapter. These cascades are dual to warped throat geometries with regions of different warping.

In Chapter 10, we construct an infinite family of quiver gauge theories that are AdS/CFT dual to a corresponding class of horizon Sasaki-Einstein manifolds with explicit metrics. The computation of central charges and baryon R-charges in the gauge theory are shown to agree with the corresponding calculation on the gravity side of the AdS/CFT correspondence. The results reported in this chapter represent a significant progress in our understanding of the AdS/CFT correspondence, passing from the two explicit Sasaki-Einstein metrics with known CFT duals that were previously at hand to an infinite set of CFT/dual Sasaki-Einstein metric pairs.

The problem of gauge theories on D-branes over singularities is revisited in Chapter 11. We introduce new brane constructions that are dual to gauge theories on D3-branes probing arbitrary toric singularities, which we call Brane Tilings. They encode both the quiver and the superpotential of the gauge theory. Brane tilings give a connection to dimer models and considerably simplify the study of these theories. In particular, the previously laborious task of finding the moduli space of the gauge theory is reduced to the computation of the determinant of the Kasteleyn matrix of a graph. This is by far the simplest method known so far for the computation of toric moduli spaces of gauge theories.

The material we report in this thesis covers part of the author's work during his graduate studies, which appears in a series of publications [43, 52, 44, 53, 56, 61, 57, 54, 14, 60, 59, 58].

Chapter 2

Branes

In addition to fundamental strings, string theories have a plethora of extended p-dimensional objects (with (p+1)-dimensional worldvolumes). They receive the generic name of **p-branes** and generalize the usual notion of a 2-dimensional membrane. Branes play a key role in our current understanding of String Theory. We refer the reader to [148, 150, 149] for comprehensive reviews. The present picture is that the five consistent string theories and 11d supergravity are all connected by duality transformations [70, 101, 168, 155, 163, 165]. This strongly supports the idea that they correspond to different limits of a single subjacent theory, M-theory. D-branes are crucial in order to be able to map the entire set of BPS objects between dual theories.

The low energy dynamics of branes is described by gauge theories living in their worldvolume. In addition to gauge fields, their fluctuations can also give rise to charged matter fields. Interesting gauge theories can be engineered with branes in different configurations, combining them with other extended objects such as orientifold planes and by embedding them in non-trivial geometries. Motivated by this, we present in this chapter a brief overview of the five consistent string theories and 11d supergravity and their branes.

2.1 Massless spectrum of string theories

For various discussions, such as the classification of possible branes, it is sufficient to consider the low energy, massless degrees of freedom of String Theory. The existence of (p+1)-form gauge fields implies that string theories couple to appropriate branes. The coupling of branes to gauge field generalize the notion of electric and magnetic coupling of electromagnetism which, in d dimensions, read

$$
\begin{aligned}
\textbf{Electric coupling: p-brane} \qquad & d * F^{(p+2)} = Q_E \delta^{(d-p-1)} \\
\textbf{Magnetic coupling: (d-p-4)-brane} \qquad & dF^{(p+2)} = Q_M \delta^{(d-p-1)}
\end{aligned}
\qquad (2.1.1)
$$

where $F^{(p+2)}$ is the (p+2)-form field strength.

Massless fields transform in irreducible representations of the little group. Counting the number of degrees of freedom for each type of massless field in arbitrary dimensions d is straightforward. For d dimensions the little group is $SO(d-1)$ and we have the following counting:

Field	Degrees of freedom
Symmetric, traceless 2-tensor (graviton)	$d(d-3)/2$
p-form	$\binom{d-2}{p}$
Spinor	$2^{\frac{d-3}{2}}$
Gravitino	$(d-3)2^{\frac{d-3}{2}}$

$$(2.1.2)$$

In preparation for our classification of p-branes, we now describe the massless field content of 11d supergravity and the different string theories

2.1.1 M-theory

A full formultation of M-theory is still unknown, but its low energy limit is described by eleven dimensional supergravity. Eleven-dimensional supergravity is the theory

with largest possible space-time supersymmetry and Poincaré invariance. The limit in the number of dimensions follows from the fact that consistent non-trivial field theories cannot have massless particles with spin greater than two. Upon dimensional reduction, 11d supergravity leads to Type IIA supergravity.

Using the expressions in (2.1.2), we determine the number of degrees of freedom in the 11d massless supergravity multiplet. It consists of the graviton G_{MN}, with $11 \cdot 8/2 = 44$ degrees of freedom, a 3-form $C^{(3)}$ with $\begin{pmatrix} 9 \\ 3 \end{pmatrix} = 84$ degrees of freedom and the gravitino ψ_M with $8.2^4 = 128$ degrees of freedom. Where the indices $M, N = 0, \ldots, 10$. We immediately verify that the supergravity multiplet has an equal number of bosonic and fermionic degrees of freedom, 128, as expected in a supersymmetric theory.

2.1.2 Type IIA

In Type IIA string theory right-movers and left-movers transform under different spacetime supersymmetries of opposite chirality. Hence, the theory is non-chiral. Its massless content corresponds to Type IIA supergravity. Massless fields are organized into irreducible representations of the ten-dimensional little group $SO(8)$.

The massless fields in the closed sector are organized as follows

$$
\begin{array}{lll}
\textbf{Bosons} & NS - NS & \mathbf{8_v} \otimes \mathbf{8_v} = \mathbf{1} + \mathbf{28_v} + \mathbf{35_v} = \phi + B^{(2)} + g^{(2)} \\
 & R - R & \mathbf{8_c} \otimes \mathbf{8_s} = \mathbf{8_v} + \mathbf{56_v} = C^{(1)} + C^{(3)} \\
\textbf{Fermions} & NS - R & \mathbf{8_v} \otimes \mathbf{8_s} = \mathbf{8_c} + \mathbf{56_c} \\
 & R - NS & \mathbf{8_c} \otimes \mathbf{8_v} = \mathbf{8_s} + \mathbf{56_s}
\end{array}
\tag{2.1.3}
$$

where NS and R indicate the Neveu-Schwarz and Ramond sectors that follow from the the periodicity of the worldsheet spinors in the quantization of the superstring [73, 147].

The $\mathbf{56_c}$ and $\mathbf{56_s}$ representations arise from combining a vector and a spinor of $SO(8)$ and thus correspond to spin 3/2 particles, i.e. gravitinos.

37

Alternatively, Type IIA supergravity can be obtained by dimensional reduction of 11d supergravity along x_{10}, without refering to quantization of String Theory. The representations of the eleven-dimensional little group $SO(9)$ decompose into the ones of $SO(8)$ as follows

$$
\begin{array}{llll}
& SO(9) & \supset & SO(8) \\
C^{(3)}: & \mathbf{84} & \to & \mathbf{28} + \mathbf{56_v} \\
g^{(2)}: & \mathbf{44} & \to & \mathbf{1} + \mathbf{8_v} + \mathbf{35} \\
\psi_\alpha^\mu: & \mathbf{128} & \to & \mathbf{8_s} + \mathbf{8_c} + \mathbf{56_s} + \mathbf{56_c}
\end{array}
\tag{2.1.4}
$$

In addition, Type IIA supergravity has a 9-form $C^{(9)}$ with 10-form field strength F_{10}. The standard action term $\int F_{10} * F_{10}$ gives the equation of motion $d * F_{10} = 0$, from which $*F_{10} = 0$ follows. The solution is thus constant but very interesting. The real importance of this form was noticed in [148], where it was understood that it generates a contribution to the cosmological constant

2.1.3   Type IIB

The massless spectrum of Type IIB is given by Type IIB supergravity. In this case, there are also two spacetime supersymmetries but of the same handedness. Thus, the theory is chiral. Type IIB supergravity cannot be obtained by dimensional reduction or restriction of a higher dimensional theory. The spectrum of Type IIB supergravity is

$$
\begin{array}{lll}
\textbf{Bosons} & NS - NS & \mathbf{8_v} \otimes \mathbf{8_v} = \mathbf{1} + \mathbf{28_v} + \mathbf{35_v} = \phi + B^{(2)} + g^{(2)} \\
& R - R & \mathbf{8_s} \otimes \mathbf{8_s} = \mathbf{1} + \mathbf{28_c} + \mathbf{35_c} = C^{(0)} + C^{(2)} + C^{(4)+} \\
\textbf{Fermions} & NS - R & \mathbf{8_v} \otimes \mathbf{8_s} = \mathbf{8_s} + \mathbf{56_s} \\
& R - NS & \mathbf{8_s} \otimes \mathbf{8_v} = \mathbf{8_s} + \mathbf{56_s}
\end{array}
\tag{2.1.5}
$$

where again we have organized the fields into different sectors corresponding to the quantization of the superstring.

The self-duality of the 35_c representation of $SO(8)$ indicates the self-duality of the 5-form field strength $F_5 = dC^{(4)+}$. It is not known how to introduce a covariant action that leads to self-duality of F_5 as an equation of motion. Hence, the standard approach is to consider covariant equations of motion and then impose $F_5 = *F_5$ by hand. The 56_s representations correspond to gravitinos.

It is also useful to introduce a 10-form $C^{(10)}$. This form is not dynamical, i.e. has no propagating degrees of freedom, since it cannot have a kinetic term in 10 dimensions (its field strength would be an 11-form).

2.1.4 Type I

The spectrum of Type IIB supergravity presented in the previous section is given by the tensor product of two identical super Yang-Mills multiplets $(8_v + 8_c)$. In this case, it is possible to impose a graded symmetrization of the product, leading to

$$
\begin{aligned}
[(8_v + 8_c) \otimes (8_v + 8_c)]_{\text{graded sym}} &= (8_v + 8_v)_{\text{sym}} + (8_v + 8_c) + (8_c + 8_c)_{\text{antisym}} \\
&= (1 + 28_c + 35_v)_B + (8_s + 56_s)_F
\end{aligned}
$$

$$(2.1.6)$$

From a string theory point of view, the symmetrization comes from **orientifolding**, i.e. taking the quotient by worldsheet parity Ω, of the left-right symmetric Type IIB string [152, 98, 31, 68].

The NS-NS 2-form is odd under Ω and then is projected out when performing the orientifold quotient. There is a surviving 2-form $C^{(2)}$ that comes from the R-R sector and transforms in the 28_c of $SO(8)$. The additional bosonic fields are the dilaton ϕ in the 1 representation and the graviton $g^{(2)}$ in the 35_v.

The orientifold projection kills one linear combination of the two gravitinos, a 56_s, of Type IIB supergravity. The spectrum in (2.1.6) is the one of chiral Type I supergravity in ten dimensions. It corresponds to the $\mathcal{N} = 1$ gravity multiplet in $d = 10$, with 64 bosonic and 64 fermionic degrees of freedom. In addition, the non-dynamical RR 10-form $C^{(10)}$ of Type IIB survives the orientifold projection.

This is a chiral theory and thus we have to be concerned about possible anomalies. The spectrum, as listed in (2.1.6), has gravitational chiral anomalies. The anomalies are canceled by including an $\mathcal{N} = 1$ vector multiplet with gauge group $SO(32)$.

$$
\begin{array}{llll}
\textbf{Bosons} & NS & \mathbf{8_v} & SO(32) \text{ gauge bosons} \\
\textbf{Fermions} & R & \mathbf{8_c} & SO(32) \text{ gauginos}
\end{array}
\qquad (2.1.7)
$$

From a string theory point of view, the vector multiplet comes from an open sector ending on space-time filling D9-branes that is required for consistency in order to cancel RR tadpoles [68].

2.1.5 Heterotic string theories

Heterotic strings exploit the fact that the right and left moving modes of closed strings are decoupled. In heterotic strings, the right moving modes are taken to be those of type II superstrings. Hence, the critical dimension is 10. The left moving modes are those of the bosonic string and live in 26 target space dimensions. The 16 extra directions do not correspond to physical dimensions but are compactified on a lattice.

The 16d lattice is severely constrained by modular invariance which requires it to be even and self-dual. Such lattices only exist in dimensions multiple of 8. There are only two examples in 16 dimensions: the $E_8 \times E_8$ and the $spin(32)/\mathbb{Z}_2$ lattices, giving rise to the $E_8 \times E_8$ and $SO(32)$ heterotic theories. Their massless spectrum is given by the $\mathcal{N} = 1$ 10d gravity multiplet presented in (2.1.6) coupled to $E_8 \times E_8$ or $SO(32)$ vector multiplets. It is interesting to note that the massless content of the $SO(32)$ theory is identical to the one of Type I.

2.2 Classification of branes

Armed with the spectra of massless forms presented above, we are ready to classify the brane content of M-theory and the different string theories according to the electric and magnetic couplings in (2.1.1). Branes in the five 10d string theories can be organized in two categories according to the dependence of their tensions on the

string coupling g_s. One the one hand, there are "solitonic" or Neveu-Schwarz (NS) branes, which are the magnetic duals of fundamental strings and have tensions that go as $1/g_s^2$. On the other hand, there are Dirichlet (D) branes, whose tensions go as $1/g_s$.

2.2.1   M-theory

The existence of the 3-form field $C^{(3)}$ in 11d supergravity indicates that there are two types of extended objects in M-theory. One of them, the M2-brane, has a 2+1 dimensional worldvolume and couples electrically to $C^{(3)}$. In addition there is a 5+1 M5-brane, which couples magnetically to $C^{(3)}$. These two M-branes give rise to all the branes of the 10-dimensional string theories.

2.2.2   Type IIA

From the p-form gauge fields in (2.1.3), we see that Type IIA string theory possesses the following set of branes:

$$
\begin{array}{|l|c|c|c|}
\hline
 & B^{(2)} & C^{(1)} & C^{(3)} \\
\hline
\text{Electric} & F1 & D0 & D2 \\
\hline
\text{Magnetic} & NS5 & D6 & D4 \\
\hline
\end{array}
\tag{2.2.8}
$$

In addition, there is a D8-brane that sources C^9 which, as discussed in Section 2.1.2. has constant field strength and generates a cosmological constant.

2.2.3   Type IIB

The massless spectrum in (2.1.5) corresponds to the following branes:

$$
\begin{array}{|l|c|c|c|c|}
\hline
 & B^{(2)} & C^{(0)} & C^{(2)} & C_{+}^{(4)} \\
\hline
\text{Electric} & F1 & D(-1) & D1 & D3 \\
\hline
\text{Magnetic} & NS5 & D7 & D5 & D3 \\
\hline
\end{array}
\tag{2.2.9}
$$

Type IIB string theory has also D9-branes, which source the non-dynamical $C^{(10)}$ discussed in 2.1.2. They fill the entire spacetime and correspond to open strings whose endpoints are free to move in 10 dimensions, i.e. with Neumann boundary conditions in all directions.

2.2.4 Type I

From (2.1.6), we get the brane content of Type I string theory:

	$C^{(2)}$
Electric	$D1$
Magnetic	$D5$

(2.2.10)

Similarly to what happens for Type IIB, there are also D9-branes in this case. It is interesting to notice that, since the NS-NS 2-form field $B^{(2)}$ does not survive the orientifold projection, there are no NS5-branes in Type I string theory.

2.2.5 Heterotic

We have seen that, similarly to what happens for Type I, the massless spectrum in the closed sector of both heterotic theories is given by the $\mathcal{N} = 1$ gravity multiplet in $d = 10$ presented in (2.1.6). In this case, though, the 2-form is sourced by NS5-branes via magnetic coupling. These are the only branes of heterotic theories.

2.2.6 Orientifold planes

Orientifolds are other interesting extended objects of string and M-theory. They can be combined with branes to engineer gauge theories. An orientifold p-plane (Op-plane) extends in (p+1) dimensions and is the fixed plane of the combined action of $\mathbb{Z}_2$ reflections in the coordinates and worldsheet parity transformation Ω. That is, they are the fixed space under:

$$x^I(z, \bar{z}) \leftrightarrow -x^I(\bar{z}, z) \quad I = p + 1, \ldots, 9 \tag{2.2.11}$$

An Op-plane is charged under the same RR gauge fields and breaks the same half of supersymmetry than a parallel Dp-brane. At least for weak string coupling, orientifold planes are non-dynamical objects.

2.3 A microscopic description of D-branes

In the sections above, we have taken a low energy approach to the classification of extended objects in string/M-theory. We started from a macroscopic, low energy supergravity description, and identified fundamental strings, D-branes, NS5-branes and M-branes as the sources of the different p-form massless fields. This strategy has the advantage of allowing a rapid identification of the brane content of each string theory and M-theory but fails to provide a microscopic description for them.

The string theory description of Dp-branes is indeed very simple: they are $p + 1$-dimensional defects in spacetime where open strings can end. Namely, they are defined by imposing Neumann boundary conditions on $p+1$ directions and Dirichlet boundary conditions in the remaining $9 - p$ [148].

$$
\begin{aligned}
&\textbf{Neumann:} \quad \partial_\sigma X^\mu(\sigma, t)|_{\sigma=0,\pi} \qquad \mu = 0, \ldots, p \\
&\textbf{Dirichlet:} \quad \partial_t X^\mu(\sigma, t)|_{\sigma=0,\pi} \qquad \mu = p + 1, \ldots, 9
\end{aligned}
\tag{2.3.12}
$$

The generalization of (2.3.12) to open strings stretching between different branes, of possibly different dimensionalities, is straightforward.

Computation of one loop diagrams in string theory shows that D-branes source the graviton, dilaton and RR fields [148], and that their tension (equal to the RR charge since they are BPS objects) is

$$
T_{Dp} = \frac{1}{g_s \ell_s^{p+1}}
\tag{2.3.13}
$$

The microscopic description of D-branes thus agrees with the identification of D-branes as the sources of RR fields that we made in the previous section.

2.4 Gauge theories in the worldvolume of D-branes

The effective action for the D-brane theory is given by a supersymmetric Dirac-Born-Infeld action coupled by a Wess-Zumino term to the closed sector fields in the bulk $S = S_{DBI} + S_{WZ}$ [127], where

$$
\begin{aligned}
S_{DBI} &= -\mu_p \int d^{p+1}\xi e^{-\Phi} \text{Tr}\left\{[-\det(G_{ab} + B_{ab} + 2\pi\alpha' F_{ab})]^{1/2}\right\} \\
S_{WZ} &= i\mu_p \int d^{p+1}\xi \text{Tr}\left[\exp(2\pi\alpha' F_2 + B_2) \wedge \sum_r C^{(r)}\right]
\end{aligned}
\tag{2.4.14}
$$

where G_{ab} and B_{ab} are the components of the NS-NS fields parallel to the D-brane and F_{ab} is the field strength of the $U(1)$ gauge field living on the brane. The string length is realated to α', which has length-squared units, by $\ell_s = \alpha'^{1/2}$. The sum in S_{WZ} runs only over the r-form fields present in the particular supergravity (IIA, IIB, etc) under consideration. The integral picks the form that matches the appropriate power of F_2 and B_2 coming from the exponential. The tension of the Dp-brane is $\mu_p e^{-\Phi}$.

We now consider a limit in which the D-brane theory is described by SYM gauge theory on the world volume of the D-brane. In order to do so, we have to decouple the massless modes on the D-brane from the tower of massive open string modes on the D-brane and the closed string fields, including gravity, in the bulk. While taking this limit we want to preserve a finite g_{SYM}^2 for the resulting gauge theory. Its value can be read from (2.4.14) by expanding S_{DBI} to quadratic order and is

$$
g_{SYM}^2 = \frac{1}{(2\pi\alpha')^2 T_{Dp}} = \ell_s^{p-3} g_s
\tag{2.4.15}
$$

Thus, the gauge theory limit corresponds to $\ell_s \to 0$ with $g_s \to 0$ for $p < 3$ and $g_s \to \infty$ for $p > 3$. For $p = 3$, g_{SYM}^2 is independent of g_s, and the $\ell_s \to 0$ limit corresponds to $\mathcal{N} = 4$ SYM in 3+1 dimersions.

For a single D-brane, the low energy limit corresponds to the dimensional reduction of 9+1 dimensional $\mathcal{N} = 1$ SYM with $U(1)$ gauge group to $p + 1$ dimensions. The low energy degrees of freedom are scalars and gauge fields plus the appropriate

fermions required by supersymmetry. The action is given by

$$S = \frac{1}{g_{SYM}^2} \int d^{p+1}x \left(\frac{1}{4} F_{\mu\nu} F^{\mu\nu} + \frac{1}{\ell_s^4} \partial_\mu X^I \partial^\mu X^I \right) \tag{2.4.16}$$

The gauge bosons of the $U(1)$ theory correspond to open strings with both endpoints on the single D-brane under consideration as depicted in Figure 2-1.a. They are pointlike, since the mass of a string state is given by the string tension multiplied by its length.

(a)   **(b)**
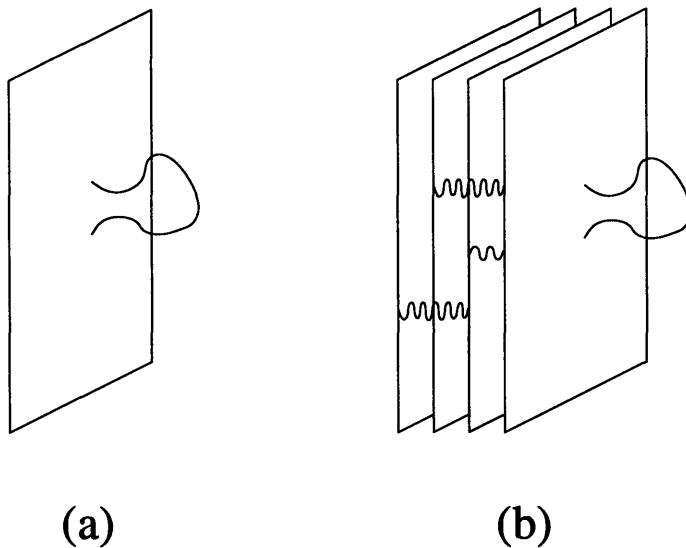
Figure 2-1: Open strings ending on: a) a single D-brane and b) a stack of D-branes.

Let us now consider the case of N parallel Dp-branes. Since they are BPS objects, the forces among the D-branes vanish. This follows from the cancellation between the attraction due to NS-NS fields (such as the graviton) and the repulsion due to R-R fields. As above, each D-brane has $U(1)$ gauge bosons on their worldvolume. In addition, there are massive states corresponding to strings stretching between different D-branes as shown in Figure 2-1, with masses dictated by the separation between the D-branes. We can keep track of both endpoints of the strings by associating to them fundamental and antifundamental $U(N)$ Chan-Patton indices. Thus, the strings naturally give rise to the adjoint representation of $U(N)$. When the D-branes are brought together and become coincident the non-diagonal states become massless. These are the W bosons of the enhanced $U(N)$ gauge group [169].

45

In this case, the decoupling limit previously considered leads to maximally supersymmetric $U(N)$ SYM in p+1 dimensions. The effective action is obtained by dimensional reduction of 9+1 dimensional $U(N)$ SYM. The kinetic term is given by

$$\mathcal{L}_{kin} = \frac{1}{g_{SYM}^2} \left(\frac{1}{4} F_{\mu\nu} F^{\mu\nu} + \frac{1}{\ell_s^4} \mathcal{D}_\mu X^I \mathcal{D}^\mu X^I \right) \tag{2.4.17}$$

with the covariant derivative $\mathcal{D}_\mu X^I = \partial^\mu X^I - i[A_\mu, X^I]$ and field strength $F_{\mu\nu} = \partial_{[\mu} A_{\nu]} - i[A_\mu, A_\nu]$

The 9-p scalars X^I transform in the adjoint representation of $U(N)$ and are subject to the potential

$$V \sim \frac{1}{\ell_s^8 g_{SYM}^2} \sum_{I,J} \text{Tr}[X^I, X^J]^2 \tag{2.4.18}$$

Separating the D-branes, the off-diagonal components of the scalars and the charged gauge bosons become massive. The gauge group thus becomes higgsed according to $U(N) \rightarrow U(1)^N$ (other patterns of higgsing are possible for non-generic positions of the D-branes).

2.5 String theory branes from M-theory

The tension of an extended object is defined as Energy/Volume, where the volume corresponds to its spatial directions. Thus, for a p-brane with p spatial directions the tension has dimensions $[E]/[L]^p = 1/[L]^{p+1}$. M-theory does not have any dimensionless parameter. It only has one dimensionful parameter, the 11d Planck length ℓ_P. Thus, we have $T_{M_2} \sim 1/\ell_P^3$ and $T_{M_5} \sim 1/\ell_P^6$. The precise relation between T_{M_2} and T_{M_5} follows from Dirac quantization and is given by

$$T_{M_5} = \frac{1}{2\pi} T_{M_2}^2 \tag{2.5.19}$$

In 10d string theories, there are two fundamental parameters. One of them, the string coupling g_s, is dimensionless, while the other one, the string length ℓ_s, is

dimensionful. The tensions of extended objects are functions of both of them. Since the D-brane tensions come from a disk diagram, they are all proportional to g_s^{-1}. The dependence on the characteristic length of the theory follows the same reasoning that in 11d. Hence,

$$T_{Dp} = \frac{1}{g_s \ell_s^{p+1}} \tag{2.5.20}$$

Properties of the various extended objects discussed above can be easily derived by considering their origin in 11d M-theory. All the branes of the ten-dimensional string theories descend from the M2 and M5-branes in eleven dimensions. By computing the tensions of different extended objects, it is possible to establish a mapping between 10d and 11d parameters. As an example, we now consider the construction of Type IIA branes starting from M-theory.

As we have discussed above, Type IIA string theory is obtained by compactifying M-theory on $\mathbb{R}^{1,9} \times S^1$. The x^{10} direction is compactified on a circle of radius R_{10}. The M-theory origin of Type IIA branes is the following:

- **Fundamental string:** M2-brane wrapped around x^{10}. Equating the tension of the wrapped membrane and the fundamental string, we get the first relation between IIA and M-theory parameters

$$\frac{R_{10}}{\ell_p^3} = \frac{1}{\ell_s^2} \tag{2.5.21}$$

- **D0-brane:** Kaluza-Klein (KK) mode of the graviton with momentum $1/R_{10}$ along x^{10}. Equating the masses of the KK mode of the graviton and the D0-brane we get the second relation

$$R_{10} = g_s \ell_s \tag{2.5.22}$$

- **D2-brane:** M2-brane not wrapping x^{10}.

- **D4-brane:** M5-brane wrapped around x^{10}.

- **NS5-brane:** M5-brane not wrapping x^{10}.

- **D6-brane:** Kaluza-Klein monopole.

- **D8-brane:** the corresponding object in M-theory, the M9-brane, is not fully understood. Its tension is R_{10}^3/ℓ_p^{12} [41].

Chapter 3

Toric geometry

A central part of this thesis is devoted to the construction of gauge theories by means of D-brane probes over singularities. Much of our studies will be focused on a particular but rich type of singularities, namely **toric singularities**. We now present the main concepts of **toric geometry**. For more detailed discussions we refer the reader to [62, 9, 139].

In addition, Chapter 6 introduces a related approach to toric varieties, constructing them as m-dimensional torus fibrations T^m over some base spaces, and encoding the information about degenerations of the fibrations in toric skeletons (also known as (p,q) webs).

A d-complex dimensional complex projective space is defined as

$$\mathbb{CP}^d = (\mathbb{C}^{d+1} - (0,\ldots,0))/\mathbb{C}^* \tag{3.0.1}$$

The origin is removed to ensure a well behaved quotient by the group $\mathbb{C}^*$, which acts on $\vec{x} \in \mathbb{C}^{d+1}$ according to $(x_1,\ldots,x_{d+1}) \to (\lambda x_1,\ldots,\lambda x_{d+1})$, with $\lambda \in \mathbb{C} \neq 0$. A d-complex dimensional toric variety V^d is a generalization of a complex projective space, in

$$V^d = (\mathbb{C}^n - F)/\mathbb{C}^{*(n-d)} \tag{3.0.2}$$

in which we quotient by $(n-d)$ $\mathbb{C}^*$ actions and we remove a set of points F in order

for such quotient to be well defined. The action of $\mathbb{C}^{*(n-d)}$ on the $\mathbb{C}^n$ coordinates is defined by $(n-d)$ charge vectors Q^a as

$$\lambda_a : (x_1, \ldots, x_n) \to (\lambda_a^{Q_1^a} x_1, \ldots, \lambda_a^{Q_n^a} x_n), \qquad a = 1, \ldots, n - d \qquad (3.0.3)$$

The charges can be arranged into a matrix $Q = (Q_i^a)$ that will be of later use. This approach to toric varieties is known as the **holomorphic quotient**.

Alternatively, we can perform the quotient by $\mathbb{C}^{*(n-d)}$ in two steps, decomposing each $\mathbb{C}^* = \mathbb{R}^+ \times U(1)$. This approach is called the **symplectic quotient**. We first fix the $\mathbb{R}^{+(n-d)}$ levels via a moment map

$$\sum_{i=1}^{n} Q_a^i |x_i|^2 = \xi_a, \qquad a = 1, \ldots, n - d \qquad (3.0.4)$$

for some real parameters ξ_a. We refer to these equations D-terms. This is because they are actually the D-terms of an $\mathcal{N} = 2$ gauged linear sigma model (GLSM)with target space $\mathbb{C}^n$ which reduces in the infrared to a non-linear sigma model whose target space is the toric variety V^d [167]. Finally, we quotient by the $U(1)^{(n-d)}$ action defined by the charge matrix Q (which gives the gauge groups and corresponding charges of the GLSM). Generic non-zero values of the ξ_a's lead to a full resolution of the singularity. Setting them to non-generic values (i.e. with some linear combinations equal to zero) produces a **partial resolution**. This idea plays a central role in Chapter 5, since it can be used to determine the gauge theories for certain toric singularities, starting from the known gauge theories for other geometries, such as Abelian orbifolds.

A simple way to represent a toric singularity is by means of a **toric diagram**. A toric diagram for a d-complex dimensional toric variety is a set of points in the integer lattice $\mathbb{N} = \mathbb{Z}^{(d)}$. The toric diagram consists of n vectors $\vec{v}_i$, $i = 1, \ldots, n$. Each $\vec{v}_i$ represents an homogeneous coordinate z_i. The $\vec{v}_i$'s satisfy linear relations of the form

$$\sum_{i=1}^{n} Q_a^i \vec{v}_i = 0 \qquad (3.0.5)$$

with $Q_a^i \in \mathbb{Z}$. Taking a basis of $\vec{Q}_a$, where $a = 1, \ldots, n - d$, we construct a charge

matrix Q. In other words, Q is given by the kernel of a matrix whose columns are the $\vec{v}_i$'s. The matrix Q computed this way, is precisely the one that determines the $U(1)^{(n-d)}$ action of the symplectic quotient.

When the toric variety is Calabi-Yau, the toric diagram is simplified. In fact the manifold is Calabi-Yau if and only if there exist a vector $\vec{h}$ in the lattice $\mathbb{M}$ dual to $\mathbb{N}$ such that

$$< \vec{h}, \vec{v}_i >= 1 \quad \forall \, \vec{v}_i \tag{3.0.6}$$

In other words, the toric diagram lives on an $(n-1)$-dimensional hyperplane at unit distance from the origin. This means that the 3-complex dimensional toric Calabi-Yaus that we will study are represented by toric diagrams that are effectively 2-dimensional.

Let us illustrate these ideas with a concrete example. Figure 3-1 shows the toric diagram for the well known example of the conifold.
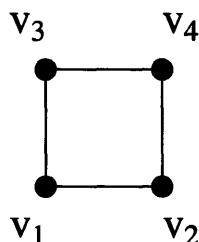
Figure 3-1: Toric diagram for the conifold.

The four nodes in the toric diagram are

$$\vec{v}_1 = (0,0,1) \quad \vec{v}_2 = (1,0,1) \quad \vec{v}_3 = (0,1,1) \quad \vec{v}_4 = (1,1,1) \tag{3.0.7}$$

where we have added to all vectors in the two dimensional toric diagram a third coordinate that follows from (3.0.6).

Using these vectors as columns, we construct the matrix

51

$$G = \begin{pmatrix} 0 & 1 & 0 & 1 \\ 0 & 0 & 1 & 1 \\ 1 & 1 & 1 & 1 \end{pmatrix} \qquad (3.0.8)$$

Then, $ker(G) = (-1, 1, 1, -1)$. That is, the linear relations among these vectors are generated by a single $\vec{Q}_1 = (-1, 1, 1, -1)$. Hence the toric diagram in Figure 3-1 describes a toric variety defined by

$$-|x_1|^2 + |x_2|^2 + |x_3|^2 - |x_4|^2 = \xi_1 \qquad (3.0.9)$$

modulo a $U(1)$ action given by the charge matrix

$$\begin{pmatrix} x_1 & x_2 & x_3 & x_4 \\ -1 & 1 & 1 & -1 \end{pmatrix} \qquad (3.0.10)$$

For $\xi_1 = 0$ in (3.0.9) we have the singular conifold. The cases of $\xi_1 > 0$ and $\xi_1 < 0$ give rise to two resolutions of the conifold singularity related by flop transitions.

Chapter 4

Egineering gauge theories using branes

String Theory has been widely used to study the dynamics of gauge theories. In doing so, it sometimes provides a completely new interpretation of field theory results. The relation goes in both directions, and gauge theories can be used to understand String Theory processes. The main ingredient in this connection is that, as we discussed in Chapter 2, the low energy dynamics of D-branes is described by SYM on their world volume, with different amounts of supersymmetry depending on the specific configuration. Several ways of constructing gauge theories using D-branes have been developed. We now review the main strategies employed: brane setups [86], geometric engineering [114, 115] and brane probes [39, 110, 125, 84].

4.1 Hanany-Witten setups

Brane setups were introduced by Hanany and Witten in [86]. They involve branes suspended between branes and extend the simple stacks of parallel branes discussed in Section 2.4. By combining different types of branes and orienting them properly, it is possible to reduce the amount of supersymmetry and introduce new matter. This approach is particularly simple and intuitive because it involves **flat branes** in **flat space**. Distances and motions in the brane picture are mapped to parameters and

moduli of the gauge theories.

We can understand the main virtues of this approach with a simple example. Let us consider one of the brane configurations studied in [86], which corresponds to the construction of $d = 3$ $\mathcal{N} = 4$ supersymmetric gauge theories. We show the setup for an $U(2)$ gauge group without matter in Figure 4-1.
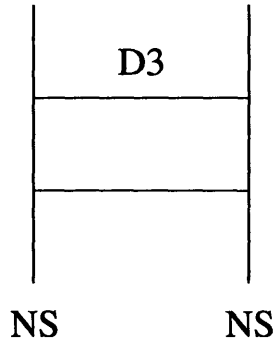
Figure 4-1: Hanany-Witten configuration for $d = 3$ $\mathcal{N} = 4$ gauge theory in 2+1 dimensions with $U(2)$ gauge group

The configuration involves NS5-branes and D3-branes spanning the following directions

	x^0	x^1	x^2	x^3	x^4	x^5	x^6	x^7	x^8	x^9
NS	●	●	●	●	●	●	–	–	–	–
$D3$	●	●	●	–	–	–	●	–	–	–

In the $g_s \to 0$ limit, the NS5-branes are much heavier that the D3-branes, and they can be regarded as non-dynamical objects whose positions determine certain parameters of the gauge theory living on the D3-branes. The D3-branes have a finite length L_6 in the x^6 direction. Hence, the low energy gauge theory on them is 2+1 dimensional. The brane configuration breaks 1/4 of the original supersymmetries, leaving 8 supercharges, i.e. $\mathcal{N} = 4$ in 3 dimensions.

The ten dimensional Lorentz group $SO(1,9)$ is broken down to $SO(1,2) \times SO(3)_V \times SO(3)_H$. $SO(1,2)$ acts on (x^0, x^1, x^2), $SO(3)_V$ on (x^3, x^4, x^5) and $SO(3)_H$ on (x^7, x^8, x^9). The double covers of $SO(3)_V$ and $SO(3)_H$ are $SU(2)_V$ and $SU(2)_H$. The V and H subindices indicate that they act as symmetries of the Coulomb and Higgs branches,

54

respectively. The R-symmetry of the gauge theory is $SO(4) = SU(2)_V \times SU(2)_H$. i.e. it corresponds to rotational symmetries of the brane configuration.

The three dimensional gauge coupling is determined by the separation between the NS5-branes L_6

$$\frac{1}{g^2} = \frac{L_6}{g_s} \tag{4.1.1}$$

Relative motion of the NS5-branes in the (x^7, x^8, x^9) directions map to FI parameters in the gauge theory. Flavors can be incorporated by adding D5-branes in $(x^0, x^1, x^2, x^7, x^8, x^9)$.

Mirror symmetry of the 3-dimensional gauge theory [105] corresponds to S-duality of the brane configuration [86]. In addition, looking at these brane constructions from a different perspective it is possible to establish a correspondence between the Coulomb branch of the 3d gauge theories and the moduli space of magnetic monopoles of the $SU(2)$ gauge theory broken to $U(1)$ that lives on the worldvolume of the NS5-branes [86]. These are typical examples of the simplifications and intuition we obtain about the dynamics and duality of field theories when they are embedded in string theory constructions.

Since its conception, the field of brane setups has been extremely fruitful and constructions of gauge theories in several dimensions, with different amounts of supersymmetry and gauge groups, have been developed since they were introduced (see for example [69] for a review of some of these constructions). The (p, q) web constructions of Chapter 6 are examples of this type.

4.2 Geometric engineering

Geometric engineering [114, 115] corresponds to considering Type IIA or IIB string theory compactified on a Calabi Yau. In the case of a CY3-fold, the resulting theory has $\mathcal{N} = 2$ supersymmetry in four dimensions.

D-branes wrapping internal cycles in the CY give rise to gauge and matter fields, that become massless when the cycles shrink to zero size. All the information that

is relevant for the field theory limit is encoded in the local structure of the geometry. Then, for the purpose of studying the field theory, the compact Calabi-Yau can be replaced by a non-compact ALE singularity. These singularities have an ADE classification, i.e. they are associated to the Dynkin diagrams of simply-laced algebras. The quiver diagram of the resulting gauge theory turns out to be equal to the corresponding Dynkin diagram.

4.3 D-brane probes

A third approach for the construction of gauge theories consists on taking a String Theory background and probe it with D-branes [39, 110, 125, 84]. The background geometry dictates the amount of supersymmetry, matter content, gauge group, and interactions of the gauge theory on the D-branes. Of particular interest are singular geometries, since they can give rise to reduced SUSY and chiral theories. This method will be used all along this thesis.

Gauge theories on D-branes at orbifold singularities are particularly simple to compute. Orbifolds are obtained by performing a quotient by the action of an orbifold group. The orbifold group acts on spacetime coordinates and, in the presence of D-branes, on the Chan-Patton degrees of freedom at the endpoints of open strings. The gauge theory for the orbifold is obtained by considering the images of the original D-branes and projecting into invariant states [39].
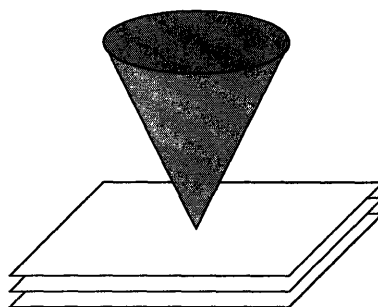
Figure 4-2: Stack of D-branes can be located over singularities to engineer interesting gauge theories.

Chapters 5 and 6 will introduce methods for computing the gauge theories on

D-branes over more general toric singularities. The quantum dynamics of the background is encoded in the quantum behaviour of the gauge theory. We will exploit this fact in Chapter 9. The problem of finding gauge theories on D-branes probing arbitrary toric singularities will be revisited in Chapter 11.

Chapter 5

Symmetries of Toric Duality

In this chapter we elucidate the nature of toric duality dubbed in hep-th/0003085 in the construction for world volume theories of D-branes probing arbitrary toric singularities. This duality will be seen to be due to certain permutation symmetries of multiplicities in the gauged linear sigma model fields. To this symmetry we shall refer as "multiplicity symmetry." We present beautiful combinatorial properties of these multiplicities and rederive all known cases of torically dual theories under this new light. We also initiate an understanding of why such multiplicity symmetry naturally leads to monodromy and Seiberg duality. Furthermore we discuss certain "flavor" and "node" symmetries of the quiver and superpotential and how they are intimately related to the isometry of the background geometry, as well as how in certain cases complicated superpotentials can be derived by observations of the symmetries alone. This chapter is based on [43].

5.1 Introduction

The study of string theory on various backgrounds, in particular space-time singularities, is by now an extensively investigated matter. Of special interest are algebraic singularities which locally model Calabi-Yau threefolds so as to produce, on the world-volume of D-branes transversely probing the singularity, classes of supersymmetric gauge theories.

Using the techniques of the gauged linear sigma model [167] as a symplectic quotienting mechanism, *toric geometry* has been widely used [8, 38, 138, 11] to analyse the D-brane theories probing toric singularities. The singularity resolution methods fruitfully developed in the mathematics of toric geometry have been amply utilised in understanding the world-volume gauge theory, notably its IR moduli space, which precisely realises the singularity being probed.

To deal with the problem of finding the gauge theory on the D-brane given an arbitrary toric singularity which it probes, a unified algorithmic outlook to the existing technology [8, 38, 138, 11] of *partial resolution* of Abelian orbifolds has been established [45]. One interesting byproduct of the algorithm is the harnessing of its *non-uniqueness* to explicitly construct various theories with vastly different matter content and superpotential which flow in the IR to the same moduli space parametrised by the toric variety [45, 46]. In fact these theories are expected [48, 12] to be completely dual in the IR as field theories. The identification of the moduli space is but one manifestation, in addition, they should have the same operator spectrum, same relevant and marginal deformations and correlation functions. The phenomenon was dubbed **toric duality**.

Recently this duality has caught some attention [48, 12, 32, 143, 24], wherein three contrasting perspectives, respectively brane-diamond setups, dual variables in field theory as well as $\mathcal{N} = 1$ geometric transitions, have lead to the same conjecture that *Toric Duality is Seiberg Duality for $\mathcal{N} = 1$ theories with toric moduli spaces*. In addition, the same phases have been independently arrived at via (p, q)-web configurations [80].

The Inverse Algorithm of [45] remains an effective - in the sense of reducing the computations to nothing but linear algebra and integer programming - method of deriving toric (and hence Seiberg) dual theories. With this convenience is a certain loss of physical and geometrical intuition: what indeed is happening to the fields (both in the sigma model and in the brane world-volume theory) as one proceed with the linear transformations? Moreover, in the case of the cone over the third del Pezzo surface (dP_3), various phases have been obtained using independent methods

[48, 12, 24] while they have so far not been attained by the Inverse Algorithm.

The purpose of this writing is clear. We first supplant the present shortcoming by explicitly obtaining all phases of dP_3. In due course we shall see the true nature of toric duality: that the unimodular degree of freedom whence it arises as claimed in [46] - though such unimodularity persists as a symmetry of the theory - is but a special case. It appears that the quintessence of toric duality, with regard to the Inverse Algorithm, is certain **multiplicity** of fields in the gauged linear sigma model. Permutation symmetry within such multiplicities leads to torically dual theories. Furthermore we shall see that these multiplicities have beautiful combinatorial properties which still remain largely mysterious.

Moreover, we also discuss how symmetries of the physics, manifested through "flavor symmetries" of multiplets of bi-fundamentals between two gauge factors, and through "node symmetries" of the permutation automorphism of the quiver diagram. We shall learn how in many cases the isometry of the singularity leads us to such symmetries of the quiver. More importantly, we shall utilise such symmetries to determine, very often uniquely, the form of the superpotential.

The outline of this section is as follows. In Section 5.2 we present the multiplicities of the GLSM fields for the theories $\mathbb{C}^2/\mathbb{Z}_n$ as well as some first cases of $\mathbb{C}^3/(\mathbb{Z}_k \times \mathbb{Z}_m)$ and observe beautiful combinatorial properties thereof. In Section 5.3 we show how toric duality really originates from permutation symmetries from the multiplicities and show how the phases of known torically dual theories can be obtained in this new light. Section 5.4 is devoted to the analysis of node and flavor symmetries. It addresses the interesting problem of how one may in many cases obtain the complicated forms of the superpotential by merely observing these symmetries. Then in Section 5.5 we briefly give an argument why toric duality should stem from such multiplicities in the GLSM fields in terms of monodromy actions on homogeneous coordinates. We conclude and give future prospects in Section 5.6.

5.2 Multiplicities in the GLSM Fields

We first remind the reader of the origin of the multiplicity in the homogeneous coordinates of the toric variety as described by Witten's gauged linear sigma model (GLSM) language [167]. The techniques of [8, 38, 138, 11] allow us to write the D-flatness and F-flatness conditions of the world-volume gauge theory on an equal footing.

At the end of the day, the $U(1)^n$ $\mathcal{N} = 1$ theory with m bi-fundamentals on the D-brane is described by c fields p_i subject to $c - 3$ moment maps: this gives us the $(c - 3) \times c$ charge matrix Q_t. The integral cokernel of Q_t is a $3 \times c$ matrix G_t; its columns, up to **repetition**, are the nodes of the three-dimensional toric diagram corresponding to the IR moduli space of the theory. These c fields p_i are the GLSM fields of [167], or in the mathematics literature, the so-called *homogeneous coordinates* of the toric variety [30]. The details of this forward algorithm from gauge theory data to toric data have been extensively presented as a flow-chart in [45, 46] and shall not be belaboured here again.

The key number to our analyses shall be the integer c. It is so that the $(r + 2) \times c$ matrix T describes the integer cone dual to the $(r + 2) \times m$ matrix K coming from the F-terms. As finding dual cones (and indeed Hilbert bases of integer polytopes) is purely an algorithmic method, there is in the literature so far no known analytic expression for c in terms of m and r; overcoming this deficiency would be greatly appreciated.

A few examples shall serve to illustrate some intriguing combinatorial properties of this multiplicity.

We begin with the simple orbifold $\mathbb{C}^3/\mathbb{Z}_n$ with the $\mathbb{Z}_n$ action on the coordinates (x, y, z) of $\mathbb{C}^3$ as $(x, y, z) \rightarrow (\omega^a x, \omega^b y, \omega^{-1} z)$ such that ω is the nth root of unity and $a + b - 1 \equiv 0 (\mod n)$ to guarantee that $Z_n \subset SU(3)$ so as to ensure that the resolution is a Calabi-Yau threefold. This convention in chosen in accordance with the standard literature [8, 38, 138, 11].

Let us first choose $a = 0$ so that the singularity is effectively $\mathbb{C} \times \mathbb{C}^2/\mathbb{Z}_n$; with the toric diagram of the Abelian ALE piece we are indeed familiar: the fan consists of a

single 2-dimensional cone generated by e_2 and $ne_1 - e_2$ [62]. This well-known $\mathcal{N} = 2$ theory, under such embedding as a $\mathbb{C}^3$ quotient, can thus be cast into $\mathcal{N} = 1$ language. Applying the Forward Algorithm of [8, 38, 138, 11] to the $\mathcal{N} = 1$ SUSY gauge theory on this orbifold should give us none other than the toric diagram for $\mathbb{C}^2/\mathbb{Z}_n$. This is indeed so as shown in the following table. What we are interested in is the matrix G_t, whose integer nullspace is the charge matrix Q_t of the linear sigma model fields. We should pay special attention to the repetitions in the columns of G_t.

5.2.1 $\mathbb{C}^2/\mathbb{Z}_n$

We present the matrix G_t, whose columns, up to **multiplicity**, are the nodes of the toric diagram for $\mathbb{C}^2/\mathbb{Z}_n$ for some low values of n:

We plot in Figure 5-1 the above vectors in $\mathbb{Z}^3$ and note that they are co-planar, as guaranteed by the Calabi-Yau condition. The black numbers labelling the nodes are the multiplicity of the vectors (in blue) corresponding to the nodes in the toric diagram.
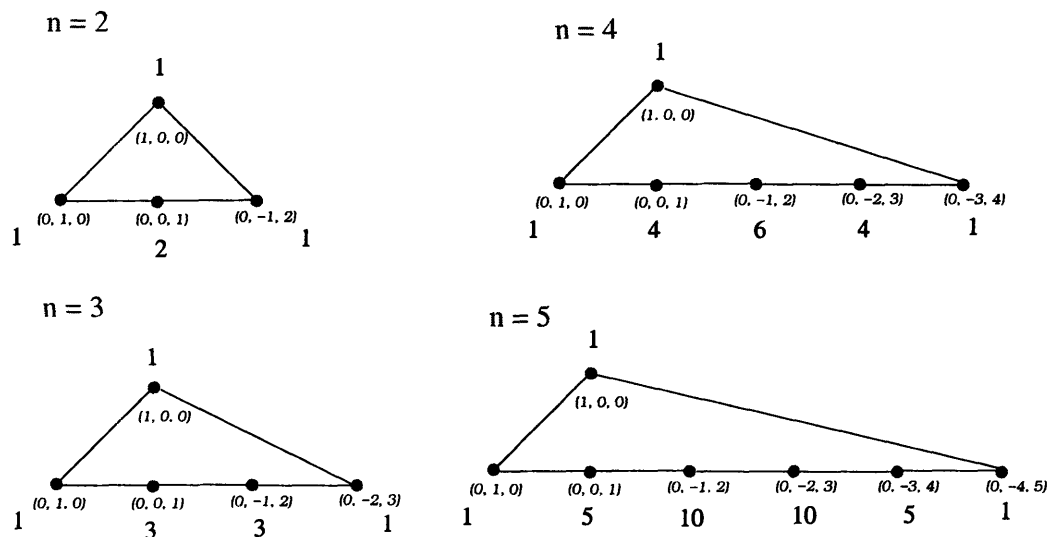
Figure 5-1: The familiar toric diagrams for $\mathbb{C}^2/(\mathbb{Z}_k \times \mathbb{Z}_m)$, but with the multiplicity of the sigma model fields explicitly labelled.

These toric diagrams in Figure 5-1 are indeed as expected and are the well-known examples of $\mathbb{C}^2/\mathbb{Z}_n$. Now note the multiplicities: a pattern in accordance with Pascal's

triangle can clearly be observed. For general n, we expect 1's on the extremal vertices of the triangles while for the ith internal colinear node, we have multiplicity $\binom{n}{i}$. Therefore for this case

$$c = \sum_{i=1}^{n} \binom{n}{i} + 1 = 2^n + 1 \tag{5.2.1}$$

We show this explicitly in the appendix.

5.2.2 $\mathbb{C}^3/(\mathbb{Z}_k \times \mathbb{Z}_k)$

As pointed out in [45], in the study of arbitrary toric singularities of local Calabi-Yau threefolds, one must be primarily concerned with the 3-dimensional Abelian quotient $\mathbb{C}^3/(\mathbb{Z}_k \times \mathbb{Z}_k)$. Partial resolutions from the latter using the Inverse Algorithm suffices to handle the world volume gauge theory. Such quotients have also been extensively investigated in [8, 38, 138, 11, 146, 74].

As is well-known, the toric diagrams for these singularities are $(k + 1) \times (k + 1)$ isosceles triangles. However current restrictions on the running time prohibits constructing the linear sigma model to high values of k. We have drawn these diagrams for the first two cases, explicating the multiplicity in Figure 5-2. From the first two cases we already observe a pattern analogous to the above $\mathbb{C}^2/\mathbb{Z}_n$ case: each side of the triangle has the multiplicity according to the Pascal's Triangle. This is to be expected as one can partially resolve the singularity to the $\mathbb{C}^2$ orbifold. We still do not have a general rule for the multiplicity of the inner point, except in the special case of $\mathbb{C}^3/(\mathbb{Z}_3 \times \mathbb{Z}_3)$, where it corresponds to the sum of the multiplicities of its neighbouring points. For contrast we have also included $\mathbb{Z}_2 \times \mathbb{Z}_3$, the multiplicities of whose outside nodes are clear while those of the internal node still elude an obvious observation.

5.3 Toric Duality and Multiplicity Symmetry

What we shall see in this section is that the numerology introduced in the previous section is more than a combinatorial curio, and that the essence of **toric duality**
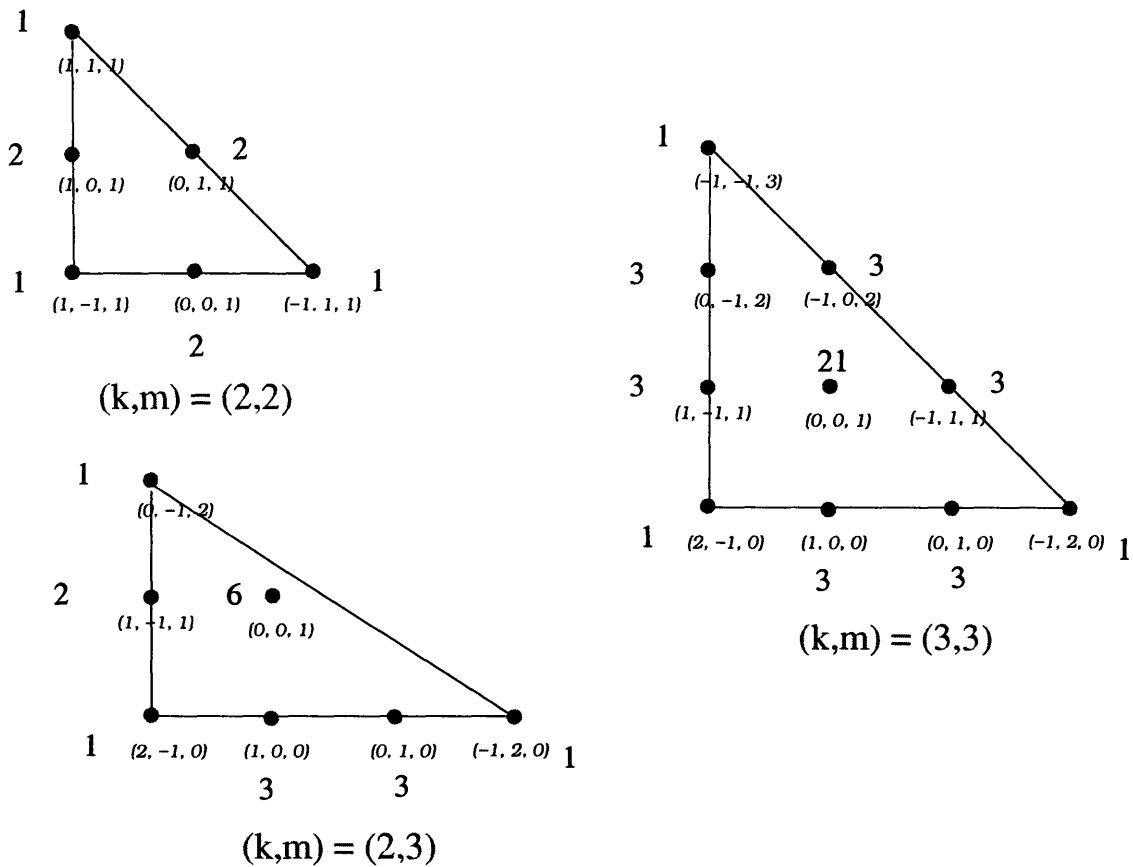
Figure 5-2: The familiar toric diagrams for $\mathbb{C}^2/\mathbb{Z}_n$, but with the multiplicity of the sigma model fields explicitly labelled.

lies within the multiplicity of linear sigma model fields associated to each node of the toric diagram.

Some puzzles arose in [48, 12] as to why not all of the four Seiberg dual phases of the third del Pezzo surface could be obtained from partially resolving $\mathbb{C}^3/(\mathbb{Z}_3 \times \mathbb{Z}_3)$. In this section we shall first supplant this shortcoming by explicitly obtaining these four phases. Then we shall rectify some current misconceptions of toric duality and show that the unimodular transformations mentioned in [46] is but a special case and that

PROPOSITION 5.3.1 *Toric duality is due to the multiplicity of the gauged linear sigma model fields associated to the nodes of the toric diagram of the moduli space.*

Let us address a subtlety of the above point. By toric duality we mean so in the

65

restricted sense of confining ourselves to the duality obtainable from the canonical method of partial resolution, which guarantees physicality. There are other sources of potentially dual theories posited in [45, 46] such as the "F-D ambiguity" and the "repetition ambiguity." Because these do not necessarily ensure the gauge theory to have well-behaved matter content and superpotential and have yet to be better understood, the toric duality we address here will not include these cases.

5.3.1 Different Phases from a Unique Toric Diagram

Let us recapitulate awhile. In [46] the different phases of gauge theories living on D-branes probing toric singularities were studied. The strategy adopted there was to start from toric diagrams related by unimodular transformations. Different sets of toric data related in this way describe the same variety. Subsequently, the so called Inverse Algorithm was applied, giving several gauge theories as a result. These theories fall into equivalence classes that correspond to the phases of the given singularity.

In this section we show how indeed all phases can be obtained from a single toric diagram. The claim is that they correspond to different multiplicities of the linear σ-model fields that remain massless after resolution. In order to ensure that the final gauge theory lives in the world volume of a D-brane, we realize the different singularities as partial resolutions of the $\mathbb{C}^3/(\mathbb{Z}_3 \times \mathbb{Z}_3)$ orbifold (Figure 5-3).

The resolutions are achieved by turning on Fayet-Iliopoulos terms. Then some fields acquire expectation values in order to satisfy D-flatness equations. As a result, mass terms for some of the chiral superfields are generated in the superpotential. Finally, these massive fields can be integrated out when considering the low energy regime of the gauge theory. Alternatively, we can look at the resolution process from the point of view of linear σ-model variables. The introduction of FI parameters allows us to eliminate some of them. The higher the dimensionality of the cone in which the ζ_i's lie, the more fields (nodes on the toric diagram) we can eliminate. In this way, we can obtain the sub-diagrams that are contained in a larger one, by deleting nodes with FI parameters.

In the following, we present the partial resolutions of $\mathbb{C}^3/(\mathbb{Z}_3 \times \mathbb{Z}_3)$ that lead to
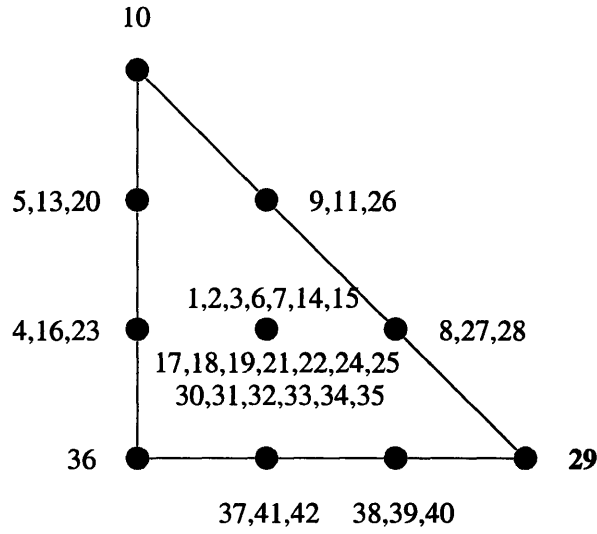
Figure 5-3: Toric diagram of $\mathbb{C}^3/(\mathbb{Z}_3 \times \mathbb{Z}_3)$, with the GLSM fields labelled explicitly (q.v. [45]).

the different phases for the F_0, dP_2 and dP_3 singularities.

5.3.2 Zeroth Hirzebruch surface

F_0 has been shown to have two phases [45, 46]. The corresponding quiver diagrams are presented in Figure 8-4. The superpotentials can be found in [45, 46] and we will present them in a more concise form below in (5.3.3) and (5.3.4). Indeed we want to rewrite them in a way such that the underlying $SU(2) \times SU(2)$ global symmetry of these theories is explicit. Geometrically, it arises as the product of the $SU(2)$ isometries of the two $\mathbb{P}^1$'s in $F_0 = \mathbb{P}^1 \times \mathbb{P}^1$.

The matter fields lie in the following representations of the global symmetry group

	$SU(2) \times SU(2)$		$SU(2) \times SU(2)$
X_{12}^i	$(\square, \cdot)$	X_{12}^i	$(\square, \cdot)$
X_{23}^i	$(\cdot, \square)$	X_{23}^i	$(\cdot, \square)$
X_{34}^i	$(\square, \cdot)$	X_{43}^i	$(\square, \cdot)$
X_{41}^i	$(\cdot, \square)$	X_{14}^i	$(\cdot, \square)$
		X_{31}^{ij}	$(\square, \square)$

dual on 4 $\Longrightarrow$

$$(5.3.2)$$

67
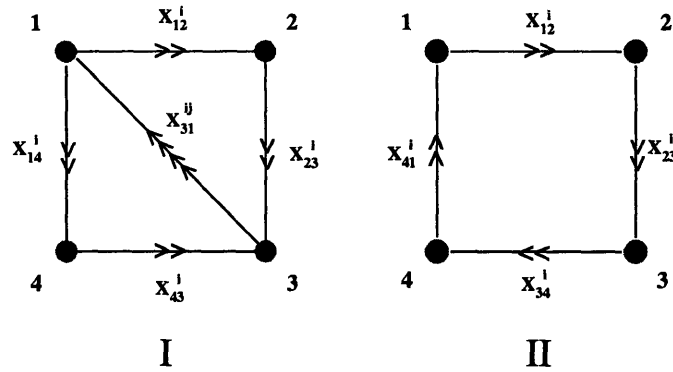
Figure 5-4: Quiver diagrams of the two torically dual theories corresponding to the cone over the zeroth Hirzebruch surface F_0.

It was shown in [48, 12, 24] that these two theories are indeed Seiberg duals. Therefore, they should have same global symmetries as inherited from the same geometry. For example, if we start from phase II and dualize on the gauge group 4, we see that the dual quarks X_{43}^i and X_{14}^i are in the complex conjugate representations to the original ones, while the X_{31}^{ij}'s are in $(\Box, \Box)$ since they are the composite Seiberg mesons ($X_{31}^{ij} = X_{34}^i X_{41}^j$). The corresponding superpotentials have to be singlets under the global symmetries. They are given by

$$W_{II} = \epsilon_{ij} X_{12}^i X_{34}^j \epsilon_{mn} X_{23}^m X_{41}^n \tag{5.3.3}$$

$$W_I = \epsilon_{ij}\epsilon_{mn} X_{12}^i X_{23}^m X_{31}^{jn} - \epsilon_{ij}\epsilon_{mn} X_{41}^i X_{23}^m X_{31}^{jn} \tag{5.3.4}$$

We identify W_{II} as the singlet appearing in the product X_{12} X_{34} X_{23} X_{41} = $(\Box, \cdot) \otimes (\Box, \cdot) \otimes (\cdot, \Box) \otimes (\cdot, \Box)$, while W_I is the singlet obtained from X_{12} X_{23} X_{31} − X_{41} X_{43} X_{31} = $(\Box, \cdot) \otimes (\cdot, \Box) \otimes (\Box, \Box) - (\cdot, \Box) \otimes (\Box, \cdot) \otimes (\Box, \Box)$. In [46] we obtained these two phases by unimodular transformations of the toric diagram. Now we refer to Figure 5-5, where we make two different choices of keeping the GLSM fields during partial resolutions. We in fact obtain the two phases from the same toric diagram with different multiplicities of its nodes. This is as claimed, torically (Seiberg) dual phases are obtained from a single toric diagram but with different resolutions of the multiple GLSM fields. We have checked that the same result holds if we perform unimodular
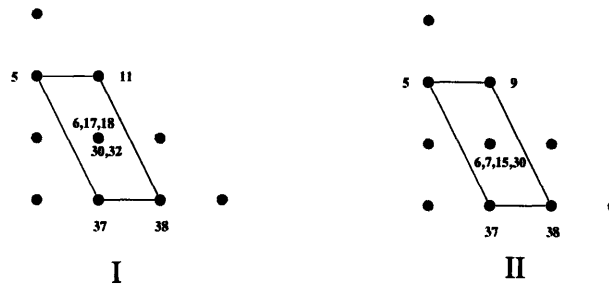
Figure 5-5: Toric diagrams of the two torically dual theories corresponding to the cone over the zeroth Hirzebruch surface F_0, with the surviving GLSM fields indicated explicitly.

transformations and make different choices out of the multiplicities for each of these $SL(3; \mathbb{Z})$-related toric diagrams. Every diagram could give all the phases.

5.3.3 Second del Pezzo surface

Following the same procedure, we can get the two phases associated to dP_2 by partial resolutions conducing to the same toric diagram. These theories were presented in [48, 12]. The GLSM fields surviving after partial resolution are shown in Figure 5-6.
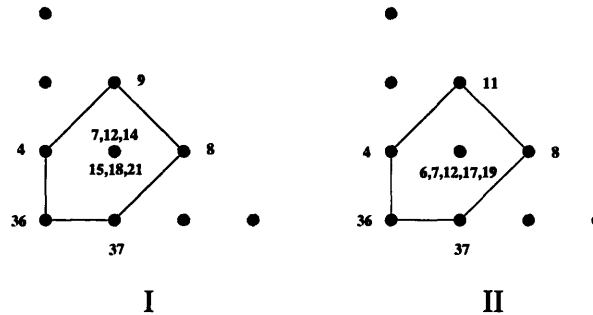
Figure 5-6: Toric diagrams of the two torically dual theories corresponding to the cone over the dP_2, with the surviving GLSM fields indicated explicitly.

5.3.4 Third del Pezzo surface

There are four known phases that can live on the world volume of a D-brane probing dP_3. They were obtained using different strategies. In [48], the starting point was a phase known from partial resolution of $\mathbb{C}^3/(\mathbb{Z}_3 \times \mathbb{Z}_3)$ [46]. Then, the phases

69

were found as the set of all the Abelian theories which is closed under Seiberg duality transformations. In [12] the phases were calculated as partial resolutions of the $\mathbb{C}^3/(\mathbb{Z}_3 \times \mathbb{Z}_3)$ orbifold singularity. Finally, an alternative approach was elaborated in [24], where four dimensional, $\mathcal{N} = 1$ gauge theories were constructed wrapping D3, D5 and D7 branes over different cycles of Calabi-Yau 3-folds. From that perspective, the distinct phases are connected by geometric transitions.

The partial resolutions that serve as starting points for the Inverse Algorithm to compute the four phases are shown in Figure 5-7. With these choices we do indeed obtain the four phases of the del Pezzo Three theory from a single toric diagram without recourse to unimodular transformations.
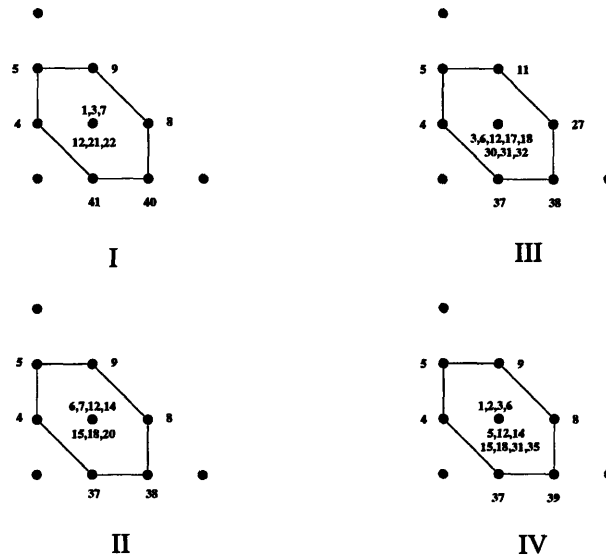
Figure 5-7: Toric diagrams of the four torically dual theories corresponding to the cone over the dP_3, with the surviving GLSM fields indicated explicitly.

Having now shown that all the known cases of torically dual theories can be obtained, each from a single toric diagram but with different combinations from the multiplicity of GLSM fields, we summarise the results in these preceding subsections (cf. Figure 5-8).

We see that as is with the cases for the Abelian orbifolds of $\mathbb{C}^2$ and $\mathbb{C}^3$, in Section 5.2, the multiplicity of the outside nodes is always 1 while that of the internal node is at least the sum of the outside nodes. What is remarkable is that as we choose different combinations of GLSM models to acquire VEV and be resolved, what remains are

Singularity	Phase	Central GLSM Fields	Target Space Fields
F_0	I	5	12
	II	4	8
dP_2	I	6	13
	II	5	11
dP_3	IV	11	18
	III	8	14
	II	7	14
	I	6	12

Table 5.1: The number of GLSM multiplicities in the centre of the toric diagram versus the number of fields in the final gauge theory.

different number of multiplicities for the internal node, each corresponding to one of the torically dual theories. This is what we have drawn in Figure 5-8.
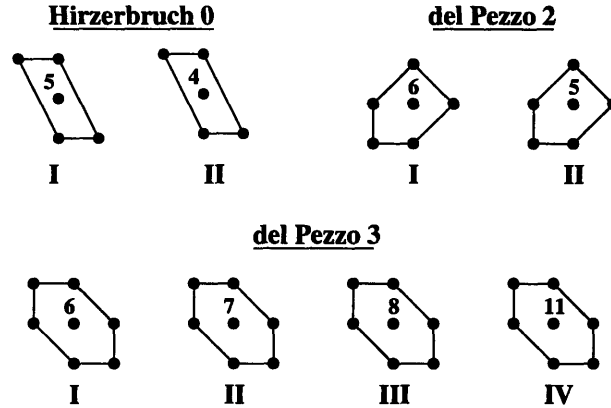
Figure 5-8: GLSM multiplicities in the toric diagrams associated to the dual theories. The outside nodes each has a single GLSM corresponding thereto, i.e., with multiplicity 1.

5.3.5 GLSM versus target space multiplicities

Let us pause for a moment to consider the relation between the multiplicities of linear σ-model and target space fields. We present them in (5.1).

We can immediately notice that there exist a correlation between them, namely the phases with a larger number of target space fields have also a higher multiplicity of the GLSM fields. Bearing in mind that partial resolution corresponds (from the point of view of the GLSM) to eliminating variables and (from the original gauge

theory perspective) to integrating out massive fields, we can ask whether different phases are related by an operation of this kind. An important point is that, on the gauge theory side, the elimination of fields is achieved by turning on non-zero vevs for bifundamental chiral fields. Apart from generating mass terms for some fields, bifundamental vevs higgs the corresponding gauge factors to the diagonal subgroups. As a consequence gauge symmetry is always reduced. All the theories in Table 5.1 have the same gauge group, so we conclude that they cannot be connected by this procedure.

5.4 Global Symmetries, Quiver Automorphisms and Superpotentials

As we mentioned before, the calculation of the superpotential is not an easy task, so it would be valuable to have guiding principles. Symmetry is definitely one of these ideas. We have seen that the isometry $SU(2) \times SU(2)$ of $\mathbb{P}^1 \times \mathbb{P}^1$ suffices to fix the superpotential of $\mathbf{F_0}$. We will now see that the $SU(3)$ isometry of $\mathbb{C}^3/\mathbb{Z}_3$ does the same job for dP_0. These examples tell us that the symmetry of a singularity is a very useful piece of information and can help us in finding and understanding the superpotential. Indeed our ultimate hope is to determine the superpotential by direct observation of the symmetries of the background.

Before going into the detailed discussion, we want to distinguish two kinds of symmetries, which are related to the background in the closed string sector, that can be present in the gauge theory. The first one is the isometry of the variety. For example, the $SU(2) \times SU(2)$ of $\mathbb{P}^1 \times \mathbb{P}^1$ and $SU(3)$ of $\mathbb{C}^3/\mathbb{Z}_3$. These symmetries are reflected in the quiver by the grouping of the fields lying in multiple arrows into representations of the isometry group. We will call such a symmetry **flavor symmetry**. As we have seen, this flavor symmetry is very strong and in the aforementioned cases can fix the superpotential uniquely.

The second symmetry is a remnant of a continuous symmetry, which is recovered

in the strong coupling limit and broken otherwise. For del Pezzo surfaces dP_n we expect this continuous symmetry to be the Lie group of E_n. We will refer to it as the **node symmetry**, because under its action nodes and related fields in the quiver diagram are permuted. We will show that using the node symmetry we can group the superpotential terms into a more organized expression. This also fixes the superpotenial to some level.

We will begin this section by discussing how symmetry can guide us to write down the superpotential using dP_3 as an example. Then for completeness, we will consider the other toric del Pezzo and the zeroth Hirsebruch surface and will present a table summarizing our results.

5.4.1 del Pezzo 3

The node symmetries of dP_3 phases have been discussed in detail in [12]. It was found that they are D_6, $\mathbb{Z}_2 \times \mathbb{Z}_2$, $\mathbb{Z}_2 \times \mathbb{Z}_2$ and D_6 for models I, II, III and IV respectively (where D_6 is the dihedral group of order 12). For the convenience of the reader, we remark here that in the notation of [48], these models were referred to respectively as II, I, III and IV therein. Here we will focus on how the symmetry enables us to rewrite the superpotentials in an enlightening and compact way. Furthermore, we will show how they indeed in many cases fix the form of the superpotential. This is very much in the spirit of the geometrical engineering method of obtaining the superpotential [24, 32, 143] where the fields are naturally organised into multiplets in accordance with Hom's of (exceptional collections of) vector bundles.

We recall that the complete results, quiver and superpotential, were given in [12, 48] for the four phases of dP_3. Our goal is to re-write them in a much more illuminating way. First we give the quiver diagrams of all four phases in Figure 5-9. In this figure, we have carefully drawn the quivers in such a manner that the symmetries are obviously related to geometric actions (rotations and reflections) on them; this is what we mean by quiver automorphism. Now let us move on to see how the symmetry determines the superpotentials.

Let us first focus on model I. We see that its quiver exhibits a D_6 symmetry of
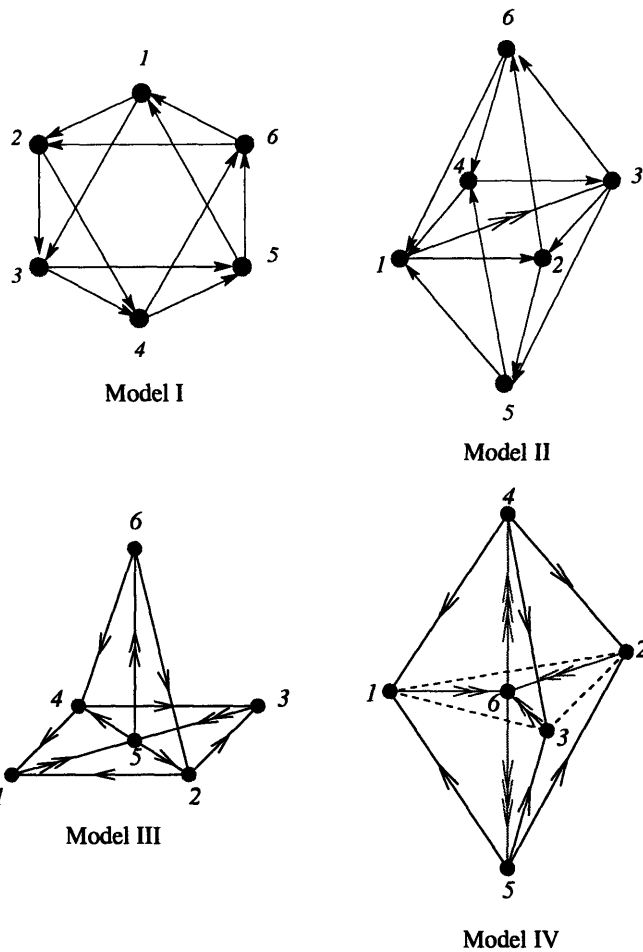
Figure 5-9: Quiver diagrams of the four torically dual theories corresponding to the cone over dP_3. We see explicitly the node symmetries to be respectively: D_6, $\mathbb{Z}_2 \times \mathbb{Z}_2$, $\mathbb{Z}_2 \times \mathbb{Z}_2$ and D_6.

the Star of David. This quiver has the following closed loops (i.e. gauge invariant operators): one loop with six fields, six loops with five fields, nine loops with four fields and two loops with three fields. Our basic idea is following:

- If a given loop is contained in the superpotential, all its images under the node symmetry group also have to be present;

- Since we are dealing with affine toric varieties we know that every field has to appear exactly twice so as to give monomial F-term constraints [45];

- Moreover, in order to generate a toric ideal, the pair must have opposite signs.

We will see that these three criteria will be rather discriminating. The gauge

invariants form the following orbits under the action of D_6 (by $(a, b, c \ldots n)$ we mean the term $X_{ab}X_{bc} \ldots X_{na}$ in the superpotential):

(1) $\{(1, 2, 3, 4, 5, 6)\}$

(2) $\{(1, 2, 3, 4, 5), (2, 3, 4, 5, 6), (3, 4, 5, 6, 1), (4, 5, 6, 1, 2), (5, 6, 1, 2, 3), (6, 1, 2, 3, 4)\}$

(3) $\{(1, 2, 3, 5), (2, 3, 4, 6), (3, 4, 5, 1), (4, 5, 6, 2), (5, 6, 1, 3), (6, 1, 2, 4)\}$

(4) $\{(1, 2, 4, 5), (2, 3, 5, 6), (3, 4, 6, 1)\}$

(5) $\{(1, 3, 5), (2, 4, 6)\}$

$$(5.4.5)$$

This theory has 12 fields, thus all the terms in the superpotential must add up to 24 fields. This leaves us with only two possibilities. One is that the superpotential is just given by the six quartic terms in **(3)** and the other is that $W = $ **(1)** $+$ **(4)** $+$ **(5)**. The first possibility is excluded by noting the following. The field X_{12} shows up in $(1, 2, 3, 5)$ with positive sign (which let us assume *ab initio* to be positive coefficient at this moment), so the sign in front of $(6, 1, 2, 4)$ must be negative, forcing the sign in front of $(2, 3, 4, 6)$ to be positive because of the field X_{46}. Whence the sign in front of $(1, 2, 3, 5)$ must be negative due to the field X_{23}, contraciting our initial choice. So the toric criterion together with the node symmetry of the quiver leaves us with only one possibility for the superpotential. We can represent the gauge invariant terms as

$$\bigcirc = X_{12}X_{23}X_{34}X_{45}X_{56}X_{61}; \quad \triangle = X_{13}X_{35}X_{51}; \quad \bigtriangledown = X_{24}X_{46}X_{62};$$
$$\square = X_{23}X_{35}X_{56}X_{62}; \quad \diamondsuit = X_{13}X_{34}X_{46}X_{61}; \quad \lozenge = X_{12}X_{24}X_{45}X_{51}.$$

where the sign has been determined by toric criteria. This gives the following nice schematic representation for the superpotential as:

$$W_I = \bigcirc - (\square + \diamondsuit + \lozenge) + (\triangle + \bigtriangledown) = \bigcirc - \mathbb{Z}_3(\square) + \mathbb{Z}_2(\triangle).$$

This is of course the same as the one given in [48, 12].

Model II has a $\mathbb{Z}_2 \times \mathbb{Z}_2$ node symmetry. One $\mathbb{Z}_2$ is a mirror reflection with respect to the plane (1234) and the other $\mathbb{Z}_2$ is a π rotation with respect to the (56) line

accompanied by the reversing of all the arrows (charge conjugation of all fields). From the quiver and the action of the symmetry group, we see that the gauge invariants form the following orbits:

$$\begin{aligned}
&\textbf{(1)} \ \{(2,6,4,1,3),(2,5,4,1,3)\} \\
&\textbf{(2)} \ \{(2,6,4,3),(2,5,4,3),(4,1,2,6),(4,1,2,5)\} \\
&\textbf{(3)} \ \{(2,6,1),(2,5,1),(3,6,4),(3,5,4)\} \\
&\textbf{(4)} \ \{(6,1,3),(5,1,3)\}
\end{aligned}$$ (5.4.6)

Since we have 14 fields, all terms in the superpotential must add to give 28 fields. Taking into account the double arrow connecting nodes 1 and 3, we see that orbits containing 13 fields should appear four times. There are four possible selections giving a total 28 fields: $(2) + (3)$; $(2) + (4) + (4)$; $(1) + (4) + (3)$ and $(1) + (4) + (4) + (4)$. The first choice gives three X_{26} fields while the fourth gives three X_{61} fields. These must be excluded. We do not seem to have a principle to dictate to us which one of the remaining is correct.

However, experience has lead us to observe the following patten: *fields try to couple to different fields as often as possible.* In second choice the field X_{26} always couples to X_{64} while in the third choice it couples to both X_{64} and X_{61}. Using our rule of thumb, we select the third choice which will turn out to be the correct one.

Next let us proceed to write the superpotential for this third choice. Let us take the term $+X_{12}X_{26}X_{61}$ as our starting point. since the field X_{12} appears again in the loop $X_{12}X_{25}X_{51}$, it must have negative sign. Using same reason we can write down orbits $(1) + (3)$ as

$$[X_{12}X_{26}X_{61} - X_{12}X_{25}X_{51} + X_{36}X_{64}X_{43} - X_{35}X_{54}X_{43}]$$
$$+[-X_{26}X_{64}X_{41}Y_{13}X_{32} + X_{25}X_{54}X_{41}?X_{32}]$$

where we have chosen arbitrarily the field Y_{13} from the doublet (X_{13}, Y_{13}) and left the ? mark undetermined (either to be Y_{13} or X_{13}). Then we use another observed fact that *multiple fields such as (X_{13}, Y_{13}) are also transformed under the action of the*

symmetry generators. Since loops $(2, 6, 4, 1, 3), (2, 5, 4, 1, 3)$ are exchanged under the $\mathbb{Z}_2$ action, we should put X_{13} in the ? mark.

Finally we can write down the orbit (**4**) which is uniquelly fixed to be $+[-X_{61}X_{13}X_{36} + X_{51}Y_{13}X_{35}]$.

Combining all these considerations we write down the superpotential as

$$
\begin{aligned}
W_{II} &= [X_{12}X_{26}X_{61} - X_{12}X_{25}X_{51} + X_{36}X_{64}X_{43} - X_{35}X_{54}X_{43}] \\
&\quad + [-X_{61}X_{13}X_{36} + X_{51}Y_{13}X_{35}] + [-X_{26}X_{64}X_{41}Y_{13}X_{32} + X_{25}X_{54}X_{41}X_{13}X_{32}] \\
&= (\mathbb{Z}_2 \times \mathbb{Z}_2)[\triangle] + \mathbb{Z}_2[\triangledown] + \mathbb{Z}_2[\lozenge],
\end{aligned}
$$

where $\triangle := X_{12}X_{26}X_{61}$, $\triangledown := X_{61}X_{13}X_{36}$ and $\lozenge := X_{26}X_{64}X_{41}Y_{13}X_{32}$. Once again, symmetry principles has given us the correct result without using the involved calculations of [48, 12].

Model III posesses a $\mathbb{Z}_2 \times \mathbb{Z}_2$ node symmetry: one $\mathbb{Z}_2$ is the reflection with respect to plane (246) while the other $\mathbb{Z}_2$ is a reflection with respect to plane (136). Under these symmetry action, the orbits of closed loops are

$$
\begin{aligned}
&(\mathbf{1}) \ \{(4, 1, 5, 6), (4, 3, 5, 6), (2, 1, 5, 6), (2, 3, 5, 6)\} \\
&(\mathbf{2}) \ \{(4, 1, 5), (4, 3, 5), (2, 1, 5), (2, 3, 5)\}
\end{aligned}
\tag{5.4.7}
$$

Furthermore, the sum of these two oribts gives 28 fields which is as should be because we again have 14 fields. Using the same principles as above we can write down the superpotential as

$$
\begin{aligned}
W_{III} &= [X_{41}X_{15}X_{54} - X_{54}X_{43}X_{35} + Y_{35}X_{52}X_{23} - X_{52}X_{21}Y_{15}] \\
&\quad + [-X_{41}Y_{15}X_{56}X_{64} + X_{64}X_{43}Y_{35}Y_{56} - X_{23}X_{35}X_{56}X_{62} + X_{62}X_{21}X_{15}Y_{56}] \\
&= (\mathbb{Z}_2 \times \mathbb{Z}_2)[\triangle + \square],
\end{aligned}
$$

where $\triangle := X_{41}X_{15}X_{54}$ and $\square := -X_{41}Y_{15}X_{56}X_{64}$. Let us explain above formula. First let us focus on the first row of superpotential. Under the $\mathbb{Z}_2$ action relative to plane (246) we transfer $X_{41}X_{15}X_{54}$ to $X_{54}X_{43}X_{35}$, while under the $\mathbb{Z}_2$ action relative

77

to plane (136) we transfer $X_{41}X_{15}X_{54}$ to $-X_{52}X_{21}Y_{15}$. This tell us that (X_{15}, X_{35}) and (Y_{15}, Y_{35}) are $\mathbb{Z}_2|_{246}$ multiplets while (X_{15}, Y_{15}) and (X_{35}, Y_{35}) are $\mathbb{Z}_2|_{136}$ multiplets. The same $\mathbb{Z}_2 \times \mathbb{Z}_2$ action works on the second row of superpotential if we notice that (X_{56}, Y_{56}) are permuted under both $\mathbb{Z}_2|_{246}$ and $\mathbb{Z}_2|_{136}$ action. The only thing we need to add is that since X_{15} in term $X_{41}X_{15}X_{54}$ so we must choose Y_{15} in term $-X_{41}Y_{15}X_{56}X_{64}$ to make the field X_{41} couple to different fields. This will fix the relationship between the first row and the second row. Again we obtain the result of [48, 12] by symmetry.

For model IV, there is a $\mathbb{Z}_3$ symmetry rotating nodes (123) and a $\mathbb{Z}_2$ reflection symmetry around plane (123). There is also a further symmetry that will be useful in writing W: a mirror reflection relative to plane (145). The closed loops are organized in a single orbit

$$\{(1,6,4), (2,6,4), (3,6,4), (1,6,5), (2,6,5), (3,6,5)\} \qquad (5.4.8)$$

This orbit will appear twice due to the multiple arrows. Using the $\mathbb{Z}_3$ symmetry first we write down the terms $[X_{41}X_{16}X_{64} + X_{43}X_{36}Y_{64} + X_{42}X_{26}Z_{64}]$ where the triplet of fields (X_{64}, Y_{64}, Z_{64}) are rotated under the $\mathbb{Z}_3$ also. Next using the $\mathbb{Z}_2$ symmetry relative to plane (145), we should get $-(X_{41}Y_{16}?)$ where we do not know whether ? should be Y_{64} or Z_{64}. However, at this stage we have the freedom to fix it to be Y_{64}, so we get $[-X_{41}Y_{16}Y_{64} - X_{43}Y_{36}Z_{64} - X_{42}Y_{26}X_{64}]$. Notice that in principle we can have $[-X_{41}Y_{16}Y_{64} - X_{43}Y_{36}X_{64} - X_{42}Y_{26}Z_{64}]$ as well. However, this choice does not respect the $\mathbb{Z}_3$ symmetry and X_{42} couples to same field Z_{64} twice. Now we act with the other $\mathbb{Z}_2$ symmetry and get $[X_{51}Y_{16}X_{65} + X_{53}Y_{36}Y_{65} + X_{52}Y_{26}Z_{65}]$. Finally we are left with the term $-[X_{51}X_{16}? + X_{53}X_{36}? + X_{52}X_{26}?]$ where $\mathbb{Z}_3$ symmetry gives two ordered choices (Y_{65}, Z_{65}, X_{65}) or (Z_{65}, X_{65}, Y_{65}). We do not know which one should be picked. The correct choice is $-[X_{51}X_{16}Y_{65} + X_{53}X_{36}Z_{65} + X_{52}X_{26}X_{65}]$ which happens to have

78

the same order as the second row. Putting everything together we get

$$W_{IV} = [X_{41}X_{16}X_{64} + X_{43}X_{36}Y_{64} + X_{42}X_{26}Z_{64}]$$
$$- [X_{41}Y_{16}Y_{64} + X_{43}Y_{36}Z_{64} + X_{42}Y_{26}X_{64}]$$
$$+ [X_{51}Y_{16}X_{65} + X_{53}Y_{36}Y_{65} + X_{52}Y_{26}Z_{65}]$$
$$- [X_{51}X_{16}Y_{65} + X_{53}X_{36}Z_{65} + X_{52}X_{26}X_{65}]$$
$$= (\mathbb{Z}_4 \times \mathbb{Z}_3)[\triangle],$$

where $\triangle := X_{41}X_{16}X_{64}$. This is again in agreement with known results.

5.4.2 Hirzebruch 0

The two phases of F_0 were considered in Section 5.3.2. We saw that they both have an $SU(2) \times SU(2)$ flavor symmetry coming from the isometries of $\mathbb{P}^1 \times \mathbb{P}^1$. Besides that, they also have a $\mathbb{Z}_2 \times \mathbb{Z}_2$ node symmetry. For phase II, one of the $\mathbb{Z}_2$ actions interchanges $(12) \leftrightarrow (34)$ while the other interchanges $(23) \leftrightarrow (41)$. For phase I, one $\mathbb{Z}_2$ exchanges $2 \leftrightarrow 4$, while the second $\mathbb{Z}_2$ interchanges $1 \leftrightarrow 3$ and charge conjugates all the fields. The superpotentials can be fixed uniquely by flavor symmetry as (cf. (5.3.3) and (5.3.4))

$$W_I = \epsilon_{ij}\epsilon_{mn}X_{12}^i X_{23}^m X_{31}^{jn} - \epsilon_{ij}\epsilon_{mn}X_{41}^i X_{23}^m X_{31}^{jn}$$
$$W_{II} = \epsilon_{ij}X_{12}^i X_{34}^j \epsilon_{mn}X_{23}^m X_{41}^n$$

where the way we wrote them exhibits both flavor and node symmetries. However, as it can be seen easily, if we only use node symmetry, there are several choices to write down the superpotential just like in the case of phase IV of dP_3. The reason for that is because we have too many multiple arrows in the quiver. In these situations, it is hard to determine how these multiple arrows transform under the discrete node symmetry. Here we are saved by utilising the additional flavor symmetry.

79

5.4.3   del Pezzo 0

The quiver for this model is presented in Figure 5-10. This is a well known example and has also been discussed in [24, 17]. The $SU(3)$ isommetry of $\mathbb{P}^2$ appears as an $SU(3)$ flavor symmetry. The three fields lying on each side of the triangle form fundamental representations of $SU(3)$. Furthermore, this theory has a $\mathbb{Z}_3$ node symmetry that acts by cyclically permuting the nodes (123). After all the cone over del Pezzo 0 is none other than the resolution $\mathcal{O}_{\mathbb{P}^2}(-3) \mapsto \mathbb{C}^3/\mathbb{Z}_3$. Bearing these symmetries in mind, we can write down the superpotential uniquely as

$$W = \epsilon_{\alpha\beta\gamma} X_{12}^{(\alpha)} X_{23}^{(\beta)} X_{31}^{(\gamma)} \tag{5.4.9}$$

which is explicitly invariant under both $SU(3)$ (α, β and γ indices) and $\mathbb{Z}_3$ cyclic permutations of (123).
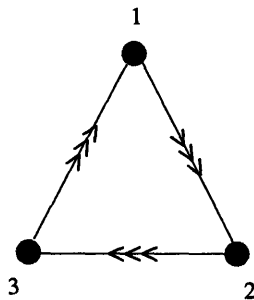
Figure 5-10: The quiver diagram for the theory corresponding to the cone over dP_0.

5.4.4   del Pezzo 1

The quiver for this model is shown in Figure 5-11. This theory has a $\mathbb{Z}_2$ node symmetry that acts by interchanging (23) $\leftrightarrow$ (14) and charge conjugating all the fields. From this symmetry, we have the following orbits of closed loops

$$\begin{aligned} &\textbf{(1)}\ \{(1,2,3,4)\} \\ &\textbf{(2)}\ \{(1,3,4),(2,3,4)\} \end{aligned} \tag{5.4.10}$$

We need 20 fields in the superpotential which can be obtained by using each orbit twice. Furthermore, this theory has an $SU(2)$ flavor symmetry with respect to which the triplet between nodes $3, 4$ splits into the doublet X_{34}^α and a singlet X_{34}^3. This flavor symmetry comes from the blow up of $\mathbb{P}^2$ at one point $[1, 0, 0]$ which breaks the $SU(3)$ isometry to $SU(2)$. Using these inputs we get the superpotential uniquely as

$$W = \left[\epsilon_{\alpha\beta} X_{34}^\alpha X_{41}^\beta X_{13} - \epsilon_{\alpha\beta} X_{34}^\alpha X_{23}^\beta X_{42} \right] + \epsilon_{\alpha\beta} X_{12} X_{34}^3 X_{41}^\alpha X_{23}^\beta \qquad (5.4.11)$$

where we can see that under the $\mathbb{Z}_2$ transformation the two terms in the brackets transform into one another, while the last one is invariant.
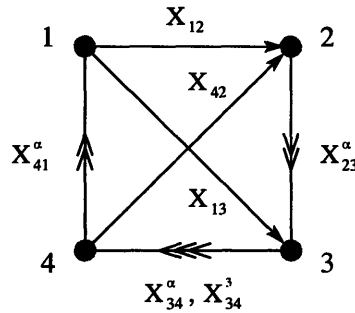
Figure 5-11: The quiver diagram for the theory corresponding to the cone over dP_1.

5.4.5 del Pezzo 2

The first phase of dP_2 has a $\mathbb{Z}_2$ node symmetry that interchanges nodes 1 and 2. The quiver for the phase I is given in Figure 5-12. From this we read out the orbits of closed loops:

$$\begin{aligned}
&(\mathbf{1}) \ \{(4, 1, 5, 3), (4, 2, 5, 3)\} \\
&(\mathbf{2}) \ \{(4, 1, 5), (4, 2, 5)\} \qquad\qquad (5.4.12) \\
&(\mathbf{3}) \ \{(3, 1, 5), (3, 2, 5)\}
\end{aligned}$$

Since we need a total of 26 fields in the superpotential, the only solution consistent with the toric condition is $W = (\mathbf{1}) + (\mathbf{2}) + (\mathbf{3}) + (\mathbf{3})$. Knowing this we can write down the superpotential. First we have the terms $[X_{41} X_{15} X_{54} - X_{42} X_{25} X_{54}]$. Under this choice, (X_{15}, X_{25}) and (Y_{15}, Y_{25}) are $\mathbb{Z}_2$ multiplets. This gives us immediately

$-[X_{41}Y_{15}X_{53}X_{34} - X_{42}Y_{25}Y_{53}X_{34}]$, where we couple X_{41} to Y_{15} (likewise X_{42} to Y_{25}) because X_{41} has coupled to X_{15} in the orbit (**2**). Furthermore, we have chosen arbitrarily (X_{53}, Y_{53}) as the $\mathbb{Z}_2$ multiplets and Z_{53} as the $\mathbb{Z}_2$ singlet. Next we will have $-[X_{31}X_{15}Y_{53} - X_{32}X_{25}X_{53}]$, where we couple X_{31} to Y_{53} instead of X_{53} because this term has the negative sign[1]. The last terms are obviously $+[X_{31}Y_{15}Z_{53} - X_{32}Y_{25}Z_{53}]$. Adding all pieces together we get

$$
\begin{aligned}
W_I \;=\;& [X_{41}X_{15}X_{54} - X_{42}X_{25}X_{54}] - [X_{41}Y_{15}X_{53}X_{34} - X_{42}Y_{25}Y_{53}X_{34}] \\
& - [X_{31}X_{15}Y_{53} - X_{32}X_{25}X_{53}] + [X_{31}Y_{15}Z_{53} - X_{32}Y_{25}Z_{53}].
\end{aligned}
$$

Model I   Model II
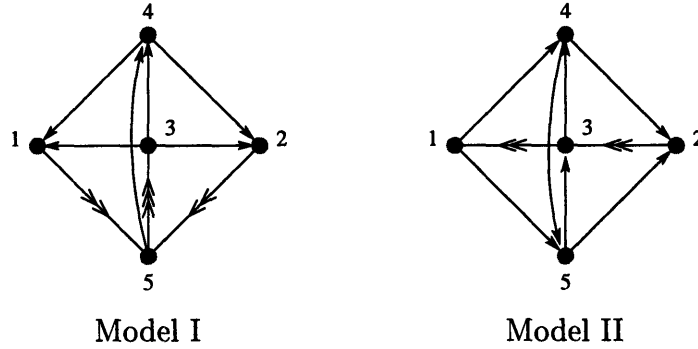
Figure 5-12: Quiver diagrams for the two models corresponding to the cone over dP_2.

Now we move to phase II. The quiver is given by Figure 5-12. It has a $\mathbb{Z}_2$ symmetry that interchanges nodes $1 \leftrightarrow 2$ and $4 \leftrightarrow 5$ and charge conjugates all the fields. From this we read out the orbits of closed loops:

$$
\begin{aligned}
&(\mathbf{1}) \; \{(1,4,5,2,3)\} \\
&(\mathbf{2}) \; \{(1,4,2,3),(1,5,2,3)\} \\
&(\mathbf{3}) \; \{(1,4,5,3),(3,4,5,2)\} \\
&(\mathbf{4}) \; \{(3,1,5),(3,4,2)\} \\
&(\mathbf{5}) \; \{(4,5,3)\}
\end{aligned}
\qquad (5.4.13)
$$

We need 22 fields in the superpotential. The only consistent choice results in $W_{II} =$

---

[1]Here we do not consider the Z_{53} because it is the singlet under the $\mathbb{Z}_2$ action.

(1)+(2)+(4)+(5). Orbits **1** and **5** give the terms $[X_{45}X_{53}X_{34}] - [X_{14}X_{45}X_{52}X_{23}X_{31}]$. Notice that under the $\mathbb{Z}_2$ action (X_{23}, X_{31}) are a doublet as well as (Y_{23}, Y_{31}). Now we consider orbit **4**. $\mathbb{Z}_2$ action tell us that there are two choices, $-[X_{53}Y_{31}X_{15} + X_{34}X_{42}Y_{23}]$ or $-[X_{53}X_{31}X_{15} + X_{34}X_{42}X_{23}]$, where the sign is determined by X_{53} of orbit **5**. However, field $X_{23}X_{31}$ at orbit 1 tell us that the second choice should have positive sign and give a contradiction. This fixes the first choice. Finally the orbit **2** gives $+[Y_{23}X_{31}X_{15}X_{52} + X_{42}X_{23}Y_{31}X_{14}]$ where the field X_{31} couples to X_{15} because the field X_{15} has coupled to Y_{31} at orbit **4** (for the same reason X_{42} couples to X_{23}). Combining everything, we get

$$
\begin{aligned}
W \;=\; & [X_{34}X_{45}X_{53}] - [X_{53}Y_{31}X_{15} + X_{34}X_{42}Y_{23}] \\
& + [Y_{23}X_{31}X_{15}X_{52} + X_{42}X_{23}Y_{31}X_{14}] - [X_{23}X_{31}X_{14}X_{45}X_{52}]. \quad (5.4.14)
\end{aligned}
$$

5.4.6 Summary

Let us make some remarks before ending this section. The lesson we have learnt is that symmetry considerations can become a powerful tool in determining the physics. These symmetries are inherited *a fortiori* from the isometries of the singularity which we probe. They exhibit themselves as "flavor symmetries", i.e., grouping of multiplets of arrows between two nodes, as well as "node symmetries," i.e., the automorphism of the quiver itself. Relatively straight-forward methods exist for determining the matter content while the general techniques of reconstructing the superpotential are rather involved. The discussion of this section may serve to shed some light.

First we see that using symmetry we can group the terms in the superpotential into a more compact and easily understood way. Second, in some cases, the symmetry can fix the superpotential uniquely. Even if not so, we can still constrain it significantly. For example, in the toric case, we can see which closed polygons (gauge invariant operators) will finally show up in the superpotential. Combining some heuristic arguments, we even can write down the superpotential completely. This is indeed far more convenient than any known methods of superpotential calculations circulated

amongst the literature.

However, we remark that application of Seiberg duality does tend to break the most obvious symmetry deducible from geometry alone in certain cases. Yet we can still find a phase which exhibits maximal symmetry of the singularity. Without much ado then let us summarise the results (the most symmetric case) in Table 5.2.

5.5 Multiplicity, Divisors and Monodromy

Now let us return to address the meaning of the multiplicities. Some related issues have been raised under this light in [141, 34]. First recall some standard results from toric geometry. Our toric data is given by a matrix G_t of dimension $3 \times c$, whose columns (up to multiplicity) are the generators $\vec{v_j} := G_t^{ij}$ of the cone (fan) in $\mathbb{Z}^3$. Its integer cokernel is thus a $(c-3) \times c$ matrix Q_t, which provides $c-3$ relations $(\sum_j q_j v_j = 0$ with $q_j := Q_t^{ij})$ among the v_i and hence a $(\mathbb{C}^*)^{c-3}$ action in $\mathbb{C}^c$ so that the symplectic quotient is the $c - (c-3) = 3$ dimensional toric singularity in which we are interested. Let the coordinates of $\mathbb{C}^c$ be $(z_1, \ldots, z_c)$, then the torus action is given as

$$(z_1, \ldots, z_c) \sim (\lambda^{Q_t^{i1}} z_1, \ldots, \lambda^{Q_t^{ic}} z_c)$$

for $i = 1, \ldots, (c-3)$ and $\lambda \in \mathbb{C}^*$.

5.5.1 Multiplicity and Divisors

It is well-known [62] that for any toric variety X with fan Σ each 1-dimensional cone corresponds to a Cartier divisor[2] of X. Since all our toric singularities are Calabi-Yau and have the endpoints of v_i coplanar, this simply means that *each node of the toric diagram corresponds to a Cartier divisor of X.* In terms of our coordinates, each

---

[2]A brief reminder on Cartier divisors. A Cartier divisor D is determined by a sheaf of nonzero rational functions f_a on open cover $\bigcup_a U_a$ such that the transition function f_a/f_b on overlaps $U_a \cap U_b$ are nowhere zero. It determines an (ordinary) Weil divisor as $\sum_V \mathrm{ord}_V(D)V$ for co-dimension 1 subvarieties V, where ord is the order of the defining equation f of V. The sheaf generated by f_a is clearly a subsheaf of the sheaf of rational functions on X; the former is called the Ideal Sheaf, denoted as $\mathcal{O}(-D)$.

	Quiver	Superpotential	Symmetry
$\mathbf{F}_0$		$$W = \epsilon_{ij} X_{12}^i X_{34}^j \epsilon_{mn} X_{23}^m X_{41}^n$$	$\mathbb{Z}_2 \times \mathbb{Z}_2$
dP_0		$$W = \epsilon_{\alpha\beta\gamma} X_{12}^\alpha X_{23}^\beta X_{31}^\gamma$$	$\mathbb{Z}_3$
dP_1		$$W = \left[\epsilon_{\alpha\beta} X_{34}^\alpha X_{41}^\beta X_{13} - \epsilon_{\alpha\beta} X_{34}^\alpha X_{23}^\beta X_{42} \right] + \epsilon_{\alpha\beta} X_{12} X_{34}^3 X_{41}^\alpha X_{23}^\beta$$	$\mathbb{Z}_2$
dP_2		$$\begin{aligned} W_I = \; & [X_{41}X_{15}X_{54} - X_{42}X_{25}X_{54}] - [X_{41}Y_{15}X_{53}X_{34} - X_{42}Y_{25}Y_{53}X_{34}] \\ & -[X_{31}X_{15}Y_{53} - X_{32}X_{25}X_{53}] + [X_{31}Y_{15}Z_{53} - X_{32}Y_{25}Z_{53}] \end{aligned}$$	$\mathbb{Z}_2$
dP_3		$$W = \bigcirc + (\square + \lozenge + \obliqueslash) + (\triangle + \triangledown);$$ $\bigcirc = X_{12}X_{23}X_{34}X_{45}X_{56}X_{61};$ $\quad \triangle = X_{13}X_{35}X_{51};$ $\quad \triangledown = X_{24}X_{46}X_{62};$ $\square = X_{23}X_{35}X_{56}X_{62};$ $\quad \lozenge = X_{13}X_{34}X_{46}X_{61};$ $\quad \obliqueslash = X_{12}X_{24}X_{45}X_{51}.$	$\mathbb{Z}_2 \times \mathbb{Z}_3$

Table 5.2: Summary of the maximally symmetric phases.

node v_i corresponds to a divisor D determined by the hyperplane $z_i = 0$ of the ideal sheaf $\mathcal{O}(D)$. Multiplicities in the toric data simply means that to each node v_i with multiplicity m_i we must now associate a divisor $D^{\oplus m_i}$ so that the sheaf is generated by sections $z_i^{m_i}$ of $\mathcal{O}(m_i D)$.

Let us rephrase the above in more physical terms. The multiplicity m_i in the GLSM fields (homogeneous coordinates) p_i corresponding to node v_i simply means the following. The gauge invariant operators (GIO) are in the form $\prod_j X_j$ constructed in terms of the original world volume fields X_j; each X_j is then writable as products of the gauged linear sigma model fields p_i. It is these GIO's that finally parametrise the moduli space; i.e., algebraic relations among these GIO's by virtue of the generating variables p_i are precisely the algebraic equation of the toric variety which the D-brane probes. Multiplicities in p_i simply means that the m_i fields $(p_i)_{k=1,...,m_i}$ must appear together in each of the expressions X_j in terms of p's.

There is therefore, in describing the moduli space of the world-volume theory by the methods of the linear sigma model, an obvious symmetry, *per construtio*: the cyclic permutation of the fields p_i, or equivalently the cyclic symmetry on the section $z_i^{m_i}$. We summarise this in the following:

PROPOSITION 5.5.2 *Describing the classical moduli space of the world-volume $\mathcal{N} = 1$ SUSY gauge theory using the gauge linear sigma model prescription leads to an obvious permutation symmetry in the sigma model fields (and hence in the toric geometry) which realises as a product cyclic group*

$$\prod_i \mathbb{Z}_{m_i} \qquad \text{with} \qquad \sum_i m_i = c.$$

The index i runs over the nodes v_i (of multiplicity m_i) of the toric diagram.

One thing to note is that there is in fact an additional symmetry, in light of the unimodular transformation mentioned in [46], and in fact there is a combined obvious symmetry of

$$\prod_i \mathbb{Z}_{m_i} \times SL(3; \mathbb{Z}).$$

The above symmetry arises as a vestige of the very construction of the GLSM approach of encoding the moduli space and its geometrical meaning in terms of sections of the ideal sheaf tensored by itself multiple times is now clear. What is not clear is the necessity of its emergence. Points have arisen in the existing literature [11, 141] that the multiplicity of p_i (or what was referred to as a redundancy of the homogeneous coordinates) ensures that the D-brane does not see any non-geometrical phases. This is to say that of the $c\,p_i$'s, at each point in the Kähler moduli space, only a subset (chosen in accordance with Proposition 5.5.2) is needed to describe the toric singularity M. Which coordinates we choose depends on the region in the Kähler moduli, i.e., how we tune the FI-parametres in the field theory. In summary then, the Forward Algorithm in computing the moduli space of the $\mathcal{N} = 1$ gauge theory encodes more than merely the complex structure of the toric singularity M, but also the Kähler structure of the resolution, given here in terms of the pair $(M, \mathcal{O}(m_i D))$, where $\mathcal{O}(m_i D)$ are sheafs of rational functions as determined by the multiplicities m_i.

5.5.2 Partial Resolutions

Now let us turn to the Inverse Algorithm of finding the gauge theory given a toric singularity. This is a good place to point out that the process used in the standard Inverse Algorithm, commonly referred to as "partial resolution" is strictly somewhat of a misnomer. The process of "partial resolution" is a precise toric method [62, 30] of refining a cone - the so-called "star-division" - into ones of smaller volume (when the volume is one, i.e., the generating lattice vectors are neighbourwise of determinant 1, the singularity is completely resolved). Partial resolutions in the sense of [11, 45, 46], where we study not the refinement but rather a sub-polytope of the toric diagram (in other words one piece of the refinement), has another meaning.

We recall that for the cases of interest one begins with the cone of $D' = \mathbb{C}^3/(\mathbb{Z}_k \times \mathbb{Z}_k)$, then resolves it completely into the fan $\Sigma_{\widetilde{D'}}$ for $\widetilde{D'} = \mathbb{C}^3/\widetilde{(\mathbb{Z}_k \times \mathbb{Z}_k)}$. The given toric singularity D for which we wish to construct the gauge theory is then a cone $\sigma \subset \Sigma_{\widetilde{D'}}$. It is then well-known (see e.g. [30, 160]) that the variety D is a closed subvariety of D'.

It was pointed out in [37] (at least for Abelian orbifolds) that each additional field in a GLSM gives rise to a line bundle R over the final toric moduli space. Let us adhere to the notation of [37, 34]; the Grothendick group $K(M)$ of coherent sheafs over M are generated by a basis $\{R_i\}$ of such line bundles. Now take a basis $\{S_i\}$ for $K^c(M)$, the compactly supported K-group of M, which is dual to $K(M)$ in the sense that there exists a natural pairing [106]

$$(R, S) = \int_M \mathrm{ch}(R)\mathrm{ch}^c(S)\mathrm{Td}(M), \qquad R \in K(M), \quad S \in K^c(M)$$

in the context of the McKay Correspondence [71, 162, 135, 129, 90, 158, 88].

Indeed the S_i's are precisely linear combinations of the sheafs $\mathcal{O}(m_j D)$ mentioned earlier and so each S can be represented as $\mathcal{O}(\sum_{ij} s_{ij} m_{ij} D_i)$, summed over the divisors D_i, of multiplicity m_{ij}, and with coefficients s_{ij}. Finally we have the push-forward of the sheafs S_i to compact cycles $C \subset M$, giving a basis $\{S_{C_i}\}$.

With this setup one can compute the quiver of the gauge theory on the D-branes probing M using the following prescription for the adjacency matrix

$$a_{ij} = \int_M \mathrm{ch}(R_i)\mathrm{ch}^c(S_{C_j})\mathrm{Td}(M).$$

Of course, homological algebraic calculations on exceptional collections of sheafs over M (c. f. e. g. [100, 99, 71, 162, 135, 129, 80]) are equivalent to the above. We use this language of the R, S basis because the $\{S_{C_i}\}$ are explicitly generated by the sections z_{ij}^m where we recall m_{ij} to be the multiplicity of the j-th node.

Our final remark is that there in fact exists a natural *monodromy* action which is none other than the Fourier-Mukai transform

$$\mathrm{ch}(S) \to \mathrm{ch}(S) - (S', S)\mathrm{ch}(S'), \qquad (5.5.15)$$

giving rise to a permutation symmetry among the $\{S_{C_i}\}$. In the language of [100, 99, 71, 162, 135, 129], this is a mutation on the exceptional collection. In the language of (p, q)-branes and geometrical engineering [100, 99, 80], this is Picard-Lefschetz

monodromy on the vanishing cycles. What we see here is that the multiplicity endows the $\{S_{C_i}\}$ with an explicit permutation symmetry (generated by the matrices m_{ij}) of which the monodromy (5.5.15) is clearly a subgroup. Therefore we see indeed that the multiplicity symmetry naturally contains a monodromy action which in the language of [45, 46] is toric duality, or in the language of [48, 12], Seiberg duality.

Of course one observes that the multiplicity gives more than (5.5.15); this is indeed encountered in our calculations. Many choices of partial resolutions by different choices of multiplicities result in other theories which are not related to the known ones by any monodromy. What is remarkable is that all these extra theories do not seem physical in that they either have ill-behaved charge matrices or are not anomaly free. It seems that the toric dual theories emerging from the multiplicity symmetry, in addition to the restriction of physicality, are constrained to be monodromy related, or in other words, Seiberg dual. We do point out that toric duality could give certain "fractional Seiberg dualities" [47]; such Seiberg-like transformations have also been pointed out in [24].

What we have given is an implicitly algebro-geometric argument, rather than an explicit computational proof, for why toric duality should arise from multiplicity symmetry. We await for a detailed analysis of our combinatorial algorithm.

5.6   Conclusions

In studying the D-brane probe theory for arbitrary toric singularities, a phenomenon where many different $\mathcal{N} = 1$ theories flow to the same conformal fixed point in the IR, as described by the toric variety, was noted and dubbed "toric duality" [45]. Soon a systematic way of extracting such dual theories was proposed in [46]. There it was thought that the unimodular degree of freedom in the definition of any toric diagram was key to toric duality.

In this chapter we have addressed that the true nature of toric duality results instead from the multiplicity of the GLSM fields associated to the nodes of the toric diagram. The unimodularity is then but a special case thereof.

We have presented some first cases of the familiar examples of the Abelian quotients $\mathbb{C}^2/\mathbb{Z}_n$ and $\mathbb{C}^3/(\mathbb{Z}_m \times \mathbb{Z}_k)$ and observed beautiful combinatorial patterns of the multiplicities corresponding to the nodes. As the process of finding dual cones is an algorithmic rather than analytic one, at this point we do not have proofs for these patterns, any further than the fact that for $\mathbb{C}^2/\mathbb{Z}_n$, the total multiplicity is $2^n + 1$. It has been suggested to us by Gregory Moore that at least the 2^n behaviour could originate from the continued fraction which arises from the Hirzebruch-Jung resolution of the toric singularity. Using this idea to obtain expressions for the multiplicities, or at least the total number of GLSM fields, would be an interesting pursuit in itself.

We have shown that all of the known examples of toric duality, in particular the theories for cones over the Zeroth Hirzebruch, the Second and Third del Pezzo Surfaces, can now be obtained from any and each of unimodularly equivalent toric diagrams for these singularities, simply by choosing different GLSM fields to resolve. The resulting multiplicities once again have interesting and yet unexplained properties. The outside nodes always have only a single GLSM field associated thereto while the interior node could have different numbers greater than one, each particular to one member of the torically dual family.

As an important digression we have also addressed the intimate relations between certain isometries of the target space and the symmetries exhibited by the terms in the superpotential and the quiver. We have argued the existence of two types of symmetries, namely "flavor symmetry" and "node symmetry", into whose multiplets the fields in the superpotential organise themselves. In fact in optimistic cases, from the isometry of the underlying geometry alone one could write down the superpotential immediately. In general however the symmetry arguments are not as powerful, though we could still see some residuals of the isometry. Moreover, Seiberg dualities performed on the model may further spoil the discrete symmetry. We conjecture however that there does exist a phase in each family of dual theories which does maximally manifest the flavor symmetry corresponding to the global isometry as well as the node symmetry corresponding to the centre of the Lie group one would observe in the closed string sector. We have explicitly shown the cases of the cones over the

90

toric del Pezzo surfaces.

Finally we gave some arguments of why such multiplicities should determine toric duality. Using the fact that nodes of toric diagrams correspond to divisors and that there is a natural monodromy action on the set of line bundles and hence the divisor group, we see that permutation symmetry among the multiplicities can indeed be realised as this monodromy action. Subsequently, as Seiberg duality is Picard-Lefshetz monodromy [24], it is reasonable to expect that toric duality, as a consequence of multiplicity permutation, should lead to Seiberg duality. Of course this notion must be made more precise, especially in the context of the very concrete procedures of our Inverse Algorithm. What indeed do the multiplicities mean, both for the algebraic variety and for the gauge theory? This still remains a tantalising question.

5.7 Appendix: Multiplicities in $\mathbb{C}^2/z^n$ singularities

Let us see that it is possible to perform a general systematic study of the multiplicities of linear σ-model fields. As an example, we will focus here on the specific case of A_{n-1} singularities. They produce $\mathcal{N} = 2$ gauge theories with quivers given by the Dynkin diagrams of the A_{n-1} ($SU(n)$) Lie algebras (Figure 5-13). These singularities correspond to the $\mathbb{C}^2/\mathbb{Z}^n$ orbifolds.
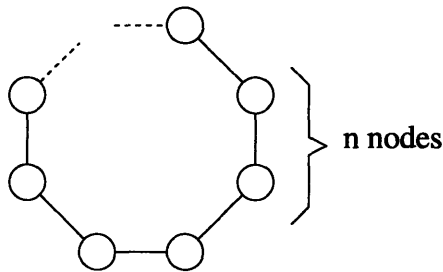
Figure 5-13: Quiver diagram for an A_{n-1} singularity.

There are n adjoint fields ϕ_i's, n Q_i's in bifundamentals and n $\tilde{Q}_i$'s in antibifundamentals. The superpotential is

$$W = \sum_{i=1}^{n} (\phi_i - \phi_{i+1})\tilde{Q}_i Q_i \qquad (5.7.16)$$

with the identification $\phi_{n+1} = \phi_1$. The moduli space is determined by solving D and F-flatness equations. D-flat directions are parametrized by the algebraically independent holomorphic gauge invariant monomials that can be constructed with the fields, so the moduli space can be found by considering the conditions imposed on this gauge invariant operators by the F-flatness conditions

$$\frac{\partial W}{\partial \phi_i} = \tilde{Q}_i Q_i - \tilde{Q}_{i-1} Q_{i-1} = 0 \qquad (5.7.17)$$

$$\frac{\partial W}{\partial \tilde{Q}_i} = (\phi_i - \phi_{i+1})Q_i = 0$$

$$\frac{\partial W}{\partial Q_i} = (\phi_i - \phi_{i+1})\tilde{Q}_i = 0$$

where no summation over repeated indices is understood. Looking at the Higgs branch, the last two equations in (5.7.17) imply

$$\phi_1 = \phi_2 = ... = \phi_n \qquad (5.7.18)$$

while the first one gives [3]

$$Q_i = \tilde{Q}_i^{-1} \tilde{Q}_{i-1} Q_{i-1} \qquad (5.7.19)$$

Iterating (5.7.19) we see that

$$Q_i = \tilde{Q}_i^{-1} \tilde{Q}_1 Q_1 \qquad (5.7.20)$$

Thus, we see that the original $3n$ fields can be expressed in terms of only $n + 2$

---

[3]In the general case of N D-branes sitting on the singularity, the Q_i's become matrices and cannot be inverted

$$\phi_i = \phi_1 \qquad (5.7.21)$$

$$Q_i = \tilde{Q}_i^{-1}\tilde{Q}_1 Q_1$$

$$\tilde{Q}_i$$

Following [45], we can use the toric geometry language to encode the relations between monomials into a matrix K, which defines a cone

$$K^T = \left(\begin{array}{c|ccccc|cccccc}
 & \phi_1 & \cdots & \phi_n & Q_2 & \cdots & \cdots & Q_n & Q_1 & \tilde{Q}_1 & \cdots & \cdots & \cdots & \tilde{Q}_n \\
\hline
\phi_1 & 1 & \cdots & 1 & 0 & 0 & \cdots & 0 & 0 & 0 & \cdots & \cdots & \cdots & 0 \\
Q_1 & 0 & \cdots & 0 & 1 & 1 & \cdots & 1 & 1 & 0 & \cdots & \cdots & \cdots & \vdots \\
\tilde{Q}_1 & \vdots & & \vdots & 1 & 1 & \cdots & 1 & 0 & 1 & & & & \vdots \\
\vdots & \vdots & & \vdots & -1 & 0 & \cdots & 0 & \vdots & 0 & \ddots & & & \vdots \\
\vdots & \vdots & & \vdots & 0 & -1 & & \vdots & \vdots & & & \ddots & & \vdots \\
\vdots & \vdots & & \vdots & \vdots & & \ddots & \vdots & \vdots & & & & \ddots & \vdots \\
\tilde{Q}_n & 0 & \cdots & 0 & 0 & & & -1 & \vdots & & & & & 1
\end{array}\right)$$

$$(5.7.22)$$

5.7.1 Finding the general dual cone

In what follows, we will discuss linear combinations, linear independence and generators, in the restricted sense of linear combinations with coefficients in $\mathbb{Z} > 0$. The reader should keep this in mind.

The dual cone of matrix K consists of all vectors $v \in \mathbb{Z}^{n+2}$ such that $v.k \geq 0$ for any column k of the matrix K^T. We can generate any vector in $\mathbb{Z}^{n+2}$ making linear combinations of vectors with entries ± 1 and 0. Looking carefully at (5.7.22), we see that K^T contains a $(n+2) \times (n+2)$ identity submatrix, formed by the first and the last $n+1$ columns. This forbids -1 entries. Then the T matrix is given by a set of vectors from those 2^{n+2} with 0 and 1 components which satisfy the following

conditions:

<u>1</u>) $v.k \geq 0 \; \forall \; k$

<u>2</u>) All v's in the dual cone are linearly independent.

<u>3</u>) They generate all the v's such that satisfy condition 1 (that is, we do not have to add extra vectors to our set).

Let us see that we can find a set of vectors that satisfy these three conditions for any n. Then, we would have found the dual cone for the general A_{n-1} singularity. We will first propose some candidate vectors, and then we will check that they indeed satisfy the requirements.

Vectors	Number
$(1, 0, ..., 0)$	1
$(0, 1, 0, ...$ all 0 and 1 combinations $...)$	2^{n-1}
$(0, 0, 1, ...$ all 0 and 1 combinations $...)$	2^{n-1}

$$(5.7.23)$$

which give a total of $2^n + 1$ vectors. From the expression of K^T (5.7.22), we immediately check that (1) is satisfied. Looking at the first three entries of the vectors, we see they are all linearly independent (not only in our restricted sense of $\mathbb{Z} > 0$ linear combinations), then (2) is true.

Finally, we have to check that every v for which $v.k \geq 0$ can be obtained from this set. In fact, all the vectors with 0,1 components can be generated, except those of the form $(0, 0, 0, ...$ at least a 1 $...)$. But these have $v.k \leq 0$ for k being any of the Q_2 to Q_n columns of K^T, so we have shown that (3) is also true.

Summarising, using the notation of [45], the dual cone for a general A_{n-1} singularity can be encoded in the following T matrix

94

$$T = \left(\begin{array}{c|cc|cc} 1 & 0 \;\;\ldots\;\;\ldots\; 0 & 0 \;\;\ldots\;\;\ldots\; 0 \\ 0 & 1 \;\;\ldots\;\;\ldots\; 1 & 0 \;\;\ldots\;\;\ldots\; 0 \\ \vdots & 0 \;\;\ldots\;\;\ldots\; 0 & 1 \;\;\ldots\;\;\ldots\; 1 \\ \hline\hline \vdots & \text{all combinations} & \text{all combinations} \\ \vdots & \underbrace{\text{of 0's and 1's}}_{2^{n-1}} & \underbrace{\text{of 0's and 1's}}_{2^{n-1}} \end{array} \right) \tag{5.7.24}$$

We see that there are $2^n + 1$ linear σ-model fields. This is consistent with claim made in Section 5.2 that the field multiplicity of each node of the toric diagram is given by a Pascal's triangle, since

$$\sum_{i=1}^{n} \binom{n}{i} + 1 = 2^n + 1 \tag{5.7.25}$$

Chapter 6

Geometric dualities in 4d field theories and their 5d interpretation

We study four-dimensional $\mathcal{N} = 1$ gauge theories arising on D3-branes probing toric singularities. Toric dualities and flows between theories corresponding to different singularities are analyzed by encoding the geometric information into (p,q) webs. A new method for identifying quiver symmetries of the four-dimensional theories using the brane webs is developed. Five-dimensional theories are associated with the theories on the D3-branes by using (p,q) webs. This leads to a novel interpretation of Seiberg duality, which can be mapped to the crossing of curves of marginal stability in five dimensions. The work presented in this chapter is based on [52].

6.1 Introduction

The purpose of this chapter is to look at gauge theories living on D3-branes probing toric singularities from three completely different perspectives, studying not only the transition between toric dual theories but also the flow between theories corresponding to different geometries. These complementary approaches are summarized in Figure 6-1. We will discuss how different physical processes manifest in the three languages. In the first place, we will study directly the $\mathcal{N} = 1$ theories in $d = 4$. In this context, toric duals are related by Seiberg dualities, while theories for different geometries

correspond to (un)higgsings. The second viewpoint is purely geometric, and the continuous flow between theories is achieved by blow-ups and blow-downs of the corresponding non-compact Calabi-Yau. Finally, every theory under study has an associated five dimensional $\mathcal{N} = 1$, $SU(2)$ partner [1]. The correspondence follows from considering M theory on the different CY threefolds. In this language, there exist a one to one mapping between the change of parameters that interpolates between four dimensional toric dual theories and the change of the BPS spectrum in five dimensions (crossing of curves of marginal stability). The key objects interconnecting these three descriptions are (p, q) webs.
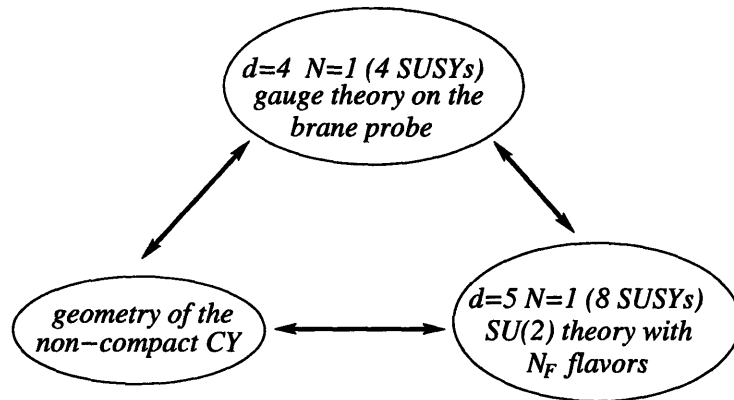
Figure 6-1: The three alternative perspectives that will be developed in this chapter. The connections between them will be made using (p, q) webs.

The organization of this chapter is as follows. In Section 6.2, we review the main concepts of (p, q) web constructions and toric geometry. In Section 6.3, we explain how to extract the quiver for the four dimensional theory that appears in the world volume of D3-branes probing a toric variety whose toric data is encoded in a given (p, q) web. Section 6.4 is devoted to understanding the flow between toric duals and theories associated with different singularities as geometric transitions and (un)higgsings. Section 6.5 shows the full power of (p, q) webs in establishing quiver symmetries of the four dimensional gauge theories. In Section 6.6, we use the mapping from (p, q) webs to five dimensional theories to introduce a third perspective for toric duality and

---

[1] Five dimensional $\mathcal{N} = 1$ theories have 8 supercharges. This is the number of SUSYs that is preserved by the (p, q) web configuration when condition 6.2.2 is satisfied.

geometric transitions, namely there is a one to one correspondence between the continuous change of parameters and subsequent flops in (p, q) webs which is associated to toric duality and a change in the five dimensional BPS spectrum.

6.2 A review of (p, q) webs and toric geometry

6.2.1 (p, q) webs and five dimensional theories

In [4, 5] (p, q) webs were introduced as brane constructions to study five dimensional theories. They are Type IIB string theory configurations in which 5-branes share four spatial directions and time. The remaining dimension of the 5-branes world volumes lie on a plane parametrized by the (x, y) coordinates. Every (p, q) web can be associated to a $\mathcal{N} = 1$ gauge theory living in the $4 + 1$ dimensions common to all the 5-branes. Each brane has a (p, q) charge which is related to its tension

$$T_{p,q} = |p + \tau q| T_{D_5} \qquad (6.2.1)$$

and to its slope

$$\Delta x : \Delta y = p : q \qquad (6.2.2)$$

where T_{D_5} is the D5-brane tension and τ is the complex scalar of Type IIB (which we have chosen equal to i in 6.2.2). The last condition assures that $1/4$ of the SUSYs is preserved. Branes can join at vertices, where (p, q) charge is conserved,

$$\sum_i p_i = \sum_i q_i = 0 \qquad (6.2.3)$$

where the sum is performed over all the branes ending at a given vertex. It is easy to see that 6.2.1, 6.2.2 and 6.2.3 imply the equilibrium of the web.

These theories were thoroughly studied in [5]. We will give here a brief explanation of how the five dimensional parameters can be read off from the (p, q) webs. All through this chapter we will deal with $SU(2)$ theories, so we choose an $SU(2)$ model

with one flavor to exemplify all the relevant concepts (Figure 6-2). Color branes are finite parallel branes (depicted in red in the figure). Their separation is parametrized by the expectation value of a $U(1)$ scalar ϕ. For $\phi = 0$, both color branes coincide and we have an unbroken $SU(2)$ gauge symmetry. When $\phi > 0$, $SU(2)$ is broken down to $U(1)$ and the W gauge boson gets a mass $m_W = \phi$. The bare value of the gauge coupling is given by the length of the color branes when $\phi = 0$ (see Figure 6-2)

We can add a flavor to this theory. This is represented by a semi-infinite brane parallel to the color branes (green brane in Figure 6-2). For $\phi = 0$ this brane corresponds to a quark multiplet in the **2** representation of $SU(2)$. When ϕ grows, the gauge group is higgsed to $U(1)$ and the **2** gives rise to two quark states with $m_{1,2} = \phi/2$. A bare mass for the quarks can be introduced by displacing the flavor brane with respect to the middle position between the color branes. In this case, the quark masses become $m_{1,2} = |m \pm \phi/2|$.
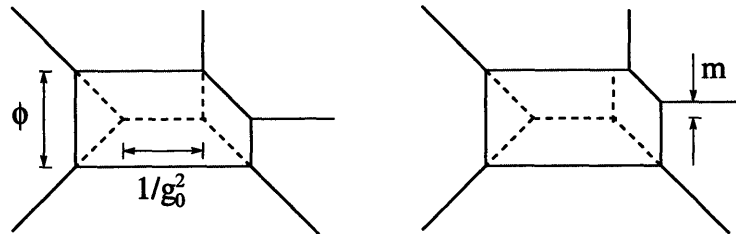
Figure 6-2: A (p,q) web corresponding to an $SU(2)$ theory with one flavor.

BPS saturated states correspond to string webs ending perpendicularly on the five branes. The rules governing the construction of string webs are identical to the ones we discussed for brane webs. The monopole tension is calculated as the area of the closed face of the web. The masses of BPS states and the monopole tension can be expressed in terms of ϕ, g_0 and the quark bare masses.

6.2.2 Toric geometry

Toric geometry and (p,q) webs are closely related. Toric geometry studies varieties that admit a $U(1)^d$ action, in general with fixed points (for a complete treatment see

[62]). These spaces are described by specifying shrinking cycles and relations between them. An alternative description of these geometries is in terms of (p, q) webs. It is possible to see that the connection between both descriptions consists simply on that the brane web is a representation of the toric skeleton (for a complete discussion of the relation see [130]).

We will focus on cones over two complex dimensional toric varieties. They can be understood as T^2 fibrations over $\mathbb{C}$. Lines and vertices in the web represent fixed points of the $U(1)$ actions (i.e. places where the fibration becomes degenerate). Lines correspond to vanishing 1-cycles, while points describe vanishing 2-cycles. The process of blowing-up a point in a given variety consists of replacing it by a 2-sphere. The toric representation of a 2-sphere is a segment. Then we see that if the points we choose to blow up are vertices in the web, we just have to replace them by segments.

We conclude this brief introduction by developing the toric representation for a specific example, the zeroth Hirzebruch surface F_0. F_0 is equal to $\mathbb{P}^1 \times \mathbb{P}^1$, so we can think about it as a 2-sphere fibered over another 2-sphere. This representation is shown in Figure 9.8.a. Now we want to interpret this geometry as a T^2 fibration over $\mathbb{C}$. A natural way to do this is by associating the vertical positions $y_{1,2}$ on the two 2-spheres to the two coordinates in the complex plane. Then, we associate to every point on $\mathbb{C}$ a 2-torus given by the product of the two circles parallel to the equators at the corresponding y_i. The full construction is presented in Figure 9.8.b. The C_2 circle vanishes at the north and south poles of the small sphere, represented torically by the two vertical lines. Analogously, the two horizontal lines correspond to the north and south poles of the big sphere. Both C_1 and C_2 vanish at the four vertices of the rectangle. From this discussion we also see that the sizes of the different compact 2-cycles are given by the lengths of the segments in the toric skeleton.

6.3 Four dimensional quivers from (p, q) webs

Let us study how to obtain the quiver for the four dimensional $\mathcal{N} = 1$ theory that appears on the world volume of a D3-brane probing the type of singularities we are
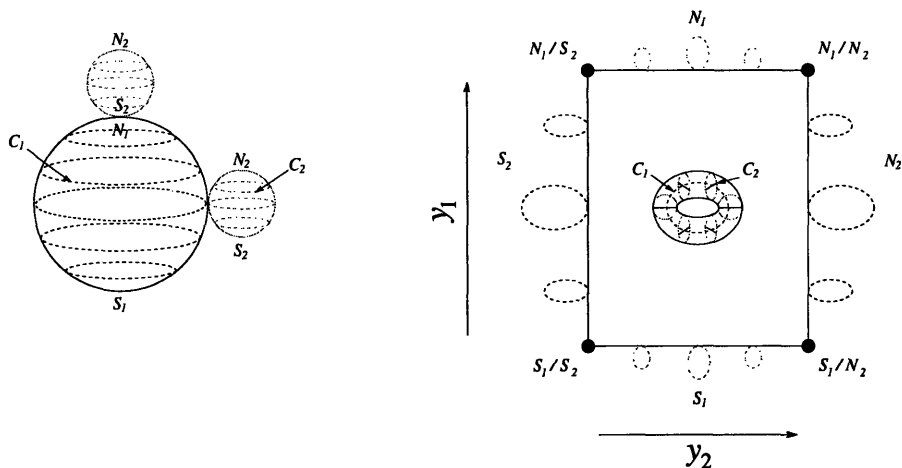
Figure 6-3: Toric representation of $F_0 = \mathbb{P}^1 \times \mathbb{P}^1$.

considering. A possible approach consists of obtaining the singularity as a partial resolution of an abelian orbifold, whose associated gauge theory is well understood. This approach was pursued in [45] and further developed in [46, 12, 43] to get the theories for the zeroth Hirzebruch and the toric del Pezzo surfaces as partial resolutions of $\mathbb{C}^3/(\mathbb{Z}_3 \times \mathbb{Z}_3)$.

A second alternative exploits the geometric information encoded in the (p, q) web. Each factor of the gauge group is given by a fractional brane, which is a bound state of D3, D5 and D7-branes. D3-branes span the four directions transverse to the singularity and thus are located at 0-cycles inside the toric variety. Analogously, D5-branes wrap 2-cycles and D7-branes wrap the compact 4-cycle. Some possible configurations are sketched in Figure 6-4. The mirror Type IIA geometries associated to these models were studied in [80]. It was found there that 0, 2 and 4-cycles map to 3-cycles, and D3-branes become D6-branes wrapping a T^3. The bifundamental matter content is given by the intersection matrix of the 3-cycles. Furthermore, each 3-cycle S_i wraps a 1-cycle C_i of a smooth elliptic fiber that becomes degenerate at some point z_i. Each C_i carries a (p_i, q_i) charge, and the intersection numbers for the 3-cycles can be calculated as

$$^{\#}(S_i . S_j) = {}^{\#}(C_i . C_j) = \det \begin{pmatrix} p_i & q_i \\ p_j & q_j \end{pmatrix} \tag{6.3.4}$$

102

The (p, q) charges of the 1-cycles are those of the external legs of the web. This suggests a profound connection between the (p, q) web and the gauge theory in four dimensions. Each node in the web corresponds to the fractional brane of one gauge group factor. When probing the singularity with N D3-branes, these gauge groups are all $SU(N)$. The external leg associated with it gives the (p, q) charges of the 1-cycle in the mirror manifold used to compute the matter content using the intersections with other 1-cycles.

D3   D5   D7
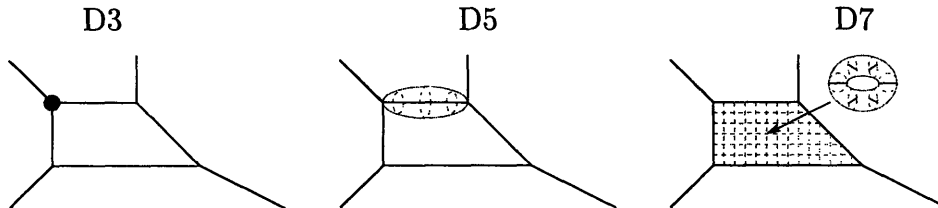
Figure 6-4: Possible D3, D5 and D7-branes located at 0-cycles and wrapping compact 2 and 4 cycles, respectively.

As it has already been noticed in [80], (p, q) charge conservation at every node of the web ($\sum_i (p_i, q_i) = 0$) guarantees the absence of anomalies in the four dimensional gauge theory. This is the case if every node of the quiver has a same number of incoming and outcoming arrows. Choosing the i-th node, we have

$$
N_{in}^{(i)} - N_{out}^{(i)} = \sum_{j \neq i} \det \begin{pmatrix} p_i & q_i \\ p_j & q_j \end{pmatrix} = \sum_{j \neq i} (q_i p_j - p_i q_j) \tag{6.3.5}
$$

$$
= q_i \sum_{j \neq i} p_j - p_i \sum_{j \neq i} q_j = -q_i p_i + q_i p_i = 0
$$

Thus we see that the theory is anomaly free.

We conclude this section with an explicit example of how the quiver theory is constructed from the brane web. We consider the case of dP_1. A possible (p, q) web for this geometry is presented in Figure 6-5.

We read the (p, q) charges of the 1-cycles from the external legs of the web. They are
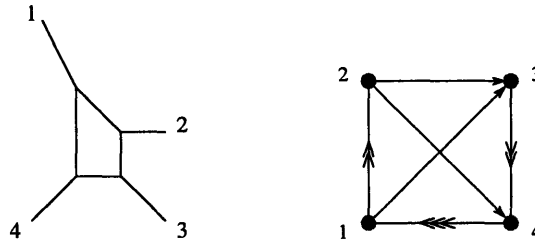
Figure 6-5: A (p, q) web for dP_1 and its associated quiver.

$$(p_1, q_1) = (-1, 2) \qquad (p_2, q_2) = (1, 0)$$
$$(p_3, q_3) = (1, -1) \qquad (p_4, q_4) = (-1, -1) \tag{6.3.6}$$

Using 6.3.4, it is straightforward to calculate the intersection numbers

$$^\#(C_1.C_2) = -2 \qquad {}^\#(C_1.C_3) = -1 \qquad {}^\#(C_1.C_4) = 3$$
$$^\#(C_2.C_3) = -1 \qquad {}^\#(C_2.C_4) = -1 \qquad {}^\#(C_3.C_4) = -2 \tag{6.3.7}$$

The sign of the intersection numbers indicate the orientation of the corresponding bifundamental fields. The resulting quiver is presented in Figure 6-5, where we have explicitly labeled the nodes according to the associated external legs.

6.4 Geometric transitions

In what follows, we will apply the observations in Sections 2 and 3 to obtain the phases of F_0 and of all del Pezzo surfaces up to dP_3. We will use (p, q) web diagrams as representations of the probed geometries and will study which are the resulting theories after successive blow-ups and blow-downs. This method proves to be very powerful and gives all the phases associated with different singularities without doing any calculation!

6.4.1 Blow-ups, unhiggsing and (p, q) webs

Del Pezzo surfaces are constructed by blowing-up up to eight generic points on $\mathbb{P}^2$. When the number of blown up points is less than or equal to three, the $SL(3, \mathbb{C})$

104

symmetry of $\mathbb{P}^2$ can be used to map the generic positions of these points to any desired location. In particular, these can be chosen to be vertices of the web configuration. Thus, all possible blow-ups of up to three points can be studied by blowing-up vertices of the web. Using the (p, q) web description of a sphere, the blow-up of a point is obtained by replacing it by a segment. The (p, q) charges of the two external legs at the endpoints of the blown-up 2-cycle are given by the charges of the original external leg.

The inverse process, a blow-down of a compact 2-cycle to a point, is given in the (p, q) web description by the replacement of a segment by a point, and the subsequent combination of the external legs attached at the end points of the segment. For the four dimensional gauge theory this process is simply a higgsing of the $SU(N)$ groups associated to both external legs to the linear combination of them under which the bifundamental field that gets a non-zero vev is neutral.
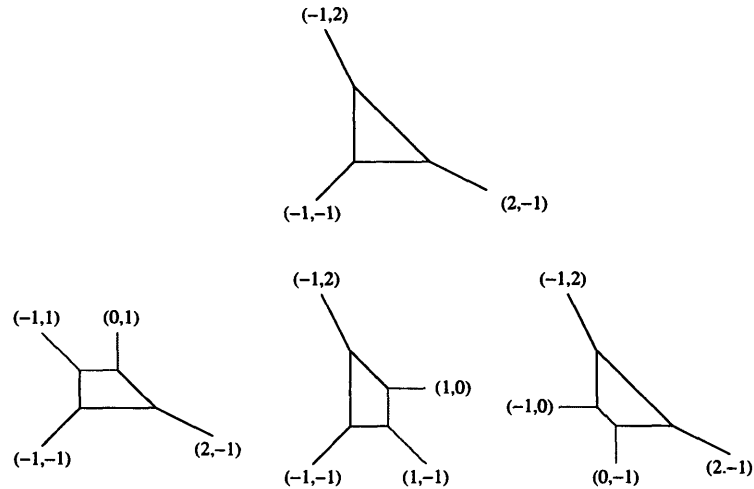
Figure 6-6: Possible blow-ups of dP_0. All the resulting theories are equivalent.

Let us use this method to calculate all the phases associated to D3-branes probing cones over toric del Pezzo surfaces. The starting point is a (p, q) web describing dP_0 (Figure 6-6). We have identified in red the branes obtained as a result of a blow-up. Once we have the resulting webs, we can calculate the intersection matrix and the quiver as in 6.3.4. The three webs in Figure 6-6 are related by $SL(2, \mathbb{Z})$ transformations, and describe the only phase of dP_1.

The next step is taking any of the equivalent webs for dP_1 (what we obtain is independent of our choice) and performing all possible blow-ups. The results are shown in Figure 6-7. After calculating the associated quivers we conclude that these webs represent two different theories. These are exactly the two toric dual models encountered in [46] for dP_2. At this point a new feature, which will persist for other geometries, appears: the existence of (p, q) webs with parallel external legs. These models are completely sensible as long as the 4d gauge theories are concerned. However, these theories present problematic issues when a 5d interpretation of the webs is intended. They may exhibit a leakage of 5d global charges due to states corresponding to strings stretching between parallel branes, and can also have directions in the moduli space along which the superpotential is not convex [5]. These drawbacks can be eliminated by providing a suitable UV completion of the theories, embedding them into larger (p, q) webs.
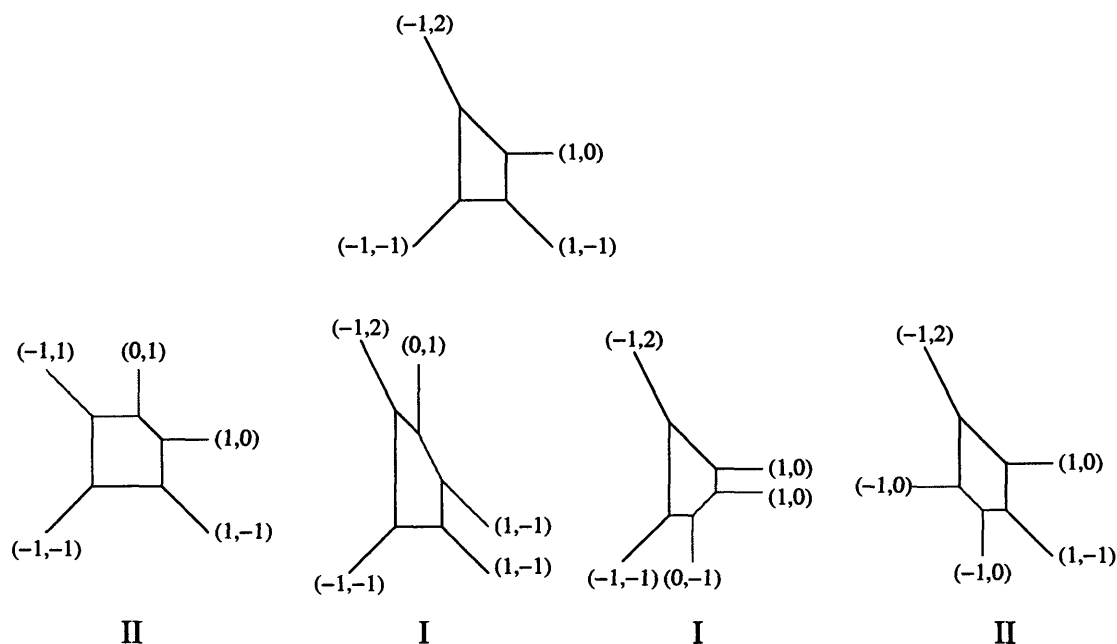
Figure 6-7: Possible blow-ups of dP_1. They correspond to two inequivalent phases.

We now move on, take one representative for each phase of dP_2 and proceed to blow-up points. At this point, it is not possible to blow-up any vertex in the web, since in some cases this would lead to crossing external legs (additional compact 4-cycles).

106

The theories coming from the first phase and second phase of dP_2 are presented in figures 6-8 and 6-9. Computing the quivers we obtain the four toric phases of dP_3 [48, 12].
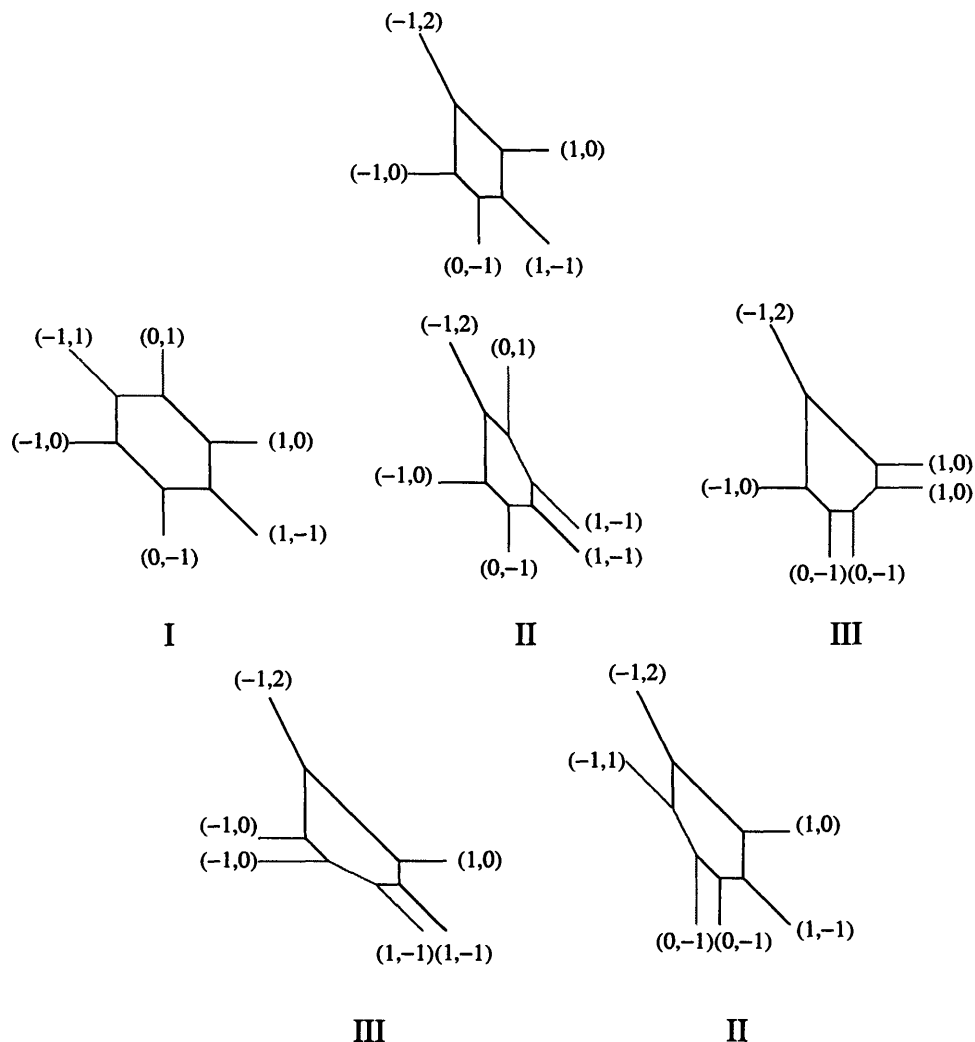
Figure 6-8: Possible blow-ups of phase I of dP_2.

The $SL(3,\mathbb{C})$ freedom is exhausted after blowing up three points on $\mathbb{P}^1$. Thus, we cannot map a further generic point to a vertex of the web and then blow it up. This is a manifestation of the fact that dP_n surfaces do not admit a toric description beyond $n = 3$. Nevertheless, we can study the theories obtained from dP_3 after a non-generic toric blow-up. We summarize the possibilities in Figure 6-10. These (p, q) webs define two quiver theories that are studied in detail in [44].
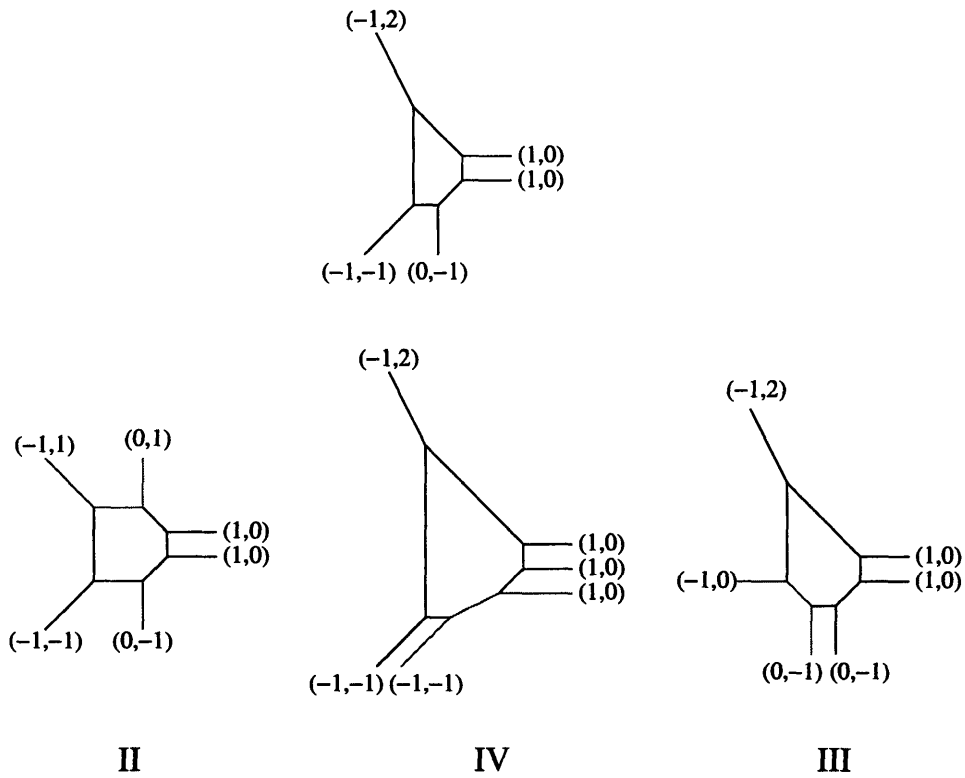
Figure 6-9: Possible blow-ups of phase II of dP_2.

We close this section by emphasizing that different Seiberg dual phases can be understood as related by blowing-down a 2-cycle and blowing-up a point. This is nothing more than an $SL(3,\mathbb{C})$ transformation relocating one of the blown-up point in $\mathbb{P}^2$. In this way, the set of Seiberg duality transformations (that do not change the rank of the gauge groups, keeping them all equal) G_S satisfies

$$G_S \subset \frac{SL(3,\mathbb{C})}{SL(2,\mathbb{Z})} \tag{6.4.8}$$

By the quotient by $SL(2,\mathbb{Z})$, we mean that those transformations that trivially do not change the intersection matrix, and hence do not lead to a dual phase, should be eliminated. Furthermore we see that, since there are elements in $SL(3,\mathbb{C})$ that do not preserve the intersection numbers, some singularities can be represented by both (p,q) webs with parallel legs and by (p,q) webs without them.
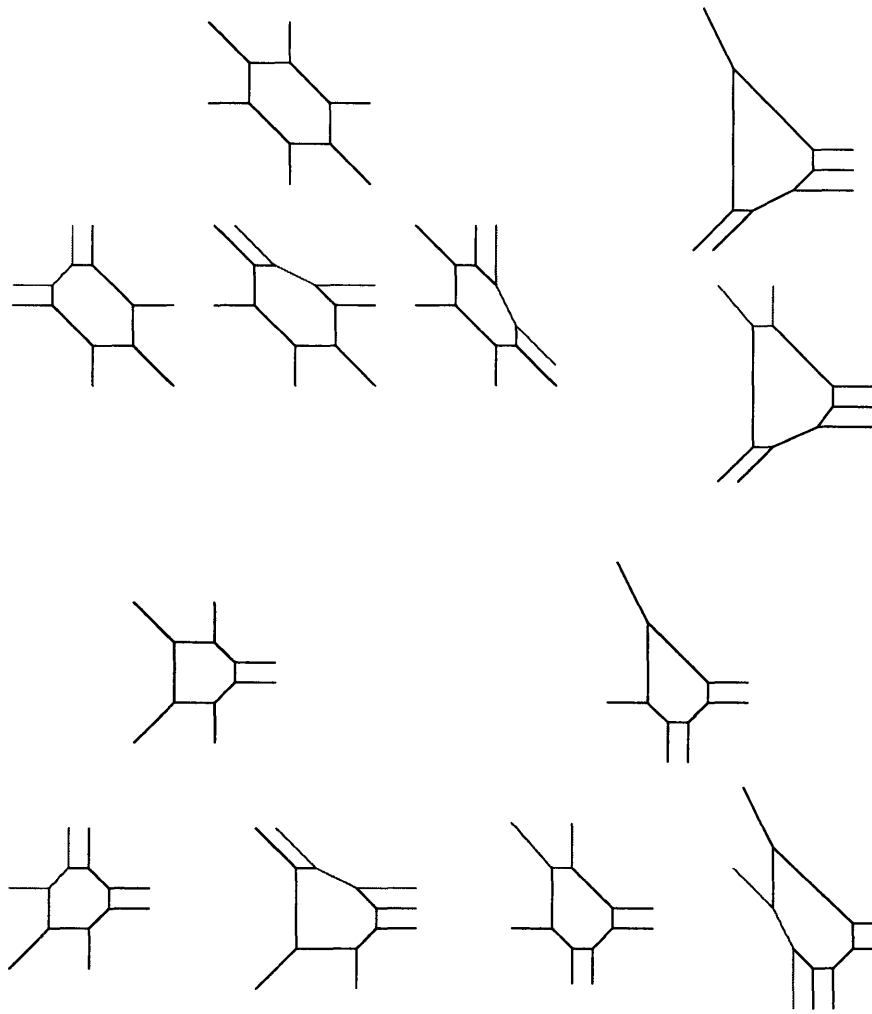
Figure 6-10: Possible blow-ups of the four phases of dP_3 at non-generic points. We have suppressed (p, q) charges for simplicity.

6.4.2 The two phases of F_0

The techniques introduced in Section 6.4.1 can be used to study, for another example, how different phases and singularities are interconnected by the geometric processes of blowing-up points and shrinking 2-cycles. In Figure 6-11 we present a possible path connecting the two phases of F_0. Starting from phase I, we blow up two points, arriving at model II of dP_3. The last step in the flow consists of shrinking two 2-cycles to zero size, combining the corresponding external legs.

The intersection matrices for both phases can be computed using 6.3.4, and are presented in the appendix.
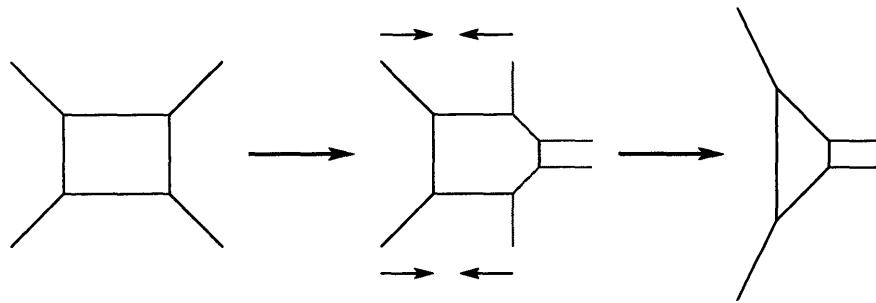
Figure 6-11: A possible transition between the two phases of F_0, by blowing-up two points and blowing-down two 2-cycles.

6.4.3 Higgsings as blow-downs

We have mentioned in Section 6.4.1 that blow-ups of the geometry correspond to unhiggings when we look at them from the perspective of the four dimensional gauge theory on the world volume of the brane probing the singularity. Conversely, the blow-down of a compact 2-cycle to a point translates into the higgsing of two $S(N)$ factors to a single $SU(N)$ by giving a non-zero expectation value to a bifundamental chiral field.

As we have discussed, compact 2-cycles are represented by the internal finite segments of the (p, q) web, their length given by the volume of the corresponding $\mathbb{P}^1$'s. Thus, we see the beautiful interplay between the two descriptions of the process. When blowing-down, we reduce the length of a segment. When this length vanishes, the external legs that are located at its endpoints are combined, adding their (p, q) charges. The two original $SU(N)$'s merge into a single one. The resulting linear combination depends on the relation between the coupling constants and is such that a bifundamental field charged under the original gauge groups is neutral with respect to it.

The (p, q) description of the original and final geometries allows an immediate identification of which vev we have to turn on in the gauge theory in order to flow down to the desired theory. Furthermore, it supplies a correspondence between gauge groups in the original and final theories. An explicit example of a blow-down from dP_3 to dP_2 will help to clarify these concepts. Let us connect the transition between

110

the theories in Figure 6-12. From the respective webs, we already see that they are related by the combination of nodes 2 and 3.
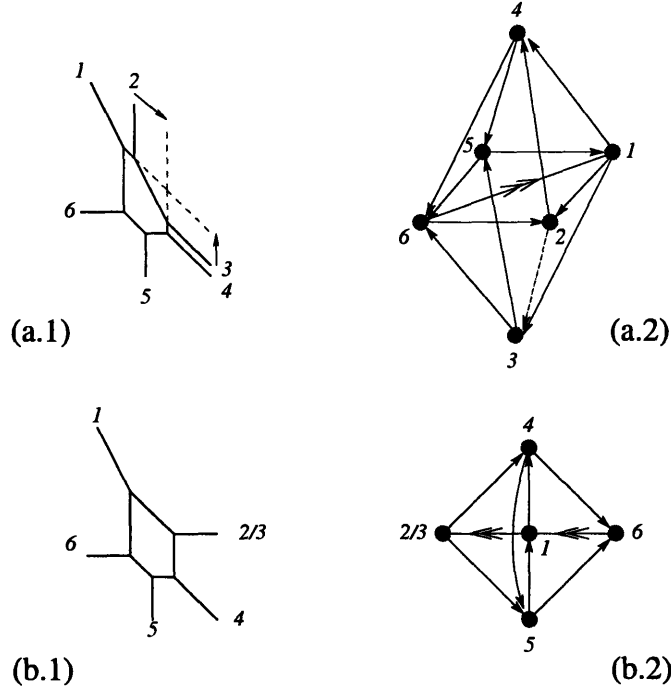
Figure 6-12: Higgsing from dP_3 (a.1) to dP_2 (b.1) by blowing down a 2-cycle. Their corresponding quivers are a.2 and b.2.

Before going on, let us notice that we have represented both quivers in a way that makes their symmetries explicit. The identification of these symmetries is immediate following the rules that will be presented in Section 6.5. Theory A has a $\mathbb{Z}_2 \times \mathbb{Z}_2$ node symmetry. The first $\mathbb{Z}_2$ interchanges nodes 3 and 4. The second $\mathbb{Z}_2$ acts as a π rotation around the (34) axis and a charge conjugation of all fields. These two symmetries disappear when we combine 2 and 3, but a new $\mathbb{Z}_2$ symmetry that interchanges $2/3 \leftrightarrow 6$, $4 \leftrightarrow 5$ and charge conjugate all fields appears in model B. At this point we can calculate the intersection matrices and see that theory A has 14 fields, while theory B has 11. One of the missing fields is the one getting a non-zero vev, so we can already see that masses for two fields will be generated when higgsing (notice that we know that this mass term will appear without looking at any superpotential!) [2].

---

[2] It is indeed very simple to understand how these two fields acquire masses. In the brane web language, the combined 2/3 leg is parallel to the existing 6, making the original ϕ_{62} and ϕ_{36} disappear.

The original superpotential is [45, 46]

$$W_A = \phi_{62}\phi_{24}\phi_{46} + \phi_{51}\phi_{14}\phi_{45} - \phi_{62}\phi_{23}\phi_{36} - \phi_{51}\phi_{13}\phi_{35} + \phi_{13}\phi_{36}\phi_{61} \qquad (6.4.9)$$

$$+\phi_{14}\phi_{46}\tilde{\phi}_{61} + \phi_{23}\phi_{35}\phi_{56}\tilde{\phi}_{61}\phi_{12} - \phi_{24}\phi_{45}\phi_{56}\phi_{61}\phi_{12}$$

The combination of legs 2 and 3 corresponds to turning on a non-zero vev for ϕ_{23} in 6.4.9. When doing so, $SU(N)^{(2)} \times SU(N)^{(3)}$ is broken down to a single $SU(N)$, under which ϕ_{23} is neutral. At the same time two fields, ϕ_{62} and ϕ_{36}, become massive as predicted. We are interested in the IR limit of this theory, so we integrate them out using their equations of motion. Setting $< \phi_{23} >= 1$, the resulting superpotential is

$$W = -\phi_{51}\phi_{13}\phi_{35} + \phi_{51}\phi_{14}\phi_{45} + \phi_{14}\phi_{46}\tilde{\phi}_{61} + \phi_{35}\phi_{56}\tilde{\phi}_{61}\phi_{12} \qquad (6.4.10)$$

$$+\phi_{13}\phi_{24}\phi_{46}\phi_{61} - \phi_{24}\phi_{45}\phi_{56}\phi_{61}\phi_{12}$$

which is exactly the superpotential of the dP_2 theory under consideration [45, 46].

An application, partial resolutions of $\mathbb{C}^3/(\mathbb{Z}_3 \times \mathbb{Z}_3)$

In Sections 6.4.1 and 6.4.2, we obtained all the gauge theories associated to blow-ups of $\mathbb{P}^2$ and $\mathbb{P}^1 \times \mathbb{P}^1$ in a constructive way, identifying at every step the possible geometric blow-ups. On the other hand, in section 6.4.3 we traced the connection between blow-downs, higgsings and transformations of the (p, q) webs. Let us now consider an example where all these tools and ideas converge.

The four phases of dP_3 were presented in Section 6.4.1. Furthermore, we have associated specific (p, q) webs to each of them. These theories were obtained in [48, 12] by the method of partial resolution of $\mathbb{C}^3/(\mathbb{Z}_3 \times \mathbb{Z}_3)$. Let us see how these

---

This is due to the existence of a $(\phi_{62}\phi_{23}\phi_{36})$ cubic term in the superpotential, which becomes a mass term after giving a non-zero expectation value to ϕ_{23}. However, the reader should be aware that the general situation is that not all gauge invariant operators permitted by a given $(p.q)$ web (alternatively by its associated quiver) appear in the corresponding superpotential.

$$\mathbb{C}^3/(\mathbb{Z}_3 \times \mathbb{Z}_3)$$

Model I

$$\phi_{91}, \phi_{34}, \phi_{67}$$

Model II

$$\phi_{34}, \phi_{67}, \phi_{68}$$

Model III

$$\phi_{91}, \phi_{24}, \phi_{34}$$

Model IV

$$\phi_{71}, \phi_{81}, \phi_{91}$$
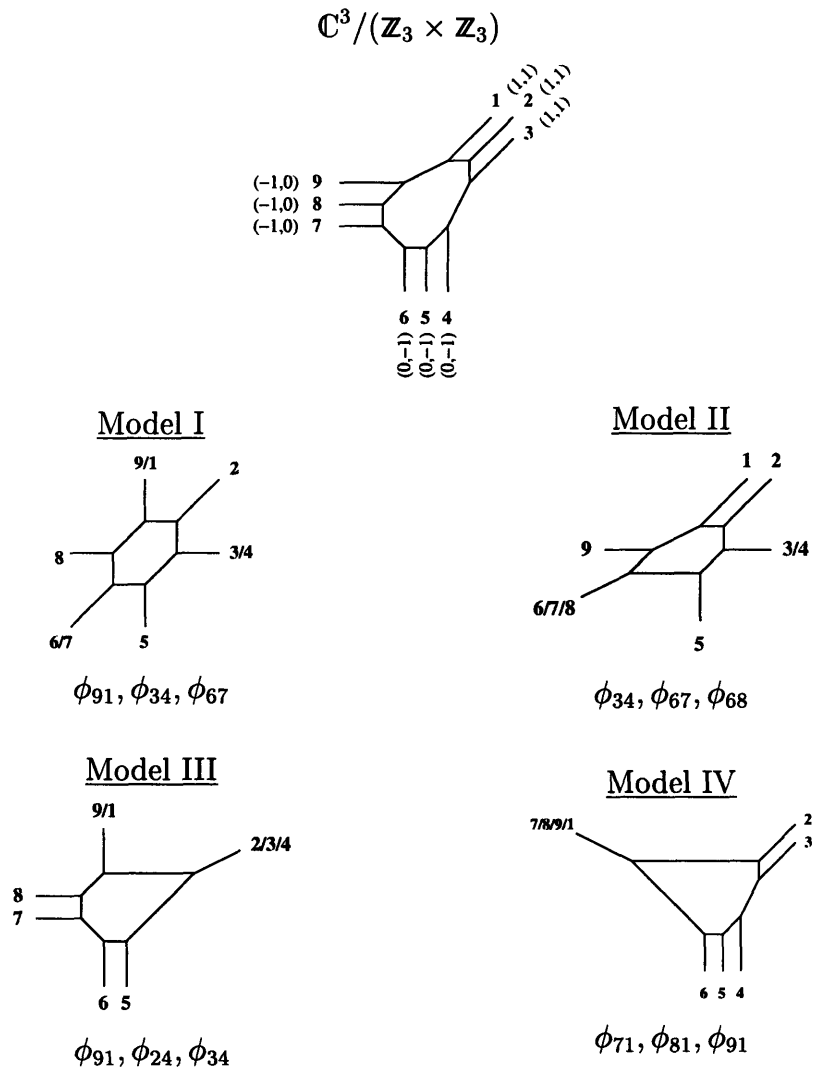
Figure 6-13: The four dP_3 phases obtained as partial resolutions (higgsings) of $\mathbb{C}^3/(\mathbb{Z}_3 \times \mathbb{Z}_3)$. We indicate the scalars that get a non-zero vev in each case.

results can be recovered immediately using our techniques. The starting point is the (p, q) web for $\mathbb{C}^3/(\mathbb{Z}_3 \times \mathbb{Z}_3)$ (Figure 6-13). In each case, we easily see which external legs have to be combined in order to get the desired phase. This is not the end of the story, the web construction also tells which fields have to get a non-zero vev in the original theory, they are the fields associated to the non-vanishing intersections of the combined 2-cycles. We summarize our results in Figure 6-13, indicating the scalars that get a non-zero expectation value.

113

6.5 Symmetries of the four dimensional gauge theory

An appealing feature of the (p,q) language is that it makes quiver symmetries of the gauge theory evident. We will consider here two examples of how thes symmetries manifest themselves in the brane representation. These symmetries have been studied in [12, 43], along with their importance as a tool for determining the structure of superpotentials.

S_n symmetries: These symmetries appear when the web brane configuration has sets of n parallel external legs (in the geometric language non-compact 2-cycles with the same (p,q) charges). Parallel branes have vanishing mutual intersections, while their intersections with the rest of the branes are identical. Due to this identity of the intersections, the gauge groups associated with parallel legs can be permuted leaving the quiver invariant. The symmetry group in this case is the full S_n permutation group. These discrete symmetries get enhanced to a continuous $SU(n)$ when the parallel branes coincide. In Figure 6-14 we show phase IV of dP_3 as an example. The three parallel red legs give rise to a S_3 symmetry between red nodes in the quiver, while there is a $\mathbb{Z}_2$ symmetry that interchanges blue nodes coming from the parallel blue branes.

$\mathbb{Z}_2$ axial symmetries: this is another example of symmetries that can be read directly from the (p,q) webs. They appear whenever the web has an axis of symmetry. In these cases the theories are invariant under exchange of gauge groups associated to external legs at both sides of the axis and charge conjugation of all fields. Is it important to notice that these reflections are indeed a subset of a larger set of transformations, given by all the $GL(2, \mathbb{Z})$ symmetries that map the webs onto themselves (i.e. that preserve the (p,q) charges of external legs). We have chosen to discuss $\mathbb{Z}_2$ reflections because they are the simplest of these symmetries, but we will also be considering the case of rotations later in this section. As an example, we present phase II of dP_3 in Figure 6-15. The two webs in Figure 6-15 are equivalent, and corre-
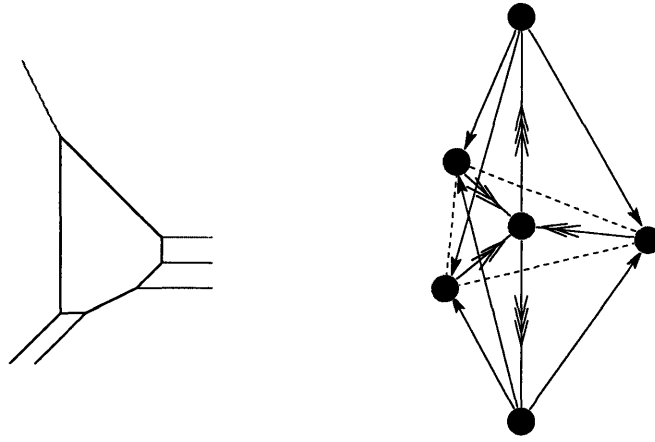
Figure 6-14: (p, q) web for phase IV of dP_3. We have colored the external branes giving rise to the different $SU(N)$ factors accordingly to their transformation properties under quiver symmetries.

spond to the same phase. We have presented both in order to illustrate how the same symmetry can arise in differently looking webs. Moreover, this example illustrates how the symmetry axis can sometimes be hidden. As it can be seen in the example, the axis can be made evident by an $SL(2, \mathbb{Z})$ change of (p, q) basis, which preserves the intersection numbers between cycles and simply corresponds to a variation in the complex scalar τ in 6.2.1.

For this example,

$$
\begin{aligned}
e_1 &= (1, 0) & e_1' &= (1, 0) \\
e_2 &= (0, 1) & e_2' &= (1, 1)
\end{aligned}
\tag{6.5.11}
$$

The two bases are related by the $SL(2, \mathbb{Z})$ matrix

$$
C = \begin{pmatrix} 1 & 1 \\ 0 & 1 \end{pmatrix}
\tag{6.5.12}
$$

Based on the preceding observations, we can use the (p, q) webs listed in the appendix and make an immediate classification of the mentioned node symmetries that appear in each model. The results are summarized in Table 6.1.

Three of the models deserve a more detailed explanation. The first of them is
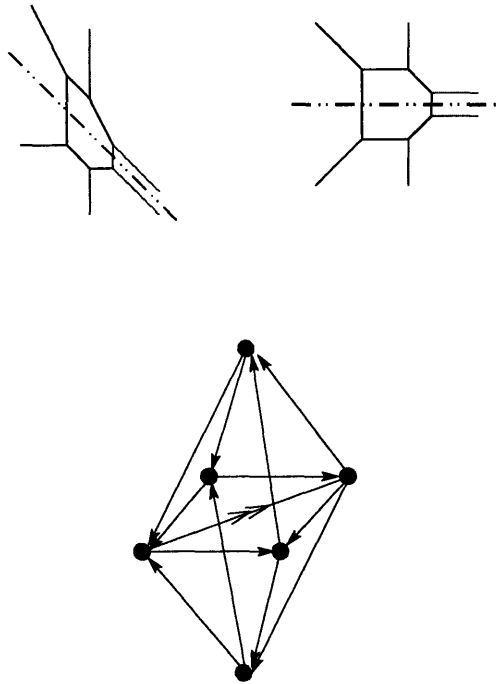
Figure 6-15: Two different (p, q) webs for phase II of dP_3. Once again, nodes of the same color transform into one another by the quiver symmetries.

dP_0, whose (p, q) web has an obvious $\mathbb{Z}_2$ axis of symmetry going along one of its legs. Furthermore, the three external legs are equivalent under $SL(2, \mathbb{Z})$ transformations that "rotate" the web. As a result, the full node symmetry group of dP_0 is D_3. An identical reasoning applies to the first phase of dP_3, which has an evident $\mathbb{Z}_2$ axis, and whose six external legs are equivalent under $SL(2, \mathbb{Z})$, leading to a D_6 symmetry. Finally, the fourth phase of dP_3 has one set of two and another one of three parallel external legs. According to our rules, this corresponds to a $\mathbb{Z}_2 \times S_3 = D_6$ symmetry.

6.6 Geometric transitions from the perspective of five dimensional theories

As we have discussed, (p, q) webs give a representation of the moduli space of $\mathcal{N} = 1$ theories in 4 dimensions, for those cases in which the moduli space admits a toric description. For these models, brane webs are simply the toric skeletons representing vanishing cycles. At the same time, (p, q) webs can be used to study 5 dimensional

116

Singularity	Phase	Node Symmetry
F_0	I	$\mathbb{Z}_2 \times \mathbb{Z}_2$
	II	$\mathbb{Z}_2 \times \mathbb{Z}_2$
dP_0		D_3
dP_1		$\mathbb{Z}_2$
dP_2	I	$\mathbb{Z}_2$
	II	$\mathbb{Z}_2$
dP_3	I	D_6
	II	$\mathbb{Z}_2 \times \mathbb{Z}_2$
	III	$\mathbb{Z}_2 \times \mathbb{Z}_2$
	IV	D_6

Table 6.1: Classification of node symmetries.

$\mathcal{N} = 1$ gauge theories living in the $4 + 1$ common dimensions of the branes. The purpose of this section will be to understand the translation of the four dimensional concepts of Seiberg duality and of different phases to the five dimensional language. While doing so, we will get some nice dynamical information about the five dimensional theories.

6.6.1 Five dimensional interpretation of the theories

We have already discussed how (p, q) webs lead to 5 dimensional $SU(N_c)$ theories with N_F flavors. The number of colors is given by the number of parallel internal branes. For all the cases we are studying, the (p, q) webs possess only one closed face (i.e. a single compact 4-cycle in the geometric interpretation), and have a pair of parallel internal branes, so they will be associated with $SU(2)$ theories. In all the webs sketched in Figures 6-6 to 6-11, it is possible to identify at least one such a pair of parallel finite branes that play the role of color branes.

Of the N_L external legs of a web, four have to be the supporting structure of color branes. It is also possible to see that in all the studied webs, after we identify the supporting branes, the remaining ones result to be parallel to color branes, thus admitting an interpretation as $N_F = N_L - 4$ flavor branes. Putting all these things together we see that F_0 phases will be associated to $SU(2)$ with no flavors, while dP_n theories will be represented in five dimensions by $SU(2)$ models with $N_F = n - 1$.

There are two theories that require a more careful interpretation. The first one is the well-known case of dP_0. Having only three external legs, this theory is understood as $SU(2)$ with -1 flavors. We can extend the reasoning in the following way, any time we face a theory where we cannot identify $N_L - 4$ legs as flavors, we blow up N points until reaching a model with the usual interpretation. This theory will have $N_L + N - 4$ flavors. Then we say that the number of flavors in the original theory is $(N_L + N - 4) - N$. The other special case is phase IV of dP_3, which is shown in Figure 6-16 together with the same (p, q) web blown-up at one point. According to our previous statements, the five dimensional interpretation of this model is $SU(2)$ with $3 - 1$ flavors.
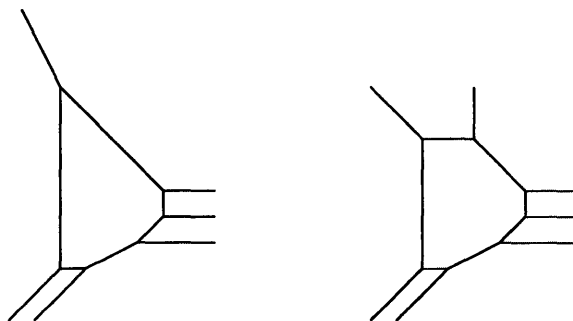
Figure 6-16: Phase IV of dP_3. It can be interpreted in five dimensions as $SU(2)$ with 3-1 flavors.

6.6.2 Different limits in moduli space, a first example

Let us start studying how the flow between theories can be interpreted as adding a flavor to the corresponding five dimensional gauge theory and considering different, eventually infinite, limits in parameter space. To do so, let us focus on the example of a transition between one of the phases of F_0 and dP_1. The main point here is to realize that in both brane configurations one of the external legs can be understood as coming from a junction between two branes, one of which is a flavor brane. When taking the location of this junction very far away from the core of the (p, q) web, the configurations become those studied in Sections 6.4.1 and 6.4.2. The position of the flavor brane is parametrized by the bare mass of the quark. When it becomes infinite,

the quark decouples leaving us with pure $SU(2)$ theories with no flavors.

Figure 6-17 shows how in the limit $m \to -\infty$ we have the second phase of F_0, for $|m| < \phi/2$ we get phase I of dP_2 and finally we obtain dP_1 for $m \to \infty$.
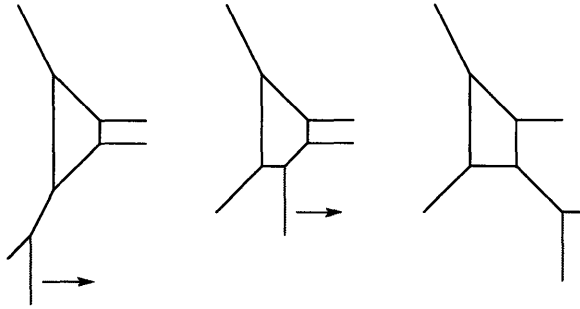
Figure 6-17: Flowing from F_0 to dP_1 by tuning the bare mass of the quark from $m \to -\infty$ to $m \to \infty$.

6.6.3 Geometrical blow-ups as tuning bare masses

Encouraged by the example presented in the previous section, we can ask whether this is a general feature and we may indeed interpret all geometrical transitions of the type we are considering as tuning the bare mass for some quark. After inspecting Figures 6-6 to 6-11 we conclude that this in fact is true!

The way of seeing this is that, in all cases, one of the two external legs connected to a 2-cycle coming from a blown-up point is parallel to a pair of finite segments in the inner face of the (p, q) webs. Thus, this external leg can be understood as a flavor brane, while the two finite branes play the role of $SU(2)$ color branes. We can think about the blowing-up process as bringing the flavor brane from infinity ($m \to \pm\infty$) until it reaches the body of the web. We can repeat this process indefinitely. One important point that has to be kept in mind is that, after each step, the two branes acting as color branes can change (and thus the orientation of the flavor brane we have to consider).

Figure 6-18 shows an example of a flow $dP_1 \to dP_2 \; II \to dP_3 \; II$, illustrating how the direction of color and flavor branes can change at each step. As an aside, this example also shows an interesting situation, the fact that at some point in the blow-
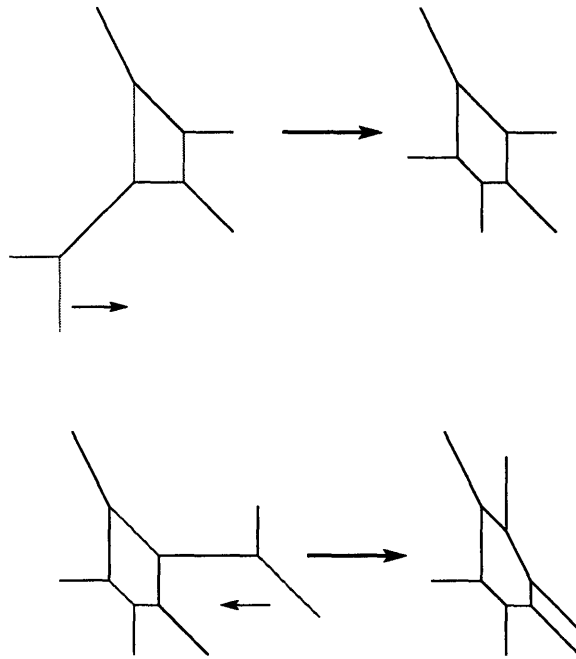
Figure 6-18: Flow $dP_1 \rightarrow dP_2 \ II \rightarrow dP_3 \ II$, obtained by bringing bare masses to finite values.

up process there can be more than one possible choices of which branes to consider color branes. We see that, before the second blow-up, another legitimate choice would have been the two vertical finite branes.

6.6.4 BPS spectrum

BPS states in the five dimensional theory are given by webs of strings ending on the 5-brane web [5]. We will use this construction to see how BPS spectra of different phases are related. Let us consider the two phases of dP_2 since they constitute one of the simplest examples. We will also restrict our analysis to BPS states associated to string webs with only two and three end points (the extension to other states is immediate). The corresponding configurations are shown in Figure 6-19.

Both spectra are quite different. Specifically there is no analog of state b of phase II in phase I. Nevertheless, we have seen that both the geometric picture and the five dimensional one in terms of varying parameters suggest that the passage between different phases is a continuous process.
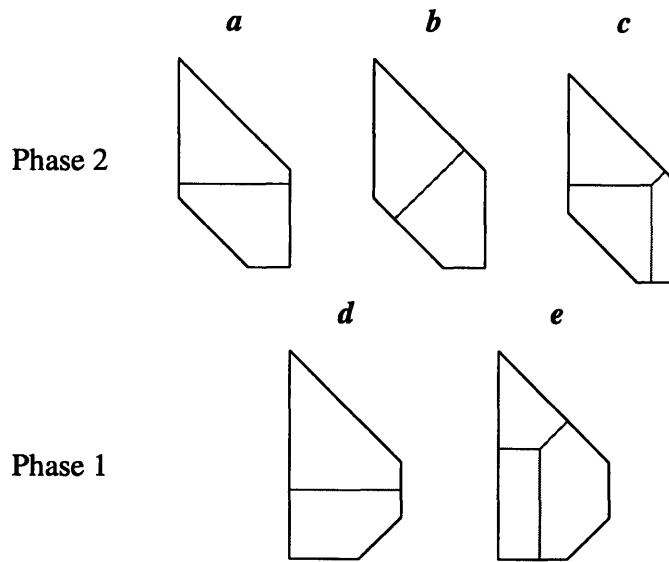
Figure 6-19: Some BPS states for phases I and II of dP_2. String junctions are represented in red. For simplicity, we have suppressed the external legs of the (p, q) webs.

Let us understand how the two spectra are continuously connected. To do so, we follow the fate of state b as we flow between phases II and I. In Figure 6-20 we show different stages of this transition. The starting point is phase II and we gradually reduce the size of the blue 2-cycle. From stages 2 and 3 we see that, as the blue cycle approaches zero size, state b becomes degenerate with one state of type c (both of them in the BPS spectrum of phase II). State c survives the transition, becoming state e of phase I. The final step consists on shrinking the blue 2-cycle to a point and blowing up the green point. In conclusion state b undergoes a continuous transformation into state e, going through a point at which both states have the same mass.

We have understood that, for the specific case of geometric transitions between dP_2 phases, BPS states corresponding to string junctions with support on collapsing 2-cycles cease to exist as these 2-cycles shrink to a point, but become degenerate with other BPS states that remain in the spectrum. The same conclusion can be reached in the general case.

The string junctions (BPS states in five dimensions) that can in principle disappear abruptly are those ending on shrinking blown-up 2-cycles (exceptional curves). It is

121
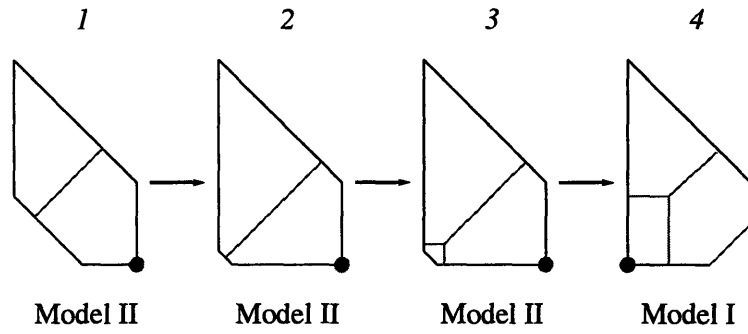
Figure 6-20: Continuous flow between BPS states of the two phases of dP_2.

easy to see (and Figures 6-6 to 6-11 illustrate this fact) that external legs attached to exceptional curves are parallel to internal branes ending on the corresponding segment of the (p, q) web. The general situation is presented in Figure 6-21, where the charges of internal branes are shown in brackets, and those of external legs in parentheses.
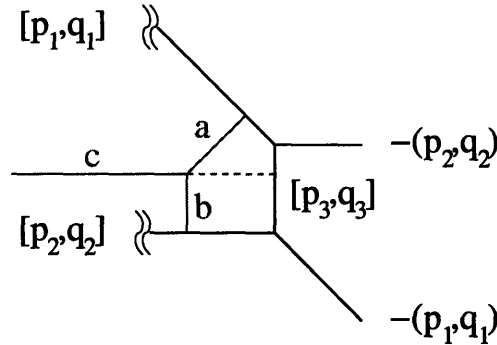
Figure 6-21: Continuous connection between BPS states in the general case.

(p, q) charge conservation fixes the slope of the shrinking brane to be given by

$$[p_3, q_3] = [p_1 - p_2, q_1 - q_2] \tag{6.6.13}$$

Let us now consider the string junction shown in red in Figure 6-21, which can be part of a larger BPS configuration. Its a and b legs are perpendicular to branes 1 and 2. Thus

$$(p_a, q_a) = (q_1, -p_1)$$
$$(p_b, q_b) = (-q_2, p_2) \tag{6.6.14}$$

Once again, (p, q) charge conservation implies

$$(p_c, q_c) = (q_1 - q_2, -p_1 + p_2) = (q_3, -p_3) \qquad (6.6.15)$$

Then, string c is perpendicular to brane 3. We can now follow a reasoning identical to the one used previously for dP_2. As brane 3 goes to zero size, legs a and b of the string junction can be negligibly small, and the corresponding BPS state becomes degenerate with the one ending directly on brane 3. This concludes our proof of the continuity of BPS spectra in the general case.

We discussed in Section 6.4.1 how Seiberg dual theories are related by the combination of a blow-down and a blow-up in the non-compact Calabi-Yau probed by the D3-brane. The arguments presented in this section lead us to an important conclusion: Seiberg duality between theories in four dimensions appears in the associated five dimensional models as crossing curves of marginal stability.

6.6.5 Continuity of the monopole tension

In this section we will calculate another five dimensional quantity, the monopole tension, and study how its values for different theories are related

Let us consider the example of the two phases of dP_2, which in five dimensional language correspond to $SU(2)$ theories with one flavor. Calculating the monopole tensions for these two phases (which is simply the area of the inner face of the (p, q) web [5]) we find

$$
\begin{aligned}
T_M^{(I)} &= \frac{7}{8}\phi^2 + \left(\frac{1}{g_0^2} + \frac{m}{2}\right)\phi - \frac{m^2}{2} \\
T_M^{(II)} &= \frac{7}{8}\phi^2 + \frac{\phi}{g_0^2} - \frac{m^2}{2}
\end{aligned}
\qquad (6.6.16)
$$

We see that this quantity has a different functional dependence on the parameters when we consider the two theories. Another question (whose answer is obvious from the (p, q) web picture) is what the value of $T_M^{(I)}$ is when $m = \phi/2$. In this situation

we know that one of the quarks becomes massless, while the other one gets the same mass as the gauge boson $m_Q = \phi$. The tension in this case becomes

$$T_M = \phi^2 + \frac{\phi}{g_0^2} \qquad (6.6.17)$$

which is exactly that for dP_1. Once again, the transition is continuous.

6.7 Conclusions

We have studied dualities and flows between gauge theories living on D3-branes probing toric singularities. We have found (p, q) webs very useful for this task, and for establishing relations among the probed geometry, the four dimensional theories on the world volume of the branes and five dimensional $SU(2)$ associated theories.

In Section 6.4 we have interpreted the flow between the four dimensional theories corresponding to the zeroth Hirzebruch and the del Pezzo surfaces as geometric transitions in the probed singularities. We also established the geometric transformations connecting toric dual models. In doing so, the (p, q) web representation of the toric varieties became not only a useful pictorial representation of the process, but a whole computational tool. The process of obtaining all the theories is reduced to doing successive blow-ups and to calculate intersection matrices. This simplicity can be contrasted with methods previously employed for the same task, based on partial resolutions of $\mathbb{C}^3/(\mathbb{Z}^3 \times \mathbb{Z}^3)$, which are computationally much more involved. Another advantage of the (p, q) web approach is that it offers a geometric intuition at every point of the process.

Furthermore, we studied the connection between blow-downs(ups) and (un)higgsings in the four dimensional theories. When doing so, the associated (p, q) webs permit the immediate identification of which field must acquire a non-zero vev. This was exemplified by getting the partial resolutions of $\mathbb{C}^3/(\mathbb{Z}^3 \times \mathbb{Z}^3)$ that give the four toric dual theories corresponding to dP_3.

Section 6.5 was devoted to study how quiver symmetries can be read off from (p, q) webs. The web constructions make these symmetries evident. The identification of

the symmetry groups is reduced to counting parallel external legs and finding axes of symmetry.

In Section 6.6 we initiated the exploration of a new perspective for geometric transitions. Exploiting the connection provided by (p, q) webs, we developed the interpretation of the studied theories as five dimensional $SU(2)$ gauge theories with N_F flavors. We showed how geometrical blow-ups can be understood as bringing flavors from infinite bare mass. We proved that BPS spectra of two theories connected by a geometric transition are continuously connected. In this language, the transition corresponds to crossing a curve of marginal stability. We also studied the continuous relation between the monopole tensions in two such theories.

6.8 Appendix: Gauge theories for branes on toric singularities

In this appendix we summarize the theories studied throughout this chapter. For each of them we give a (p, q) web and its quiver [3]. For the del Pezzo surfaces, we also include the corresponding fractional brane charges. These charges were calculated with the procedure described in [80], which uses the map between 3-cycles in the mirror manifold and vector bundles on the del Pezzo surfaces of [100, 99]. The purpose of their inclusion is to exemplify how the combination and splitting of external legs of the (p, q) webs are associated to the same operations on the fractional brane charges.

---

[3]In some of the quivers we have charge conjugated all the fields in order to follow the ones presented in the references [45, 46, 48, 43].

Cone over F_0

F_0 has two phases. Phase I has 12 fields, while Phase II has 8.

(p,q) web	Quiver	Intersection matrix
		$\mathcal{I}_I = \begin{pmatrix} 0 & -2 & -2 & 4 \\ 2 & 0 & 0 & -2 \\ 2 & 0 & 0 & -2 \\ -4 & 2 & 2 & 0 \end{pmatrix}$
		$\mathcal{I}_{II} = \begin{pmatrix} 0 & -2 & 0 & 2 \\ 2 & 0 & -2 & 0 \\ 0 & 2 & 0 & -2 \\ -2 & 0 & 2 & 0 \end{pmatrix}$

(6.8.18)

Cone over dP_0
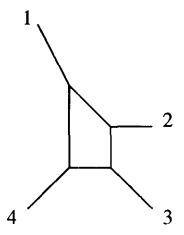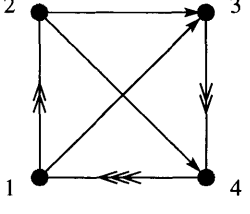
dP_0 has one phase with 9 fields.

(p,q) web	Quiver	Intersection matrix	Fractional brane charges
		$\mathcal{I} = \begin{pmatrix} 0 & -3 & 3 \\ 3 & 0 & -3 \\ -3 & 3 & 0 \end{pmatrix}$	$ch(F_1) = (2, -\ell, -1/2)$ $ch(F_2) = (-1, \ell, -1/2)$ $ch(F_3) = (-1, 0, 0)$

(6.8.19)

126
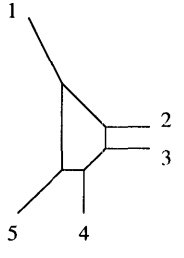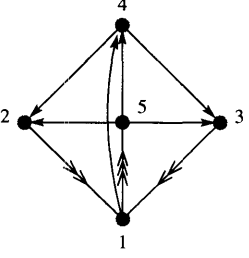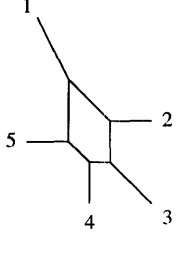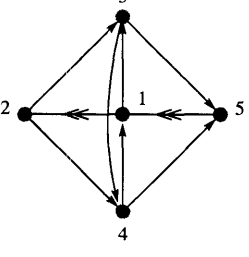
Cone over dP_1

dP_1 has one phase with 10 fields.

(p,q) web	Quiver	Intersection matrix	Fractional brane charges
		$\mathcal{I} = \begin{pmatrix} 0 & -2 & -1 & 3 \\ 2 & 0 & -1 & -1 \\ 1 & 1 & 0 & -2 \\ -3 & 1 & 2 & 0 \end{pmatrix}$	$ch(F_1) = (2, -\ell, -1/2)$ $ch(F_2) = (0, E_1, -1/2)$ $ch(F_3) = (-1, \ell - E_1, 0)$ $ch(F_4) = (-1, 0, 0)$

$$(6.8.20)$$

Cone over dP_2
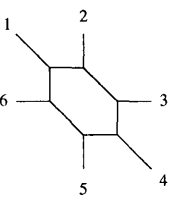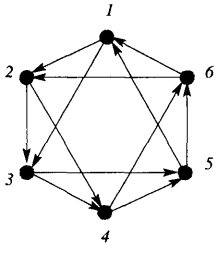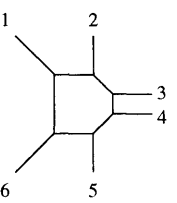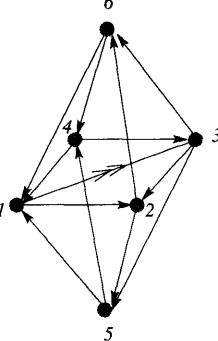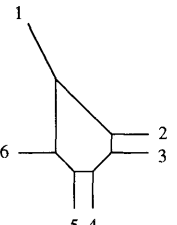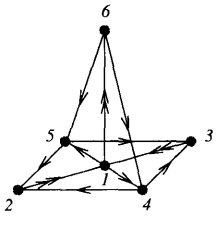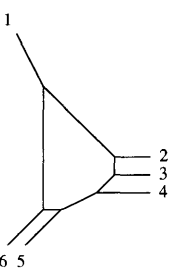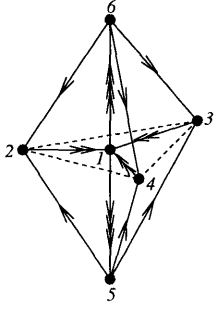
dP_2 has two phases, with 13 and 11 fields.

(p,q) web	Quiver	Intersection matrix	Fractional brane charges
		$\mathcal{I}_I = \begin{pmatrix} 0 & -2 & -2 & 1 & 3 \\ 2 & 0 & 0 & -1 & -1 \\ 2 & 0 & 0 & -1 & -1 \\ -1 & 1 & 1 & 0 & -1 \\ -3 & 1 & 1 & 1 & 0 \end{pmatrix}$	$ch(F_1) = (2, -\ell, -1/2)$ $ch(F_2) = (0, E_1, -1/2)$ $ch(F_3) = (0, E_2, -1/2)$ $ch(F_4) = (-1, \ell - E_1 - E_2, 1/2)$ $ch(F_5) = (-1, 0, 0)$
		$\mathcal{I}_{II} = \begin{pmatrix} 0 & -2 & -1 & 1 & 2 \\ 2 & 0 & -1 & -1 & 0 \\ 1 & 1 & 0 & -1 & -1 \\ -1 & 1 & 1 & 0 & -1 \\ -2 & 0 & 1 & 1 & 0 \end{pmatrix}$	$ch(F_1) = (2, -\ell, -1/2)$ $ch(F_2) = (0, E_1, -1/2)$ $ch(F_3) = (-1, \ell - E_1, 0)$ $ch(F_4) = (-1, E_2, 1/2)$ $ch(F_5) = (0, -E_2, -1/2)$

$$(6.8.21)$$

Cone over dP_3

dP_3 has four phases, with 12, 14, 14 and 18 fields.

(p,q) web	Quiver	Intersection matrix	Fractional brane charges
		$$\mathcal{I}_I = \begin{pmatrix} 0 & -1 & -1 & 0 & 1 & 1 \\ 1 & 0 & -1 & -1 & 0 & 1 \\ 1 & 1 & 0 & -1 & -1 & 0 \\ 0 & 1 & 1 & 0 & -1 & -1 \\ -1 & 0 & 1 & 1 & 0 & -1 \\ -1 & -1 & 0 & 1 & 1 & 0 \end{pmatrix}$$	$ch(F_1) = (1, -\ell + E_3, 0)$ $ch(F_2) = (1, -E_3, -1/2)$ $ch(F_3) = (0, E_1, -1/2)$ $ch(F_4) = (-1, \ell - E_1, 0)$ $ch(F_5) = (-1, E_2, 1/2)$ $ch(F_6) = (0, -E_2, -1/2)$
		$$\mathcal{I}_{II} = \begin{pmatrix} 0 & -1 & -1 & -1 & 1 & 2 \\ 1 & 0 & -1 & -1 & 0 & 1 \\ 1 & 1 & 0 & 0 & -1 & -1 \\ 1 & 1 & 0 & 0 & -1 & -1 \\ -1 & 0 & 1 & 1 & 0 & -1 \\ -2 & -1 & 1 & 1 & 1 & 0 \end{pmatrix}$$	$ch(F_1) = (1, -\ell + E_3, 0)$ $ch(F_2) = (1, -E_3, -1/2)$ $ch(F_3) = (0, E_1, -1/2)$ $ch(F_4) = (0, E_2, -1/2)$ $ch(F_5) = (-1, \ell - E_1 - E_2, 1/2)$ $ch(F_6) = (-1, 0, 0)$
		$$\mathcal{I}_{III} = \begin{pmatrix} 0 & -2 & -2 & 1 & 1 & 2 \\ 2 & 0 & 0 & -1 & -1 & 0 \\ 2 & 0 & 0 & -1 & -1 & 0 \\ -1 & 1 & 1 & 0 & 0 & -1 \\ -1 & 1 & 1 & 0 & 0 & -1 \\ -2 & 0 & 0 & 1 & 1 & 0 \end{pmatrix}$$	$ch(F_1) = (2, -\ell, -1/2)$ $ch(F_2) = (0, E_1, -1/2)$ $ch(F_3) = (0, E_3, -1/2)$ $ch(F_4) = (-1, \ell - E_1 - E_3, 1/2)$ $ch(F_5) = (-1, E_2, 1/2)$ $ch(F_6) = (0, -E_2, -1/2)$
		$$\mathcal{I}_{IV} = \begin{pmatrix} 0 & -2 & -2 & -2 & 3 & 3 \\ 2 & 0 & 0 & 0 & -1 & -1 \\ 2 & 0 & 0 & 0 & -1 & -1 \\ 2 & 0 & 0 & 0 & -1 & -1 \\ -3 & 1 & 1 & 1 & 0 & 0 \\ -3 & 1 & 1 & 1 & 0 & 0 \end{pmatrix}$$	$ch(F_1) = (2, -\ell, -1/2)$ $ch(F_2) = (0, E_1, -1/2)$ $ch(F_3) = (0, E_2, -1/2)$ $ch(F_4) = (0, E_3, -1/2)$ $ch(F_5) = (-1, \ell - E_1 - E_2 - E_3, 1)$ $ch(F_6) = (-1, 0, 0)$

$$(6.8.22)$$

Chapter 7

Duality Walls, Duality Trees and Fractional Branes

We compute the NSVZ beta functions for $\mathcal{N} = 1$ four-dimensional quiver theories arising from D-brane probes on singularities, complete with anomalous dimensions, for a large set of phases in the corresponding duality tree. While these beta functions are zero for D-brane probes, they are non-zero in the presence of fractional branes. As a result there is a non-trivial RG behavior. We apply this running of gauge couplings to some toric singularities such as the cones over Hirzebruch and del Pezzo surfaces. We observe the emergence in string theory of "Duality Walls," a finite energy scale beyond which Seiberg duality does not proceed. We also identify certain quiver symmetries as T-duality-like actions in the dual holographic theory. The content of this chapter is based on [56].

7.1 Introduction

Understanding renormalization group flows out of conformal fixed points of super-symmetric gauge theories is of vital importance in fully grasping the AdS/CFT Correspondence beyond super-conformal theories and brings us closer to realistic gauge theories such as QCD. In particular, the $\mathcal{N} = 1$ gauge theories arising from world-volume theories of D-brane probes on Calabi-Yau singularities have been extensively

studied under this light. Dual to these theories are the so-called non-spherical horizons of AdS [125, 110, 116, 1, 121, 138].

A prominent example, the conifold singularity, was analysed by Klebanov and Strassler (KS) in [119] where the RG flow takes the form of a duality cascade. Here, we have a theory with two gauge group factors and four associated bi-fundamental fields. With the addition of appropriate D5-branes, the theory is taken out of conformality in the infra-red. Subsequently, the two gauge couplings evolve according to non-trivial beta functions. Whenever one of the couplings becomes strong, we should perform Seiberg duality to migrate into a regime of weak coupling [119]. And so on we proceed *ad infinitum*, generating an intertwining evolution for the couplings. This is called the a **duality cascade**. The dual supergravity (SuGRA) solution, happily aided by our full cognizance of the metric on the conifold, can be studied in detail and matches the field-theory behavior.

The generalization of this phenomenon to other geometries is hindered by the fact that the conifold is really the only geometry for which we know the metric. Nevertheless nice extensions from the field theory side have been performed. Notably, in [50], the cascade has been recast into properties of the Cartan matrix of the quiver [108, 88, 89]. Then Seiberg duality becomes Weyl reflections in the associated root space. The UV behaviour would thus depend markedly on whether the Cartan matrix is hyperbolic (with a single negative eigenvalue and the rest positive) or not. Indeed for some simple quiver examples without consideration of stringy realization, it was shown that the RG flow converges in the UV and surprisingly there is a finite accumulation point at which the scale of the dualizations pile up. This opens the question of what is the possible UV completions of these field theories. Such fundamental limitation on the scale of the theory was originally dubbed **duality walls** in [159].

The issue seems to persist as one studies generalizations of the conifold geometry and in realizations in string theory. As a first example that is chiral and arising from standard string theory constructions, [85] discussed the case of our familiar $\mathbb{C}^3/\mathbb{Z}_3$ singularity. Using naïve beta-functions without consideration for the anomalous dimensions, [85] analysed in detail how one encounters duality walls for this string

theoretic gauge theory.

Indeed, even without making reference to explicit metrics and supergravity solutions, it is possible to study this problem from a gauge theory perspective. Extensive methodology and catalogues of non-spherical horizons have been in circulation (q.v. e.g. [138, 75, 20, 96, 39, 79, 11], and Chapters 5 and 6. for an infinite family with explicit Sasaki-Einstein metrics). A particular class for which an algorithmic outlook was partaken is the toric singularities of which the conifold and the $\mathbb{C}^3/\mathbb{Z}_3$ orbifold are examples [11, 45, 53]. For these geometries, Seiberg-like dualities dubbed "Toric Duality" [45, 48, 12] have been labouriously investigated. Consecutive application of such a duality on a given theory essentially translates to a systematic application of certain quiver transformation rules. These rules can be understood from many fruitful perspectives: as ambiguities in the Inverse Toric Algorithm [45]; or as monodromy transformations of wrapped cycles around the singularity [29, 99, 47, 24]; or as braiding relations in (p, q) sevenbrane configurations [47]; or as mutations in helices of exceptional collections of coherent sheafs [99]; or as tilting functors in the D-brane derived category [18, 22], etc.

A key feature of such a duality is the **tree structure** of the space of dual theories. As we dualise upon a node in the quiver at each stage, a new branch blossoms. The topology of the tree is important. For example, whether there are any closed cycles which would signify that certain dualities may be trapped within a group of theories.

We are therefore naturally inspired by the conjunction of the toy model in [85] and our host of techniques from toric duality. Dualization in the tree is precisely the desired cascading procedure. A first care which needs to be taken is a thorough analysis of the beta-function, including the **anomalous dimensions**. Happily, the form of the exact beta function with the anomalous dimensions has been computed by [142] for $\mathcal{N} = 1$ gauge theories and by [128] for quiver theories in particular.

In $\mathcal{N} = 1$ SCFT theories, the 't Hooft anomaly for the $U(1)_R$ charge determines all anomalous dimensions of chiral operators. These however are determined up to global non-R flavour symmetries. Computationally one must resort to finding such additional symmetries. In the quiver cases, this can be done by guided inspection of

131

the quiver diagrams [43].

The nice work by [102] posited a maximization principle to systematically determine the R-symmetry and hence all anomalous dimensions. Namely one must maximise a certain combination of the $U(1)$ charges. This quantity is called a in the canonical literature and together with c they constitute the central charges of the SCFT. Indeed it is believed that a obeys a 4d version of Zamolodchikov's c-theorem, decreasing monotonically along an RG flow towards the IR. The central charge a shall be for us, a measure of the number of degrees of freedom in the field theory. In the AdS dual, it corresponds to the 5d horizon volume of the singular geometry.

The organization of this chapter is as follows. We will first require three ingredients the combination of which will form the crux of our calculation. The first piece we need is four dimensional $\mathcal{N} = 1$ super conformal field theory (SCFT), especially quiver theories. In particular we remind the reader of the computations of anomalous dimensions in the beta function. This will be the subject of §7.2. The second piece we need is the so-called "duality trees" which arise from iterative Seiberg-like dualizations of quiver theories. This, with concrete examples from the zeroth del Pezzo, will constitute §7.3. The final piece we need is to recall the rudiments of the Klebanov-Strassler "cascade" for the quiver theory associated to the conifold. We do this in §7.4.

Thus equipped, we examine a simple but illustrative gauge theory in §7.5. This quiver theory arises from D3-branes probing the singular complex cone over the zeroth Hirzebruch surface. We have studied it in detail in Chapters 5 and 6. The duality tree for the conformal phases of the theory form a flower. With the appropriate addition of fractional branes to take us away from conformality, we compute the beta function running in §7.5.2, by determining, using the abovementioned maximization principle, all anomalous dimensions. We will find in §7.5.3 that there is indeed a duality wall, viz., an energy scale beyond which dualities cannot proceed. Interestingly, certain quiver automorphism symmetries can be identified with T-duality-like actions in the dual AdS theory.

Such analyses are well adapted and easily generalizable to arbitrary quiver the-

ories. As a final example, we present the case of the cone over the first del Pezzo surface in §7.6. This case exhibits another interesting phenomenon which we call "toric islands."

We end with concluding remarks and prospects in §7.7.

7.2 Computing Anomalous Dimensions in a SCFT

We devote this section to a summary of beta-functions in 4D $\mathcal{N} = 1$ SCFT and of how to compute in particular the anomalous dimensions. Later, we will make extensive use of the values of these anomalous dimensions.

The necessary and sufficient conditions for a $\mathcal{N} = 1$ supersymmetric gauge theory with superpotential to be conformally invariant, i.e., a SCFT, are (1) the vanishing of the beta function for each gauge coupling and (2) the requirement that the couplings in the superpotential be dimensionless. Both these conditions impose constraints on the anomalous dimensions of the matter fields, that is, chiral operators of the theory. This is because supersymmetry relates the gauge coupling beta functions to the anomalous dimensions of the matter fields due to the form of the Novikov-Shifman-Vainshtein-Zakharov(NSVZ) beta functions. [142, 128].

The examples which we study are a class of SUSY gauge theories known as quiver theories. These have product gauge groups of the form $\prod_i SU(N_{c_i})$ together with N_{f_i} bifundamental matter fields for the i-th gauge factor. There is also a polynomial superpotential. The SCFT conditions for these quiver theories can be written as:

$$\beta_i \sim 3N_{c_i} - N_{f_i} + \frac{1}{2}\sum_j \gamma_j = 0$$

$$-d(h) + \frac{1}{2}\sum_k \gamma_k = 0 \qquad (7.2.1)$$

where β_i is the beta-function for the i-th gauge factor, and γ_j, the anomalous dimensions. The index j labels the fields charged under the j-th gauge group factor while k indexes the fields appearing in the k-th term of the superpotential with coupling h, whose naïve mass dimension is $d(h)$.

These conditions (7.2.1) constitute a linear system of equations. However they do not always uniquely determine the anomalous dimensions because there will be more variables than constraints. One or more of the γ's are left as free parameters. Intriligator and Wecht [102] provided a general method for fixing this freedom in aribitrary 4D SCFT, whereby completely specifying the anomalous dimensions. They showed that the R-charges of the matter fields, which in an SCFT are related to the γ's, are those that (locally) maximize the central charge a of the theory. The central charge a is given in terms of the R-charges by

$$a = \frac{3}{32}(3\text{Tr}R^3 - \text{Tr}R) ,\tag{7.2.2}$$

where the trace is taken over the fermionic components of the vector and chiral multiplets.

In a quiver theory with gauge group $\prod_i SU(N_i)$ and chiral bifundamental multiplets with multiplicities f_{ij} between the i-th and j-th gauge factors (the matrix f_{ij} is the adjacency matrix of the quiver), we can give an explicit expression for (7.2.2) in terms of the R-charges R_{ij} of the lowest components of the bifundamentals

$$a = \frac{3}{32}\left[2\sum_i N_i^2 + \sum_{i<j} f_{ij}N_iN_j\left[3(R_{ij}-1)^3 - (R_{ij}-1)\right]\right] .\tag{7.2.3}$$

Parenthetically, we remark that in some cases, such as the ones to be discussed in §7.4 and §7.5, anomalous dimensions can be fixed by using some discrete symmetries by inspecting the quiver and the form of the superpotential, without the need to appeal to the systematic maximization of a.

Now in (7.2.3) we need to know the R-charges. However, in a SCFT the conformal dimension D of a chiral operator is related to its R-charge by $D = \frac{3}{2}|R|$. Moreover, the relation between D and γ is $D = 1 + \frac{\gamma}{2}$. Therefore we can write the R-charges and hence (7.2.3) in terms of the anomalous dimensions by

$$\frac{3}{2}|R| = 1 + \frac{\gamma}{2} .\tag{7.2.4}$$

134

Therefore, after solving the conformality constraints (7.2.1) we can write a in terms of the still unspecified γ's by (7.2.3) and then maximize it in order to completely determine all the anomalous dimensions.

The freedom in the anomalous dimensions after using the SCFT conditions reflects the presence of non-anomalous $U(1)$ flavor symmetries in the IR theory. Initially, there is one $U(1)$ flavor symmetry for each arrow of the quiver. All the matter fields lying on an arrow have the same charge under this $U(1)$. Now we must impose the anomaly free condition for each node, this is the condition that for the adjacency matrix f_{ij} at the i-th node we have

$$\sum_j f_{ij} N_j = \sum_j f_{ji} N_j \ . \tag{7.2.5}$$

In other words, the ranks of the gauge groups, as a vector, must lie in the integer nullspace of the antisymmetrised adjacency matrix:

$$(f - f^T)_{ij} \cdot \vec{N} = 0 \ . \tag{7.2.6}$$

Indeed the matrix $(f - f^T)$ is the intersection matrix of the quiver in geometrical engineering of these theories (q.v. e.g. [80, 99, 47]). After imposing this condition (7.2.6), we are left with (# of arrows - # of nodes) non-anomalous $U(1)$'s. The invariance of the superpotential reduces their number even more, giving one linear relation between their charges for each of its terms. But the number of independent such relations is not always sufficient to eliminate all the abelian flavor symmetries. The charges of those that still remain in the IR can indeed be read off from the expressions for the anomalous dimensions of the fields in terms of those that remain free after imposing the conditions (7.2.1).

The way in which the charge matrix of the remaining $U(1)$ flavor symmetries appears in this framework is as the matrix of coefficients that express the anomalous dimensions of the bifundamental fields as linear combinations of numerical constants and some set of independent anomalous dimensions. Specifically, suppose we start

with n anomalous dimensions and that the solution to (7.2.1) specifies k of them in terms of the other $n - k$:

$$\gamma_i = \gamma_{0_i} + q_{ij}\gamma_j \quad, \quad i = 1, \ldots, k \quad, \quad j = k + 1, \ldots, n. \tag{7.2.7}$$

The corresponding R-charges are related to the γ's by $R = \frac{\gamma \pm 2}{3}$. The charges of the matter fields under these residual $U(1)$'s from are given by the q_{ij} matrix in (7.2.7). The constants γ_{0_i} are mapped to the test values of R charges. It is important to keep in mind that it is possible to change the basis of $U(1)$'s (correspondingly the set of independent anomalous dimensions), in which case the charge matrix would be modified.

7.3 Duality Structure of SUSY Gauge Theories: Duality Trees

Having reminded ourselves of the methodology of computing anomalous dimensions, we turn to the next ingredient which will prepare us for the cascade phenomenon, viz., the **duality trees** which arise from Seiberg-like dualities performed on the quivers. Duality trees provide an interesting way to encode dual gauge theories and their relations. This construction was introduced in [24], for the specific case of D3-branes probing a complex cone over dP_0, the zeroth del Pezzo surface.

In general, for a quiver theory with adjacency matrix f_{ij} and n gauge group factors, there are n different choices of nodes on which to perform Seiberg duality. In other words, we can dualize any of the n nodes of the quiver to obtain a new one, for which we again have n choices for dualization. We recall that dualization on node i_0 proceeds as follows. Define $I_{in} :=$ nodes having arrows going into i_0, $I_{out} :=$ those having arrow coming from i_0 and $I_{no} :=$ those unconnected with i_0.

1. Change the rank of the node i_0 from N_c to $N_f - N_c$ with $N_f = \sum_{i \in I_{in}} f_{i,i_0} N_i = \sum_{i \in I_{out}} f_{i_0,i} N_i$;

2. $f_{ij}^{dual} = f_{ji}$ if either $i, j = i_0$;

3. Only arrows linking I_{in} to I_{out} will be changed and all others remain unaffected;

4. $f_{AB}^{dual} = f_{AB} - f_{i_0 A} f_{B i_0}$ for $A \in I_{out}$, $B \in I_{in}$;

   If this quantity is negative, we simply take it to mean an arrow going from B to A. This step is simply the addition of the Seiberg dual mesons (as a mass deformation if necessary).

We remark that the fourth of these dualization rules accounts for the antisymmetric part of the intersection matrix, which does not encode bi-directional arrows. Such subtle cases arise when there are no cubic superpotentials needed to give masses to the fields associated with the bi-directional arrows. This situation appears for example in some of the theories studied in [44] and [49].

The subsequent data structure is that of a tree, where each site represents a gauge theory, with n branches emanating therefrom, connecting it to its dual theories. This is called a **duality tree**. We will see that duality trees exhibit an extremely rich structure, with completely distinct topologies for the branches for gauge theories coming from different geometries.

As an introduction, let us recall the simple example considered in [24, 47]. The probed geometry in this case was a complex cone over dP_0. This cone is simply the famous non-compact $\mathbb{C}^3/\mathbb{Z}_3$ orbifold singularity. The generic quiver for any one in the tree of Seiberg dual theories for this geometry will have the form as given in Figure 7-1. The superpotential is cubic because there are only cubic gauge invariant operators in this theory, given by closed loops in the quiver diagram.

Since there are three gauge group factors, there will be three branches coming out from each site in the duality tree. The tree is presented in Figure 7-2. For clarity we colour-coded the tree so that sites of the same colour correspond to equivalent theories, i.e., theories related to one another by some permutation of the gauge groups and/or charge conjugation of all fields in the quiver (in other words theories whose quivers are permutations and/or transpositions of each other). We have also included, the quivers to which the various coloured sites correspond in Figure 7-3.
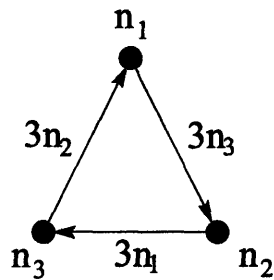
Figure 7-1: Generic quiver for any of the Seiberg dual theories in the duality tree corresponding to a D3-brane probing $\mathbb{C}^3/\mathbb{Z}_3$, the complex cone over dP_0.
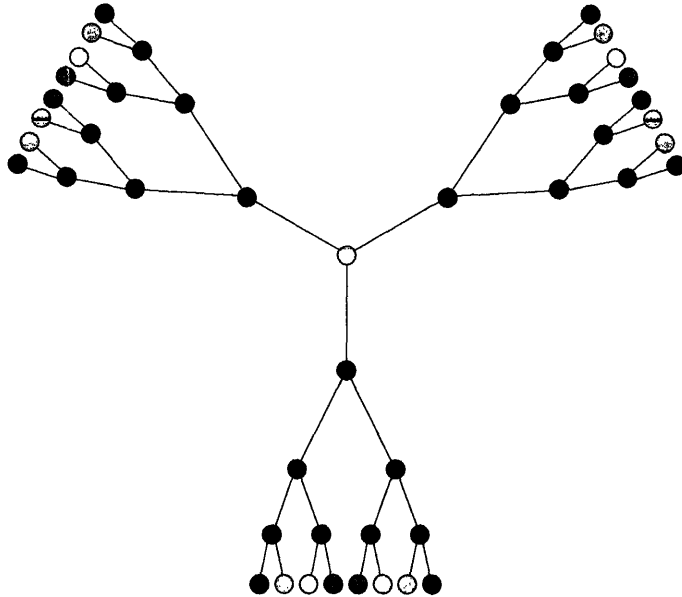
Figure 7-2: Tree of Seiberg dual theories for dP_0. Each site of the tree represents a gauge theory, and the branches between sites indicate how different theories are related by Seiberg duality transformations.

One important invariant associated with an algebraic singularity is the trace of the total monodromy matrix around the singular point. This can typically be recast into an associated Diophantine equation in the intersection numbers, i.e., the f_{ij}'s [29, 36, 47]. This equation captures all the theories that can be obtained by Seiberg duality and hence classifies

From Figure 7-1, we see that there exists a simple relation between the intersection numbers and the ranks of the gauge groups for dP_0, namely for rank (n_1, n_2, n_3), the intersection matrix is given by $3\begin{pmatrix} 0 & n_1 & -n_3 \\ -n_1 & 0 & n_2 \\ n_3 & -n_2 & 0 \end{pmatrix}$. The Diophantine equation in

138
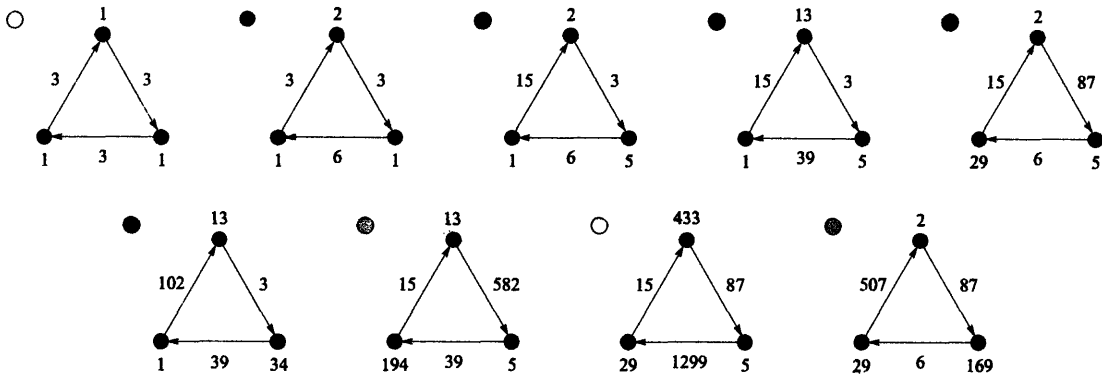
Figure 7-3: Some first cases of the Seiberg dual phases in the duality duality tree for the theory corresponding to a D3-brane probing $\mathbb{C}^3/\mathbb{Z}_3$, the complex cone over dP_0.

terms of the ranks reads

$$n_1^2 + n_2^2 + n_3^2 - 3n_1 n_2 n_3 = 0 \ . \tag{7.3.8}$$

This turns out to be the well-studied Markov equation.

It is important to stress that, up to this point, duality trees do not provide any information regarding RG flows. In fact, if the theories under study are conformal the trees just represent the set of dual gauge theories and how they are interconnected by Seiberg duality transformations within the conformal window. We will extend our discussion about this point in §7.4 and §7.5, where we will obtain non-conformal theories by the inclusion of fractional branes.

7.4 The Conifold Cascade

A famous example of successive Seiberg dualizations is the Klebanov-Strassler cascade in gauge theory [119] associated to the warped deformed conifold [119]. In light of the duality tree structure in the previous section, we now present the third and last piece of preparatory work and summarise some key features of this example, in order to illustrate the concept of duality cascade, as well as to introduce many of the methods and approximations that will be used later.

Let us begin by considering the gauge theory that appears on a stack of N D3-

branes probing the conifold. This theory has an $SU(N) \times SU(N)$ gauge symmetry. The matter content consists of four bifundamental chiral multiplets $A_{1,2}$ and $B_{1,2}$ and the quiver diagram is shown in Figure 7-4. This model has also interactions given by
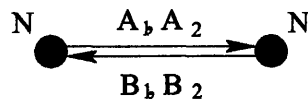
Figure 7-4: Quiver diagram for the gauge theory on N D3-branes probing the conifold.

the following quartic superpotential

$$W = \frac{\lambda}{2} \epsilon^{ij} \epsilon^{kl} \mathrm{Tr} A_i B_k A_j B_l \qquad (7.4.9)$$

for some coupling λ, and where we trace over color indices.

This gauge theory is self dual under Seiberg duality transformations, by applying the duality rules in §7.3. Accordingly, its duality tree is the simplest one, consisting of a single point representing the $SU(N) \times SU(N)$ theory, which transforms into itself when dualizing either of its two gauge groups. This is shown in Figure 7-5.

Figure 7-5: The "duality tree" of the conifold. Its single site represents the standard $SU(N) \times SU(N)$ theory. The closed link coming out the site and returning to it represents the fact that the theory, being self-dual, transforms into itself under Seiberg duality.

We will see below that when we apply the procedure for finding anomalous dimensions outlined in §7.3 to this specific case, taking into account its symmetries, we conclude that all the anomalous dimensions are in fact equal to $-1/2$ and that the theory is conformal, i.e. both the gauge and superpotential couplings have vanishing beta functions and (7.2.1) are satisfied. In order to induce a non-trivial RG flow the theory has to be deformed. A possible way of doing this is by the inclusion of fractional branes [119]. It is straightforward to see what kind of fractional branes can be introduced.

In general, introducing fractional branes is done by determining, for a given quiver, the most general gauge groups consistent with anomaly cancellation. Now recall from (7.2.6), possible ranks of the gauge factors must reside in the integer nullspace of the intersection matrix. Therefore a basis for probe and fractional branes is simply given by a basis for this nullspace. For the conifold, we find that the most general gauge group is $SU(N + M) \times SU(N)$. We will refer to N as the number of **probe branes** and to M as the number of **fractional branes**.

We see that indeed, for any non-vanishing M, there is no possible choice of anomalous dimensions satisfying (7.2.1) and thus we are indeed moving away from the conformal point. This case has been widely studied (see [119, 94, 95] and references therein) and leads to a **duality cascade**. What this means is that at every step in the dualization procedure of this now non-conformal quiver theory, one of the gauge couplings is UV free while the other one is IR free. As we follow the RG flow to the IR, we reach a scale at which the inverse coupling of the UV free gauge factor vanishes. At this point, it is convenient to switch to a more suitable description of the physics, in terms of different microscopic degrees of freedom, by performing a Seiberg duality transformation on the strongly coupled gauge group. This procedure generates the duality cascade when iterated. Indeed, the tree of Figure 7-5 can be interpreted as representing a duality cascade modulo fractional brane contributions.

7.4.1 Moving Away from the Conformal Point

Let us now study this cascade in detail, setting the framework we will later use to analyze cascades for general quiver theories. Recall, from (7.2.1), that a key ingredient required for the computation of the beta functions are the values of the anomalous dimensions. We have already provided a method to compute anomalous dimensions in the absence of fractional branes, that is, in a conformal theory, in §7.2. There is no analogue for such a procedure when the theory is taken away from conformality. However we will assume, for all the theories we will consider, that

$$\gamma = \gamma_c + O(M/N)^2 \,, \tag{7.4.10}$$

141

where γ_c is the value of the given anomalous dimension at the conformal point. This assumption will be justified for various non-trivial examples in Chapter 8, where we construct supergravity solutions dual duality cascades.

The expression (7.4.10) is of great aid to us as it gives us the control over the anomalous dimensions we were pursuing. Inspecting (7.2.1), we see that because the departure of the γ's from their conformal values is of order $(M/N)^2$ at large N, the order (M/N) contributions to the beta functions can be computed simply by substituting the anomalous dimensions calculated at the conformal point into (7.2.1), and using the gauge groups with the M corrections.

Let us be concrete and proceed to compute the cascade for this example. First let us consider the anomalous dimensions at the conformal point where $M = 0$. They are the result of requiring the beta functions for both $SU(N)$ gauge groups and for the single independent coupling in the superpotential to vanish in accordance with (7.2.1). In this case, these three conditions coincide and are reduced to

$$\gamma_{c,A} + \gamma_{c,B} = -1 , \tag{7.4.11}$$

where $\gamma_{c,A}$ (resp. $\gamma_{c,B}$) is the critical value for the anomalous dimension for field A (resp. B). Once we take into account the symmetry condition $\gamma_{c,A} = \gamma_{c,B}$, we finally obtain

$$\gamma_c = -1/2 . \tag{7.4.12}$$

Now let us consider the beta functions for the gauge couplings in the non-conformal case of $M \neq 0$. They are

$$\begin{aligned} SU(N+M) : & \quad \beta_{g_1} = N(1 + \gamma_A + \gamma_B) + 3M \\ SU(N) : & \quad \beta_{g_2} = N(1 + \gamma_A + \gamma_B) + (-2 + \gamma_A + \gamma_B)M. \end{aligned} \tag{7.4.13}$$

Note that there is no solution to the vanishing of these beta functions for $M \neq 0$. Replacing the anomalous dimensions at the conformal point $\gamma_c = -1/2$ in (7.4.13)

we obtain the leading contribution to the beta functions

$$
\begin{aligned}
SU(N+M): \quad & \beta_{g_1} = +3M \\
SU(N): \quad & \beta_{g_2} = -3M \ .
\end{aligned}
\tag{7.4.14}
$$

Since the theory at any point in the cascade is given by the quiver in Figure 7-4 with gauge group replaced by $SU(N + (n+1)M) \times SU(N + nM)$ for some $n \in \mathbb{Z}$ (where the role of the two gauge groups is permuted at every step), we see that the gauge couplings run as shown in Figure 7-6, where the beta function for each gauge group changes from $\pm 3M$ to $\mp 3M$ with each dualization. In Figure 7-6 we use the standard notation to which we adhere throughout this thesis: the squared inverse couplings are denoted as $x_i = 1/g_i^2$ and the logarithm of the scale is $t = \log \mu$.

An important feature of this RG flow is that the separation between successive dualizations in the t axis remains *constant* along the entire cascade. We will see in §7.5.3 how the gauge theory for a D3-brane probing more general geometries, such as a complex cone over the Zeroth Hirzebruch surface, can exhibit a dramatically different behavior.
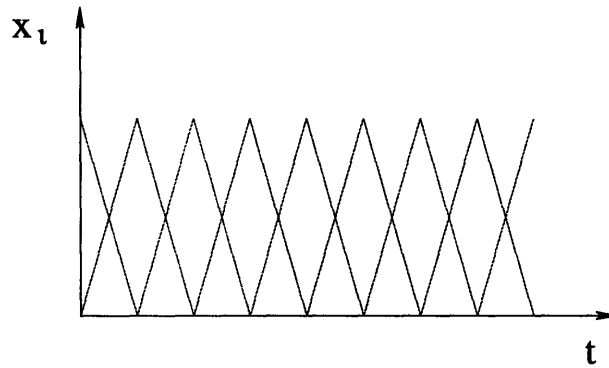
Figure 7-6: Running of the inverse square gauge couplings $x_i = \frac{1}{g_i^2}$, i=1,2. against the log of energy scale $t = \log \mu$, for the conifold. The distance between consecutive dualizations is constant and the ranks of the gauge groups grow linearly with the step in the cascade.

7.5 Phases of F_0

We are now well-equipped with techniques of computing anomalous dimensions, of duality trees and duality cascades. Let us now initiate the study of some more complicated gauge theories. Our first example will be the D-brane probe theory on a complex cone over the zeroth Hirzebruch surface F_0, which is itself simply $\mathbb{P}^1 \times \mathbb{P}^1$. This is a toric variety and the gauge theory was analysed in [45].

There are some reasons motivating the choice of this theory. The first is its relative simplicity. The second is that its Seiberg dual phases generically have multiplicities of bifundamental fields greater than 2, whereby providing some interesting properties. Indeed, from the general analysis of [50, 85], a qualitative change in a RG flow towards the UV behavior is expected when such a multiplicity is exceeded. Finally, as we will discuss later, this theory admits the addition of fractional branes. The presence of fractional branes turns the theory non-conformal, driving a non-trivial RG flow. All together, this theory is a promising candidate for a rich RG cascade structure.

The duality tree in this case is shown in Figure 7-7; we shall affectionately call it the "F_0 flower," of the genus *Flos Hirzebruchiensis* and family *Floris Dualitatis*. We have drawn sites that correspond to different theories with different colours; the colour-coded theories are summarized in Figure 7-8. Since the quiver has four gauge groups, there are four possible ways of performing Seiberg duality and thus there are four branches coming out from each site of the tree. The number on each branch corresponds to the node which was dualised. A novel point that was not present in the tree for dP_0 is the existence of **closed loops**.

The possible existence of RG flows corresponding to these closed loops is constrained by the requirement that the number of degrees of freedom decreases towards the IR, in accordance to the a-conjecture/theorem. As it was stressed for the dP_0 and the conifold examples, the duality tree for F_0 merely represents the infinite set of conformal theories which are Seiberg duals. Non-vanishing beta functions and the subsequent RG flow are generated when fractional branes are included in the system. We reiterate this point: *the duality tree describes duality cascades modulo fractional*

branes. In other words, it represents a "projection" of actual cascades to the space of vanishing fractional branes.
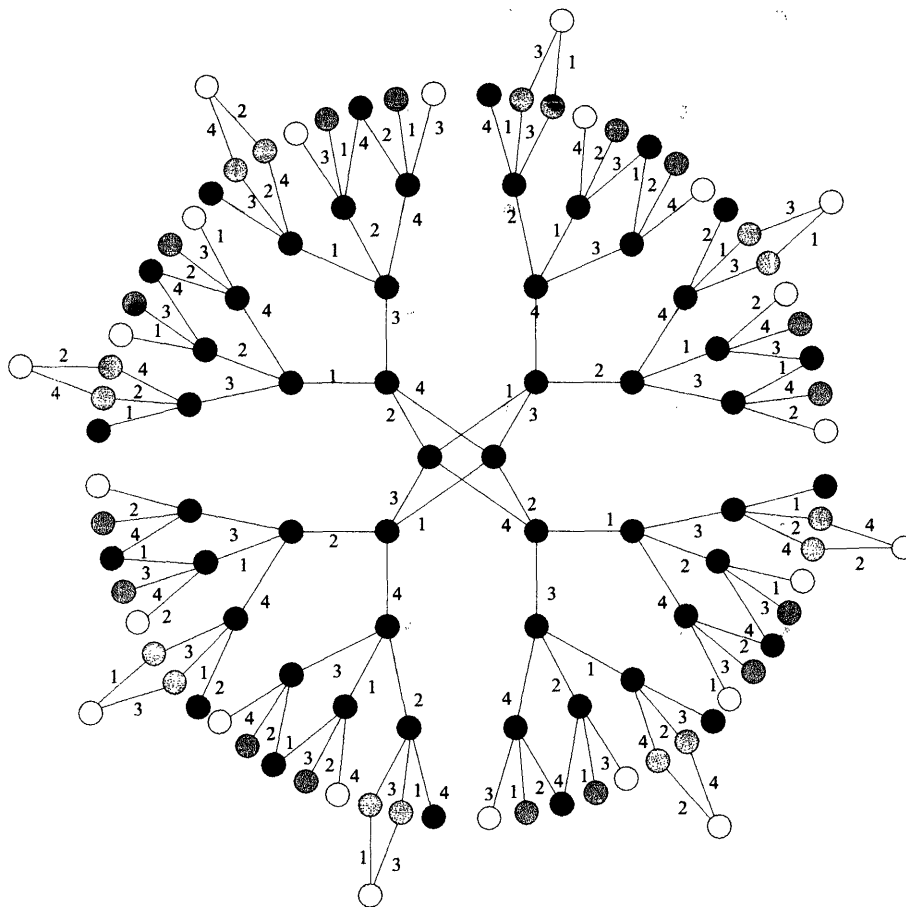
Figure 7-7: The "duality tree" of Seiberg dual theories for F_0, it is in the shape of a "flower," the *Flos Hirzebruchiensis.*

7.5.1 F_0 RG flows

In this section we will follow the RG flow towards the UV of the theory living on D3-branes probing F_0, with the addition of fractional branes to obtain a non-conformal theory. As in the conifold example, the possible anomaly free probe and fractional branes are determined by finding the integer null space of the intersection matrix that defines the quiver (7.2.6). This can be done for any of the dual quivers that appear in the duality tree, but the natural choice is the simplest of the F_0 quivers as was done in [47] which is shown in Figure 7-8 as the first one (blue dot). The intersection
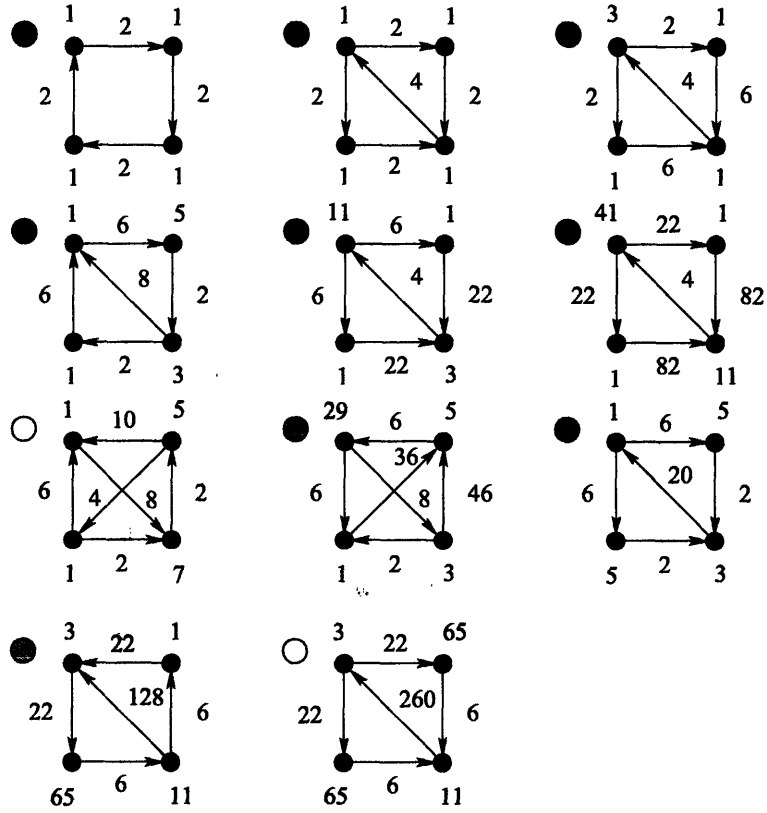
Figure 7-8: Some Seiberg dual phases for F_0.

matrix for this quiver is given by

$$A_{ij} = \begin{pmatrix} 0 & 2 & 0 & 0 \\ 0 & 0 & 2 & 0 \\ 0 & 0 & 0 & 2 \\ 2 & 0 & 0 & 0 \end{pmatrix} \Rightarrow f_{ij} = \begin{pmatrix} 0 & 2 & 0 & -2 \\ -2 & 0 & 2 & 0 \\ 0 & -2 & 0 & 2 \\ 2 & 0 & -2 & 0 \end{pmatrix} . \qquad (7.5.15)$$

A suitable basis for the nullspace of (7.5.15) is $v_1 = (1,1,1,1)$ and $v_2 = (0,1,0,1)$. Therefore, the most generic ranks for the nodes in the quiver, consistent with anomaly cancellation, are

$$(n_1, n_2, n_3, n_4) = N(1,1,1,1) + M(0,1,0,1) . \qquad (7.5.16)$$

Following the discussion in §7.4, we will refer to N as the number of probe branes and M as the number of fractional branes. The theory is then conformal for $M = 0$

and non-conformal otherwise. For $M \neq 0$, there will exist an RG cascade. The specific path to the UV is determined by the initial conditions of the flow, namely the gauge couplings at a given scale Λ_0. As we will see, very different qualitative behaviours can be obtained, depending on these initial conditions.

Under the approximation in (7.4.10), the procedure outlined in §7.2 can be applied to determine the conformal anomalous dimensions, which then can be used to work out the beta functions in the limit $M/N \ll 1$ and study the running of the gauge couplings as we flow to the UV. Let us do so in detail. The beta-functions in (7.2.1), for a quiver theory with k gauge group factors, ranks $\{n\}_i$, adjacency matrix A_{ij} and loops indexed by h corresponding to gauge invariant operators that appear in the superpotential, now becomes

$$
\begin{aligned}
\beta_{i \in \text{nodes}} &= 3n_i - \frac{1}{2}\sum_{j=1}^{k}(A_{ij} + A_{ji})n_j + \frac{1}{2}\sum_{j=1}^{k}(A_{ij}\gamma_{ij} + A_{ji}\gamma_{ji})n_j \\
\beta_{h \in \text{loops}} &= -d(h) + \frac{1}{2}\sum_{h}\gamma_{h_i h_j} \ ,
\end{aligned}
\tag{7.5.17}
$$

where in the second expression $\beta_{h \in \text{loops}}$ associated with the terms in the superpotential, the index in the sum over $\gamma_{h_i h_j}$ means consecutive arrows in a loop and $d(h)$ is determined by 3 minus the number of fields in the loop.

We will make liberal use of (7.5.17) throughout. For our example for the first phase of F_0, the ranks $(n_1, n_2, n_3, n_4) = (1, 1, 1, 1)$, together with intersection matrix from (7.5.15), (7.5.17) reads

$$
\begin{aligned}
&1 + \gamma_{1,2} + \gamma_{4,1} = 0, \quad 1 + \gamma_{1,2} + \gamma_{2,3} = 0, \quad 1 + \gamma_{2,3} + \gamma_{3,4} = 0, \\
&1 + \gamma_{3,4} + \gamma_{4,1} = 0, \quad 1 + \tfrac{1}{2}(\gamma_{1,2} + \gamma_{2,3} + \gamma_{3,4} + \gamma_{4,1}) = 0 \ ,
\end{aligned}
\tag{7.5.18}
$$

which affords the solution

$$
\{\gamma_{1,2} \to -1 - \gamma_{4,1}, \quad \gamma_{2,3} \to \gamma_{4,1}, \quad \gamma_{3,4} \to -1 - \gamma_{4,1}\} \ .
\tag{7.5.19}
$$

We see that there is one undetermined γ. To fix this we appeal to the maximization

147

principle presented in §7.2. The central charge (7.2.3) now takes the form (where $\gamma_{4,5}$ is understood to mean $\gamma_{4,1}$.

$$a = \frac{3}{4} + \frac{1}{16} \sum_{i=1}^{4} \left(1 + \frac{\left(-1 + \gamma_{i,i+1}\right)^3}{3} - \gamma_{i,i+1} \right) . \qquad (7.5.20)$$

Upon substituting (7.5.19) into (7.5.20), we obtain

$$a(\gamma_{4,1}) = -\frac{3}{8}\left(-2 + \gamma_{4,1} + \gamma_{4,1}^2\right) , \qquad (7.5.21)$$

the maximum of which occurs at $\gamma_{4,1} = -\frac{1}{2}$. And so we have, upon using (7.5.19),

$$\gamma_{1,2} = \gamma_{2,3} = \gamma_{3,4} = \gamma_{4,1} = -1/2 . \qquad (7.5.22)$$

Let us remark, before closing this section, that there is an alternative, though perhaps less systematic, procedure to determine anomalous dimensions that does not rely on the maximization of a. For every theory in the F_0 cascade the space of solutions to (7.5.18) is one dimensional. Fixing this freedom at any given point determines the anomalous dimensions in the entire duality tree. Maximization of the central charge a is a possible way of determining this free parameter. For F_0, a simple alternative is to make use of the symmetries of the theory (quiver and superpotential). Our theory (7.5.15) for example, instantly has all γ's equal by the $\mathbb{Z}_4$ symmetry of the quiver. Therefore, in conjunction with the solutions (7.5.19) to conformality, gives (7.5.22) as desired. Once the anomalous dimensions of theory (7.5.15) are determined, the freedom that existed in the conformal solutions of all the dual theories is fixed. This is done by matching the scaling dimensions of composite Seiberg mesons every time a Seiberg duality is performed and/or by noting that the anomalous dimensions of fields that are neutral under the dualized gauge group are unchanged.

7.5.2 Closed Cycles in the Tree and Cascades

Now we wish to find the analogue of the conifold cascade in §7.4 here. For this we wish to look for **closed cycles** in the duality tree (Figure 7-7). In the conifold case the theory was self dual and we cascaded by adding appropriate fractional branes. Here we do indeed see a simple cycle involving 2 sites (namely the blue and the dark green). We will call these two theories models A and B respectively and draw them in Figure 7-9. Model A is the example we addressed above.
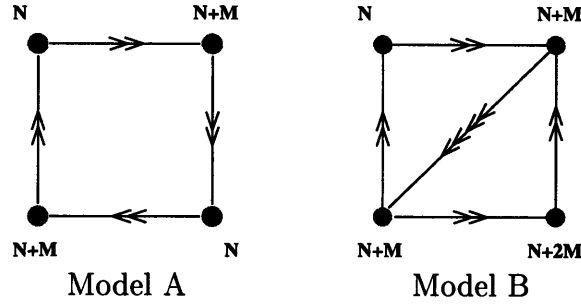
Model A   Model B

Figure 7-9: Quivers for Models A and B. Model A corresponds to the choice of ranks $(n_1, n_2, n_3, n_4)_A = N(1,1,1,1) + M(0,1,0,1)$, from which model B is obtained by dualizing node 3. It has ranks $(n_1, n_2, n_3, n_4)_B = N(1,1,1,1) + M(0,1,2,1)$.

The starting point will be model A, its superpotential and the set of gauge couplings at a scale Λ_0. We recall from (7.5.22) that the anomalous dimensions at the conformal point are $\gamma_{1,2} = \gamma_{2,3} = \gamma_{3,4} = \gamma_{4,1} = -1/2$. This leads to the following values for the beta functions for the 4 gauge group factors:

$$\beta_1 = -3M \qquad \beta_2 = 3M$$
$$\beta_3 = -3M \qquad \beta_4 = 3M \ . \tag{7.5.23}$$

These beta-functions are constants, which means that the running of x_i, the inverse squared couplings as a function of the log scale is linear, with slopes given by (7.5.23). Let us thus run x_i to the UV accordingly. We see that β_1 and β_3 are negative so at some point the inverse couplings for the first or the third node will reach 0. Which of them does so first depends on the value of the initial inverse couplings we choose for n_1 and n_3. We dualise the node for which the inverse coupling first reaches 0, say

node 3. This will give us Model B. If instead node 1 has the inverse coupling going to 0 first, we would dualise on 1 and obtain a theory that is equivalent to Model B after a reflection of the quiver (we can see this from Figure 7-7).

Next we compute the anomalous dimensions for Model B at the conformal point. In analogy to (7.5.18) and (7.5.20) we now obtain $\gamma_{1,2} = \gamma_{3,2} = \gamma_{4,3} = \gamma_{4,1} = -1/2$ and $\gamma_{2,4} = 1$, which gives the beta functions for the next step:

$$
\begin{aligned}
\beta_1 &= -3M & \beta_2 &= 0 \\
\beta_3 &= 3M & \beta_4 &= 0 \ .
\end{aligned}
\tag{7.5.24}
$$

From these we run the couplings at this stage again, find the node for which the inverse coupling first goes to 0. And dualize that node. We see a remarkable feature in (7.5.24). To the level of approximation that we are using, only the first gauge group factor has a negative beta function. This implies that the next node to be dualized is precisely node 1. Performing Seiberg duality thereupon takes us to a quiver that is exactly of the form of Model A, only with the ranks differing in contributions proportional to M, i.e., different fractional brane charges.

By iterating this procedure it is possible to see that the entire cascade corresponds to a chain that alternates between type A and type B models. Furthermore, the length of the even steps of the cascade, measured on the $t = \log \mu$ axis is constant. The same statement applies to the length of the odd steps. This cascade is presented in Figure 7-10 for the initial conditions $(x_1, x_2, x_3, x_4) = (2, 1, 1, 0)$.

7.5.3   Duality wall

We have seen in §7.5.2 that models A and B form a closed cascade and are not connected to the other theories in the F_0 duality tree by the RG flow, regardless of initial conditions. This motivates the study of duality cascades having other Seiberg dual theories as their starting points. The simplest choice corresponds to the model in Figure 7-11. This theory is obtained from Model A by Seiberg dualizing node 2 followed by 1. We will call this Model C.
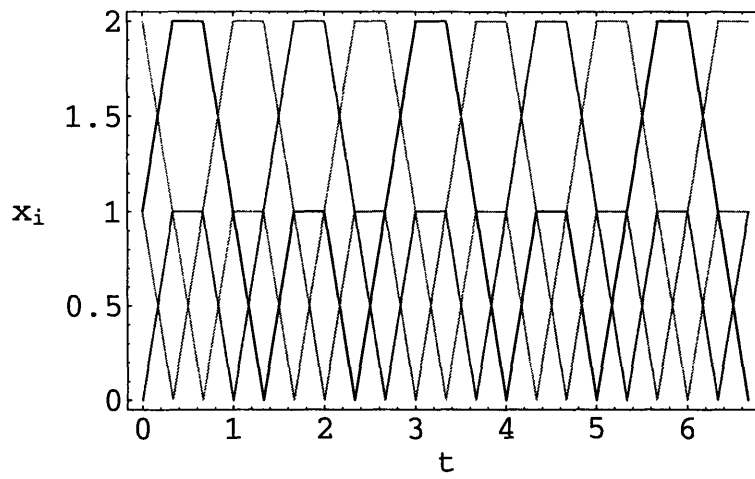
Figure 7-10: Duality cascade alternating between the A and B toric models. The colouring scheme is such that orange, black, green, and red respectively represent nodes 1, 2, 3 and 4.
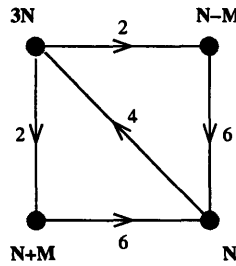
Figure 7-11: Model C for the F_0 theory. It is obtained from dualising node 2 and then 1 from the simplest Model A.

Decreases in the Step

Applying the formalism developed in previous sections we can proceed to compute, for any initial condition, the RG cascade as the theory evolves to the UV. The starting point is the computation of the anomalous dimensions for Model C at the conformal point. These, by the techniques above, turn out to be $\gamma_{1,2} = \gamma_{1,4} = -3/2$, $\gamma_{2,3} = \gamma_{4,3} = 5/2$ and $\gamma_{3,1} = -1$. Using them to calculate the beta functions, we obtain

$$\begin{array}{ll} \beta_1 = 0 & \beta_2 = -3M \\ \beta_3 = 0 & \beta_4 = 3M \ . \end{array} \tag{7.5.25}$$

With these let us evolve to the UV. Let us first consider the case in which the initial condition for the inverse gauge couplings are $(x_1, x_2, x_3, x_4) = (1, 1, 1, 0)$. Figure 7-12

151

shows the evolution of the four inverse gauge couplings both as a function of the step in the cascade and as a function of the logarithm of the scale. An interesting feature

Couplings vs. step
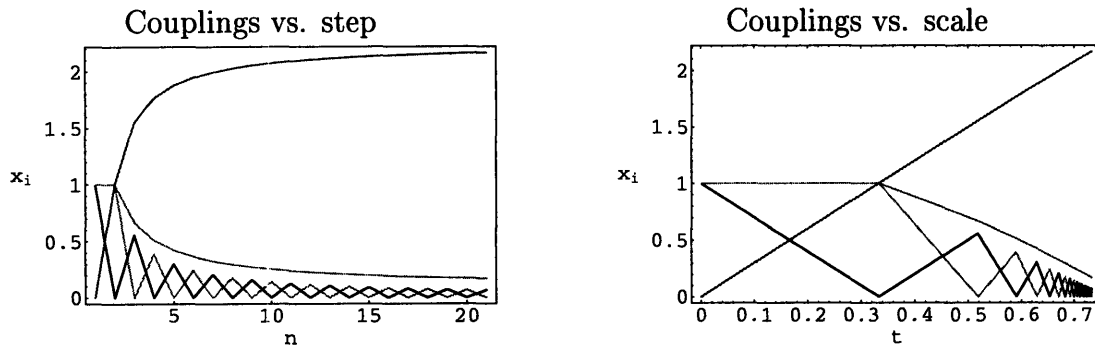
Couplings vs. scale

Figure 7-12: Evolution of gauge couplings with (a) the step in the duality cascade and (b) the energy scale for initial conditions $(x_1, x_2, x_3, x_4) = (1, 1, 1, 0)$. The colouring scheme is such that orange, black, green, and red respectively represent nodes 1, 2, 3 and 4.

is that the distance, Δ_i, between successive dualizations is monotonically decreasing. This marks a departure from the behaviors observed in the conifold cascade and from the example presented in §7.5.2, where Δ_i remained constant (cf. Figure 7-6). However, this fact does not necessarily mean the convergence of the dualization scales. Indeed, we plot the intervals Δ_i in Figure 7-13.a while Figure 7-13.b shows the resulting dualization scales. The slope of this curve is decreasing, reflecting the

Δ vs. step

Scale vs. step
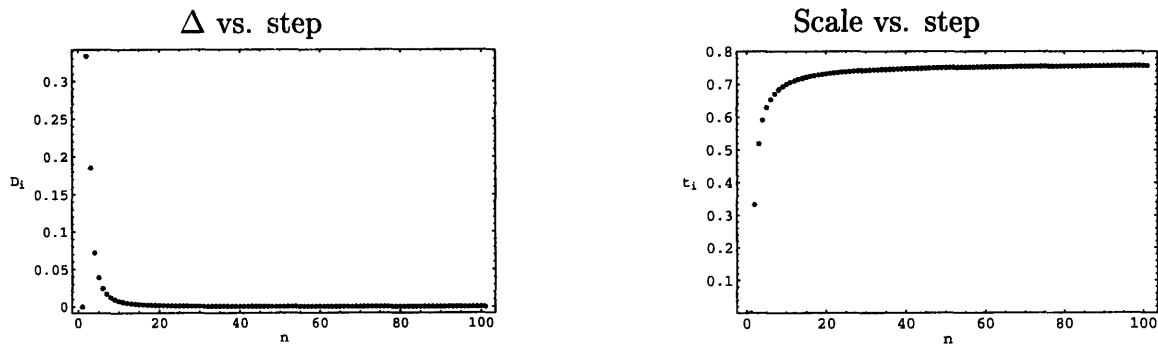
Figure 7-13: The evolution of Δ, the size of the increment during each dualization and the energy scale increase as we dualise, for the initial conditions $(x_1, x_2, x_3, x_4) = (1, 1, 1, 0)$.

decreasing behavior of Δ_i. Nevertheless, *ad infinitum*, the scale may in principle diverge. In Section 8.3, we perform an analytical study of this cascade and show that for this initial conditions the dualization scales are convergent.

A Duality Wall

Let us now consider a different set of initial conditions, given by $(x_1, x_2, x_3, x_4) = (1, 1, 4/5, 0)$. The flow of the inverse couplings is now shown in Figure 7-14.
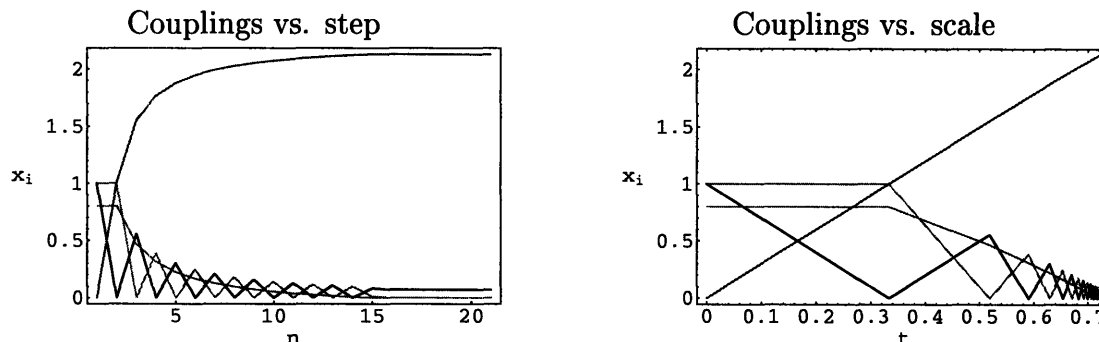
Figure 7-14: Evolution of gauge couplings with (a) the step in the duality cascade and (b) the energy scale for initial conditions $(x_1, x_2, x_3, x_4) = (1, 1, 4/5, 0)$. The colouring scheme is such that orange, black, green, and red respectively represent nodes 1, 2, 3 and 4.

A completely new phenomenon appears in this case. Something very drastic happens after the 14-th step in the cascade. As a consequence of lowering the initial value of x_3, the third node gets dualized at this step, producing an explosive growth of the number of chiral and vector multiplets in the quiver. This statement can be made precise: *at the 14-th step node 3 is dualized and the subsequent quivers have all their intersection numbers greater than 2.* In this situation the results of [50, 85] suggest that a duality wall is expected. This phenomenon is characterized by a flow of the dualization scales towards an UV *accumulation point* with an exponential divergence in the number of bifundamental fields and ranks of the gauge groups.

This asymptotic behavior can be inferred once Seiberg dualities are interpreted as Picard-Lefschetz monodromy transformations which we discuss in Section 8.3

Figure 7-14 shows a very small running of the gauge couplings beyond this point. This is not due to a vanishing of the beta functions, but to the extreme reduction of the length of the Δ_i intervals.
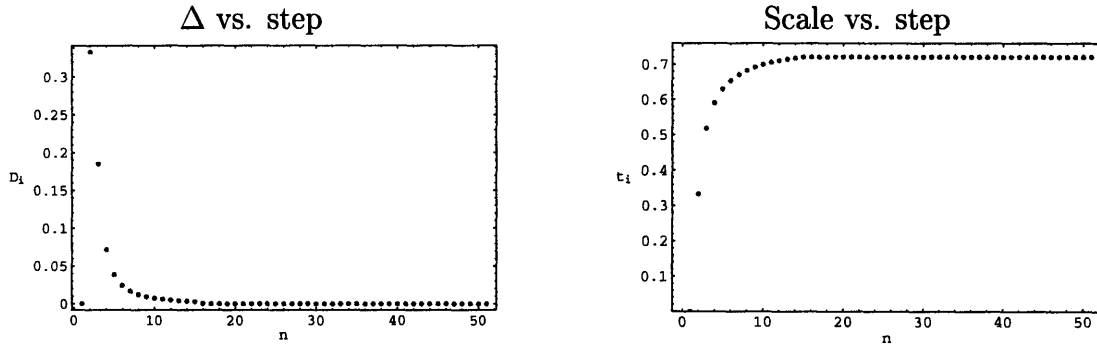
Figure 7-15: The evolution of Δ, the size of the increment during each dualization and the energy scale increase as we dualise, for the initial conditions $(x_1, x_2, x_3, x_4) = (1, 1, 4/5, 0)$.

In contrast to Figure 7-13, for the initial conditions $(1, 1, 4/5, 0)$, we have drawn the plots in Figure 7-15.a and Figure 7-15.b. Both of them indicate that a limiting scale which cannot be surpassed is reached as the theory flows towards the UV. This is precisely what we call a **duality wall.**

7.5.4 Location of the Wall

We have just seen that starting from the quiver in Figure 7-11 for F_0 with initial conditions $(x_1, x_2, x_3, x_4) = (1, 1, 4/5, 0)$ a duality wall is reached. Let us briefly examine the sensitivity of the location of the duality wall to the initial inverse couplings.

Let our initial inverse gauge couplings be $(1, x_2, x_3, 0)$, with $0 < x_2, x_3 < 1$, and we repeat the analyses in the previous two subsections. We study the running of the beta functions, and determine the position of the duality wall, t_{wall}, for various initial values. We plot in Figure 7-16, the position of the duality wall against the initial values x_2 and x_3, both as a three-dimensional plot in I and as a contour plot in II. We see that the position is a step-wise function. A similar behavior has been observed in [85] for dP_0 in the case of vanishing anomalous dimensions.

154

(I)   (II)
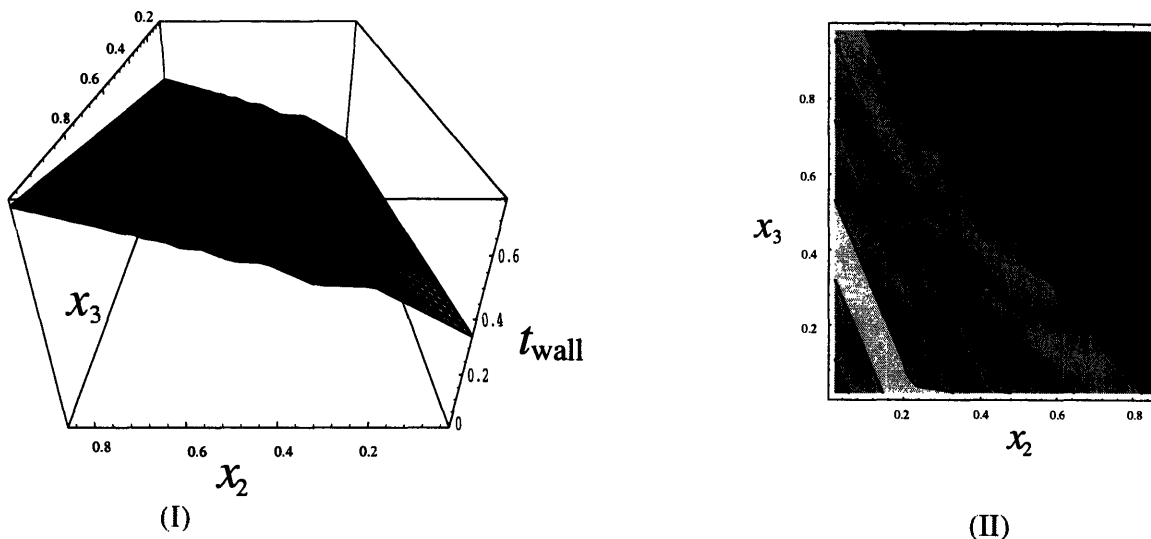
Figure 7-16: A plot of the position t_{wall} against the initial gauge coupling values $(1, x_2, x_3, 0)$. (I) is the 3-dimensional plot and (II) is the contour plot versus x_2 and x_3.

7.5.5   A $\mathbb{Z}_2$ Symmetry as T-Duality

A remarkable symmetry seems to be captured by the gauge theory discussed above. Suppose that, starting from Model C, we had decided to follow the RG flow towards the IR instead of the UV. There is a simple trick that accomplishes this task, namely to look at the flow to the the UV of a theory in which the beta functions have changed sign and where the log-scale t has been replaced by $-t$. Since we are considering beta functions that are linear in the number of fractional branes M, changing the sign of the beta functions can be interpreted as changing M to $-M$. However, upon inspecting Figure 7-11, we see that $M \leftrightarrow -M$ is nothing more than a $\mathbb{Z}_2$ reflection of the quiver along the (13) axis. Therefore, the flow to the IR that starts from Model C is simply the flow to the UV of its $\mathbb{Z}_2$ reflection. Therefore, the whole cascade we have already computed also describes, up to this reflection, the cascade to the IR.

Let us elaborate on the origin of this $\mathbb{Z}_2$ symmetry. In the holographic dual of the gauge theory, the energy scale μ is typically associated to a radial coordinate R. Then, transforming $t = \log \mu$ to $-t$ corresponds to an inversion of the radial coordinate $R \leftrightarrow 1/R$ in the holographic dual theory. Therefore this $\mathbb{Z}_2$ symmetry displayed by the gauge theory RG flow indicates a $\mathbb{Z}_2$ T-duality-like symmetry of string theory on

the underlying geometry. The scale of model C can then be interpreted as the self dual radius of the dual holographic theory. This holographic theory then exhibits a minimal length beyond which there are no further new phenomena. Every physical quantity at a scale less than this scale can be expressed in terms of a different physical quantity by applying the $\mathbb{Z}_2$ action described above. It will be very interesting to explore this symmetry further.

7.6 Phases of dP_1

We have initiated the study of duality walls for general quiver theories and in the foregoing discussion analysed in detail the illustrative example of the cone over the zeroth Hirzebruch surface. It is interesting to extend the construction of duality trees to other gauge theories and the structures and RG flows that may emerge.

Let us briefly consider perhaps the next simplest case, viz., the gauge theory on a D3-brane probing a complex cone over dP_1, the first del Pezzo surface, which is $\mathbb{P}^2$ blown up at 1 point. This is again a toric variety and the theory has been extensively studied [45, 43]. There is only one toric phase in this case[1] , whose quiver is shown in Figure 7-17; the ranks are $(1,1,1,1)$. This model is self-dual under the
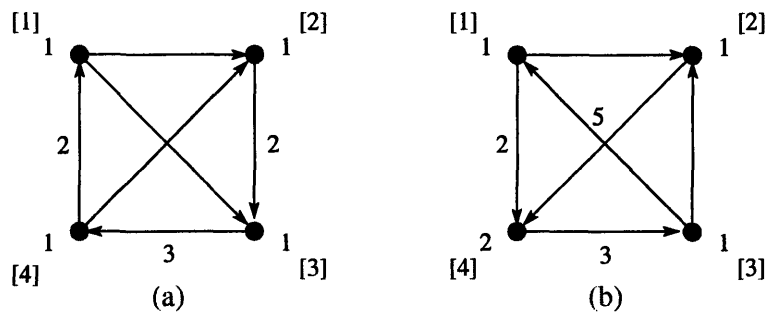
Figure 7-17: The quivers for the gauge theory arising from dP_1. (a) is the toric phase while (b) is obtained from (a) by dualising either node 3 or 4 and is a non-toric phase. The ranks of the nodes are denoted by blue square brackets.

dualizations of nodes 1 or 2, and is transformed into a theory with gauge group $SU(2N) \times SU(N) \times SU(N) \times SU(N)$ when dualizing any of the other two nodes.

_____

[1]We follow here the nomenclature of [43], where a theory was denoted toric if it had all its gauge group factors equal to $U(N)$, i.e., all the ranks are equal.

Again using the notation of (7.5.16), we denote the ranks in the conformal case, as $(2, 1, 1, 1)$. The duality tree obtained by taking into account these two models is shown in Figure 7-18. The encircled theory is the one in Figure 7-17.a and each link shows the associated dualized node. Other Seiberg dualizations of the $(2, 1, 1, 1)$ model lead to $(5, 2, 1, 1)$ and $(4, 2, 1, 1)$ theories. We have not included them in Figure 7-18 for simplicity.

● (1,1,1,1)
● (2,1,1,1)
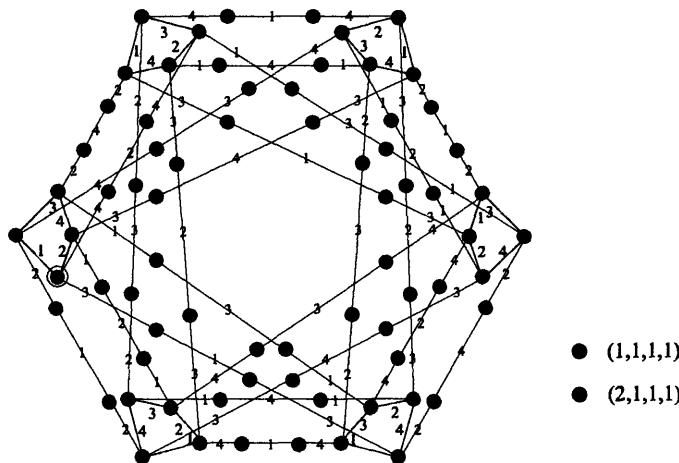
Figure 7-18: The tree of Seiberg dual theories for dP_1. There are six toric islands (sets of blue sites) in this tree.

Already at this level we can see that the duality space of dP_1 is very rich, exhibiting a phenomenon that we will call **"toric islands"** (isolated sets of toric models). Furthermore, the abundance of closed loops makes it quite different from the dP_0 and F_0 cases. The appearance of a six-fold multiplicity of islands is a result of the combinatorics that gives the possible reorderings of a given quiver. Explicitly, the number of possible re-orderings of the four nodes in the toric quiver is $4! = 24$. After grouping these toric models in islands of four, we are led to the six expected islands.

7.7 Conclusions and Prospects

In applying some recent technology to the classic conifold cascade phenomenon [119], we have here studied how duality walls arise in string theory. Endowed with the systematic methods from toric duality [45, 43] and maximization principles in de-

termining anomalous dimensions in arbitrary four-dimensional SCFT's [102, 103], we have re-examined the ideas of [50, 85] by supplanting complete anomalous dimensions to the beta functions, emerging under a fully string theoretic realization.

Indeed, armed with the vast database of "duality trees" encoding various (generalized) Seiberg dual phases of four-dimensional SCFT $\mathcal{N} = 1$ gauge theories that live on world-volumes of D3 branes probing various singular geometries, we have outlined a general methodology of analysing cascading phenomena and finding duality walls. At liberty to take advantage of the well-studied toric singularties, we have used the enlightening example of the theory corresponding to the complex cone over the zeroth Hirzebruch surface F_0. We have shown how one adds fractional branes to take the theory out of conformality and hence obtain a nontrivial running of the (inverse) gauge couplings. Thereafter, by either symmetry arguments [43] or maximization of central charge a [102], one could determine the exact form of the NSVZ beta-functions, in the limit where the number of physical branes is much larger than that of fractional ones. We have then shown how to apply this running to consecutive applications of Seiberg duality.

We find, when one identifies appropriate "closed cycles" in the tree, generalization of the conifold cascades. We also find the existence of "duality walls" (cf. Figure 7-14). This occurs whenever subsequent applications of the duality (cascade) result in the rapid decrease in the evolution, towards the UV, of the interval between dualizations, whereby creating an accumulation point onto which all asymptotic values of the couplings pile. Such a wall signifies a finite energy scale beyond which Seiberg dualities cannot proceed.

An interesting appearance is played by the $\mathbb{Z}_2$ symmetry which the beta function equations exhibit and the non-trivial action on the scale. This action simply inverts the scale and defines a critical scale, say 1, at which there is a reflection point in the physics. All phenomena above this scale are related to those below it. In the dual geometry this is reminiscent of the familiar T-duality and the critical scale corresponds to the self-dual radius of T-duality. The position of the wall is sensitive to the initial conditions, viz., the values of the gauge couplings, and exhibits a step-wise behaviour

with respect to them (cf. Figure 7-15). In next section we will study this dependence on initial conditions analytically.

Of course, our example is but the simplest of a wide class of theories. We have briefly touched upon a more involved case of the cone over the first del Pezzo surface. There, interesting "toric islands" appear, giving an even richer structure for the cascade. Several new cascades, showing widely different phenomena, will be constructed in coming sections.

Chapter 8

Chaotic Duality in String Theory

We investigate the general features of renormalization group flows near superconformal fixed points of four dimensional $\mathcal{N} = 1$ gauge theories with gravity duals. The gauge theories we study arise as the world-volume theory on a set of D-branes at a Calabi-Yau singularity where a del Pezzo surface shrinks to zero size. Based mainly on field theory analysis, we find evidence that such flows are often chaotic and contain exotic features such as duality walls. For a gauge theory where the del Pezzo is the Hirzebruch zero surface, the dependence of the duality wall height on the couplings at some point in the cascade has a self-similar fractal structure. For a gauge theory dual to $\mathbb{P}^2$ blown up at a point, we find periodic and quasi-periodic behavior for the gauge theory couplings that does not violate the a conjecture. Finally, we construct supergravity duals for these del Pezzos that match our field theory beta functions. This chapter is based on [61].

8.1   Introduction and Summary

In the previous chapter, we have considered duality cascades for a class of non-spherical horizons which are $U(1)$ bundles over the del Pezzo surfaces [85, 56]. We have observed that, in some cases, these theories exhibit a behavior that differs dramatically from the KS flow.

The numerical studies of Chapter 7 have convinced us that, sensitive to the type

of geometry as well as initial conditions, the quivers after a large number of Seiberg dualities may become hyperbolic in the language of [50]. After this, a finite energy scale is reached beyond which duality cannot proceed. This phenomenon has been dubbed a "duality wall".

In this chapter we elucidate some aspects of flows, cascades, and walls for gauge theories arising from these more general geometries using both field theory and SuGRA techniques. To begin with, a more systematic, and where possible, analytic investigation of the duality wall phenomenon is clearly beckoning. For this purpose, we will use the exceptional collection techniques that become particularly conducive for the del Pezzo surfaces [24], especially for computing the beta functions and Seiberg dualities [93, 97]. We review these matters synoptically in Section 8.2. In particular, we will formulate the general RG cascade as motion and reflections in certain **simplices** in the space of gauge couplings.

Thus girt with the analytic form of the beta functions and Seiberg duality rules [56, 93, 85], we show in Section 8.3 the existence of the duality wall at finite energy analitically. As an illustrative example, we focus on F_0, the zeroth Hirzebruch surface. In the numerical studies of Chapter 7, two types of cascading behavior were noted for F_0. Depending on initial values of couplings, one type of cascade readily caused the quiver to become hyperbolic and hence an exponential growth of the ranks, whereby giving rise to a wall. The other type, though seemingly asymptoting to a wall, was not conclusive from the data. As an application of our analytic methods, we show that duality walls indeed exist for both types and give the position thereof as a function of the initial couplings. These results represent the first example in which the position of a duality wall along with all the dual quivers in the cascade have been analytically determined. Thus, we consider it to be an interesting candidate to attempt the construction of a SuGRA dual. Interestingly, the duality wall height function is piece-wise linear [85, 56] and "fractal." A highlight of this chapter will be the demonstration that a **fractal** behavior is indeed exhibited in such RG cascades. As we zoom in on the wall-position curve, a self-similar pattern of concave and convex cusps emerges.

162

Inspired by this **chaotic behavior**, we seek further in our plethora of geometries for signatures of chaos. Moving onto the next simplest horizon, namely that of the dP_1, the first del Pezzo surface, we again study the analytic evolution of the cascade in detail. Here, we find Poincaré cycles for trajectories of gauge coupling pairs. The shapes of these cycles depend on the initial values of couplings. For some ranges, beautiful elliptical orbits emerge. This type of behavior is reminiscent of the attractors and Russian doll renormalization group flow discussed in [137, 126]. This example constitutes Section 8.4.

Finally, in Section 8.5, we move on to the other side of the AdS/CFT Correspondence and attempt to find SuGRA solutions. We rely upon the methodologies of [72] to construct solutions that are analogous to those of Klebanov and Tseytlin (KT) [120] for the conifold. The fact that explicit metrics for cones over del Pezzo surfaces are not yet known (except for dP_1 [63]) is only a minor obstacle. We are able to write down KT-like solutions, complete with the warp factor, as an explicit function of the Cartan matrices of the exceptional algebra associated with the del Pezzo.

These SuGRA solutions should be dual to field theory cascades that are similar to the original KS cascade. Identifying the precise SuGRA phenomenon which marks the duality wall remains an open and tantalizing quest.

We would like to stress the importance of possible corrections to the R-charges of the matter fields, and hence to the anomalous dimensions and beta functions. We will see that in order to be able to follow the RG cascades accurately, we need to be able to assume that the R-charges are corrected only at order $\mathcal{O}(M/N)^2$ where M is the number of D5-branes, N the number of D3-branes, and M/N a measure of how close we are to the conformal point $M = 0$. In the case of the conifold, the gauge theory possessed a $\mathbb{Z}_2$ symmetry which forced the $\mathcal{O}(M/N)$ corrections to vanish. Our del Pezzo gauge theories generally lack such a symmetry.

We have two arguments to address these concerns. First, for KS type cascades, our SuGRA solutions beta functions precisely, severely constraining any possible M/N corrections to the R-charges. For more complicated cascades involving duality walls, we lack SuGRA solutions. Nevertheless, we shall push ahead, assuming that eventu-

ally appropriate supergravity solutions will be found and that R-charge corrections, even if $\mathcal{O}(M/N)$, will not change the qualitative nature of our results. The flows which we shall soon present are so interesting that we think it worthwhile to describe them in their current, though less than fully understood state. An analogy can be made to the Navier-Stokes equation. Turbulence is observed in fluids in many different situations but is very difficult to model exactly. Instead, people have developed simple models, such as Feigenbaum's quadratic recursion relation, to understand certain qualitative features, such as period doubling. In some sense, the flows we present here are in relation to the real RG flows as Feigenbaum's analysis is to the real Navier-Stokes equation.

8.2 A Simplicial View of RG Flow

In preparation for our discussions on Renormalization Group (RG) flow in the gauge theory duals to del Pezzo horizons, we initiate our study with an abstract and recollective discussion of RG flows and duality cascades.

8.2.1 The Klebanov-Strassler Cascade

The Klebanov-Strassler (KS) flow [119] provides our paradigm for an RG cascade. In the KS flow, one starts with an $\mathcal{N} = 1$ $SU(N) \times SU(N + M)$ gauge theory with bifundamental chiral superfields A_i and B_i, $i = 1, 2$ and a quartic superpotential. The couplings associated with the two gauge groups we shall respectively call g_1 and g_2. This quiver theory can be geometrically realized as the world-volume theory of a stack of N coincident D3-branes together with M D5-branes probing a conifold singularity. The matter content and superpotential are given as follows:

$$N \bullet \xrightarrow{\quad A_{1,2} \quad} \xleftarrow[\quad B_{1,2} \quad]{} \bullet N+M \qquad W = \frac{\lambda}{2}\epsilon^{ij}\epsilon^{kl}\mathrm{Tr}A_i B_k A_j B_l \ . \qquad (8.2.1)$$

where λ is the superpotential coupling and the trace is taken over color indices.

164

For $M = 0$ the gauge theory is conformal. Indeed, the M D5-branes are added precisely to take us out of this conformal point, inducing a RG flow.

The one loop NSVZ beta function [142] determines the running of the gauge couplings. For each gauge group we have

$$\beta_i = \frac{d(8\pi^2/g_i^2)}{d\ln\mu} = \frac{3T(G) - \sum_i T(r_i)(1 - 2\gamma_i)}{1 - \frac{g_i^2}{8\pi^2}T(G)} \qquad (8.2.2)$$

where μ is a ratio of energy scales and for an $SU(N_c)$ gauge group $T(G) = N_c$ and $T(fund) = 1/2$.

Using $\gamma_i = \frac{3}{2}R_i - 1$, we can express the beta functions $\beta_{i=1,2}$ for the two gauge couplings $g_{i=1,2}$ in terms of R-charges. As is done in [119], we will work in the approximation that the denominator of (8.2.2) is neglected. Then, the beta functions become

$$\begin{aligned}
\beta_1 &= 3\left[N + (R_A - 1)(N + M) + (R_B - 1)(N + M)\right] , \\
\beta_2 &= 3\left[(N + M) + (R_A - 1)N + (R_B - 1)N\right] .
\end{aligned}$$

At the conformal point, the R-charges of the bifundamentals can be calculated from the geometry and are $R_A = R_B = 1/2$. They can also be simply determined by using the symmetries of the quiver and requesting the vanishing of the beta functions for the gauge and superpotential couplings. Generically, we would expect the R-charges to suffer $\mathcal{O}(M/N)$ corrections for $M \neq 0$. Here however, there is a $\mathbb{Z}_2$ symmetry $M \to -M$ for large N that forces the corrections to be of order at least $\mathcal{O}(M/N)^2$. Thus,

$$\beta_1 = -3M, \qquad \beta_2 = 3M \qquad (8.2.3)$$

up to $\mathcal{O}(M/N)$ corrections.

If we trust these one loop beta functions, then flowing into the IR, we see that the coupling g_2 will eventually diverge because of the positivity of β_2. According to Klebanov and Strassler, the appropriate remedy is a Seiberg duality. After the

duality, the gauge group becomes $SU(N) \times SU(N - M)$ but otherwise the theory remains the same. After this duality, the beta functions change sign: $\beta_1 = 3M$ and $\beta_2 = -3M$. This process of Seiberg dualizing and flowing can be continued for a long time in the large N limit as shown in Figure 8-1. The number of colors in the gauge groups becomes smaller and smaller. Klebanov and Strassler [119] demonstrated that when one of the gauge groups becomes trivial, the gauge theory undergoes chiral symmetry breaking and confinement. The phenomenon is realized geometrically in the SuGRA dual by a deformation of the conifold in the IR.
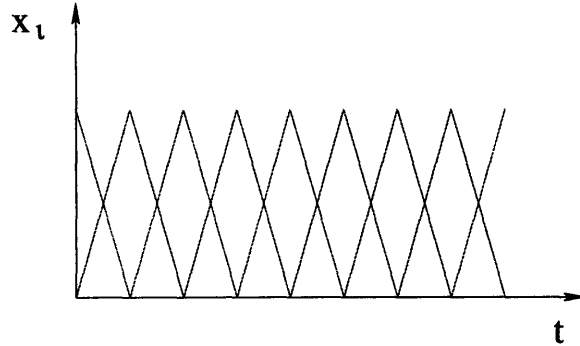
Figure 8-1: The KS cascade for the conifold. The two inverse gauge couplings $x_{i=1,2} = \frac{1}{g_i^2}$ for the two nodes evolve in weave pattern against log-energy scale t where Seiberg duality is applied whenever one of the x_i's reaches zero.

Clearly there are some weaknesses in this purely gauge theoretic approach to the RG flow of a strongly coupled gauge theory. Usually Seiberg duality is understood as an IR equivalence of two gauge theories and is not performed in the limit $g_2 \to \infty$. Can we really trust Seiberg duality here? Also, we have dropped the denominator of the full NSVZ beta function (8.2.2), which is presumably important. Nevertheless, the analysis is sound and the strongest argument for the validity of these Seiberg dualities comes not from gauge theory but from the dual supergravity theory [119]. There is a completely well-behaved supergravity solution, the KS solution of the conifold, which models this RG flow. On the gravity side, there is a radial dependence of the 5-form flux which produces a logarithmic running of the effective number of D3-branes in complete accordance with the field theory cascade, giving credence to these Seiberg dualities.

8.2.2 General RG Flows

We shall henceforth focus on the four dimensional, $\mathcal{N} = 1$ gauge theories engineered by placing D3-branes at the singularity of a Calabi-Yau threefold cone over a del Pezzo surface. We have presented thes theories in detail in Chapters 5 and 6 (see also [93, 11, 45, 43, 52] for a comprehensive discussion). With some important caveats, these theories can be treated in a fashion similar to the discussion above for the conifold.

The field content of a del Pezzo gauge theory is described compactly by a quiver. For D-branes probing the n-th del Pezzo, the number of gauge group factors in the quiver theory is equal to

$$k = n + 3 , \tag{8.2.4}$$

which is the Euler characteristic $\chi(dP_n)$. We reserve the index $i = 1, 2, \ldots k$ for labeling the nodes of the quiver. We denote the adjacency matrix of the quiver by f_{ij}. In other words, f_{ij} is the number of arrows in the quiver from node i to node j. We point out that by definition, the f_{ij} are all non-negative.

Thus given a quiver, we need to specify the ranks of the gauge groups in order to define a gauge theory. We will denote the rank of the gauge group on the i-th node by d^i, and the dimension vector by $d = (d^i)_{i=1,\ldots,k}$. As on the conifold, the ranks d^i are related to the number of branes that realize the specific gauge theory in string theory. When probing the del Pezzos, we will reserve N to denote the number of regular D3-branes, and M^I to denote the number of D5-branes. The D3-brane corresponds to a unique dimension vector which we will denote by $r = (r^i)_{i=1,\ldots k}$. In distinction to the conifold and its ADE generalizations, the possible D5-branes are constrained by chiral anomaly cancellation, and we will parametrize their dimension vectors by $s_I = (s_I^i)$ with $I = 1, 2 \ldots, n$.

Summarizing, a D-brane configuration with N regular D3-branes and M^I D5-branes of type I corresponds to the gauge group $\prod_{i=1}^{k} SU(d^i)$ with

$$d^i = r^i N + s_I^i M^I \tag{8.2.5}$$

167

and f_{ij} chiral fields X_{ij} in the $SU(d^i) \times SU(\overline{d^j})$ bi-fundamental representation.

As shown in [93, 97], the beta functions of the gauge theory can be computed effectively from geometry by taking advantage of the exceptional collection language [24, 93, 97, 47]. An exceptional collection $\mathcal{E} = (E_1, E_2, \ldots, E_k)$ is an ordered collection of sheaves, specifying the D-brane associated with each node. The intersections of the sheaves give rise to massless strings which in turn correspond to bifundamental fields in the gauge theory. $\mathcal{E}$ can roughly be thought of as a basis of branes.

An important feature of exceptional collections for us will be the ordering. The ordering of a collection induces an ordering of the nodes of the quiver. In order to use the exceptional collection technology to compute the beta functions, we must keep track of the ordering.

If a given quiver satisfies the well split condition of [93], the order of the quiver changes in a simple way under Seiberg duality. To understand the well split condition, we first need to refine our understanding of the quiver ordering. It was shown in [93] that the ordering of the quiver is only determined up to cyclic permutations. If $123 \ldots n$ is a good ordering, then so is $23 \ldots n1$. If a quiver is well split, then we can find a cyclic permutation such that for any node j, all the outgoing arrows from j go to nodes $i < j$ and all the in-going arrows into j come from nodes $i > j$. After a Seiberg duality on node j, j would become the last node in the quiver. In, [54] alternative formulation of the well split condition in terms of (p, q) webs was found.

An unproven conjecture of [93] is that the Seiberg dual of a well split quiver is again well split. The conjecture was proven for four node quivers in [93] and no counter-examples are known to the author. An appropriate understanding of ill split quivers is still lacking. For example, the correct determination of R-charges for them is still open. Indeed, the fractional Seiberg dualities encountered in [47] are problematic precisely for this reason. Ill split quivers were studied in [54]. As our examples in this chapter involve only Seiberg dualities of well split, four node quivers, we can be confident in our calculations.

In light of the exceptional collection language, we shall also make use of the matrix S which is an upper triangular matrix with ones along the diagonal and related to

f_{ij} by

$$S_{ij} = \begin{cases} f_{ij} - f_{ji} \,, & i < j \,; \\ 1 \,, & i = j \,; \\ 0 \,, & i > j \,. \end{cases} \qquad (8.2.6)$$

where we have assumed an ordering. The components S_{ij}, $i \neq j$, are still the number of arrows from node i to node j, except that now a negative entry corresponds to reversing the arrow direction. We will find it convenient to use a matrix $\mathcal{I}$ which is simply the antisymmetrized version of S (or f).

$$\mathcal{I} = S - S^t = f - f^t \qquad (8.2.7)$$

Using this, chiral anomaly cancellation can be concisely expressed as the condition that the dimension vector d be in the kernel of $\mathcal{I}$. In other words, r and the s_I form a basis of $\ker \mathcal{I}$.

Beta Functions and Flows

Methods exist in the literature for the determination of the R-charges as well as the beta function. Evaluating (8.2.2) with the quiver notation introduced above, and denoting by R_{ij} the R-charge of the bifundamental X_{ij}, one obtains for the beta function of the i-th node (cf. Eq (5.7) of [56])

$$\frac{dx_i}{d\ln \mu} = \beta_i = \left(3d^i + \frac{3}{2} \sum_{j=1}^{k} \left(f_{ij}(R_{ij} - 1) + f_{ji}(R_{ji} - 1) \right) d^j \right) \,. \qquad (8.2.8)$$

where x_i is related to the i-th gauge coupling via $x_i \equiv 8\pi^2/g_i^2$.

One very insightful approach for the determination of the R-charge is the procedure of maximization of the central charge a in the CFT as advocated in [102, 103]. We shall however adhere to the procedure of [93, 97], which gives the R-charges at the conformal point. Transcribing Eq. 49 from [85] to present notations, the R-charge

of the bi-fundamental X_{ij} is given by

$$R(X_{ij}) = 1 + \left(\frac{2}{(9-n)r^i r^j}(S_{ij}^{-1} + S_{ji}^{-1}) - 1 \right) \text{sign}(i-j) . \qquad (8.2.9)$$

It was shown in [85] that plugging (8.2.9) into (8.2.8), and going to the conformal point $d^i = r^i$, one finds $\beta_i = 0$, as expected.

The flow is induced when we leave the conformal fixed point by adding D5-branes. As in [119], we will work in the regime $M^I \ll N$. As in Chapter 7, we will assume the R-charges do not receive corrections of $\mathcal{O}(M^I/N)$. This assumption is supported by the supergravity solutions we write down in Section 8.5, which severely constrain the nature of such corrections for KS type cascades. For more general cascades with duality walls, we believe that we can still trust the qualitative nature of our results. Ignoring the corrections, the non-conformal beta functions can readily be obtained by substituting (8.2.9) into (8.2.8) for general ranks d^i. We obtain, to order M^I/N,

$$\beta_i = 3s_I^i M^I + \frac{3}{2}\sum_j \tilde{R}_{ij}s_I^j M^I , \qquad (8.2.10)$$

where we have introduced the symmetric matrix

$$\tilde{R}_{ij} = f_{ij}(R_{ij} - 1) + f_{ji}(R_{ji} - 1) . \qquad (8.2.11)$$

We will now evolve the inverse gauge couplings $x_i = 8\pi^2/g_i^2$ with the beta functions (8.2.10). Since the one-loop beta functions are constant, the evolution proceeds in step-wise linear fashion, much like the KS cascade; we have

$$\frac{8\pi^2}{g_i^2(t + \Delta t)} - \frac{8\pi^2}{g_i^2(t)} = \beta_i \Delta t \qquad (8.2.12)$$

during the step Δt in energy scale ($t = \ln \mu$), before one has to perform Seiberg duality on the node whose coupling reaches zero first.

An important constraint can be placed on this evolution. Even though now these

170

beta functions do not vanish identically, it is still the case that

$$\sum_i^k \beta_i r^i = 0 \ .$$

(8.2.13)

The reason is that this sum can be reorganized into a sum over each of the beta functions at the conformal point, and at the conformal point, each of these beta functions vanishes individually. It follows from (8.2.10) and (8.2.13) therefore, that,

$$\sum_i^k \frac{r^i}{g_i^2} = \text{constant}$$

(8.2.14)

throughout the course of the cascade; on this constraint we shall expound next.

Simplices in the Space of Couplings

The space of possible gauge coupling constants $x_i \equiv 1/g_i^2$ for a quiver with k gauge groups is a cone $(\mathbb{R}_+)^k$. The relation (8.2.14) cuts out a **simplex** in this cone. The beta functions (8.2.10) establish the direction of the renormalization group flow inside this simplex. For the KS conifold flow, having two gauge couplings, the cone is the quadrant in $\mathbb{R}^2$ parametrized by $1/g_1^2 = x > 0$ and $1/g_2^2 = y > 0$. The simplex is the line segment $x + y = \text{const}$ inside this cone. The beta functions tell us to move up and down this line segment until one or the other coupling constant diverges.

In more general cases, under the renormalization group flow, we will eventually reach a face of the simplex where one of the couplings diverges. At this point, the insight gained from the KS flow tells us we should Seiberg dualize the corresponding gauge group. After the duality, we find ourselves typically in a new gauge theory. The new gauge theory has some new associated simplex and renormalization group flow direction given by some different set of beta functions. The KS flow is very special in that the Seiberg dual theory is identical to the original one up to the total number of D3-branes N.

One imagines in general some huge collection of simplices glued together along their faces. In any given simplex, the renormalization group trajectory is a straight

line. At the faces, the trajectory "refracts". One recomputes the beta functions to find the new direction for the RG flow. In Figure 8-1 for example, we have the evolution of the couplings reflecting off the t-axis (corresponding to either $1/g_1^2$ or $1/g_2^2$ equal to zero), whereby giving the weave pattern. Note that such RG flows are generically quite sensitive to initial conditions. Slightly altering the initial couplings may alter the trajectory such that a different face of a simplex is reached. A different face corresponds to a Seiberg duality on a different node which will generically completely alter the rest of the flow. Such a sensitivity was noticed in [85, 56].

For four node quivers, the simplices are tetrahedra and the RG flow can be visualized. There is only one vector s, with components s_i, corresponding to only one D5-brane. Thus, the direction of the RG flow inside any given tetrahedron is, up to sign, independent of M. Moreover, one can show that after a duality on node i, $\beta_i \rightarrow -\beta_i$ (see the appendix for details).

Thus prepared, we can embark upon a detailed study of the RG flows and duality cascades for various concrete examples. Some of them will exhibit a KS type behavior, meaning that the cascade will periodically return to the same quiver up to a change in the number of D3-branes, showing no accumulation of dualization scales in the UV. Others will be markedly different, exhibiting duality walls. In particular, we shall describe an assortment of interesting flows for D-branes probing cones over the del Pezzo surfaces, where we will be able, in addition to numerics, to gain some quantitative analytic understanding.

8.3 Duality Walls for F_0

We begin with D-brane probe theories on the complex cone over F_0, the zeroth Hirzebruch surface. The addition of D5-branes takes us out of conformality, whereby inducing a RG flow. Detailed numerical study was undertaken in [56]. We presented the results in Chapter 7. All Seiberg dual theories for this geometry can be arranged into a web which encodes all possible duality cascades. This web takes the form of a flower and has been affectionately called the *Flos Hirzebruchiensis* (cf. Fig 7

172

cit. Ibid.). The purpose of this section is to derive analytical results for the existence of duality walls and their location. We also explain the **fractal structure** of the duality wall curve as a function of the initial couplings.

8.3.1   Type A and Type B Cascades

Before proceeding with the analytical derivations, let us make a brief summary of the findings in [56], where two classes of RG trajectories were identified. In one gauge theory realization, F_0 exhibits a Klebanov-Strassler type flow that alternates between two quivers with constant intervals in $t = \log \mu$ (for energy scale μ) between successive dualizations. This type of flow is an immediate generalization of the conifold cascade. The quivers of and the beta functions inter-connecting between the two theories are shown in Figure 8-2.

$$\beta_1 = -3M$$
$$\beta_2 = 3M$$
$$\beta_3 = -3M$$
$$\beta_4 = 3M$$

$$\beta_1 = -3M$$
$$\beta_2 = 0$$
$$\beta_3 = 3M$$
$$\beta_4 = 0$$
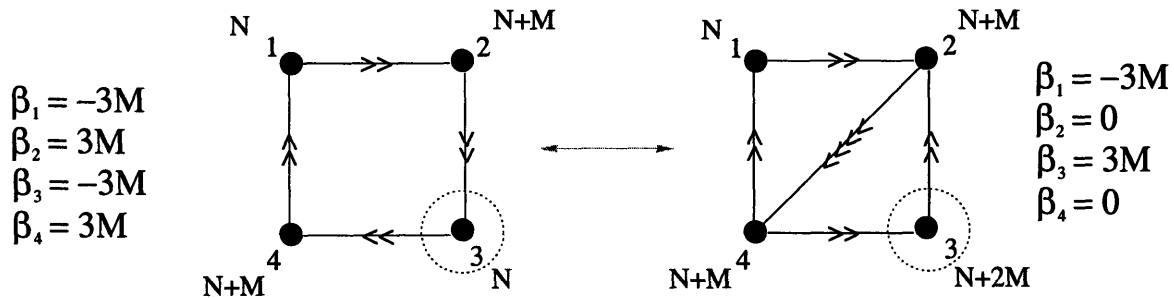
Figure 8-2: The first class of duality cascades for F_0. This is an immediate generalization of the KS conifold case and we alternate between the two theories upon dualizing node 3 of each and evolve according to the beta functions shown.

The second class of flows commences with the quiver in Figure 8-3, which is another theory in the duality flower for F_0. In this case, there is a decrease in the t interval between consecutive dualizations towards the UV, leading to the possibility of a so-called **duality wall** past which no more dualization is possible and we have an accumulation point at finite energy. Considering initial couplings of the four gauge group factors of the form $(1, x_2, x_3, 0)$, two qualitatively different behaviors were observed.

1. In theories with $x_3 > 0.9$, the cascade corresponds to an infinite set of alternate dualizations of nodes 1 and 2. The distance between dualizations is monotoni-

$$\beta_1 = 0$$
$$\beta_2 = -3M$$
$$\beta_3 = 0$$
$$\beta_4 = 3M$$
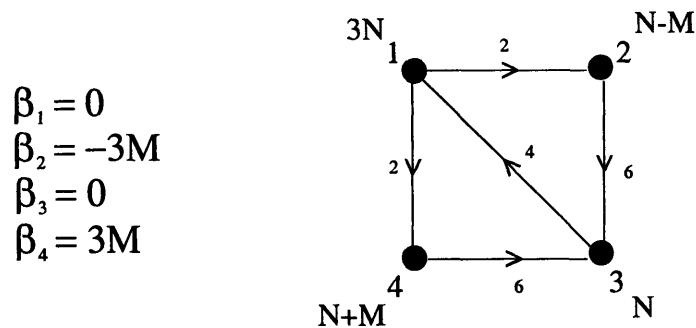
Figure 8-3: The second class of theories for F_0. Starting from this quiver and following the duality cascade give markedly different behavior from the KS case. It was seen in this case that the increment in energy scale decreases at each step and a "duality wall" may be reached [56].

cally decreasing, as was shown in Figures 7-12 and 7-13. However, no conclusive evidence of convergence to a duality wall was found in this case. We will call such a cascade an **A type cascade** and will show shortly that in this case a duality wall is indeed approached smoothly.

2. On the other hand, for $x_3 < 0.9$, the third gauge group is dualized at a finite scale. When this happens, all the intersection numbers in the quiver become larger than 2, leading to an explosive growth of the ranks of the gauge groups and the number of bifundamental chiral fields, and generating an immediate accumulation of the dualization scales. This discontinuous behavior makes duality walls evident even in numerical simulations for these flows. We will refer to these flows as **B type cascades**.

8.3.2 Duality Walls in Type A Cascade

Having elucidated the rudiments of the cascading behavior of the F_0 theories, let us explore whether there are indeed duality walls for A type cascades, which we recall to be the type for which numerical evidence is not conclusive. We shall proceed analytically. In order to do so, let us first construct the quiver at an arbitrary step k. We can regard Seiberg duality as a matrix transformation on the rank vector and the adjacency matrix as was done for example in Sec. 8.1 of [56]. An elegant way to derive the quiver at a generic position in the cascade is by realizing Seiberg duality

174

transformations as mutations in an exceptional collection (equivalently, by Picard-Lefschetz monodromy transformations on the 3-cycles in the manifold mirror to the original Calabi-Yau). We will use this language as was done in [93, 97].

Taking the exceptional collection to be $(a, b, 3, 4)$, the alternate dualizations of nodes 1 and 2 corresponds in this language to the repeated left mutation of a with respect to b. For even k $(a, b) = (1, 2)$, while for odd k $(a, b) = (2, 1)$. Figure 8-3 corresponds to $k = 1$ where the exceptional collection ordering is (2,1,3,4). This quiver is well split.

Quivers at Step k

Under Seiberg duality, the rank of the relevant gauge group changes from N_c to $N_f - N_c$. Type A cascades correspond to always dualizing node a. By explicitly constructing these RG trajectories, we will check that this assumption is indeed consistent. The exceptional collection tells us that after the duality, nodes a and b will switch places. Thus

$$N_a(k + 1) = N_b(k) \ ,$$
$$N_b(k + 1) = 2N_b(k) - N_a(k) \ . \tag{8.3.15}$$

It is immediate to prove that after k iterations, the ranks of the $SU(N_i)$ gauge groups are given by

$$N_a = (2k - 1)N + (k - 2)M \ ,$$
$$N_b = (2k + 1)N + (k - 1)M \ ,$$
$$N_3 = N \ , \tag{8.3.16}$$
$$N_4 = N + M \ .$$

The number of bifundamental fields between each pair of nodes follow from applying the usual rules for Seiberg duality of a quiver theory. In particular, we combine the bifundamentals X_{a4}, X_{ba}, and X_{a3} into mesonic operators $M_{b4} = X_{ba}X_{a4}$ and $M_{b3} = X_{ba}X_{a3}$. We introduce new bifundamentals X'_{4a}, X'_{ab}, and X'_{3a} with dual quantum numbers along with the extra term $M_{b4}X'_{4a}X'_{ab} + M_{b3}X'_{3a}X'_{ab}$ to the superpotential. We then use the superpotential to integrate out the massive fields, which appear in the quiver as bidirectional arrows between the pairs of nodes $(3, b)$ and $(4, b)$. The

resulting incidence matrix for the quiver will change such that

$$f_{ba}(k+1) = f_{ba}(k) \qquad\qquad f_{3b}(k+1) = f_{a3}(k) \qquad\qquad f_{43}(k+1) = f_{43}(k)$$

$$f_{a4}(k+1) = -f_{4b}(k) + 2f_{a4}(k) \qquad f_{4b}(k+1) = f_{a4}(k) \qquad f_{a3}(k+1) = -f_{3b}(k) + 2f_{a3}(k)$$
$$\text{(8.3.17)}$$

which can be simplified to yield

$$f_{ba}(k) = 2 \qquad\qquad f_{3b}(k) = 2(k+1) \qquad\qquad f_{43}(k) = 6$$

$$f_{a4}(k) = 2(k-1) \qquad f_{4b}(k) = 2(k-2) \qquad f_{a3}(k) = 2(k+2) \ . \qquad \text{(8.3.18)}$$

This information can be summarized in the quiver diagram in Figure 8-4.
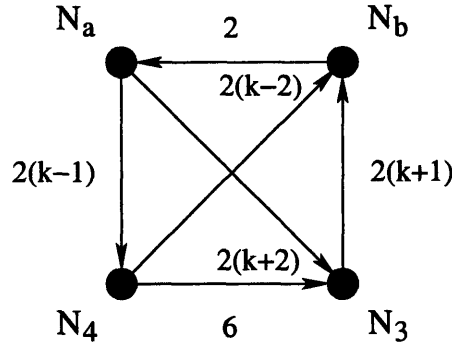
Figure 8-4: Quiver diagram at step k of a type A cascade for F_0.

With the adjacency matrix (8.3.18) and the non-conformal ranks (8.3.16), we can readily compute the beta functions from (8.2.10), to arrive at

$$\beta_a = -\frac{9(k+1)kM}{(4k+2)} \quad < 0$$
$$\beta_b = \frac{9(k-1)kM}{(4k-2)} \quad \geq 0$$
$$\beta_3 = \frac{3(7k^2-3k-4)M}{(2-8k^2)} \quad < 0$$
$$\beta_4 = \frac{3(7k^2+3k-4)M}{(-2+8k^2)} \quad > 0 \ ,$$

$$k = 1, 2, 3, \ldots$$
$$(a, b) = (2, 1); \qquad k \text{ odd} \qquad\qquad \text{(8.3.19)}$$
$$(a, b) = (1, 2); \qquad k \text{ even}$$

The RG Flow

Using the results in Section 8.3.2, we proceed to study the evolution of the dualization scales starting with the initial couplings $(1, x_2(0), x_3(0), 0)$. Let us consider the first step in the cascade. We are in a type A cascade, so $x_3(0) > 0.9$. The beta functions

are, from (8.3.19),

$$\beta_1(1) = 0, \quad \beta_2(1) = -3M, \quad \beta_3(1) = 0, \quad \beta_4(1) = 3M . \tag{8.3.20}$$

We see that only node 2 has a negative beta function at the first step and so its associated coupling will reach zero first, i.e., the first step ends with the dualization of node 2. The subsequent increment $\Delta(1)$ in the energy scale $t = \log \mu$ before the dualization is performed is equal to

$$\Delta(1) = \frac{x_2(0)}{|\beta_2(1)|} . \tag{8.3.21}$$

Applying

$$x_i(k+1) = x_i(k) + \beta_i(k+1)\Delta(k+1), \quad t(k+1) = t(k) + \Delta(k) , \tag{8.3.22}$$

we have at the end of this step

$$x_1(1) = 1, \quad x_2(1) = 0, \quad x_3(1) = x_3(0), \quad x_4(1) = \frac{3Mx_2(0)}{|\beta_2(1)|} . \tag{8.3.23}$$

So, as far as nodes 2 and 3 are concerned, the initial value $x_2(0)$ only affects the length of the first step, beyond which any information about it is erased. In order to look for the initial couplings that lead to a type A flow, recall that we have to determine the possible initial values $x_3(0)$ such that $x_3(k)$ remains greater than zero as $k \to \infty$ so that the third node never becomes dualized. Since $\beta_3(1) = 0$, this is completely independent of $\Delta(1)$ and hence independent of $x_2(0)$.

That said, let us look at the cascade at the next step. The beta functions (8.3.19) now give

$$\beta_1(2) = -\frac{27}{5}M, \quad \beta_2(2) = 3M, \quad \beta_3(2) = -\frac{9}{5}M, \quad \beta_4(2) = 3M . \tag{8.3.24}$$

Since we are interested in type A cascades, we assume that the initial value $x_3(0)$ is such that this node is never dualized. Thus, the next node to undergo Seiberg

duality is the other one with a negative beta function, namely node 1. Recalling that $x_1(1) = 1$, the consequent step in the energy scale $\Delta(2)$ is thus

$$\Delta(2) = \frac{x_1(1)}{|\beta_1(2)|} = \frac{1}{|\beta_1(2)|} \, , \tag{8.3.25}$$

and $x_1(2) = 0$ while $x_2(2) = \beta_2(2)\Delta(2)$. Proceeding similarly, the next step gives

$$\Delta(3) = \frac{\beta_2(2)}{\beta_1(2)} \frac{1}{\beta_2(3)} \, . \tag{8.3.26}$$

We see that in general, at the kth step, the interval $\Delta(k)$ is given by

$$\Delta(k) = \left[\prod_{i=2}^{k} \frac{\beta_b(i)}{|\beta_a(i)|} \right] \frac{1}{\beta_b(k)} \, , \qquad \begin{array}{ll} (a,b) = (2,1), & k \text{ odd}; \\[4pt] (a,b) = (1,2), & k \text{ even} \, , \end{array} \tag{8.3.27}$$

for $k \geq 2$. This, using (8.3.19), can be written as a telescoping product

$$M\Delta(k) = \left[\prod_{i=2}^{k} \frac{(i-1)}{(i+1)} \frac{(2i+1)}{(2i-1)} \right] \frac{(4k-2)}{9(k-1)k} \, . \tag{8.3.28}$$

Simplifying this expression we arrive at

$$M\Delta(k) = \frac{2(2k+1)(4k-2)}{27k^2(k^2-1)} \tag{8.3.29}$$

for $k \geq 2$. The total variation of the third coupling x_3, after k steps, is given by

$$x_3(k) - x_3(0) = \sum_{i=2}^{k} \Delta(i)\beta_3(i) \, . \tag{8.3.30}$$

As discussed, the boundary between type A and B cascades corresponds to initial conditions such that $x_3(k) \to 0$ for $k \to \infty$, i.e., the initial conditions that separate the regime in which node 3 gets dualized at some finite k from the one in which it never undergoes a Seiberg duality. Then,

178

$$x_3(0) - x_3(\infty) = \frac{2}{9} \sum_{i=2}^{\infty} \frac{(7i+4)}{i^2(i+1)} = \frac{4}{27}\pi^2 - \frac{5}{9} \ . \tag{8.3.31}$$

We see that this sum is approximately equal to 0.906608, in agreement with the numerical evidence, which located the transition at $x_3(0) \sim 0.9$. We will henceforth call this coupling $x_3(0)$ such $x_3(\infty) = 0$, x_{3b}, because it is a boundary value between type A and type B cascades.

Duality Walls in Type A Cascades

The computations in the previous section enable us to address one of the questions left open in [56] (see Chapter 7 of this thesis), namely whether duality walls exist in this case. Our flow, from (8.3.31), corresponds to an infinite cascade that only involves nodes 1 and 2. Let us sum up all the steps $\Delta(k)$ in the energy scale *ad infinitum*; this is equal to

$$\sum_{k=1}^{\infty} \Delta(k) = \Delta(1) + \sum_{k=2}^{\infty} \Delta(k) \ . \tag{8.3.32}$$

Using $\Delta(1) = x_2(0)/|\beta_2(1)| = x_2(0)/3M$ and (8.3.29), we see that this sum can actually be performed, giving us a finite answer. This means that there is indeed a duality wall for our type A cascades, whose value is equal to

$$t_{wall} = \frac{1}{3M} \left(x_2(0) + \frac{2\pi^2}{27} + \frac{5}{9} \right) \ . \tag{8.3.33}$$

We would like to emphasize that, although derived in the approximation of vanishing $\mathcal{O}(M/N)$ corrections to the R-charges, (8.3.33) is the first analytical result for a duality wall. Given the detailed understanding we have of every step of the cascade on the gauge theory side, this example stands as a natural candidate in which to try to look for a realization of this phenomenon in a SuGRA dual.

8.3.3 Fractal Structure of the Duality Wall Curve

Having analytically ascertained the existence and precise position of the duality wall for type A cascades, and the boundary value $x_{3b}(0)$ of the inverse squared coupling at which the cascades become type B, we now move on to address another fascinating question, hints of which were raised in [56, 85], viz., the dependence of the position of the wall upon the initial couplings. We will see that, in type B cascades, such dependence takes the form of a *self-similar* curve.

Let us focus on the one dimensional subset of the possible initial conditions given by couplings of the form $(1, 1, x_3(0), 0)$ (more general initial conditions can be studied in a similar fashion). Figure 8-5 is a plot of the position of the duality wall as a function of $x_3(0)$. Initial values $x_3(0) > x_{3b}$ correspond to type A cascades. Node 3 is not dualized in this case and thus the position of the wall is independent of $x_3(0)$ in this range, as determined by (8.3.33). From now on, we will focus on the $x_3(0) < x_{3b}$ type B region. The curve exhibits in this region an apparent piecewise linear structure as was noticed in [56] and presented in Section 7.5.4.
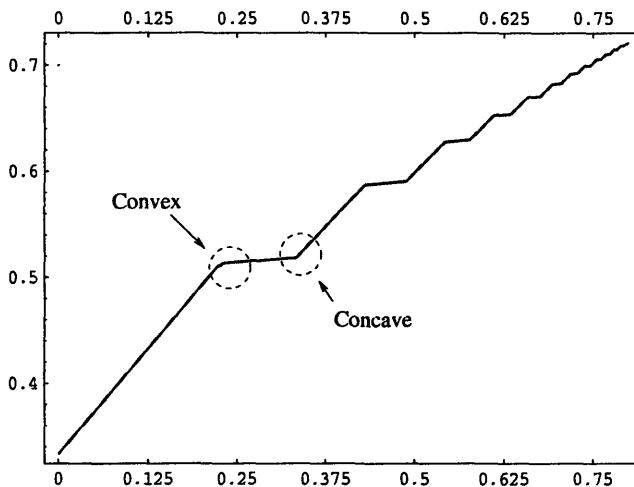
Figure 8-5: Position of the duality wall for F_0 as a function of $x_3(0)$ for initial conditions of the form $(1, 1, x_3(0), 0)$. A piecewise linear structure is seen for the type B cascade region, i.e., $x_3(0) < x_{3b} \sim 0.9$.

In order to appreciate the piecewise structure more clearly, it is useful to consider the derivative of the curve. We show in Figure 8-6 a numerical differentiation of Figure 8-5. This apparent linearity is in fact approximate, and an intricate structure

180

is revealed when we look at the curve in more detail. While exploring the origin of the different features of the curve, we will discover that a *self-similar fractal structure* emerges.
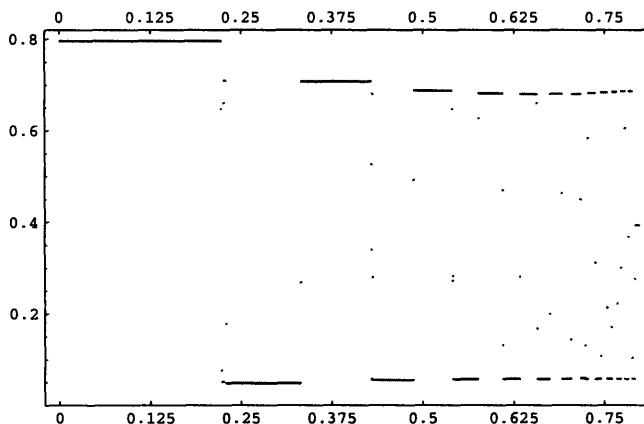
Figure 8-6: Derivative of the position of the duality wall for F_0 as a function of $x_3(0)$ for initial conditions of the form $(1, 1, x_3(0), 0)$. The appearance of the constant segments evidences further the piecewise linear behavior of position of the wall with respect to $x_3(0)$.

The most prominent features in Figure 8-5 are the **concave** and **convex cusps** at the endpoints of apparently linear intervals. In our notation (cf. figure), the bend at $\simeq 0.2$ is a convex cusp while the one at $\simeq 0.3$ is a concave one. We will explain now their origin and give analytical expressions for their positions.

As we will illustrate with examples, this kind of structure appears at those values of the couplings at which a transition between different cascades occurs. A semi-quantitative measure of how different two cascades are is given by the number of steps m that they share in common. In this sense, if a given cascade A shares m_1 steps with cascade B and m_2 with cascade C, with $m_1 > m_2$, we say that A is closer to B than to C. The general principle is that the closer the cascades between which a transition occurs at a given initial coupling, the smaller the corresponding feature in the position of duality wall versus coupling curve is.

It is important to remember what the physical meaning of our computations is. Numbering cascade steps increasing towards the UV and identifying the values of the initial couplings are just a simple way to handle the process of reconstructing a

181

duality cascade. This cascade represents a traditional RG flow in the IR direction, in which Seiberg duality is used to switch to alternative descriptions of the theory beyond infinite coupling. At some stage of this flow in the IR the model in Figure 8-3 appears, with couplings given precisely by what we called initial conditions. Thus, two cascades that share a large number of steps m in common, correspond to two RG flows initiated at different theories with large gauge groups and number of bifundamental fields in the UV that converge at some point, sharing the last m steps prior to reaching the model in Figure 8-3. Due to the fact that a duality wall exists, the independent flows before convergence of the cascades take place in a very small range of energies.

We now investigate the convex and concave cusps of the curve. Our approach consists of identifying what happens to the cascades at those special points, and then computing the corresponding values of the initial couplings analytically. Let us first consider the *concave cusps*. The m-th concave cusp corresponds to the transition from node 3 being dualized at step $m + 1$ to it being dualized at step $m + 2$. The cascades at both sides of the m-th concave cusp share the first m steps and are of the form

$$
\begin{array}{c}
2121\ldots a3 \\
\underbrace{2121\ldots a}_{m}\,b3
\end{array}
\tag{8.3.34}
$$

where $(a, b) = (1, 2)$ for m even and $(2, 1)$ for m odd. In this way, concave cusps fit in our general discussion of transitions between cascades, and we see that cusps become smaller as m is increased. The values of $x_3(0)$ that correspond to the concave cusps are obtained by setting $x_3(k) = 0$ in (8.3.30) and (8.3.31) for $k \geq 2$, i.e.

$$
x_3^{conc}(k) = \frac{2}{9} \sum_{i=2}^{k} \frac{(7i + 4)}{i^2(i + 1)} \quad k \geq 2 \ .
\tag{8.3.35}
$$

From (8.3.35), the first concave cusps are located at $x_3(0)$ equal to

$$
\frac{1}{3},\ \frac{79}{162},\ \frac{467}{810},\ \frac{2569}{4050},\ \frac{19133}{28350},\ \ldots
\tag{8.3.36}
$$

in complete agreement with the numerical values of Figures 8-5 and 8-6.

Let us move on and study the convex cusps in Figure 8-5. In analogy with (8.3.34), we claim that the mth convex cusp corresponds to cascades switching between

$$2121\ldots a3a$$
$$\underbrace{2121\ldots a}_{m}3b \tag{8.3.37}$$

with $(a, b) = (1, 2)$ for m even and $(2, 1)$ for m odd. In order to check whether the proposal in (8.3.37) is correct, we proceed to compute the positions for the cusps that it predicts. The calculation is similar to the one in §8.3.2 and we only quote its result here

$$x_3^{conv}(k) = \frac{(4+7k)(10+49k+50k^2+14k^3)}{9k^2(1+k)^2(3+22k+14k^2)} + \frac{2}{9}\sum_{i=2}^{k-1}\frac{(7i+4)}{i^2(i+1)} , \qquad k \geq 2 . \tag{8.3.38}$$

Equation (8.3.35) determines the following positions for the first convex cusps

$$\frac{70}{309}, \frac{21773}{50544}, \frac{76733}{141750}, \frac{457831}{750060}, \frac{83386559}{126809550}, \ldots \tag{8.3.39}$$

which are in perfect accordance with Figures 8-5 and 8-6, whereby validating (8.3.37).

The Fractal: Something fascinating happens when the duality wall curve is studied in further detail. Although convex cusps appear as such when looking at the curve at a relatively small resolution as in Figure 8-5, an infinite fractal series of concave and convex cusps blossoms when we zoom in further and further. As an example, we show in Figure 8-7 successive amplifications of the area around the first convex cusp, indicating the dualization sequences associated to each side of a given cusp. According to our previous discussion, this cusp is located at $x_3(0) = 70/309$ and corresponds to the transition between two cascades differing at the third step: $232\ldots$ and $231\ldots$. Figure 8-7.b zooms in. We can appreciate that what originally seemed to be a convex cusp becomes a pair of convex cusps with a concave one in the middle. Furthermore,

the value of $x_3(0)$ given by (8.3.38) is in fact the one that corresponds to this originally hidden concave cusp. The new convex cusps are of a higher order, corresponding to transitions between cascades at the 4th step. The first one in Figure 8-7.b corresponds to $2323\ldots \to 2321\ldots$ while the second one is associated to $2312\ldots \to 2313\ldots$. We see in Figure 8-7.c how each of the convex cusps splits again into two 5th order convex cusps with a concave one in between.

This procedure can be repeated indefinitely. We conclude that concave cusps are fundamental, while an infinite self-similar structure that corresponds to increasingly closer cascades can be found by expanding convex cusps.

Figure 8-7: uccesive amplifications of the regions around convex cusps show the self-similar nature of the curve for the position of the wall versus $x_3(0)$. We show the first steps of the cascades at each side of the cusps, indicating between parentheses the first dualizations that are different.

8.4 RG Flows and Quasiperiodicity

Having expounded in detail the analytic treatment of RG flows for the zeroth Hirzebruch theory as well as their associated fractal behavior, let us move on to see what novel features arise for more complicated geometries. We recall the next simplest del Pezzo surface is the blow up of $\mathbb{P}^2$ at 1 point, the so-called dP_1. The gauge theory for D3-brane probes on the cone over dP_1 was constructed via toric algorithms in [45]. There are infinitely many quiver gauge theories which are dual to this geometry. Their connections under Seiberg duality can be encoded in a duality tree. When D5-branes are included, the duality tree becomes a representation of the possible paths followed by a cascading RG flow. The tree for dP_1 appears in Figure 7-18. This tree contains isolated sets of quivers with conformal ranks $r = (1, 1, 1, 1)$, denoted toric islands in [56]. We will find quasiperiodicity of the gauge couplings for RG cascades among these islands.

8.4.1 Initial Theory

We are interested in studying the RG flow of a gauge theory corresponding to dP_1. For simplicity, let us choose one of the dual quivers with a relatively small number of bifundamentals. Our quiver is described by the following (we have also included the inverse matrix as a preparation to compute the R-charges):

$$
S = \begin{pmatrix} 1 & -2 & -1 & 3 \\ 0 & 1 & -1 & -1 \\ 0 & 0 & 1 & -2 \\ 0 & 0 & 0 & 1 \end{pmatrix}, \quad S^{-1} = \begin{pmatrix} 1 & 2 & 3 & 5 \\ 0 & 1 & 1 & 3 \\ 0 & 0 & 1 & 2 \\ 0 & 0 & 0 & 1 \end{pmatrix}.
$$

(8.4.40)

We start with a gauge theory with N D3-branes and M D5-branes, $M \ll N$, corresponding to gauge groups

$$SU(N + M) \times SU(N + 3M) \times SU(N) \times SU(N + 2M) . \qquad (8.4.41)$$

Chiral anomaly cancellation is satisfied since the D3-brane vector $r = (1, 1, 1, 1)$ and the D5-brane vector $s = (1, 3, 0, 2)$ are in the kernel of $S - S^T$. In fact, the kernel of $S - S^T$ is two dimensional, and these are the only kinds of D-branes that are allowed. The R-charges of the bifundamental fields at the conformal point are then, using (8.2.9),

$$
\begin{aligned}
R(X_{32}) &= \frac{1}{4} , \\
R(X_{21}) &= R(X_{43}) = \frac{1}{2} , \\
R(X_{42}) &= R(X_{31}) = R(X_{14}) = \frac{3}{4} .
\end{aligned}
\qquad (8.4.42)
$$

As before, we assume the conformal R-charges get corrections only at order $(M/N)^2$. Subsequently, using (8.2.10) we calculate the one loop beta functions for the four gauge groups to be

$$\beta/M = (-15/4, 27/4, -27/4, 15/4) . \qquad (8.4.43)$$

8.4.2 RG Flow

As discussed above, we let the gauge couplings evolve according to the beta functions and we perform a Seiberg duality on the gauge group factor whose coupling diverges first. Interestingly, a Seiberg duality on node 2 or 3 produces the same quiver up to permutation (with the rank of the dualized gauge group appropriately modified). On the other hand, Seiberg duality on nodes 1 or 4 produces a different quiver with larger numbers of bifundamentals.

In the next section, we will perform a numerical study of the possible flows. We will see how certain RG flows involve a single type of quiver and periodically return to the starting point up to a change in the number of D3-branes. These cases are

the dP_1 analogues of the KS cascade. We will also discover other more intricate flows with a beautiful structure, depending on the initial conditions.

Poincaré Orbits

Let us explore the two-dimensional space of initial couplings $(c-x_3(0)-x_4(0), 0, x_3(0), x_4(0))$, where c is some constant that fixes the overall normalization. Next, choose some initial value for the pair $(x_3(0), x_4(0))$ and evolve the cascade for a large number of steps. An interesting way of visualizing these flows is the following. We keep all the values of (x_3, x_4) which are both non-zero, i.e., when either node 1 or 2 but neither node 3 nor 4 is dualized. A subsequent scatter plot can be made for these values, and is presented in Figure 8-8 for various choices of initial conditions, which are identified by different colors.

We see different types of behavior according to the initial conditions. First, there are elliptical trajectories. They correspond to cascades that only involve $r = (1, 1, 1, 1)$ quivers. In the language of [56], the entire RG flow takes place within a single toric island. Other trajectories jump among three squashed ellipses. These cascades consist of both quivers with $r = (1, 1, 1, 1)$ and $r = (2, 1, 1, 1)$ (and its permutations) and correspond to hopping around the six toric islands. Finally, other flows have a diffuse scatter plot, and correspond to cascades that travel to quivers with arbitrarily large gauge groups. Outside the stable elliptical orbits, numerically we find sensitive dependence on the initial conditions.

For the periodic trajectories, it is indeed possible to show analytically that (x_3, x_4) give rise to the parametric equation for an ellipse with respect to the parameter n [61], in accord with the scatter plots (c) and (d) in Figure 8-8.

Though one might worry, there is in fact no contradiction between this periodic behavior and the expectation that under RG flow, there will be fewer degrees of freedom in the IR than in the UV. This expectation has been encoded more precisely in the so-called a-conjecture (see for example [102, 10] for a recent discussion). One can associate to any four-dimensional conformal theory a central charge denoted a which can be interpreted as a measure of the number of degrees of freedom in the
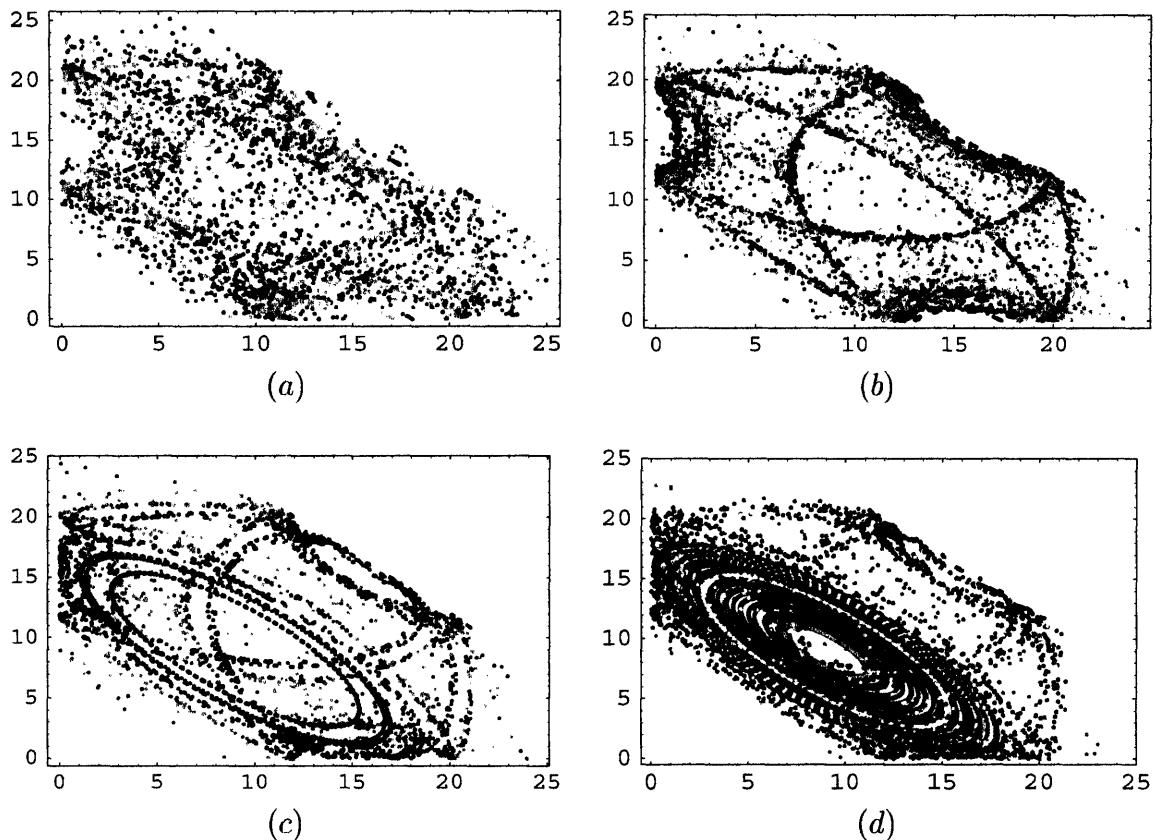
Figure 8-8: Scatter plot of (x_3, x_4) that are non-zero during 800 dualization steps for the initial value $(32 - x_3(0) - x_4(0), 0, x_3(0), x_4(0))$. In each plot, $(x_3(0), x_4(0))$ is allowed to range over a rectangular region with lower left corner L, upper right corner R, and minimum step size in the $x_3(0)$ and $x_4(0)$ directions equal to δ_3 and δ_4 respectively. (a) $L = (9, 15\frac{7}{8})$, $R = (10, 16\frac{2}{8})$, $\vec{\delta} = (\frac{1}{4}, \frac{1}{8})$; (b) $L = (9, 15\frac{3}{8})$, $R = (10, 15\frac{6}{8})$, $\vec{\delta} = (\frac{1}{4}, \frac{1}{8})$; (c) $L = (2, 6)$, $R = (5, 9)$, $\vec{\delta} = (1, 1)$; (d) $L = (7, 11)$, $R = (9, 17)$, $\vec{\delta}(1, \frac{1}{2})$. We use a different color for every set of initial conditions.

theory. According to the a-conjecture, given UV and IR conformal fixed points, $a_{UV} > a_{IR}$. Now for our field theory analysis to be valid, our gauge theories should never be very far away from conformality, where this distance is measured by the $\mathcal{O}(M/N)$ corrections. One expects therefore that a can be loosely defined at any point in the RG cascade and moreover that a should be non-increasing as we move into the IR. Recall that $a \sim \sum_\psi R(\psi)^3$ where the sum runs over the R-charges of all the fermions in the theory [7, 6]. From the structure of these quiver theories, one sees that $a \sim N^2$ and moreover after a sequence of four dualities for the dP_1 flow

188

above, $N \to N - 4M$. Thus a is indeed decreasing as we move into the IR despite the periodic behavior of the gauge couplings.

The scatter plots are reminiscent of the Poincaré surface-of-section (SoS) plots used in the study of chaotic dynamics. We recall that a Poincaré SoS is a surface in phase space which cuts the trajectory of a system. If the trajectory is periodic or quasiperiodic, the accumulation of intersection points where the trajectory cuts the surface often produces cycles. In our case, instead of phase space, the RG cascade is a trajectory inside the space of couplings, which we recall from §8.2.2 to be a glued set of tetrahedra. The ellipses we observe are sections thereof. In the above plots, we have actually superimposed different surfaces, $x_2 = 0$ and $x_1 = 0$, but a symmetry has kept the picture from getting muddled.

8.5   Supergravity Solutions for del Pezzo Flows

In the above, we have discussed in detail the RG flows for some del Pezzo gauge theories from a purely field-theoretic point of view. This is only half of the story according to the AdS/CFT Correspondence. It is important to find type IIB supergravity solutions that are dual to these field theory flows. As already emphasized [119], the main reason to trust that Seiberg duality cascades occur for the KS solution is not the field theory analysis but that it is reproduced by a well behaved supergravity solution. The purpose of this section is to investigate these dual solutions.

Surprisingly, even without a metric for the del Pezzos, we can demonstrate the existence of and almost completely characterize some of their supergravity solutions. The solutions we find are analogous to the Klebanov-Tseytlin (KT) solution [120] for the conifold. Recall that the KS solution is well behaved everywhere and asymptotes to the KT solution in the ultraviolet (large radius). The KT solution, on the other hand, is built not from the warped deformed conifold but from the conifold itself and thus has a singularity in the infrared (small radius).

8.5.1 Self-Dual (2,1) Solutions

To put these type IIB SuGRA solutions in historical context, note that they are closely related to a solution found by Becker and Becker [13] for M-theory compactified on a Calabi-Yau four-fold with four-form flux. One takes the four-fold to be a three-fold $\mathbf{X}$ times T^2 and then T-dualizes on the torus, as was done in [78, 33]. The crucial point here is that the resulting complexified three-form flux has to be imaginary self-dual and a harmonic representative of $H^{2,1}(\mathbf{X})$ to preserve supersymmetry. Graña and Polchinski [72] and also Gubser [76] later noticed that the KT and KS supergravity solutions were examples of these self-dual (2,1) type IIB solutions. (Indeed, the authors of [119] also mention that their complexified three-form is of type (2,1).)

Let us briefly review the work of Graña and Polchinski. The construction begins with a warped product of $\mathbb{R}^{3,1}$ and a Calabi-Yau three-fold $\mathbf{X}$:

$$ds^2 = Z^{-1/2}\eta_{\mu\nu}dx^\mu dx^\nu + Z^{1/2}ds_{\mathbf{X}}^2 , \qquad (8.5.44)$$

where the warp factor $Z = Z(p)$, $p \in \mathbf{X}$, depends on only the Calabi-Yau coordinates. We are interested in the case where $\mathbf{X}$ is the total space of the complex line bundle $\mathcal{O}(-K)$ over the del Pezzo dP_n. Here K is the canonical class. The manifold $\mathbf{X}$ is noncompact.

There exists a class of supersymmetric solutions with nontrivial flux

$$G_3 = F_3 - \frac{i}{g_s}H_3 \qquad (8.5.45)$$

where $F_3 = dC_2$ is the RR three-form field strength and $H_3 = dB_2$ the NSNS three-form. To find a supergravity solution, the complex field strength G_3 must satisfy several conditions: G_3 must

1. be supported only in $\mathbf{X}$;

2. be imaginary self-dual with respect to the Hodge star on $\mathbf{X}$, i.e., $\star_{\mathbf{X}} G_3 = iG_3$;

3. have signature $(2, 1)$ with respect to the complex structure on $\mathbf{X}$; and finally,

190

4. be harmonic.

If these conditions are met, a supergravity solution exists such that the RR field strength F_5 obeys

$$dF_5 = -F_3 \wedge H_3 \, , \tag{8.5.46}$$

and the warp factor satisfies

$$(\nabla_{\mathbf{X}}^2 Z)\mathrm{vol}(\mathbf{X}) = g_s F_3 \wedge H_3 \, , \tag{8.5.47}$$

where $\mathrm{vol}(\mathbf{X})$ is the volume form on $\mathbf{X}$. In particular, $\mathrm{vol}(\mathbf{X}) = r^5 dr \wedge \mathrm{vol}(\mathbf{Y})$ where $\mathbf{Y}$ is the (5 real-dimensional) level surface of the cone $\mathbf{X}$. The axion vanishes and the dilaton is constant: $e^\phi = g_s$.

8.5.2 (2,1) Solutions for the del Pezzo

Let us construct such a G_3 for the del Pezzos. As a first step, we construct the metric on $\mathbf{X}$. Let $h_{a\bar{b}}$ be a Kähler-Einstein metric on dP_n such that $R_{a\bar{b}} = 6h_{a\bar{b}}$. Indeed, we only know of the existence of and not the explicit form[1] of $h_{a\bar{b}}$. We want to consider the case where $\mathbf{X}$ is a cone over dP_n. In this case, the metric on $\mathbf{X}$ can be written [20, 19] as

$$ds_{\mathbf{X}}^2 = dr^2 + r^2\eta^2 + r^2 h_{a\bar{b}} dz^a d\bar{z}^{\bar{b}} \, , \tag{8.5.48}$$

where $\eta = \left(\frac{1}{3}d\psi + \sigma\right)$. The one-form σ must satisfy $d\sigma = 2\omega$ where ω is the Kähler form on dP_n and $0 \leq \psi < 2\pi$ is the coordinate on the circle bundle over dP_n.

Next, we describe a basis of self-dual and anti-self-dual harmonic forms on dP_n.[2] We begin with the Kähler form ω. Locally, dP_n looks like $\mathbb{C}^2$ and $2\omega \sim dz^1 \wedge d\bar{z}^{\bar{1}} + dz^2 \wedge d\bar{z}^{\bar{2}}$. Thus locally, it is easy to see that ω is self-dual under the operation of the Hodge star. Because the Hodge star is a local operator, ω must be self-dual

---

[1]Such a metric is known not to exist for dP_1 and dP_2. See for example [161].

[2]We would like to thank Mark Stern and James M$^{\mathrm{c}}$Kernan for the following argument.

everywhere. Now, recall our dP_n are Einstein. Thus

$$\omega = 6iR_{a\bar{b}}dz^a \wedge dz^{\bar{b}} = 6i\partial\bar{\partial}\ln\sqrt{\det h} \ . \tag{8.5.49}$$

Clearly $d\omega = (\partial + \bar{\partial})\omega = 0$ whence ω must be closed. It follows that ω is a self-dual harmonic form on dP_n.

There exists a cup product (bilinear form) Q on $H^{1,1}(dP_n)$ defined as

$$Q(\phi,\xi) = \int_{dP_n} \phi \wedge \xi \ , \qquad \phi,\xi \in H^{1,1}(dP_n) \ . \tag{8.5.50}$$

The Hodge Index Theorem states that Q has signature $(+,-,\ldots,-)$. For dP_n, $h^{2,0} = 0$ while $h^{1,1} = n+1$, there being n other harmonic $(1,1)$ forms on dP_n in addition to ω. We denote these harmonic forms as ϕ_I, $I = 1,\ldots,n$. Let us pick a basis for Q such that

$$\phi_I \wedge \omega = 0 \ . \tag{8.5.51}$$

From the above discussion of ω one sees that

$$0 < \int \omega \wedge \star\omega = \int \omega \wedge \omega \tag{8.5.52}$$

where the inequality follows from the definition of the Hodge star and the equality from the fact that ω is self-dual. Hence the ϕ_I span a vector space V where

Recall that the Hodge star in two complex dimensions squares to one: $\star\star\phi = \phi$. Thus we can diagonalize $\star$ on V such that $\star\phi_I = \pm\phi_I$. However, if $\star\phi_I = \phi_I$, then one would find $\int \phi_I \wedge \phi_I > 0$, in contradiction to the fact that Q has purely negative signature on V. We conclude that the ϕ_I must all be purely anti-self-dual, $\star\phi_I = -\phi_I$.

With these preliminaries, it is now straightforward to construct G_3. We let

$$F_3 = \sum_{I=1}^{k} a^I \eta \wedge \phi_I \ , \qquad H_3 = \sum_{I=1}^{k} a^I g_s \frac{dr}{r} \wedge \phi_I \ , \tag{8.5.53}$$

192

for expansion coefficients a^I. Hence,

$$G_3 = \sum_{I=1}^{k} a^I \left(\eta - i\frac{dr}{r}\right) \wedge \phi_I \ . \tag{8.5.54}$$

This is a solution because by construction, G_3 is harmonic and is supported on $\mathbf{X}$ so conditions (1) and (4) are met. Moreover, $(dr/r + i\eta)$ is a holomorphic one-form on $\mathbf{X}$. Therefore, G_3 must have signature $(2,1)$ because ϕ is a $(1,1)$ form. Furthermore, it is easy to check that $\star_{\mathbf{X}} G_3 = iG_3$. Thus, conditions (2) and (3) are also met.

D5-Branes The number of D5-branes in this SUGRA solution is given by the Dirac quantization condition on the RR flux. More precisely, we have an integrality condition on the integral of F_3 over compact three-cycles in the level surface $\mathbf{Y}$ of the cone $\mathbf{X}$. Given a basis $\mathcal{H}^J$ ($J = 1, \ldots n$) of such cycles, we impose that writing

$$\int_{\mathcal{H}^J} F_3 = 4\pi^2 \alpha' M^J \ , \tag{8.5.55}$$

must give integer M^J. From the construction of $\mathbf{Y}$, it follows that $\mathcal{H}^J$ will be some circle bundle over a curve $D^J \subset dP_n$ while the circumference of the circle is $2\pi/3$. Subsequently, equation (8.5.55) reduces to

$$\sum_I a^I \int_{D^J} \phi_I = 6\pi \alpha' M^J \ . \tag{8.5.56}$$

To understand the curve D^J, we take a closer look at the divisors that correspond to elements of $H^{1,1}(dP_n)$. Because dP_n is $\mathbb{P}^2$ blown up at n points, there will be a divisor H corresponding to the hyperplane in $\mathbb{P}^2$ and exceptional divisors E_i ($i = 1, \ldots, n$) for each of the blow ups. Essentially because two lines intersect at a point, $Q(H,H) = H \cdot H = 1$. From the blow-up construction, we also know that $Q(E_i, E_j) = E_i \cdot E_j = -\delta_{ij}$. Finally, $E_i \cdot H = 0$ because the blow-ups are at general position. We see explicitly that Q has signature $(+, -, -, \ldots, -)$. From Poincaré duality, there is a one-to-one map from the differential forms ω and ϕ_I to the divisors H and E_i, which we now explore.

The first chern class of $\mathbb{P}^2$ is $c_1(\mathbb{P}^2) = 3H$. By the adjunction formula, it follows that $c_1(dP_n) = 3H - \sum_{j=1}^{n} E_j$. Locally, the first chern class can be expressed in terms of the Ricci tensor,

$$c_1(dP_n) = i\frac{R_{a\bar{b}}}{2\pi}dz^a \wedge d\bar{z}^{\bar{b}} , \tag{8.5.57}$$

and then from the Einstein condition (8.5.49), we find that

$$\omega = \frac{\pi}{3}c_1(dP_n) . \tag{8.5.58}$$

Thus, by (8.5.51), the ϕ_I must be orthogonal to $c_1(dP_n)$. This orthogonality condition has an astonishingly beautiful (and well known) consequence. The orthogonal complement of $3H - \sum_j E_j$ is the weight lattice of the corresponding exceptional Lie group $\mathcal{E}_n$. In this language the ϕ_I must lie in this weight lattice.

We now return to the question, what are the curves D^J in the integral (8.5.56)? The problems we need to worry about in defining the D^J are essentially the same problems we need to worry about in trying to quantize the flux in a far simpler system, that of a collection of point electric charges in three dimensions. In drawing a sphere (or perhaps some shape with more complicated topology) around each charge, we want to make sure that the sphere wraps around the selected charge exactly once and no other charges.

For the dP_n, this condition translates into the requirement that

$$\int_{D^J} \phi_I = \int_{dP_n} \phi_I \wedge c_1(D^J) = \delta_I^J . \tag{8.5.59}$$

Because $\phi_I \wedge \omega = 0$, only the component of $c_1(D^J)$ orthogonal to $c_1(dP_n)$ need be defined. Let us choose $c_1(D^J) \wedge \omega = 0$. To avoid surrounding charges more than once, we need to make the D^J "as small as possible". Thus we choose the $c_1(D^J)$ to be the generators of the weight lattice. The condition (8.5.59) then implies that the ϕ_I generate the root lattice. For example, for dP_3, we could choose $\phi_1 = E_1 - E_2$, $\phi_2 = E_2 - E_3$, and $\phi_3 = H - E_1 - E_2 - E_3$. Indeed, the bilinear form (8.5.50) can be

written in the basis

$$\int_{dP_n} \phi_I \wedge \phi_J = -A_{IJ} \tag{8.5.60}$$

where A_{IJ} is the Cartan matrix for the $\mathcal{E}_n$ root lattice.

Finally, using (8.5.53), (8.5.56) and (8.5.59), we can normalize F_3 and H_3, giving us

$$a^J = 6\pi\alpha' M^J \; ; \tag{8.5.61}$$

hence the number M^J of D5-branes is fixed in our SUGRA solutions. From a perturbative point of view, we can think of this SUGRA solution as arising from the back reaction of D5-branes wrapped around vanishing curves C_I of $\mathbf{X}$, which are the Poincaré duals of the ϕ_I. This follows from the definition $dF_3 = \sum a^I d(\eta \wedge \phi_I) = \sum a^I \delta_{C_I}$.

D3-branes Having discussed some detailed algebraic geometry for the dP_n, we are now ready to quantize the number N of D3-branes as well. The condition reads, using (8.5.46),

$$\int_{\mathbf{Y}} F_5 = (4\pi^2\alpha')^2 N \; , \tag{8.5.62}$$

where $F_5 = \mathcal{F} + \star_{10}\mathcal{F}$, and

$$\mathcal{F} = \sum_{I,J} a^I a^J g_s \ln(r/r_0)\eta \wedge \phi_I \wedge \phi_J \; . \tag{8.5.63}$$

Therefore one finds, using (8.5.60) and (8.5.61),

$$N = \frac{3}{2\pi} g_s \ln(r/r_0) \sum_{I,J} M^I A_{IJ} M^J \tag{8.5.64}$$

for large r. In other words, the number of D3-branes grows logarithmically with the radius.

Warp Factor Now, recalling from [20] that for $\mathbf{Y} = dP_n$,

$$\int_{\mathbf{Y}} \mathrm{vol}(\mathbf{Y}) = \frac{\pi^3}{27}(9 - n) \; , \tag{8.5.65}$$

195

we can use (8.5.53) and (8.5.47) to solve for the warp factor. The equation reads

$$\left[\frac{\partial^2}{\partial r^2} + \frac{5}{r} \frac{\partial}{\partial r} \right] Z(r) = \frac{(6\pi \alpha' g_s)^2}{\text{Vol}(\mathbf{Y})} \frac{2\pi}{3r} \sum_{I,J} M^I A_{IJ} M^J \, . \tag{8.5.66}$$

This yields

$$Z(r) = \frac{2 \cdot 3^4}{9-n} \alpha'^2 g_s^2 \left(\frac{\ln(r/r_0)}{r^4} + \frac{1}{4r^4} \right) \sum_{I,J} M^I A_{IJ} M^J \, . \tag{8.5.67}$$

In short, we have found the analog of the Klebanov-Tseytlin solution, a solution that is perfectly well behaved at large radius but has a curvature singularity at small radius $Z(r_*) = 0$. We envision that there is some similar warped deformed del Pezzo solution which resolves the singularity, just as the warped deformed conifold of the KS solution resolved the singularity of the KT solution. An analysis of such IR deformations, from a field theory and toric geometry perspectives, is the subject of Chapter 9.

8.5.3 Gauge Couplings

In order to move towards a comparison between SUGRA and gauge theory, let us determine the gauge couplings on probe branes inserted into the geometry we have discussed above. To begin with, let us study D3-branes. Their gauge coupling is simply proportional to the string coupling, g_s, which as we have seen is constant in the self-dual (2,1) solutions. In gauge theory, this is expressed by the fact that the sum of gauge couplings (8.2.14) is independent of the scale.

We can also probe with D5-branes. Consider a D5-brane wrapped on a curve $C_I \subset dP_n \subset \mathbf{Y}$ at a fixed radial position r in $\mathbf{X}$. We take C_I to be the Poincaré dual of the harmonic two-form ϕ_I. As is well-known (see, e.g., [94]), the gauge coupling on such a brane is related to the integral of the NS 2-form around C_I by

$$x_I = \frac{8\pi^2}{g_I^2} = -\frac{1}{2\pi \alpha' g_s} \int_{C_I} B_2 \, . \tag{8.5.68}$$

Thus, using the expression for B_2 by integrating H_3 from (8.5.53), as well as the value

of a^J from (8.5.61), we find

$$x_I = -3 \ln r \sum_J \int_{C_I} \phi_J M^J .$$ (8.5.69)

This yields for the beta function

$$\beta_I = \frac{dx_I}{d \ln r} = -3(C_I \cdot C_J) M^J ,$$ (8.5.70)

where $C_I \cdot C_J = \int \phi_I \wedge \phi_J$ is the *intersection pairing* of two-cycles in dP_n and the sum on J is implied.

To compare this result with gauge theory, we first need to recall the fact from section 8.2.2 that a D5 brane wrapped around C_I is associated with a certain combination of fractional branes that we have encoded in the vector $s_I = (s_I^i)$. Thus, the beta function β_I is related to the beta functions of the fractional branes via

$$\beta_I = \sum_i s_I^i \beta_i ,$$ (8.5.71)

Inserting the expression for β_i from (8.2.10), we obtain the gauge theory expression

$$\beta_I = 3 \sum_i s_I^i s_J^i M^J + \frac{3}{2} \sum_{ij} s_I^i \tilde{R}_{ij} s_J^j M^J$$ (8.5.72)

where $\tilde{R}$ is given in (8.2.11). Let us now use the vanishing of the beta function for the conformal theory (corresponding to putting $d^i = r^i$ in (8.2.8) and using (8.2.10)) to rewrite the first term as

$$\sum_i s_I^i s_J^i = -\frac{1}{2} \sum_{ij} s_I^i s_J^i \tilde{R}_{ij} \frac{r^j}{r^i} .$$ (8.5.73)

Using the definition of $\tilde{R}_{ij}$ in (8.2.11), we find the gauge theory result

$$
\begin{aligned}
\beta_I &= \frac{3}{2}\sum_{ij} \tilde{R}_{ij}\left(s_I^i s_J^j - s_I^i s_J^i \frac{r^j}{r^i}\right)M^J \\
&= \frac{3}{2}\sum_{ij} f_{ij}(R_{ij}-1)\left(s_I^i s_J^j + s_I^j s_J^i - s_I^i s_J^i \frac{r^j}{r^i} - s_I^j s_J^j \frac{r^i}{r^j}\right)M^J \, . \quad (8.5.74)
\end{aligned}
$$

To finish up and relate this long-winded expression to the intersection pairing in (8.5.70), we need to rely on certain results concerning baryonic $U(1)$ charges in quiver gauge theories related to del Pezzos [138, 103, 97, 96]. First of all, these baryonic $U(1)$ charges are in one-to-one correspondence with possible non-conformal deformations. In formulas, one can write all baryonic $U(1)$ charges Q_I as a sum

$$
Q_I = \sum_i q_I^i Q_i \qquad (8.5.75)
$$

where Q_i is a charge associated with the nodes of the quiver and is equal to $+1$ for incoming arrows and -1 for outgoing arrows. In other words,

$$
Q_I(X_{ij}) = q_I^j - q_I^i \, . \qquad (8.5.76)
$$

For purposes of anomaly cancellation, these charges are related to the null vectors s_I^i of $\mathcal{I} = S - S^t$ via [103, 97]

$$
q_I^i r^i = s_I^i \, . \qquad (8.5.77)
$$

It was then shown in [97] that the baryonic $U(1)$ charges Q_I are also in one-to-one correspondence with curves C_I in the del Pezzo orthogonal to the Kähler class. Moreover, it was shown in [97] that one could identify the intersection product of the curves C_I as the cubic anomaly associated with the baryonic charges Q_I,

$$
C_I \cdot C_J = \frac{1}{2}\mathrm{tr}R Q_I Q_J \, . \qquad (8.5.78)
$$

Now let us relate this cubic anomaly to the beta functions.

$$
\begin{aligned}
(\mathrm{tr} R Q_I Q_J)\, M^J \;&=\; M^J \sum_{i,j} f_{ij}(R_{ij}-1) Q_I(X_{ij}) Q_J(X_{ij}) r^i r^j \\
&=\; M^J \sum_{i,j} f_{ij}(R_{ij}-1)(q_I^j - q_I^i)(q_J^j - q_J^i) r^i r^j \\
&=\; -M^J \sum_{i,j} f_{ij}(R_{ij}-1)\Big(s_I^i s_J^j + s_I^j s_J^i - s_I^i s_J^i \frac{r^j}{r^i} - s_I^j s_J^j \frac{r^i}{r^j}\Big) = -\frac{2}{3}\beta_I \, .
\end{aligned}
$$

This expression, upon substituting into the SuGRA result (8.5.70), gives the gauge theory result for the beta function in (8.5.74), whereby giving us the link we needed.

8.5.4 Discussion

On the one hand it is impressive that we can write down such a complicated supergravity solution that encodes interesting field theoretic behavior without knowing the precise metric on the del Pezzos. On the other, it is a little disappointing that we have found no smoking gun for the existence of duality walls from the supergravity perspective.

Let us consider the implications of this KT-like solution for del Pezzos. Such a solution indicates that the dual del Pezzo field theory should behave like the KS field theory. In other words, one expects a sequence of Seiberg dualities where as we move into the UV, the number of D3-branes gradually increases, the number of D5-branes remains fixed, and no duality wall is reached. We have seen such behavior for some of the phases of the del Pezzos. For example, the Model A/Model B flow of [56] and the dP_1 flow considered here exhibit such behavior. Several other examples will be constructed in Chapter 9.

Our supergravity solutions severely constrain possible $\mathcal{O}(M/N)$ corrections to the R-charges for KS type flows. In particular, both on the field theory side and on the supergravity side, we saw that the sum of the beta functions (8.2.14) must vanish. Additionally, we calculated the n β_I for dP_n both in field theory and in supergravity and saw that the two expressions agreed. In total, we have $n+1$ constraints on $n+3$

beta functions. Thus, any corrections to the beta functions for KS flows must lie in the remaining two dimensional vector space. (Note that for the original KT solution for the conifold, the two constraints are enough eliminate any possible corrections to the two beta functions.)

We have also seen behavior vastly different from KS type cascades. For example, for the F_0 surface, we saw duality walls. Note also in this flow that the number of D3-branes does not increase but is pinned by nodes three and four. Presumably there is some other supergravity solution which describes this flow. One way of constructing a more general type of supergravity solution would be to try to construct F_3 with a dependence on dr or to start with a non-conical metric on **X**.

Chapter 9

Multi-Flux Warped Throats and Cascading Gauge Theories

In this chapter we describe duality cascades and their infrared behavior for systems of D3-branes at singularities given by complex cones over del Pezzo surfaces (and related examples), in the presence of fractional branes. From the gauge field theory viewpoint, we show that D3-branes probing the infrared theory have a quantum deformed moduli space, given by a complex deformation of the initial geometry to a simpler one. This implies that for the dual supergravity viewpoint, the gauge theory strong infrared dynamics smoothes out the naked singularities of the warped throat solutions with 3-form fluxes constructed in Chapter 8, describing the cascading RG flow of the gauge theory. This behavior thus generalizes the Klebanov-Strassler deformation of the conifold. We describe several explicit examples, including models with several scales of strong gauge dynamics. In the regime of widely separated scales, the dual supergravity solutions should correspond to throats with several radial regions with different exponential warp factors. These rich throat geometries are expected to have interesting applications in compactification and model building. Throughout our studies, we also construct explicit duality cascades for gauge theories with irrational R-charges, obtained from D-branes probing complex cones over dP_1 and dP_2. The material we present in this chapter is based on [59].

9.1 Introduction

The preceding sections have been devoted to the study of cascading gauge theories. We have seen that their ultraviolet (UV) behavior is markedly different from that of ordinary field theories. Instead of having a UV fixed point, they have an infinite tower of dual theories with a steadily increasing number of colors and matter fields towards the UV. This increase can sometimes be linear as in [119], or can be much faster, with a power law or even exponential behavior. In the latter cases, the dualization scales generally present a UV accumulation point, leading to a duality wall [85, 56].

A supergravity solution describing the UV region of the conifold cascade was found by Klebanov and Tseytlin (KT) in [120]. This solution is well behaved at large energies but has a naked singularity in the infrared (IR). A full solution, which asymptotes the one of KT at large energies but is well behaved in the IR was later presented by Klebanov and Strassler (KS) in [119]. Instead of being based on the singular conifold, it is constructed using the *deformed conifold*. The 3-cycle inside the deformed conifold remains of finite size in the IR, avoiding the singular behavior. On the gauge theory side, the IR singularity is eliminated by strong coupling effects, whose scale is related to the dual 3-cycle size.

In [61], UV solutions, similar to that of KT, were constructed for complex cones over del Pezzo surfaces dP_n, for $3 \leq n \leq 8$. These supergravity solutions were presented in Section 8.5. They also suffer from the same problems in the IR. Contrary to what happens for the conifold, explicit metrics describing either the non-spherical horizons or their deformations are not known. Therefore it remains an open question to develop methods to understand the infrared behavior of these theories in their dual versions. The purpose of this chapter is to use the strong coupling dynamics of the dual gauge theories to extract as much information as possible regarding these deformations. In particular we will show a precise agreement between the field theory analysis of D3-branes probing the infrared of the cascades and the complex deformations of the initial geometries. This strongly supports the existence of completely smooth supergravity descriptions of the complete RG flow for (some of) these non-

conformal gauge theories. In addition, our techniques are valid for other geometries, suggesting the existence of cascades and infrared deformations for other quiver gauge theories.

Although our examples are analogous to the conifold in some respects, the gauge theories and corresponding geometries are notably richer in others. For instance, we will encounter that these gauge theories generically give rise to several dynamical scales. In the regime of widely separated scales, the flow among these scales is to a great approximation logarithmic. The supergravity duals thus correspond to logarithmic throats with different warp factors, patched together at some transition scales. Clearly these topologically richer throats deserve further study.

Before proceeding, it is important to point out that our analysis shows that a smoothing of the singularity by a complex deformation may not be possible for some geometries, or even for all possible assignments of fractional branes in a geometry. Our methods give a clear prescription for when this is the case. A class of examples of this kind is provided by the countable infinite family of 5d horizons with $S^2 \times S^3$ topology, for which explicit metrics have been constructed in [65, 63, 66, 64, 134]. These geometries are labeled by two positive integers $p > q$ and are denoted $Y^{p,q}$. In [14], the quiver theories living on the world-volume of D3-branes probing metric cones over $Y^{p,q}$ geometries were derived. We review this work in Chapter 10. Impressive checks of the AdS/CFT correspondence for these models, such as matching the field theory R-charges and central charge $a = c$ with the corresponding geometric computations were carried out in full generality [14]. Recently, warped throat supergravity solutions dual to cascades in the $Y^{p,q}$ quivers were constructed in [92]. These solutions exhibit a naked singularity, and we show that for the particular subclass of $Y^{p,0}$ a complex deformation removes the IR singularity. However, in the general case these geometries do not admit complex deformations to smooth out their infrared behavior. It would be interesting to understand such examples, and we leave this question for future research.

The chapter is organized as follows. In Section 9.2 we provide some background material.

In Section 9.2.1 we review the KS supergravity solution for the conifold, stressing, making emphasis in the IR behavior. We also discuss possible generalizations of the supergravity throats constructed in [61] and presented in Section 8.5.

In Sections 9.2.2 and 9.2.3 we present a framework to determine possible geometric deformations for general local Calabi-Yau geometries using (p, q) web diagrams, and discuss a topological property of the corresponding RG flow solutions. In section 9.2.4 we introduce our approach to show that the strong gauge theory dynamics induces the complex deformation of the initial geometries to simpler ones. These arise as quantum deformations of the moduli space of the gauge theory describing D3-branes probing the infrared dynamics.

In Section 9.3 we describe some simple examples of RG cascading flows and infrared deformations, in several cases with a single strong dynamics scale. The examples include the cone over F_0, the cone over dP_2, and the suspended pinch point (SPP) singularity. In subsequent sections we present examples with several strong dynamics scales. In Section 9.4 we study the case of the cone over dP_3, which admits a two-scale deformation following the pattern $dP_3 \rightarrow$ conifold $\rightarrow$ smooth ($\mathbb{C}^3$). In Section 9.5 we present further two-scale examples, namely $dP_4 \rightarrow$ SPP $\rightarrow$ smooth, and $PdP_3 \rightarrow \mathbb{C}^2/\mathbb{Z}_2 \rightarrow$ enhançon.

Section 9.6 contains our concluding remarks. Appendix 9.7 presents an alternative approach for the field theory analysis of the mesonic branch, while Appendix 9.8 provides a detailed description of the deformations in toric geometry. Finally Appendix 9.9 describes the field theory description of the smoothing for real cones over the $Y^{p,0}$ manifolds.

9.2   Cascading throats

In this section we lay out our approach to cascading RG flows. We first discuss the supergravity duals that describe logarithmic flows, beginning with a review of the well known conifold example and then moving on to generalizations to other geometries. We then explain how to identify extremal transitions using (p, q) web

diagrams. Finally, we discuss how these geometric deformations are generated by the strong coupling dynamics of the gauge theory.

9.2.1 Supergravity throats

To frame the forthcoming discussion, it is convenient to review the case of the conifold. The $\mathcal{N} = 1$ supersymmetric gauge theory on N D3-branes at a conifold singularity [121], in the presence of M fractional branes (i.e. D5-branes wrapped over the 2-cycle in the base of the conifold), is given by a gauge group $SU(N) \times SU(N + M)$, with two chiral multiplets A_1, A_2 in the representation $(\Box, \bar{\Box})$ and two multiplets B_1, B_2 in the representation $(\bar{\Box}, \Box)$. The superpotential is $W = A_1 B_1 A_2 B_2 - A_1 B_2 A_2 B_1$. In order to keep the notation short, we leave the superpotential couplings and the trace over color indices implicit. We will adopt this convention when presenting all the forthcoming superpotentials. As discussed in [119] and thoroughly reviewed in Chapters 7 and 8, for $M \ll N$ the theory undergoes a duality cascade as it flows to the infrared, at each step of which the highest rank gauge group becomes strongly coupled and is replaced by its Seiberg dual.

A supergravity solution describing the UV region of the conifold cascade was found by Klebanov and Tseytlin (KT) in [120]. This solution is well behaved at large energies but has a naked singularity in the infrared (IR). A full solution, which asymptotes the one of KT at large energies but is well behaved in the IR was later presented by Klebanov and Strassler (KS) in [119]. Instead of being based on the singular conifold, it is constructed using the *deformed conifold*. The 3-cycle inside the deformed conifold remains of finite size in the IR, avoiding the singular behavior. On the gauge theory side, the IR singularity is eliminated by strong coupling effects, whose scale is related to the dual 3-cycle size.

In the absence of fractional branes the gauge theory on D3-branes at a conifold singularity is superconformal, and its supergravity dual is given by Type IIB theory on $AdS_5 \times T^{1,1}$. The 5-manifold $T^{1,1}$ is topologically $S^2 \times S^3$, and may be regarded as an S^1 fibration over $S^2 \times S^2$. Denoting σ_i the 2-forms dual to the two S^2's, we define for future convenience the Kähler class $\omega = \sigma_1 + \sigma_2$ and the orthogonal combination

$\phi = \sigma_1 - \sigma_2$.

In the presence of M fractional branes, conformal invariance of the gauge theory is broken, and the supergravity dual is no longer $AdS_5 \times T^{1,1}$. In the UV, the supergravity dual is a particular case of the throats to be described in section 9.2.1. Sketchily, it is a warped version of $AdS_5 \times T^{1,1}$, with warping sourced by non-trivial RR and NSNS 3-form fluxes supported on ϕ,

$$G_3 = F_3 - \frac{i}{g_s} H_3 = M(\eta + i\frac{dr}{r}) \wedge \phi \qquad (9.2.1)$$

where η is a 1-form along the S^1 fiber in $T^{1,1}$, and r is the radial coordinate. In intuitive terms, the RR flux (related to F_3) is sourced by the fractional branes in the dual description, while the NSNS flux (related to H_3) leads to a logarithmic running of the relative inverse squared gauge coupling of the field theory. The fluxes also lead to a radially varying integral of the 5-form over $T^{1,1}$, which reproduces the decrease in the number of D3-branes in the duality cascade of the field theory. The solution does not contain, even asymptotically, an AdS_5. This is accordance with the fact that the gauge theory does not have a conformal fixed point in the presence of fractional branes.

The above solution, first studied in [120], if extended to the IR, leads to a naked singularity. Intuitively, this is because the above supergravity description misses the **strong coupling dynamics** taking place near the end of the cascade. The full solution in [119] is smooth, due to a non-trivial modification of the above ansatz in the infrared. In the IR, the geometry is a deformed conifold, and has a finite size S^3, which supports the RR 3-form flux. The size of this 3-cycle is related to the scale of strong dynamics of the dual gauge theory. The complete solution is a warped deformed conifold, with imaginary self-dual 3-form fluxes which are moreover $(2,1)$-forms and thus preserve supersymmetry [76, 72]. In the UV, the full solution asymptotes the warped version of $AdS_5 \times T^{1,1}$ described above, while in the IR it contains a non-trivial 3-cycle supporting the flux.

Overall, the gauge/gravity correspondence is a relation between the field theory,

described by fractional D3-branes on (i.e. D5-branes on the 2-cycle of) a resolved conifold, and the supergravity solution, described by 3-form fluxes on a deformed conifold. Namely a brane-flux transition taking place between two geometries related by an extremal transition where a 2-cycle disappears and is replaced by a 3-cycle [166, 25, 26, 24]. In our case the geometries under consideration are toric, and can be visualized using web or toric diagrams [4, 5]. The geometric interpretation of webs is discussed in detail in [130]. In these pictures, finite segments and faces of the initial web correspond to 2- and 4-cycles in the resolution phase, while 3-cycles correspond to segments joining the different sub-webs in the deformation phase. The geometrical transition is nicely depicted using web diagrams for the conifold geometry, as shown in Figure 9-1. The detailed geometric description of the deformation is described in Appendix 9.8.
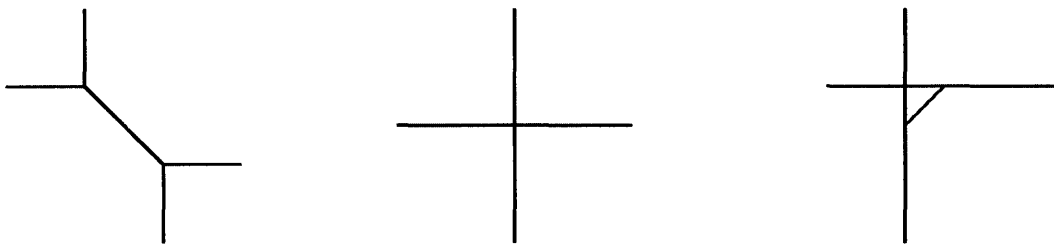
Figure 9-1: Conifold extremal transition. The finite segment in the first figure represents an S^2, with an area proportional to the length of the segment, while the green segment in the last figure corresponds to an S^3 with a volume proportional to the distance between the two infinite lines.

For future convenience, it is useful to review the matching between the deformation of the geometry and the infrared dynamics of the field theory. In particular, and following [119], we may recover the deformed conifold geometry as the moduli space of D3-branes probing the infrared end of the cascade.

A simple derivation follows by considering the infrared theory in the presence of M additional D3-branes. This is described by a conifold gauge theory with gauge group $SU(2M) \times SU(M)$, with the chiral multiplets A_r, B_r, $r = 1, 2$ and superpotential $W = A_1 B_1 A_2 B_2 - A_1 B_2 A_2 B_1$. The non-perturbative dynamics may be determined by assuming, to begin with, that the $SU(M)$ gauge factor is weakly coupled and acts as a spectator, corresponding to a global flavor symmetry. Then the gauge factor

$SU(2M)$ has $N_f = N_c$ and develops a quantum deformation of its moduli space. Introducing the four mesons $M_{rs} = A_r B_s$, which transform in the adjoint of $SU(M)$, and the baryons $\mathcal{C}$, $\tilde{\mathcal{C}}$, the quantum modified moduli space is described by

$$\det(M_{11})\det(M_{22}) - \det(M_{12})\det(M_{21}) - \mathcal{C}\tilde{\mathcal{C}} = \Lambda^{4M}, \qquad (9.2.2)$$

where Λ is the dynamical scale of the $SU(2M)$ gauge theory. The constraint may be implemented in the superpotential by introducing a Lagrange multiplier chiral field X, so it reads

$$W = M_{11}M_{22} - M_{12}M_{21} - X(\det \mathcal{M} - \mathcal{C}\tilde{\mathcal{C}} - \Lambda^{4M}), \qquad (9.2.3)$$

with $\mathcal{M}$ a $2M \times 2M$ matrix whose blocks are the $M \times M$ matrices, $M_{11}, M_{12}, M_{21}, M_{22}$. The quantum constraint forces some of the mesons or baryons to acquire vevs. As discussed in [119], the dynamics of the probes is obtained along the mesonic branch[1], which corresponds to

$$X = \Lambda^{4-4M} \quad ; \quad \mathcal{C} = \tilde{\mathcal{C}} = 0 \quad ; \quad \det \mathcal{M} = \Lambda^{4M} \qquad (9.2.4)$$

The vacuum is parametrized by the vevs of the mesons M_{ij}, subject to the quantum constraint. This can be seen to correspond to M D3-brane probes moving in a deformed conifold. To make this more manifest and to simplify the discussion, it is convenient to restrict to the Abelian case. This is sensible, because all the information about the non-Abelian gauge dynamics has been already included, and because we are not turning on baryonic degrees of freedom.[2] The moduli space of the single

---

[1] As mentioned already in [119], the baryonic branch describes instead the continuation of the cascade down to the endpoint $SU(M)$ theory. That the infrared theory at the end of the cascade is in the baryonic branch is supported by the identification in the supergravity solution of the Goldstone mode associated to the spontaneous breaking of baryon number symmetry, and the identification of the D1-brane as an axionic string [77, 154, 23].

[2] A more precise statement would be to stick to the non-Abelian case, without overall $U(1)$, but study the dynamics along the generic mesonic Higgs branch. Our results below would arise for the relative $U(1)$'s controlling the relative positions of the D-branes. The trick of simplifying the discussion by restricting to the Abelian quiver theory is a standard manipulation for branes at singularities, see [138] for further discussion.

D3-brane probe in this case is

$$M_{11}M_{22} - M_{12}M_{21} = \Lambda^4 \qquad (9.2.5)$$

namely, a deformed conifold geometry. Hence the strong coupling dynamics of the field theory encodes the deformed geometry at the infrared end of the cascade, dictating the size of the finite S^3.

The general idea is that the gauge theory living on the D-brane world volume perceives the deformed geometry that becomes important at a given scale as a quantum deformation of its moduli space. This technique will generalize to more complicated cascades and infrared behaviors in the next sections.

As we discussed, the main support for the idea of a cascading RG flow for the conifold comes from the supergravity dual description [120]. In Section 8.5, we discussed the construction of analog supergravity solutions for del Pezzo surfaces [61]. This construction of throats was originally elucidated for the case of del Pezzo surfaces. Nevertheless, its range of applicability is much broader and it is indeed suitable for any other complex cone over a 4-dimensional surface Y^4 with a Kähler-Einstein metric.

The construction of these throats is important since it illustrates that cascading RG flows appear often in quiver gauge theories. Moreover, warped throats are interesting both from the viewpoint of phenomenological applications (e.g. [67, 109, 27]) and of counting flux vacua, due to their 'attractor' behavior [35]. Our purpose in this chapter is to clarify the infrared structure of these (and similar) classes of models, a key understanding required for the above applications.

These throats contain a naked singularity at their origin, and hence are the analogs of the KT throat [120] for the conifold. In later sections we will clarify that the dual gauge theory infrared dynamics suggests that in many situations a suitable deformation of the geometry eliminates the singularity, and yields a smooth supergravity solution, the analog of the solution in [119] for the conifold.

In addition, we would like to mention that there exist more general situations,

where the conical Calabi-Yau singularity corresponds to a real cone over a Sasaki-Einstein 5-dimensional horizon X_5 as before, but X_5 cannot be constructed as a $U(1)$ fibration over a 4-dimensional Kähler-Einstein base. Simple examples of this class are provided by the complex cones over dP_1 and dP_2, where the $U(1)$ fibration over the del Pezzo surface is irregular. This fact maps, on the gauge theory side, to irrational R-charges. Moreover, recently, an infinite family of cones over 5d Sasaki-Einstein manifolds, denoted $Y^{p,q}$, with explicit metrics has been constructed [65, 63, 66, 64, 134]. Also, the dual quiver gauge theories have been found in [14]. Duality cascades for the case of $Y^{2,1}$, corresponding to the 5d horizon of a complex cone over dP_1, were constructed in [61], and duality cascades for the entire $Y^{p,q}$ family along with their supergravity duals have been recently carried out in [92]. An interesting difference with respect to the above throats is an additional dependence of the warp factor on a coordinate of the 5d horizon X_5, rather than just on the radial direction.

Finally, notice that, using our arguments in coming sections, one can show that the $Y^{p,q}$ cascades do not in general admit a geometric deformation to resolve their singularities. The only cases where this is possible correspond to cones over $Y^{p,0}$, which are in fact $\mathbb{Z}_p$ quotients of the conifold. They thus fall within our analysis, and we describe the field theory version of their smoothing in Appendix 9.9.

9.2.2 The deformed geometries

The above throats contain a naked singularity, suggesting that they miss the non-perturbative infrared dynamics of the dual gauge field theory. Hence they are the analogs of the singular solution in [120]. From the discussion of the conifold it is expected that, at least in some cases, when the infrared gauge theory dynamics is included, the dual supergravity solution corresponds to a deformed background related to the original one by an extremal transition. This transition replaces 2- and 4-cycles by 3-cycles. A general question is therefore to analyze the existence of extremal transitions on local Calabi-Yau geometries, where shrinking 4-cycles are replaced by finite size 3-cycles.

In this section we address this geometric question from several viewpoints. For

concreteness we center the discussion on the geometries given by complex cones over del Pezzo surfaces, although results generalize to other situations, as will be clear in our examples.

The general question is what are the possible deformations of the complex cones over del Pezzo surfaces. Besides its relevance to the above discussion, this question has another interesting realization. Geometries with collapsing del Pezzo surfaces lead, when used as M-theory backgrounds, to five-dimensional field theories with E_n global symmetries. The Coulomb branch is parametrized by the sizes of the 2-cycles, while the Higgs branch corresponds to extremal transitions, i.e. complex deformations of the geometry arising at the origin of the Coulomb branch, where the 4-cycle shrinks to zero size. The classification of such Higgs branches was described in [157], and shown [140] to fully agree with the geometric description.[3]

In many examples, one may use the realization of the five-dimensional field theories in terms of (p, q) webs of Type IIB fivebranes [4, 5], in order to visualize the corresponding Higgs branches. This corresponds to the situations where the geometries are toric, and the (p, q) web corresponds to the reciprocal of the collection of points in the $\mathbb{Z}^2$ integer lattice defining the toric diagram [5, 130]. In general, for toric geometries with a corresponding web, deformations exist if there are subsets of external legs which can form sub-webs in equilibrium. The deformation is described as the separation of such sub-webs. A more precise description of this in toric geometry language is illustrated in some examples in Appendix 9.8.

The (p, q) web representation of the deformation for the conifold is described in Figure 9-1, where the sub-webs correspond to straight lines. The 3-cycle in the deformed conifold corresponds to a segment stretched between the two sub-webs. For example in 5 dimensional gauge theories a D3-brane stretched between the two (p, q) sub-webs is a BPS brane on the Higgs branch, which maps to a brane wrapped on the 3-cycle in the geometry.

---

[3] A concise description of these Higgs branches is provided by the instanton moduli space of the corresponding E_n gauge theory. The relation is manifest by realizing the five-dimensional field theory in the worldvolume of D4-branes probing configurations of D8-branes/O8-planes at strong coupling, so that the global symmetry is enhanced to E_n [157]. The Higgs branch corresponds to dissolving the D4-brane as an instanton of the E_n gauge theory.

Using the toric diagrams for the cones over del Pezzo surfaces one can recover the results in [140]. Namely, for dP_0 and dP_1 there is no deformation branch, as is manifest from their toric pictures, Figure 9-2.
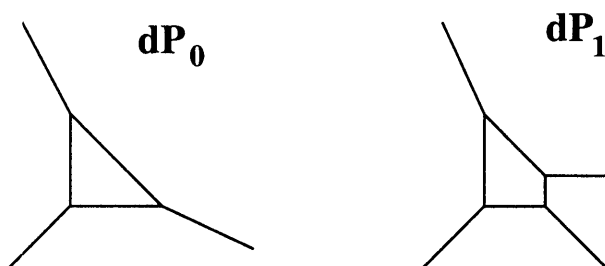
Figure 9-2: Web diagrams for the complex cones over dP_0 and dP_1. In both cases, it is impossible to split them into more than one sub-webs in equilibrium, implying there exist no complex deformations for these geometries.

On the other hand, dP_2 has a deformation, shown in Figure 9-3, which completely smoothes out the geometry. For dP_3 there are two deformation branches, one of them two-dimensional and the other one-dimensional, see Figure 9-4. Notice that the two-dimensional deformation branch may be regarded as a one-dimensional deformation to the conifold, subsequently followed by a one-dimensional deformation to a smooth space. This is more manifest in the regime of widely different sizes for the two independent 3-cycles.
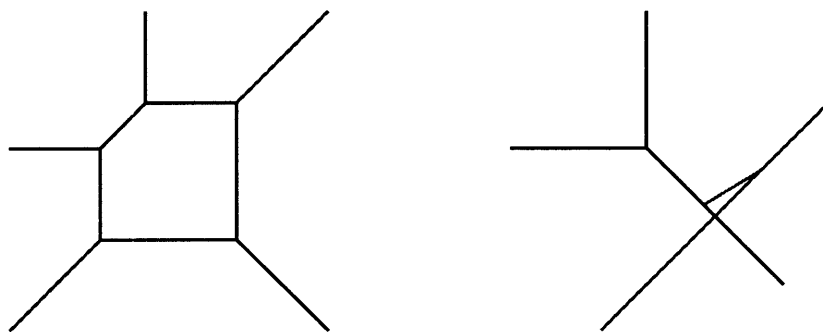
Figure 9-3: The web diagram for the complex cone over dP_2 and its complex deformation.

For higher del Pezzo surfaces, the generic geometry is not toric. However, there are closely related blow-ups of $\mathbb{P}_2$ at non-generic points, which do admit a toric description. These non-generic geometries lead to the same quivers than the del Pezzos,
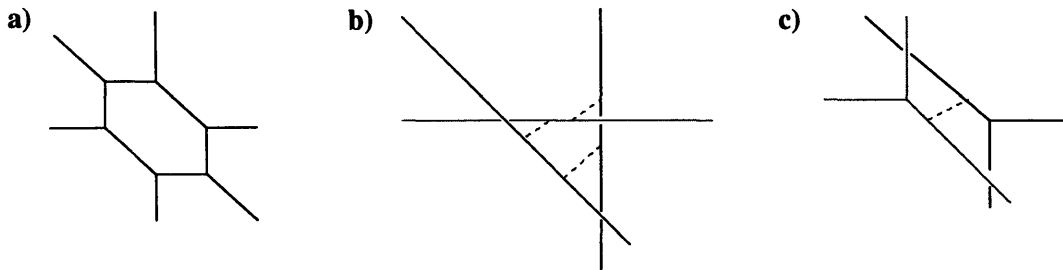
Figure 9-4: Web diagram for the complex cone over dP_3 and its two branches of complex deformation. Figure b) shows a two-dimensional deformation branch, parametrized by the sizes of two independent 3-spheres corresponding to the dashed segments (the three segments are related by a homology relation, hence only two are independent). Figure c) shows a one-dimensional deformation branch.

but with different superpotentials. For non-toric del Pezzos, some deformations are manifest in the toric representation, see Figure 9-5 for an example. Notice however that the dimensions of these deformation branches are in general lower than that for generic geometries, thus showing that some deformations of the higher del Pezzos are non-toric.
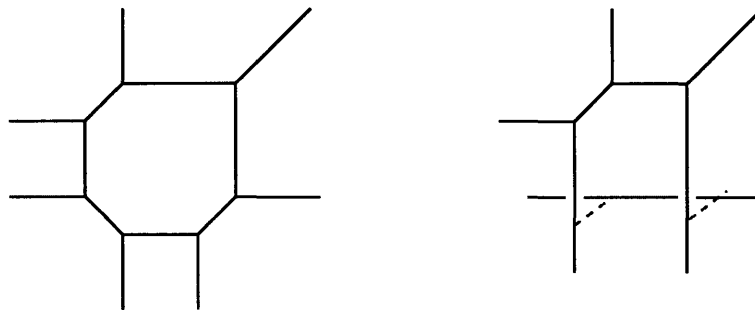
Figure 9-5: Web diagram for a cone over a non-generic blow-up of $\mathbb{P}^2$ at four points and its deformation. This geometry is toric and is closely related to dP_4. The two dashed segments correspond to two homologically equivalent 3-spheres. The left-over diagram describes a suspended pinch point singularity, which admits a further deformation not shown in the picture.

In a similar spirit, we may consider other toric geometries closely related to toric del Pezzos, but corresponding to a non-generic location of the blow-ups.[4] They are given by web diagrams associated to the so-called less symmetric quiver gauge the-

---

[4]Here the distinction between toric and quiver webs is relevant [49]. In these cases, the web diagram corresponds to the quiver web, and encodes the quiver data of a less symmetric phase of the gauge theory. On the other hand, the geometry is still described by some toric data, corresponding to a toric web, different in general from the quiver web. See [49] for a detailed discussion.

ories. For such geometries, deformations to smooth geometries exist, although the generic deformation may not be available. One example of a deformation on a non-generic version of dP_3 is shown in Figure 9-6.
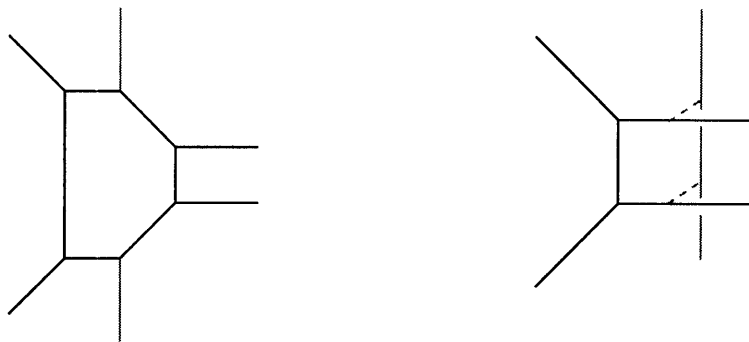
Figure 9-6: Web diagram for the cone over a non-generic dP_3 and its deformation to the orbifold $\mathbb{C}^3/\mathbb{Z}_2$.

Finally, we emphasize that the above techniques can be used to study the deformations of other geometries, even involving more than one collapsing 4-cycles. Concrete examples, like the deformations of the cone over F_0, the suspended pinch point singularity and the $Y^{p,q}$ geometries will appear in subsequent sections. It is interesting to point out that all possible complex deformations for toric varieties may not be described using the above web deformations. Nevertheless, all our examples will be of this kind. We leave the interesting question of other possible situations for future research.

9.2.3 A topological consideration

The throats on cones over dP_n constructed in [61] (and generalizations) have in principle n independent discrete parameters, the M^I, associated to the integer fluxes sourced by the n independent fractional branes one can in principle introduce in the quiver gauge theory.

However, in this section we describe a topological argument which shows that in order for a throat to have a smooth deformation at its bottom, corresponding to a geometric deformation as discussed above, the fractional brane assignments cannot be fully arbitrary. Equivalently, it is possible to use topological information about the al-

lowed deformations to derive the set of fractional branes triggering the corresponding strong infrared dynamics.

The argument is as follows. The fractional brane numbers can be measured in the throat solution by computing the flux of the RR 3-form F_3 through a 3-cycle in the 5d base of the cone (constructed as an S^1 fibration over a 2-cycle in the del Pezzo surface [5]). There are n such 3-cycles. On the other hand, in the smooth deformed geometries, one in general finds a smaller number k of 3-cycles. This implies that $n - k$ 3-cycles in the asymptotic region are homologically trivial. Consequently, only k independent choices of fractional brane numbers remain.

For each deformed geometry, the set of corresponding fractional branes, i.e. those associated to the homologically non-trivial 3-cycles, is determined as follows. Consider a given complex deformation, corresponding to the separation of sub-webs. Recall now the relation between external legs in web diagram and nodes in the quiver [80, 52]. The fractional branes associated to the deformation are those controlling the rank of the nodes corresponding to the legs in the removed sub-web. We will see some examples of this in later sections.

Notice that this does not mean there are no throat solutions for more general fractional brane assignments, but rather that they cannot be completed in terms of a purely geometric background. A systematic study of fractional branes and the dynamics they trigger is in progress [51].

9.2.4 Deformations from the gauge theory

In the previous sections, we have introduced the simple example of the conifold and discussed how the original naked singularity in the supergravity dual is cured when the strong coupling dynamics of the gauge theory is taken into account. We then reviewed how more general extremal transitions are described using toric geometry in the form of (p, q) webs.

We now describe the derivation of the geometric deformation from the viewpoint

---

[5]Although we focus on the case of del Pezzo surfaces, the discussion applies to other real four dimensional Kähler-Einstein surfaces.

of the infrared dynamics of the dual gauge theory, for a general quiver theory. As in the conifold case above, the deformation can be derived as the deformed moduli space of probes, arising from the quantum modification of the moduli space of the gauge theory. Although the basic idea follows discussions in [119], its implementation in our more involved geometries leads to richer structures.

The geometries we study have several collapsing 2-cycles on which we can wrap D5-branes, giving rise to different types of fractional branes. In order for the supergravity solutions described in Section 8.5 to be valid we will assume that the number of fractional branes of each type $M^I \ll N$. There is no constraint on the relative sizes of the M^I's. However, in order to simplify our discussion, we can consider the situation in which

$$M^1 \ll M^2 \ll \ldots \ll \ldots \ll N \tag{9.2.6}$$

Then it is natural to foresee a hierarchy of scales of strong gauge dynamics

$$\Lambda_1 \ll \Lambda_2 \ll \ldots \ll \Lambda_3 \tag{9.2.7}$$

where the Λ_I's are dynamical scales that arise when $N(\Lambda_I)$ is comparable to M_I

$$\Lambda_I \text{ such that } N(\Lambda_I) \sim M^I \tag{9.2.8}$$

We have simplified the field theory analysis by assuming the scales are well separated, although we expect that descriptions of other situations exist in both the smooth supergravity solution and the gauge theory language.

The basic structure of strong infrared dynamics is the following. Given a quiver gauge theory with fractional branes, the theory cascades down until the number of D3-branes N becomes similar to one of the fractional brane numbers, say M^{I_0}, at a scale Λ_{I_0}. For simplicity, and due to our assumption of separation of scales, we may ignore the remaining M^I's and take them to vanish. In order to simplify notation, we call $M^{I_0} = M$. Then the last step of the cascade can be probed by introducing M additional D3-branes and studying the resulting moduli space. In this situation the

216

gauge group takes the form

$$SU(2M)^m \times SU(M)^n \qquad (9.2.9)$$

In several of our examples below, the number of gauge factors with rank $2M$ is two [6], $m = 2$, but the discussion may be carried out in general. Also, in the explicit models the number of flavors for the $SU(2M)$ gauge factors is $2M$, hence equals the number of colors.

The non-perturbative dynamics may be determined by assuming, to begin with, that the $SU(M)$ gauge factors are weakly coupled and act as spectators, corresponding to global flavor symmetries. For simplicity we continue the discussion assuming also that there no arrows among $SU(2M)$ nodes, i.e. no $(2M, \overline{2M})$ matter. Under these circumstances, the strong dynamics corresponds to a set of decoupled $SU(2M)$ gauge theories with equal number of colors and flavors, which thus develop a non-perturbative *quantum modification of the moduli space*. This is best understood in terms of gauge invariant mesonic and baryonic variables. For each such gauge factor, the mesons are

$$\mathcal{M}_{ru} = A_r B_u \qquad (9.2.10)$$

with $r, u = 1, 2$, where

$$A_r : \quad (2M, \overline{M}_r) \qquad B_u : \quad (M_u, \overline{2M}) \qquad (9.2.11)$$

and the baryons have the abbreviated form

$$\mathcal{B} = [A]^{2M} \qquad \tilde{\mathcal{B}} = [B]^{2M} \qquad (9.2.12)$$

where antisymmetrization of gauge indices is understood. It is important to keep in mind that these operators are not gauge invariant when the entire gauge group

---

[6]In the (p, q) web description of the deformations presented in Section 9.2.2, this arises naturally when one of the sub-webs that are separated is simply an infinite straight line.

(and not just the factors undergoing deformation) is taken into account. This will be important when we study what happens after they develop non-zero vevs. The quantum modified moduli space is described by

$$\det \mathcal{M} - \mathcal{B}\tilde{\mathcal{B}} = \Lambda^{4M} \qquad (9.2.13)$$

The resulting infrared gauge dynamics is described by a quiver gauge theory with the $SU(2M)$ nodes removed, the corresponding flavors replaced by mesonic and baryonic degrees of freedom (both in the quiver diagram and in the superpotential), and with the quantum modified constraints enforced as superpotential interactions by means of singlet chiral field Lagrange multipliers X, of the form[7]

$$W = W_0 + X(\det \mathcal{M} - \mathcal{B}\tilde{\mathcal{B}} - \Lambda^{4M}) \qquad (9.2.14)$$

The quantum constraints force some of the meson/baryon degrees of freedom to acquire non-zero vevs. The dynamics of the probes is recovered along the mesonic branch, which corresponds to setting the baryons to zero and $X = \pm\Lambda^{4-4M}$, and saturating the constraint with meson vevs (see footnote 1). This triggers symmetry breaking of some of the $SU(M)$ factors to diagonal combinations, and makes some of the fields massive due to superpotential couplings. The resulting theory contains a set of meson fields with quantum deformed moduli space, describing the probes in the deformed geometry. In addition, there are additional gauge factors and chiral multiplets describing the geometry left-over after the complex structure deformation of the original one. In later sections we will present several examples, in which the matching between the gauge theory description of the quantum deformations and the geometric complex structure deformations is complete. This is a very satisfactory result.

There is a subtlety in fixing the sign of the vev for X. The simplest way of determining the correct one is to require that, restricting to the Abelian case, the theory

---

[7]For simplicity, we show only one Lagrange multiplier and additional superpotential term. It us understood that there is one such contribution for each strongly coupled gauge group factor.

has a superpotential allowing for a toric description of its moduli space. Concretely, that each bi-fundamental field appears with opposite signs in the two terms containing it. This recipe can be recovered from a more careful treatment of the equation of motion determining X from the initial superpotential, as discussed in a concrete example in Appendix 9.7.

After the condensation, the left-over quiver theory may correspond to a singular geometry with fractional branes, and thus will have subsequent duality cascades and condensations. The resulting RG flow takes in this case the form of a cascade with multiple dynamical scales at which the underlying geometry undergoes deformation. Explicit examples are discussed in coming sections.

9.3 Some warmup examples

In this section we would like to describe some simple examples of infrared resolutions, in situations with one-scale cascades.

9.3.1 The cone over F_0

Let us consider the case of the cone over F_0. The web diagram for this geometry is shown in Figure 9-7a, and the corresponding quiver is in Figure 9-8a.
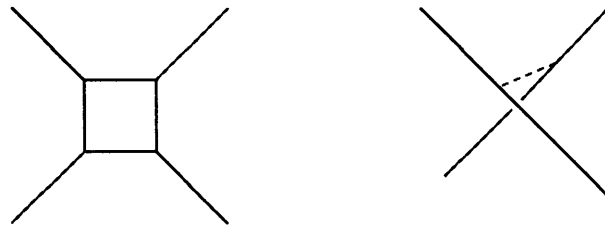
Figure 9-7: Web diagram for the complex cone over F_0, and its complex deformation to a smooth space.

The fractional brane corresponds to the rank vector $(0, 1, 0, 1)$. The superpotential for the theory is

$$W = X_{12}X_{23}Y_{34}Y_{41} - X_{12}Y_{23}Y_{34}X_{41} - Y_{12}X_{23}X_{34}Y_{41} + Y_{12}Y_{23}X_{34}X_{41} \quad (9.3.15)$$
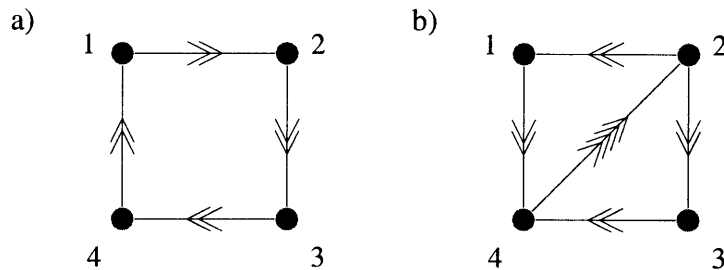
Figure 9-8: Figure a) shows the quiver diagram for the theory of D3-branes at a complex cone over F_0. Figure b) shows a dual phase of the theory, involved in the duality cascade.

in self-explanatory notation. This theory has an $SU(2) \times SU(2)$ global symmetry, which geometrically arises as the product of the $SU(2)$ isometries of the two $\mathbb{P}^1$'s in $F_0 = \mathbb{P}^1 \times \mathbb{P}^1$. It corresponds to a $\mathbb{Z}_2$ orbifold of the conifold $xy - zw = 0$ by the action $x, y, z, w \to -x, -y, -z, -w$, as first determined in [138]. This is also manifest in the dual toric diagrams, where the cone over F_0 differs from the conifold by the addition of an interior point (namely, by the refinement of the toric lattice).

This theory has a cascade, which was exhaustively studied in [56, 61], and to which we referred in Chapters 7 and 8. Introducing N D3-branes and M fractional branes, namely starting quiver 9-8a with the rank vector

$$N\,(1,1,1,1) \,+\, M\,(0,1,0,1) \tag{9.3.16}$$

the theory alternates between the two quivers in Figure 9-8a, b. Given the $\mathbb{Z}_2$ symmetry of the quiver and of the deformed geometry, it is natural to consider the situation where the UV gauge couplings of opposite nodes are equal. In this case, the duality cycle is obtained by a (simultaneous) dualization of the nodes 1 and 3, followed by a (simultaneous) dualization of 2 and 4, after which 1 and 3 are subsequently dualized, etc. Under these conditions, quiver 9-8b appears just as an intermediate step between simultaneous dualizations. In each duality cycle, the number of D3-branes decreases by $2M$ units. It is interesting to note that, regarding the geometry as a quotient of the conifold, nodes 1 and 3 descend from a single node in the quiver of the conifold, while 2 and 4 descend from the other. In this respect, the duality cascade in the

220

orbifold theory, in the situation of symmetric gauge couplings for opposite nodes in the quiver, can be regarded as directly descending from the duality cascade in the conifold theory.

The infrared end of the cascade is therefore expected to be similar to that of the conifold. In fact, this is exactly what is obtained e.g. for N a multiple of M. The gauge theory associated to the rank vector $(0, M, 0, M)$, leads to two decoupled $\mathcal{N} = 1$ SYM-like theories. In more detail, the infrared behavior may be explored by introducing M additional D3-brane probes, namely by studying the gauge theory with rank vector $(M, 2M, M, 2M)$. In the infrared the gauge factors 1 and 3 are weakly coupled, and can be considered spectators. The gauge factors 2 and 4 have $N_f = N_c$ and develop a quantum deformation of their moduli space. Following the general discussion in Section 9.2.4, we introduce the mesons

$$\mathcal{M} = \begin{bmatrix} M_{11} & M_{12} \\ M_{21} & M_{22} \end{bmatrix} = \begin{bmatrix} X_{12}X_{23} & X_{12}Y_{23} \\ Y_{12}X_{23} & Y_{12}Y_{23} \end{bmatrix}$$

$$\mathcal{N} = \begin{bmatrix} N_{11} & N_{12} \\ N_{21} & N_{22} \end{bmatrix} = \begin{bmatrix} X_{34}X_{41} & X_{34}Y_{41} \\ Y_{34}X_{41} & Y_{34}Y_{41} \end{bmatrix}$$

and the baryons $\mathcal{B}, \tilde{\mathcal{B}}, \mathcal{C}, \tilde{\mathcal{C}}$

The quantum modified superpotential reads

$$\begin{aligned} W &= M_{11}N_{22} - M_{12}N_{21} - M_{21}N_{12} + M_{22}N_{11} + \\ &+ X_1 \left(\det \mathcal{M} - \mathcal{B}\tilde{\mathcal{B}} - \Lambda^{4M} \right) + X_2 \left(\det \mathcal{N} - \mathcal{C}\tilde{\mathcal{C}} - \Lambda^{4M} \right) \end{aligned} \qquad (9.3.17)$$

where we have introduced a single strong coupling scale due to the equality of the gauge couplings along the flow.

In order to study the mesonic branch, we have

$$X_1 = \Lambda^{4-4M} \quad ; \quad \mathcal{B} = \tilde{\mathcal{B}} = 0 \quad ; \quad X_2 = \Lambda^{4-4M} \quad ; \quad \mathcal{C} = \tilde{\mathcal{C}} = 0$$

$$\det \mathcal{M} = \Lambda^{4M} \quad ; \quad \det \mathcal{N} = \Lambda^{4M} \qquad (9.3.18)$$

221

Now restricting to the Abelian case (see footnote 2), the resulting superpotential is

$$W = M_{11}N_{22} - M_{12}N_{21} - M_{21}N_{12} + M_{22}N_{11}$$
$$- M_{11}M_{22} + M_{12}M_{21} - N_{11}N_{22} + N_{12}N_{21}$$

That is, the superpotential becomes entirely quadratic. The gauge group is broken to the diagonal combination of nodes 1 and 3 by the expectation values of the mesons. Using the equations of motion, the superpotential vanishes. The only degrees of freedom are one set of mesons, due to the equations of motion, which require $\mathcal{M} = \mathcal{N}$. In addition, these mesons are subject to the quantum constraints, namely $\det \mathcal{M} = \Lambda^4$. This describes the dynamics of the probes in the deformation of the cone over F_0 to a smooth space. Indeed, at any point in the mesonic branch (in the Abelian case) the gauge group is $U(1)$ and there are three adjoint (i.e. uncharged) chiral multiplets with vanishing superpotential. This is the $\mathcal{N} = 4$ $U(1)$ SYM of D3-branes probing a smooth space.

The analogy of the above discussion with the conifold case is manifest from the orbifold description. Moreover, from the geometric viewpoint the deformation of the cone over F_0 corresponds simply to the quotient of the deformed conifold $xy - zw = \epsilon$ by the $\mathbb{Z}_2$ action $x, y, z, w \to -x, -y, -z, -w$, under which it is invariant.

The complex cone over F_0 is one of the first examples in the family of real cones over the manifolds $Y^{p,0}$ introduced in [65, 63, 66, 64, 134], namely $Y^{2,0}$. The real cones over $Y^{p,0}$ correspond to quotients of the conifold $xy - zw = 0$ by the $\mathbb{Z}_p$ action generated by

$$x \to e^{2\pi i/p}x \quad , \quad y \to e^{-2\pi i/p}y \quad , \quad z \to e^{2\pi i/p}z \quad , \quad w \to e^{-2\pi i/p}w \qquad (9.3.19)$$

(with $Y^{1,0}$ corresponding to $T^{1,1}$, the base of the conifold itself). This orbifold action is easily understood by looking at the toric diagrams for these varieties. The toric diagrams look like the diagram of the conifold with an additional refinement of the lattice.

Moreover, using the web diagrams for these varieties it follows that these are the

only examples of cones over the manifolds $Y^{p,q}$ which admit a complex deformation which smoothes the singularity. Namely, only for the case of $q = 0$ we expect that complex deformations will smooth out the naked singularity at the tip of the warped throat solutions in the presence of fluxes as in [92]. The discussion of the geometries involved and the field theory description of the smoothing is presented in Appendix 9.9.

9.3.2 First del Pezzos

Let us consider the cones over the first del Pezzo surfaces. As already mentioned, the cone over dP_0 does not admit any fractional branes, and therefore cannot be taken away from the conformal regime.

The quiver diagram for a cone over dP_1 is presented in Figure 9-9. The corresponding superpotential is
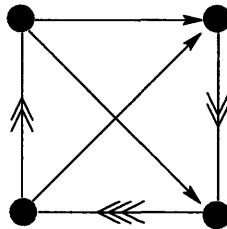
Figure 9-9: Quiver diagram for D3-branes at the cone over dP_1.

$$W = \epsilon_{\alpha\beta} X_{34}^\alpha X_{41}^\beta X_{13} - \epsilon_{\alpha\beta} X_{34}^\alpha X_{42} X_{23}^\beta + \epsilon_{\alpha\beta} X^{12} X_{34}^3 X_{41}^\alpha X_{23}^\beta \qquad (9.3.20)$$

This theory admits one kind of fractional branes, given by the rank vector $(0, 3, 1, 2)$. The addition of these fractional branes leads to an RG cascade which was first studied in [61]. The superpotential (9.3.20) preserves an $SU(2) \times U(1)$ global symmetry. The R-charges can then be determined using the a-maximization principle, and turn out to be irrational numbers [134]. Some explicit computations can be found in [21]. This is the simplest example of a singularity whose dual gauge theory has irrational R-charges. Thus, it is very interesting to understand the associated cascades in detail and we now proceed to do so.

The resulting RG flow is logarithmic and periodic. For an appropriate choice of initial couplings, the sequence of dualized nodes in a period is 2, 4, 3, 1, after which $N \to N - 4M$ and M. The quivers for several steps in the cascade are shown in Figure 9-10.
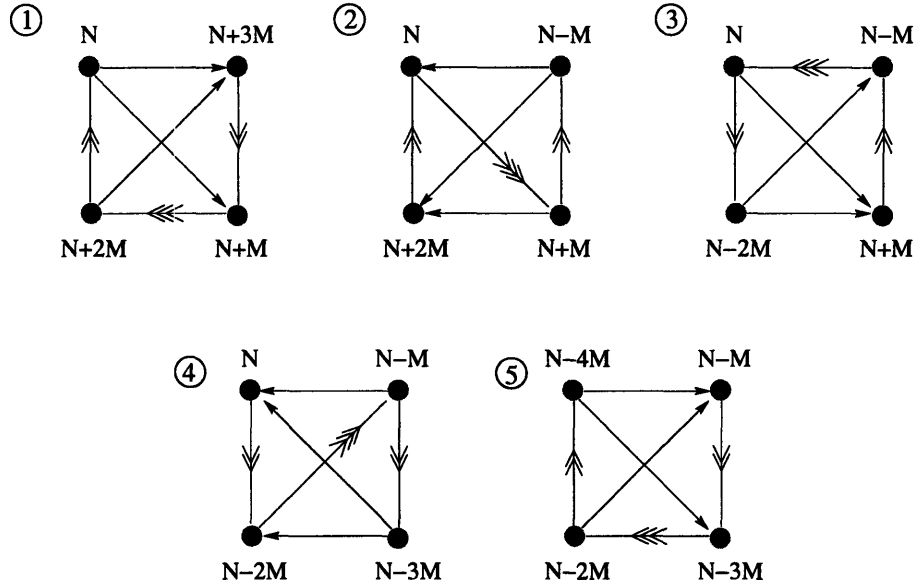
Figure 9-10: Quivers in a duality cycle in the duality cascade of dP_1. We have indicated in blue the dualized node at each step.

The beta functions at each step are

	N_1	N_2	N_3	N_4	β_1/M	β_2/M	β_3/M	β_4/M
1	N	$N+3M$	$N+M$	$N+2M$	$-10+\sqrt{13}$	$\mathbf{10-\sqrt{13}}$	$22-7\sqrt{13}$	$-22+7\sqrt{13}$
2	N	$N-M$	$N+M$	$N+2M$	$22-7\sqrt{13}$	$-10+\sqrt{13}$	$-22+7\sqrt{13}$	$\mathbf{10-\sqrt{13}}$
3	N	$N-M$	$N+M$	$N-2M$	$-22+7\sqrt{13}$	$22-7\sqrt{13}$	$\mathbf{10-\sqrt{13}}$	$-10+\sqrt{13}$
4	N	$N-M$	$N-3M$	$N-2M$	$\mathbf{10-\sqrt{13}}$	$-22+7\sqrt{13}$	$-10+\sqrt{13}$	$22-7\sqrt{13}$
5	N	$N-4M$	$N-3M$	$N-2M$	$-10+\sqrt{13}$	$10-\sqrt{13}$	$22-7\sqrt{13}$	$-22+7\sqrt{13}$

$$(9.3.21)$$

where we have indicated the beta functions of the dualized nodes with a bold font.

In addition, the supergravity dual of this flow corresponds to the $Y^{2,1}$ flow, which is a member of the class of warped throat solutions recently constructed in [92]. However, as already mentioned, the geometry does not admit a complex deformation, hence the naked singularity at the infrared is not removed by this mechanism. This

Figure 9-11: Evolution of the inverse squared couplings $x_i = 8\pi^2/g_i^2$ as a function of $t = \log\mu$ for the dP_1 cascade under consideration. UV couplings have been chosen respecting the quiver symmetries and such that the sequence given by Figure 9-10 and (9.3.21) is followed. We indicate x_1 and x_2 in green, and x_3 and x_4 in orange.

question is being addressed in [51].

The first non-trivial example of complex deformation is provided by the cone over dP_2. The web diagram is shown in Figure 9-3a, and the corresponding quiver diagram is in Figure 9-12.
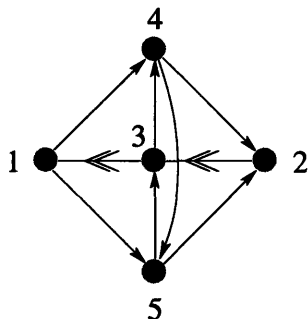
Figure 9-12: Quiver diagram for D3-branes at the cone over dP_2.

The superpotential for this theory is given by

$$
\begin{aligned}
W \;=\;& X_{34}X_{45}X_{53} - (X_{53}Y_{31}X_{15} + X_{34}X_{42}Y_{23}) \\
+\;& (Y_{23}X_{31}X_{15}X_{52} + X_{42}X_{23}Y_{31}X_{14}) - X_{23}X_{31}X_{14}X_{45}X_{52}
\end{aligned}
\qquad (9.3.22)
$$

The two independent fractional branes can be taken to correspond to the rank vectors $(1,1,0,0,0)$ and $(0,1,0,1,-1)$. The existence of an RG cascade in this theory, although expected, has not been established in the literature, neither from the field

225

theory nor the supergravity viewpoint.

Using our arguments in section 9.2.3, it is possible to see that the cascade ending in the deformation shown in figure 9-3a corresponds to the first type of fractional branes. We thus proceed to study it, taking initial ranks of the form

$$\vec{N} = N(1,1,1,1,1) + M(1,1,0,0,0) \tag{9.3.23}$$

We will consider UV couplings respecting the $\mathbb{Z}_2$ symmetry that the quiver has in the absence of fractional branes, $x_1 = x_2$ and $x_4 = x_5$.
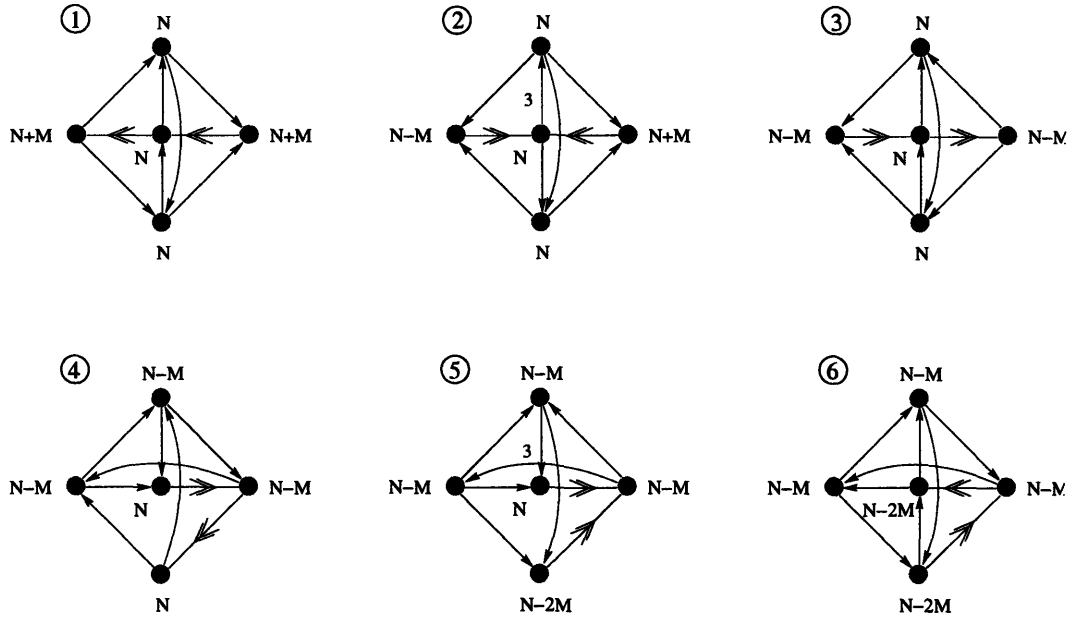
Figure 9-13: Some quivers in a duality cycle in the duality cascade of dP_2. We have indicated in blue the dualized node at each step.

The sequence of gauge group ranks and beta functions for the gauge couplings is

	N_1	N_2	N_3	N_4	N_5	β_1/M	β_2/M	β_3/M	β_4/M	β_5/M
1	$N+M$	$N+M$	N	N	N	3	3	$\frac{3}{4}(-9+\sqrt{33})$	$\frac{3}{8}(1-\sqrt{33})$	$\frac{3}{8}(1-\sqrt{33})$
2	$N-M$	$N+M$	N	N	N	-3	3	0	0	0
3	$N-M$	$N-M$	N	N	N	-3	-3	$\frac{3}{4}(9-\sqrt{33})$	$\frac{3}{8}(-1+\sqrt{33})$	$\frac{3}{8}(-1+\sqrt{33})$
4	$N-M$	$N-M$	N	$N-M$	N	$\frac{3}{8}(1-\sqrt{33})$	$\frac{3}{4}(-9+\sqrt{33})$	3	$\frac{3}{8}(1-\sqrt{33})$	3
5	$N-M$	$N-M$	N	$N-M$	$N-2M$	0	0	3	0	-3
6	$N-M$	$N-M$	$N-2M$	$N-M$	$N-2M$	$\frac{3}{8}(-1+\sqrt{33})$	$\frac{3}{4}(9-\sqrt{33})$	-3	$\frac{3}{8}(-1+\sqrt{33})$	-3

226
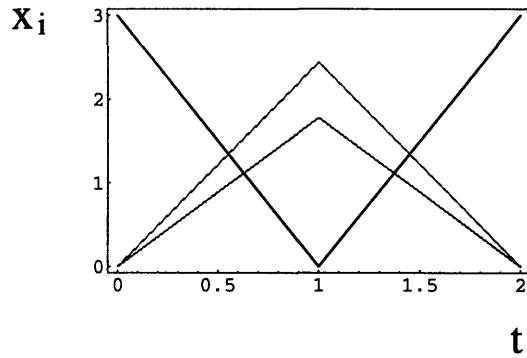
Figure 9-14: Evolution of the inverse squared couplings $x_i = 8\pi^2/g_i^2$ as a function of $t = \log\mu$ for some steps in the dP_2 cascade under consideration. UV couplings have been chosen respecting the quiver symmetries and such that the sequence given by Figure 9-13 and (9.3.24) is followed. We indicate x_1 and x_2 in black, x_3 in green, and x_4 and x_5 in magenta.

Figure 9-14 shows a typical evolution of gauge couplings in this case. For simplicity, Figure 9-13 and (9.3.24) only show six steps in the duality cascade. At the end of this pattern of dualization, one obtains a quiver similar to the original one, up to a reduction of the number of D3-branes and a rotation of the diagram. Hence continuation of this pattern eventually leads to a full duality cycle, and thus a periodic cascade.

Let us now explore the behavior of the theory for small number of regular D3-branes, which corresponds to the infrared of the RG cascade. For that, we consider M D3-branes probing the theory at the IR end of the cascade. Hence, let us consider the gauge theory described by the rank vector

$$\vec{N} = M(1,1,1,1,1) + M(1,1,0,0,0) \qquad (9.3.24)$$

In this situation nodes 1 and 2 have $N_f = N_c$ and develop a quantum deformed

moduli space. The meson fields for nodes 1 and 2 are

$$\mathcal{M} = \begin{bmatrix} M_{34} & M_{35} \\ \tilde{M}_{34} & \tilde{M}_{35} \end{bmatrix} = \begin{bmatrix} X_{31}X_{14} & X_{31}X_{15} \\ Y_{31}X_{14} & Y_{31}X_{15} \end{bmatrix}$$

$$\mathcal{N} = \begin{bmatrix} N_{43} & N_{53} \\ \tilde{N}_{43} & \tilde{N}_{53} \end{bmatrix} = \begin{bmatrix} X_{42}X_{23} & X_{52}X_{23} \\ X_{42}Y_{23} & X_{52}Y_{23} \end{bmatrix}$$

The quantum modified superpotential becomes

$$\begin{aligned} W &= X_{34}X_{45}X_{53} - (X_{53}Y_{31}X_{15} + X_{34}X_{42}Y_{23}) \\ &+ (Y_{23}X_{31}X_{15}X_{52} + X_{42}X_{23}Y_{31}X_{14}) - X_{23}X_{31}X_{14}X_{45}X_{52} \\ &+ X_1 (\det \mathcal{M} - \mathcal{B}\tilde{\mathcal{B}} - \Lambda^{4M}) + X_2 (\det \mathcal{N} - \mathcal{C}\tilde{\mathcal{C}} - \Lambda^{4M}) \end{aligned} \qquad (9.3.25)$$

Along the mesonic branch we have

$$X_1 = \Lambda^{4-4M} \quad ; \quad \mathcal{B} = \tilde{\mathcal{B}} = 0 \quad ; \quad X_2 = -\Lambda^{4-4M} \quad ; \quad \mathcal{C} = \tilde{\mathcal{C}} = 0$$

$$\det \mathcal{M} = \Lambda^{4M} \quad ; \quad \det \mathcal{N} = \Lambda^{4M} \qquad (9.3.26)$$

The appropriate signs for the vevs for X_1 and X_2 can be determined with a reasoning identical to the one in Appendix 9.7.

The expectation values for the mesons higgs the gauge group to a single diagonal combination of the nodes 3, 4 and 5. Restricting to the Abelian case, the superpotential becomes

$$\begin{aligned} W &= X_{34}X_{45}X_{53} - N_{53}M_{34}X_{45} - X_{53}\tilde{M}_{35} - X_{34}\tilde{N}_{43} \\ &+ \tilde{N}_{53}M_{35} + N_{43}\tilde{M}_{34} + M_{34}\tilde{M}_{35} - \tilde{M}_{34}M_{35} - N_{43}\tilde{N}_{53} + \tilde{N}_{43}N_{53} \end{aligned} \qquad (9.3.27)$$

Using the equations of motion for e.g. $\tilde{M}_{34}$, $\tilde{M}_{35}$ and $\tilde{N}_{43}$, we have

$$M_{34} = X_{53} \quad , \quad M_{35} = N_{43} \quad , \quad X_{33} = N_{53} \qquad (9.3.28)$$

228

Plugging this into (9.3.27) we have

$$W = X_{34}X_{45}X_{53} - X_{34}X_{53}X_{45} \tag{9.3.29}$$

Renaming $X_{34} = X$, $X_{45} = Y$ and $X_{53} = Z$, we obtain the $\mathcal{N} = 4$ field content and superpotential

$$W = X[Y, Z] \tag{9.3.30}$$

which in any event vanishes in the Abelian case, but is crucial in non-Abelian situations. Hence, the moduli space of the D3-brane probes is given by the complex deformation of the cone over dP_2 to a smooth space, as expected from the geometrical analysis.

9.3.3 The suspended pinch point

To illustrate that the ideas of cascades and infrared deformations are very general, we would like to consider a further example, based on the suspended pinch point (SPP) singularity. The web diagram for this geometry is shown in Figure 9-15a, while its deformation is in Figure 9-15b.
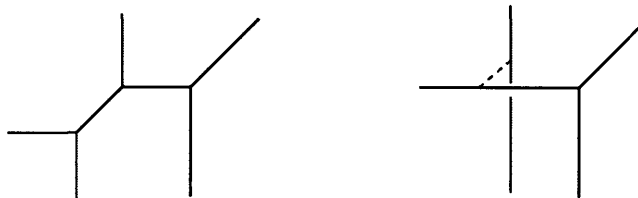
Figure 9-15: Web diagram for the SPP and its deformation to a smooth geometry.

The quiver diagram was determined in [138, 164] and is shown in Figure 9-16a, and the superpotential is

$$W = X_{21}X_{12}X_{23}X_{32} - X_{32}X_{23}X_{31}X_{13} + X_{13}X_{31}X_{11} - X_{12}X_{21}X_{11} \tag{9.3.31}$$

The ranks of the gauge factors are arbitrary, hence there are two independent fractional branes, which can be taken to be $(0, 1, 0)$ and $(0, 0, 1)$.
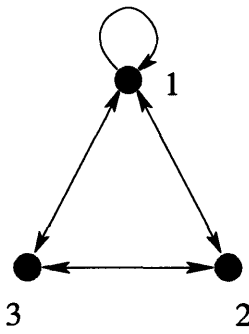
Figure 9-16: Quiver diagram for SPP.

Although it has not been described in the literature, the theory has a very nice and simple duality cascade, which as we show ends in the deformed geometry shown in Figure 9-15a. Similarly to what happens in the flows considered for dP_1 and dP_2, this cascade shares a very special feature with the conifold cascade: it is periodic and involves a single quiver. Let us consider the starting point given by the ranks

$$\vec{N} = N(1,1,1) + M(0,1,0) \tag{9.3.32}$$

By following the pattern of dualizing the most strongly coupled node at each step, we are led to a cascade that repeats the following sequence of dualizations $(2,1,3,2,1,3)$. The quiver theories at each step of this sequence are shown in Figure 9-17. As before, we have indicated in blue the node that gets dualized at each step.

In more detail, the ranks of the gauge groups and the beta functions for this series of dualizations are
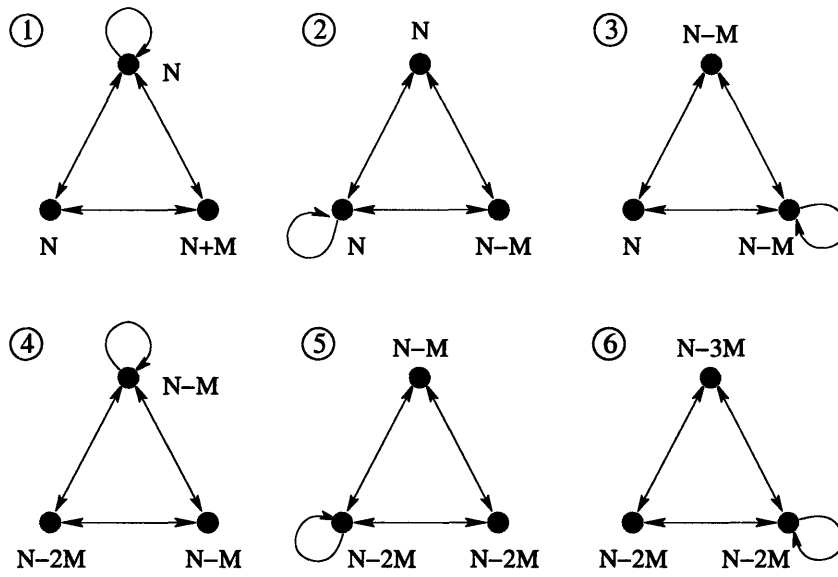
Figure 9-17: Sequence of quivers in one period of the SPP cascade. We have indicated in blue the dualized node at each step.

	N_1	N_2	N_3	β_1/M	β_2/M	β_3/M
1	N	$N + M$	N	$-3/2$	**3**	$-3/2$
2	N	$N - M$	N	**3/2**	-3	$3/2$
3	$N - M$	$N - M$	N	$-3/2$	$-3/2$	**3**
4	$N - M$	$N - M$	$N - 2M$	$3/2$	**3/2**	-3
5	$N - M$	$N - 2M$	$N - 2M$	**3**	$-3/2$	$-3/2$
6	$N - 3M$	$N - 2M$	$N - 2M$	-3	$3/2$	**3/2**
7	$N - 3M$	$N - 2M$	$N - 3M$	$-3/2$	**3**	$-3/2$

$$(9.3.33)$$

After six dualizations (step **7** in the previous table), the quiver comes back to itself, with $N \to N - 3M$ and M constant.

It is important that at every step in the cascade the most strongly coupled node is never the one with the adjoint chiral field. This allows the cascade to proceed via standard Seiberg dualizations. In the previous table, we have again used a bold font for the beta function of the dualized node at each step. It still remains to show that it is possible to choose initial couplings such that the proposed dualities take place

along the RG flow. In fact, it is possible to do so, as shown in Figure 9-18 for a particular choice of UV couplings. Moreover, the pattern is completely generic.
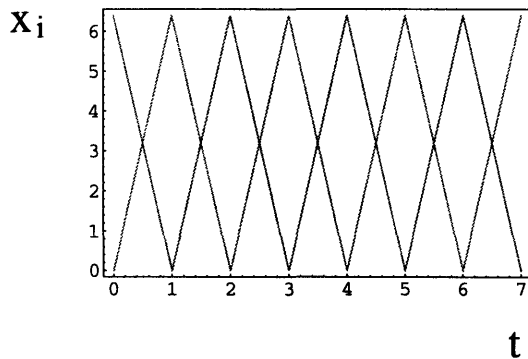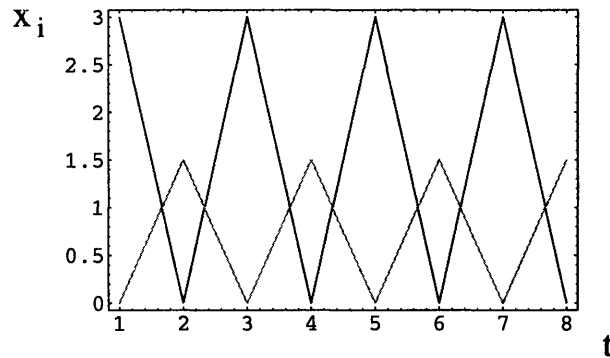

Figure 9-18: Evolution of the inverse squared couplings $x_i = 8\pi^2/g_i^2$ as a function of $t = \log\mu$ for the SPP cascade. Red lines indicate x_2 and green lines indicate x_1 and x_3.

As usual, the cascade proceeds until the effective number of D3-branes is comparable to M. At this point, we expect the gauge theory strong dynamics to take over and induce a geometric transition. Indeed, the SPP singularity admits a complex deformation, shown in Figure 9-15b. In the following we describe how this arises in the field theory.

In order to study the infrared end of the cascade, we study the gauge theory describing M D3-branes probing it. This corresponds to the quiver theory with rank vector

$$\vec{N} = M(1,1,1) + M(0,1,0) \qquad (9.3.34)$$

In this case, we only need to consider mesons and baryons for node 2. The mesons are given by

$$\mathcal{M} = \begin{bmatrix} M_{13} & M_{11} \\ M_{33} & M_{31} \end{bmatrix} = \begin{bmatrix} X_{12}X_{23} & X_{12}X_{21} \\ X_{32}X_{23} & X_{32}X_{21} \end{bmatrix} \qquad (9.3.35)$$

We now introduce the quantum constraint in the superpotential and choose the mesonic branch

$$X = \Lambda^{4-4M} \quad ; \quad \mathcal{B} = \tilde{\mathcal{B}} = 0 \qquad (9.3.36)$$

232

Restricting to the Abelian case, the superpotential reads

$$W \quad = \quad -M_{33}X_{31}X_{13} + X_{13}X_{31}X_{11} - M_{11}X_{11} + M_{33}M_{11} \qquad (9.3.37)$$

The equation of motion for M_{11} requires $X_{11} = M_{33}$, so we get

$$W \quad = \quad -M_{33}X_{31}X_{13} + X_{13}X_{31}M_{33} \qquad (9.3.38)$$

The gauge group is $SU(M)$ (due to the breaking by meson vevs $M \propto \mathbf{1}$). All three fields transform in the adjoint representation (a singlet in the Abelian case). The above theory clearly describes the field content and superpotential of $\mathcal{N} = 4$ SYM, i.e. the theory describing the smooth geometry left over after the deformation.

In addition, there remain some additional light fields, namely M_{11}, M_{13}, M_{31}, M_{33}, subject to the constraint

$$M_{13}M_{31} - M_{33}M_{11} = \Lambda^4 \qquad (9.3.39)$$

The dynamics is that of probe D3-branes in the geometry corresponding to the deformation of the SPP to flat space. This matches nicely the geometric expectation, from the web diagrams in Figure 9-15, from which we see that the result of the deformation is a smooth geometry.

The relation between the field theory and the more geometrical description of the deformation can be done also using the toric geometry language. Using the construction of the moduli space of the SPP in terms of toric data (the forward algorithm), e.g. in [138, 146], the moduli space is given by $xy = zw^2$, with

$$x = X_{13}X_{32}X_{24}, \quad y = X_{31}X_{12}X_{23}, \quad z = X_{11}, \quad w = X_{13}X_{31} \qquad (9.3.40)$$

modulo relations from the superpotential (namely, we also have e.g. $w = X_{12}X_{21}$).

Using the mesons we have

$$x = X_{13}M_{31} \; , \; y = X_{31}M_{13} \; , \; z = X_{11} = M_{33} \; , \; w = X_{13}X_{31} = M_{11} \qquad (9.3.41)$$

The monomials satisfy $xy - zw^2 = 0$ at the classical level, namely

$$X_{13}X_{31}(M_{31}M_{13} - M_{33}M_{11}) = 0 \qquad (9.3.42)$$

The quantum deformation of the moduli space of the field theory $M_{31}M_{13} - M_{33}M_{11} = \Lambda^4$, thus corresponds to

$$X_{13}X_{31}(M_{31}M_{13} - M_{33}M_{11}) = \epsilon X_{13}X_{31} \qquad (9.3.43)$$

which in terms of the monomials can be written as $xy - zw^2 = \epsilon w$ which is the description of the geometric deformation in Figure 9-15b. Thus the description we have provided has a quite direct link with the geometric description of the deformation, see Appendix 9.8. Similar computations could be carried out in the other cases.

9.4 The dP_3 example

In this and subsequent sections we present examples where there are **several scales of strong gauge dynamics** along the RG flow. They are dual to supergravity solutions with several geometric features along the radial direction. The cleanest examples are those involving several deformation scales, which separate throat-like regions with different warp factors, dual to cascading flows in the gauge theory. In this section we center on one such example, based on the cone over dP_3.

The complex cone over dP_3 has two different deformation branches, shown in Figure 9-4. Following the discussion in section 9.2.3, it is possible to directly determine the sets of fractional branes in the gauge theory that are associated to the finite size 3-cycles in the supergravity description, and which should therefore trigger the corresponding RG flow and strong dynamics. In this section we carry out the gauge

234
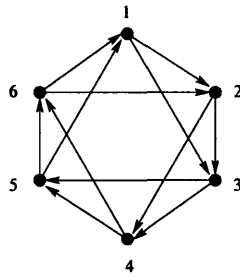
Figure 9-19: The quiver for D3-branes on the complex cone over dP_3.

theory analysis corresponding to these sets of fractional branes and describe in detail the duality cascade and infrared dynamics.

Before doing that, let us review some general features of the gauge theory. The (p, q) web diagram is shown in Figure 9-4, and the corresponding quiver gauge theory is shown in figure 9-19. The superpotential reads (see e.g. [43])

$$\begin{aligned}
W &= X_{12}X_{23}X_{34}X_{45}X_{56}X_{61} + X_{13}X_{35}X_{51} + X_{24}X_{46}X_{62} - \\
&\quad - X_{23}X_{35}X_{56}X_{62} - X_{13}X_{34}X_{46}X_{61} - X_{12}X_{24}X_{45}X_{51}
\end{aligned} \tag{9.4.44}$$

in self-explanatory notation.

A basis of fractional branes is given by the rank vectors $(1, 0, 0, 1, 0, 0)$, $(0, 0, 1, 0, 0, 1)$ and $(1, 0, 1, 0, 1, 0)$.

9.4.1 The cascade for the first branch

In this section we describe a cascading RG flow for the dP_3 theory. This duality cascade, which has not appeared in the literature, provides the dual of the throat in [61] corresponding to the appropriate choice of fractional branes.

The cone over dP_3 has a two-dimensional deformation branch, shown in Figure 9-4c, which involves two independent 3-cycles and hence two independent RR fluxes. Hence a warped throat ending in this deformation must be dual to an RG flow in the quiver gauge theory with two independent fractional branes. From the geometry, and the argument in section 9.2.3, the 3-cycles involved in the deformation correspond to
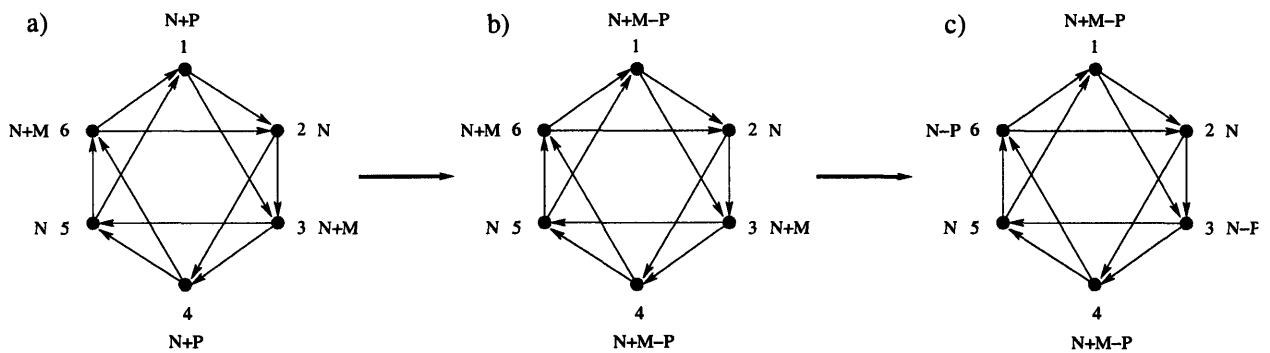
Figure 9-20: Two dualizations in the first RG cascade in dP_3. Dualized nodes are shown in blue.

the fractional branes with rank vectors $(1,0,0,1,0,0)$ and $(0,0,1,0,0,1)$.

Hence our starting point is the quiver in Figure 9-19 with ranks

$$\vec{N} = N(1,1,1,1,1,1) + P(1,0,0,1,0,0) + M(0,0,1,0,0,1) \qquad (9.4.45)$$

In addition, the $\mathbb{Z}_2$ symmetry of the external legs in the toric diagram suggests that it is natural to consider initial conditions such that the RG flow is symmetric with respect to opposite nodes in the quiver. Hence, opposite nodes are taken with equal gauge couplings at a large UV scale. In order to study the RG flow to the infrared, we center on the regime $N \gg P \gg M$, which eventually will lead to two hierarchically different scales of RG flow.

The suggested duality cascade proceeds as follows. The nodes with largest beta function are 1 and 4, so we dualize them simultaneously. The results are shown in Figure 9-20a,b (the resulting quiver may be reordered to yield a standard maximally symmetric quiver, but we need not do so). Next the most strongly coupled nodes are 3, 6, so we dualize them simultaneously. This is shown in Figure 9-20b,c.

The quiver in Figure 9-20c can be reordered into a standard maximally symmetric quiver. This is of the form of the starting quiver, with similar fractional branes, but with the effective N reduced by an amount P. We can then continue dualizing nodes 2, 5, then 1, 4, then 3, 6, etc, following the above pattern and generating a cascade which preserves the fractional branes but reduces the effective N.

236

In order to check that the suggested cascade of dualizations is consistent with an RG flow, we compute the gauge theories at each step in the cascade, along with the beta functions for the gauge couplings.

Given that $N \gg P \gg M$, we expect the cascade to be controlled by the P fractional branes of the first type in the UV. In that spirit, we study in detail the RG flow first neglecting the effect of M, which we set to zero for simplicity, under the assumption that the M fractional branes of the second type will only produce a small perturbation to the cascade constructed this way.

Let us explore in more detail that the above proposed cascade of dualizations 1,4,2,5,3,6 indeed corresponds to an RG flow. This cascade iterates between Models I and II of dP_3 in [48], and the corresponding ranks and beta functions at each step are

	N_1	N_2	N_3	N_4	N_5	N_6	β_1/P	β_2/P	β_3/P	β_4/P	β_5/P	β_6/P
1	$N+P$	N	N	$N+P$	N	N	3	$-3/2$	$-3/2$	3	$-3/2$	$-3/2$
2	$N-P$	N	N	$N+P$	N	N	-3	0	0	3	0	0
3	$N-P$	N	N	$N-P$	N	N	-3	$3/2$	$3/2$	-3	$3/2$	$3/2$
4	$N-P$	$N-P$	N	$N-P$	N	N	-2	$-3/2$	$5/2$	$-5/2$	$3/2$	2
5	$N-P$	$N-P$	N	$N-P$	$N-P$	N	$-3/2$	$-3/2$	3	$-3/2$	$-3/2$	3
6	$N-P$	$N-P$	$N-2P$	$N-P$	$N-P$	N	0	0	-3	0	0	3
7	$N-P$	$N-P$	$N-2P$	$N-P$	$N-P$	$N-2P$	$3/2$	$3/2$	-3	$3/2$	$3/2$	-3

$$(9.4.46)$$

After six dualizations (step **7** in the previous table), the quiver comes back to itself, with ranks

$$\vec{N} = (N - P)(1,1,1,1,1,1) - P(0,0,1,0,0,1) \qquad (9.4.47)$$

Thus, the theory after six steps looks like the original one, with $N \to N - P$, plus a rotation and a replacement of $P \to -P$.

Notice that in the situation which is $\mathbb{Z}_2$ symmetric with respect to opposite nodes, the above duality steps group by pairs of simultaneous dualizations, and the quivers
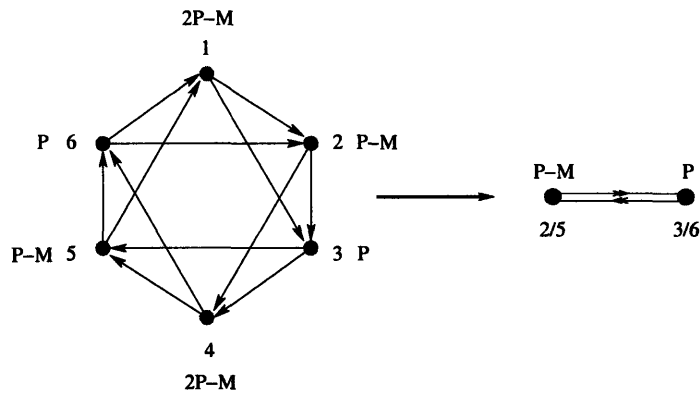
Figure 9-21: Condensation of the gauge theory of dP_3 to the gauge theory of the conifold. The nodes undergoing a deformation are indicated in green.

involved are always maximally symmetric (model I in [48]).

One may worry that in the presence of non-zero M the structure of the above cascade is destabilized. However, numerical results on the structure of cascades for a variety of choices of UV gauge couplings shows that the existence of cascades is a quite robust feature of the above choice of fractional branes (although the particular pattern of dualities involved in a cycle may be different from the above one).

Hence, the above cascade can be generalized to the situation with non-zero M, with the same result, namely there are cycles of Seiberg dualities, which leave the quiver and fractional branes invariant, but decrease the number of D3-branes in multiples of P.

The cascade proceeds until the effective N is not large compared with P. For simplicity, consider that the starting N is $N = (k+2)P - M$. Then after a suitable number of cascade steps, the ranks in the maximally symmetric quiver are $(2P - M, P - M, P, 2P - M, P - M, P)$, for nodes $(1, 2, 3, 4, 5, 6)$, as shown in Figure 9-21a. At this stage the $SU(2P - M)$ factors have $2P - M$ flavors and develop a quantum deformation of their moduli space. This should correspond to turning on one of the complex deformations of the geometry. From the structure of the left over web in the toric representation after a one-parameter deformation, see Figure 9-4b, we expect that the left over geometry should be a conifold. This is shown in Figure 9-21.

Before describing this quantum deformation in detail, let us simply mention that

238
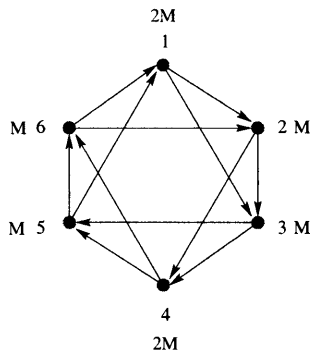
Figure 9-22: Gauge theory encoding the dynamics of D3-brane probes of the infrared of the cascade. The nodes undergoing a deformation are indicated in green.

it results in the disappearance of nodes 1 and 4, the recombination of nodes 2 and 3, and 5 and 6 respectively, due to meson vevs, and a rearrangement of the arrows. The final result is indeed a conifold quiver gauge theory, with ranks $P - M$ and P. The theory subsequently evolves towards the infrared via a Klebanov-Strassler flow, by duality cascades where the effective number of D3-branes decreases in steps of M. At the end of this cascade, there is another condensation, which corresponds to turning on the second complex deformation of the cone over dP_3 to yield a smooth space.

9.4.2 The quantum deformation to the conifold

Let us now describe the fate of the dP_3 quiver theory at the end of the first duality cascade. To simplify the discussion, we take the situation where nodes 2356 have equal rank, i.e. $M = 0$, but the generalization to non-zero M is possible. We would like to consider the gauge theory associated to a set of P D3-branes probing the infrared of the duality cascade. The corresponding quiver is shown in Figure 9-22.

Following our general discussion in section 9.2.4, the $SU(2P)$ nodes condense, so

239

we introduce the corresponding mesons

$$\mathcal{M} = \begin{bmatrix} M_{63} & M_{62} \\ M_{53} & M_{52} \end{bmatrix} = \begin{bmatrix} X_{61}X_{13} & X_{61}X_{12} \\ X_{51}X_{13} & X_{51}X_{12} \end{bmatrix}$$

$$\mathcal{N} = \begin{bmatrix} N_{36} & N_{35} \\ N_{26} & N_{25} \end{bmatrix} = \begin{bmatrix} X_{34}X_{46} & X_{34}X_{45} \\ X_{24}X_{46} & X_{24}X_{45} \end{bmatrix}$$

We also introduce the baryons $\mathcal{B}$, $\tilde{\mathcal{B}}$, $\mathcal{A}$, $\tilde{\mathcal{A}}$. The quantum constraints read

$$\det \mathcal{M} - \mathcal{B}\tilde{\mathcal{B}} = \Lambda^{4P} \quad ; \quad \det \mathcal{N} - \mathcal{A}\tilde{\mathcal{A}} = \Lambda^{4P} \tag{9.4.48}$$

where we use the same dynamical scale for both gauge groups, corresponding to the $\mathbb{Z}_2$ symmetry of opposite nodes in the quiver preserved during the flow.

The superpotential reads

$$\begin{aligned} W &= M_{62}X_{23}N_{35}X_{56} + M_{53}X_{35} + N_{26}X_{62} - \\ &- X_{23}X_{35}X_{56}X_{62} - M_{63}N_{36} - M_{52}N_{25} + \\ &+ X_1 \left(\det \mathcal{M} - \mathcal{B}\tilde{\mathcal{B}} - \Lambda^{4P} \right) + X_2 \left(\det \mathcal{N} - \mathcal{A}\tilde{\mathcal{A}} - \Lambda^{4P} \right) \end{aligned} \tag{9.4.49}$$

Going along the mesonic branch, we uncover the dynamics of the probes in the geometry at the infrared of the cascade. The mesonic branch corresponds to

$$X_1 = X_2 = \Lambda^{4-4P} \quad ; \quad \mathcal{A} = \tilde{\mathcal{A}} = 0 \quad ; \quad \mathcal{B} = \tilde{\mathcal{B}} = 0 \tag{9.4.50}$$

and the constraints on the mesons. For the most symmetric choice of meson vevs $\mathcal{M} \propto \mathbf{1}$, $\mathcal{N} \propto \mathbf{1}$, the gauge groups associated to the nodes 3 and 6, and 2 and 5, are broken to their respective diagonal combinations.

In order to simplify the discussion, we restrict to the Abelian case, where the

240

superpotential reads

$$W = M_{62}X_{23}N_{35}X_{56} - X_{23}X_{35}X_{56}X_{62} - M_{63}N_{36} - M_{52}N_{25} +$$
$$+ M_{53}X_{35} + N_{26}X_{62} + M_{63}M_{52} - M_{53}M_{62} + N_{36}N_{25} - N_{26}N_{35} \quad (9.4.51)$$

Using the equations of motion for M_{53} and N_{26}, we have $X_{35} = M_{62}$, $X_{62} = N_{35}$. Thus

$$W = X_{23}N_{35}X_{56}M_{62} - X_{23}M_{62}X_{56}N_{35} -$$
$$- M_{63}N_{36} - M_{52}N_{25} + M_{63}M_{52} + N_{36}N_{25} \quad (9.4.52)$$

Using the equations of motion for e.g. M_{63}, M_{52}, the quadratic terms disappear, and we are left with

$$W = X_{23}N_{35}X_{56}M_{62} - X_{23}M_{62}X_{56}N_{35} \quad (9.4.53)$$

Going back to the non-Abelian case, the gauge group is $SU(M)_{25} \times SU(M)_{36}$, with charged fields given by those appearing in the superpotential. These can be relabeled as $A_1 = X_{23}$ and $A_2 = X_{56}$, in the $(\square, \overline{\square})$, and $B_1 = M_{35}$, $B_2 = M_{62}$, in the $(\overline{\square}, \square)$. This is the gauge theory of D3-branes at a conifold singularity, showing that the left over geometry after the complex deformation is a conifold. It is important to note that there are some additional massless fields, which describe the dynamics of the D3-brane probe in the deformed geometry. Specifically, the quadratic terms in (9.4.52) leave two linear combinations of M_{63}, M_{52}, N_{36}, N_{25} massless. In addition, the fields M_{53} and N_{26}, which disappeared from the superpotential, also remain massless. Overall, we have light fields subject to the constraints (from $\partial W/\partial X_i = 0$)

$$M_{63}M_{52} - M_{53}M_{62} = \Lambda^{4P} \quad ; \quad N_{36}N_{25} - N_{26}N_{35} = \Lambda^{4P} \quad (9.4.54)$$

Hence the complete dynamics of the theory corresponds to one D3-probe in a geometry which is the deformation of a complex cone over dP_3 to a singular conifold.

241
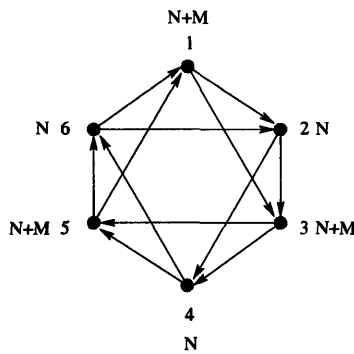
Figure 9-23: Starting point of the cascade ending in the one-parameter deformation of the cone over dP_3.

Notice also that if we consider two kinds of fractional branes, namely non-zero M in the original cascade, the quantum deformation proceeds as above, since it involves recombinations of opposite nodes which have equal ranks even for non-zero M. The resulting condensation leads to a conifold, with the two nodes of the conifold theory having different ranks, what triggers a further Klebanov-Strassler duality cascade and infrared deformation.

9.4.3 The other branch

The cone over dP_3 has a second deformation branch, which is one-dimensional, see figure 9-4c. In this section we discuss the duality cascade dual to the corresponding supergravity throat, and describe the infrared deformation in the gauge theory.

Using the relation in section 9.2.3, the one-parameter deformation branch corresponds to the choice of fractional branes in Figure 9-23. Also, due to the $\mathbb{Z}_3$ symmetry of the geometry, it is natural to propose that nodes with even/odd label have equal UV couplings, respectively.

The proposed cascade in this case goes as follows. As one flows to the infrared, the $SU(N + M)$ gauge factors become strongly coupled and should be dualized. Their simultaneous dualization is difficult, since there are bi-fundamentals joining the corresponding nodes, so we proceed sequentially, with a particular choice of ordering which is not important for the final result. We choose to dualize node 1 first. The

242
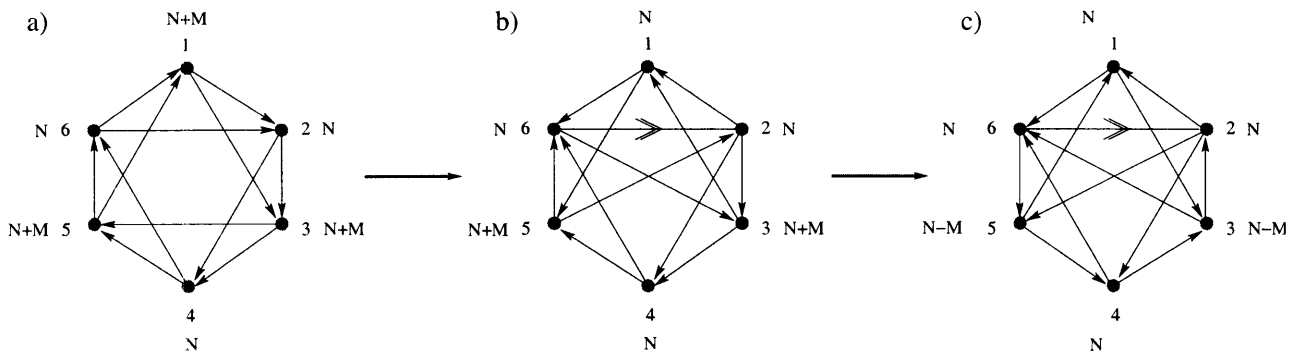
Figure 9-24: Some steps in the duality cascade. Dualized nodes are shown in blue.
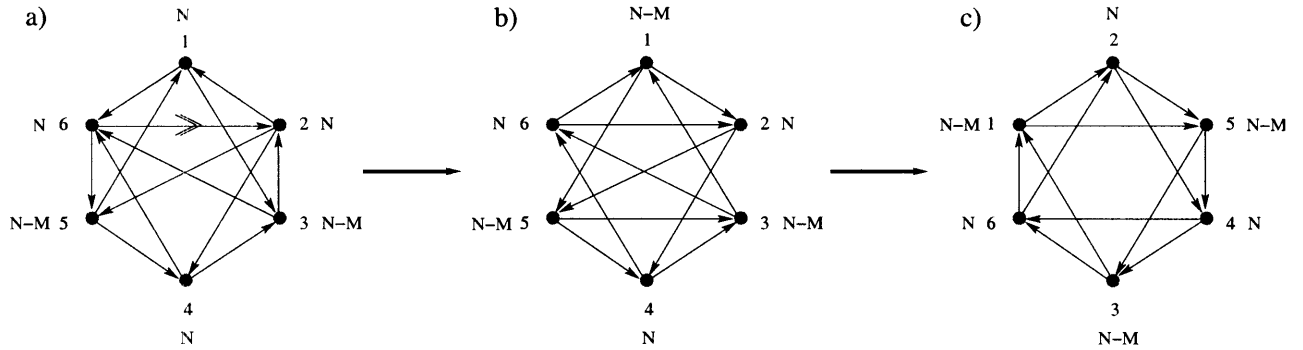
Figure 9-25: Last duality and reordering to complete the duality step. Note that the nodes of the last quiver have been reordered in order to make its $\mathbb{Z}_3$ symmetry manifest. The dualized node is shown in blue.

result is shown in Figure 9-24ab. In the resulting theory, there are no bi-fundamentals joining nodes 3 and 5, so we can now dualize them simultaneously, as shown in Figure 9-24bc.

Next, node 1 is most strongly coupled, so we dualize it again. The result is shown in Figure 9-25ab. Then, we dualize nodes 2 and 6. The final quiver is the maximally symmetric one, as can be shown by reordering the nodes as in 9-25bc. This final theory is of the same kind as the original one, but reducing the effective N in M units (and up to a rotation). Notice also that the final theory has the same nice $\mathbb{Z}_3$ symmetry between the nodes as the original one with the nodes $(2, 4, 6)$ playing the role of $(1, 3, 5)$. One can then proceed to perform the same sequence of dualizations, this time on nodes $(2, 4, 6)$, completing a full cycle of the cascade.

The above heuristic derivation is confirmed by the detailed computation, and

provides the field theory interpretation of the supergravity solution in [61], for the corresponding choice of asymptotic fluxes. The cascade proceeds until the effective number of D3-branes is comparable to that of fractional branes. At this stage, we may use the field theory to derive the strong infrared dynamics which removes the singularity by replacing it by a smooth deformed geometry.

For that purpose, we consider the dynamics of the theory at the end of the cascade, in the presence of additional D3-brane probes. Namely, we consider the quiver with ranks $(2M, M, 2M, M, 2M, M)$. In this situation, we expect that the three nodes 1, 3, 5 lead to a quantum deformed moduli space. In order to study the left-over theory, we consider performing this condensations sequentially (the order not being relevant for the final result).

Consider the strong dynamics associated to the node 1. We introduce the mesons

$$\mathcal{M} = \begin{bmatrix} M_{62} & M_{63} \\ M_{52} & M_{53} \end{bmatrix} = \begin{bmatrix} X_{61}X_{12} & X_{61}X_{13} \\ X_{51}X_{12} & X_{51}X_{13} \end{bmatrix} \qquad (9.4.55)$$

Similar to our above analysis, we implement the quantum constraint in the superpotential. We center on the mesonic branch, along which the gauge factors 6 and 2, and 5 and 3, are broken to their respective diagonal subgroups, denoted 26 and 35 henceforth. Restricting to the Abelian case, the superpotential is described by

$$\begin{aligned} W &= M_{62}X_{23}X_{34}X_{45}X_{56} + M_{53}X_{35} + X_{24}X_{46}X_{62} - X_{23}X_{35}X_{56}X_{62} \\ &- M_{63}X_{34}X_{46} - M_{52}X_{24}X_{45} - M_{62}M_{53} + M_{52}M_{63} \end{aligned} \qquad (9.4.56)$$

The combined node 35 has $N_f = N_c$ plus additional massive adjoints and flavors, which we integrate out using the equations of motion for M_{53}, X_{35}, M_{52}, M_{63}. The resulting superpotential is

$$\begin{aligned} W &= M_{62}X_{23}X_{34}X_{45}X_{56} + X_{24}X_{46}X_{62} \\ &- X_{23}M_{62}X_{56}X_{62} - X_{34}X_{46}X_{24}X_{45} \end{aligned} \qquad (9.4.57)$$

so the only fields charged under the node 35 are the massless ones. Since node 35 has

244

$N_f = N_c$ we introduce the mesons

$$\mathcal{N} = \begin{bmatrix} N_{26} & N_{24} \\ N_{46} & N_{44} \end{bmatrix} = \begin{bmatrix} X_{23}X_{56} & X_{23}X_{34} \\ X_{45}X_{56} & X_{45}X_{34} \end{bmatrix} \tag{9.4.58}$$

which, along with the corresponding baryons, satisfy a quantum deformed constraint. Along the mesonic branch, the group associated with the nodes 26 and 4 is broken down to a single diagonal combination. The superpotential is given by

$$\begin{aligned} W &= M_{62}N_{24}N_{46} + X_{24}X_{46}X_{62} - N_{26}M_{62}X_{62} \\ &\quad - N_{44}X_{46}X_{24} + N_{26}N_{44} - N_{46}N_{24} \end{aligned} \tag{9.4.59}$$

Using the equations of motion for N_{26}, N_{44}, N_{46}, N_{24}, the superpotential reads

$$W = X_{24}X_{46}X_{62} - X_{24}X_{62}X_{46} \tag{9.4.60}$$

Since these fields transform in the adjoint representation of the leftover $SU(M)$ gauge group, this is the $\mathcal{N} = 4$ SYM theory, and the result implies that the geometry after the deformation is smooth. As usual, there are some additional neutral massless fields, with quantum modified constraints, which describe the dynamics of the probe in the deformation of dP_3 to a smooth geometry. We see that the complete smoothing by a single scale is in full agreement with the geometric picture.

9.5 Further examples

In this section we apply our by now familiar techniques to study other examples of quiver gauge theories with two scales of strong infrared dynamics.

9.5.1 From $PdP_4^{(I)}$ to the Suspended Pinch Point

We now investigate a two-scale cascade which follows the sequence

$$PdP_4^{(I)} \rightarrow SPP \rightarrow \text{smooth}$$

245

where *PdP* stands for 'pseudo del Pezzo' and $PdP_4^{(I)}$ indicates the complex cone over a non-generic toric blow-up of dP_3 denoted Model I of PdP_4 in [44].

This is another simple example of the agreement between the complex deformation of the geometry, and the quantum deformation of D3-branes probing the infrared theory of fractional branes. Since the discussion of the RG flow and existence of cascades in these geometries is involved and somewhat aside our main interest, we skip their discussion and center on the gauge theory description of the deformation.

We consider the theory on a stack of D3-branes probing a complex cone over the toric variety obtained by performing a non-generic blow-up of dP_3. Figure Figure 9-26a shows the (p,q) web diagram for this geometry. We also indicate a complex deformation to the suspended pinch point (SPP) singularity.
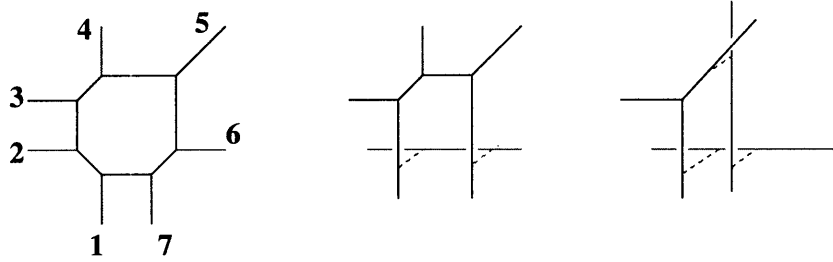
Figure 9-26: Web diagram for the $PdP_4^{(I)}$ model, its deformation to the SPP, and a further deformation to a smooth space.

The quiver diagram for this model is shown in Figure 9-27, which has a 5-block structure that is evident in the web diagram, with nodes 7, 1 and 2, 3 forming pairs.

The corresponding superpotential was derived in [44] and reads

$$
\begin{aligned}
W \; =\; & X_{24}X_{46}X_{61}X_{12} + X_{73}X_{35}X_{57} - X_{73}X_{34}X_{46}X_{67} - X_{45}X_{57}X_{72}X_{24} \\
& - X_{35}X_{56}X_{61}X_{13} + X_{51}X_{13}X_{34}X_{45} - X_{25}X_{51}X_{12} + X_{25}X_{56}X_{67}X_{72}
\end{aligned}
\tag{9.5.61}
$$

Following our arguments in section 9.2.3, the deformation we want to consider corresponds, in the gauge theory, to the choice of fractional branes

$$
\vec{N} = M(1,1,1,1,1,1,1) + M(0,1,0,0,0,1,0)
\tag{9.5.62}
$$
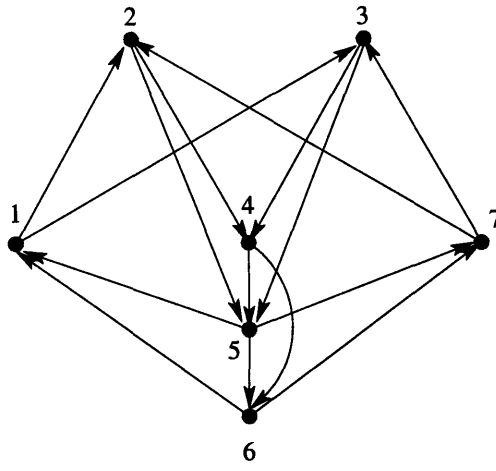
Figure 9-27: Quiver diagram for $PdP_4^{(I)}$. We show in green the nodes that undergo the deformation.

Following our general prescription, we construct the meson fields for nodes 2 and 6

$$\mathcal{M} = \begin{bmatrix} M_{14} & M_{74} \\ M_{15} & M_{75} \end{bmatrix} = \begin{bmatrix} X_{12}X_{24} & X_{72}X_{24} \\ X_{12}X_{25} & X_{72}X_{25} \end{bmatrix}$$

$$\mathcal{N} = \begin{bmatrix} N_{41} & N_{47} \\ N_{51} & N_{57} \end{bmatrix} = \begin{bmatrix} X_{46}X_{61} & X_{46}X_{67} \\ X_{56}X_{61} & X_{56}X_{67} \end{bmatrix}$$

(9.5.63)

We now introduce Lagrange multiplier chiral fields to impose the quantum modified constraints on mesons and baryons. Along the mesonic branch we have

$$X_1 = \Lambda^{4-4M} \quad ; \quad \mathcal{B} = \tilde{\mathcal{B}} = 0 \quad ; \quad X_2 = \Lambda^{4-4M} \quad ; \quad \mathcal{C} = \tilde{\mathcal{C}} = 0$$

$$\det \mathcal{M} = \Lambda^{4M} \quad ; \quad \det \mathcal{N} = \Lambda^{4M}$$

(9.5.64)

Along the mesonic branch, nodes 1, 4 and 5, 7 recombine to their respective diagonal combinations. Restricting to the Abelian case, the superpotential is

247

$$W = M_{14}N_{41} + X_{73}X_{35}X_{57} - X_{73}X_{34}N_{47} - X_{45}X_{57}M_{74}$$
$$-X_{35}N_{51}X_{13} + X_{51}X_{13}X_{34}X_{45} - M_{15}X_{51} + M_{75}N_{57} \qquad (9.5.65)$$
$$-M_{14}M_{75} + M_{15}M_{74} - N_{41}N_{57} + N_{51}N_{47}$$

Using the equations of motion for M_{14}, M_{15}, N_{57}, N_{47}, N_{51}, etc, we have

$$N_{41} = M_{75} \quad X_{51} = M_{74} \quad M_{75} = N_{41}$$
$$N_{51} = X_{73}X_{34} \quad N_{47} = X_{35}X_{13} \qquad (9.5.66)$$

The gauge group after symmetry breaking is $SU(N)_{57} \times SU(N)_{14} \times SU(N)_3$, and we have the superpotential

$$W = X_{73}X_{35}X_{57} - M_{74}X_{45}X_{57} - X_{73}X_{34}N_{47} - X_{35}X_{73}X_{34}X_{13} + M_{74}X_{13}X_{34}X_{45}$$
$$(9.5.67)$$

Relabeling the gauge group as $SU(N)_1 \times SU(N)_2 \times SU(N)_3$, and the fields as

$$M_{74} \to Y_{12} \quad , \quad X_{45} \to Y_{21} \quad , \quad X_{13} \to Y_{23} \quad , \quad X_{34} \to Y_{32}$$
$$X_{35} \to Y_{31} \quad , \quad X_{71} \to Y_{13} \quad , \quad X_{57} \to Y_{11} \qquad (9.5.68)$$

we readily see the field content and superpotential of the SPP geometry. In addition to these fields, there are some massless modes, leftover from the initial mesons. One can check that out of the eight original fields, five combinations remain massless, and they are subject to the quantum constraints, hence three degrees of freedom remain. They provide the moduli space of a D3-brane probe in the geometry given by the dP_4 deformed to a SPP.

The remaining theory may have fractional branes, triggering the cascade of the SPP that we studied in section 9.3.3, which terminates in smooth $\mathbb{C}^3$.

9.5.2 From PdP_3b to $\mathbb{C}/\mathbb{z}_2$

In this section we would like to discuss a further example of condensation, realized geometrically as the deformation of a non-generic blow-up of dP_2, the pseudo del

Pezzo denoted PdP_3b in [49], to a $\mathbb{C}^2/\mathbb{Z}_2 \times \mathbb{C}$ orbifold singularity. From the geometric viewpoint, it illustrates the fact that different phases of the quiver gauge theory may suffer different condensation processes. From the field-theoretical viewpoint, it provides an example with a different behavior for the left over theory. Namely, instead of the $\mathcal{N} = 4$ theory or a conifold-like singularity, the left-over geometry corresponds to an orbifold singularity. In the presence of fractional branes on $\mathbb{C}^2/\mathbb{Z}_2$, the theory is not conformal, but instead of running down a cascade it encounters a singularity. The smoothing of this singularity in the dual supergravity description is of enhançon type [107].

Let us consider a set of branes at a complex cone over the non-generic blow-up of dP_2 leading to the quiver gauge theory in the phase denoted Model II of PdP_3b, worked out in [49], and whose quiver diagram is shown in Figure 9-28. The corresponding toric web diagram is shown in Figure 9-29 [8].
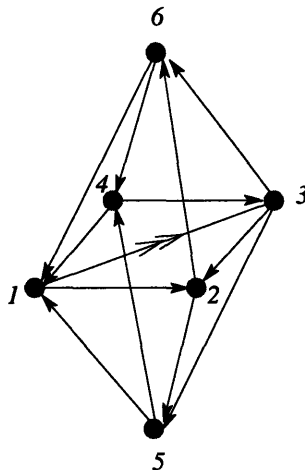
Figure 9-28: Quiver diagram for PdP_3b.

The tree level superpotential is given by

$$W_0 = X_{12}X_{25}X_{54}X_{41} + X_{26}X_{64}X_{43}X_{32} - X_{25}X_{51}Y_{13}X_{32} - X_{64}X_{41}X_{13}X_{36}$$
$$+Y_{13}X_{36}X_{61} + X_{13}X_{35}X_{51} - X_{61}X_{12}X_{26} - X_{43}X_{35}X_{54}$$

$$(9.5.69)$$

---

[8]Here we adhere to the terminology introduced in [49]. Thus, we see that the toric diagram for PdP_3b is different from the one for dP_3 and is given by the reciprocal of the (p, q) web in Figure 9-29.
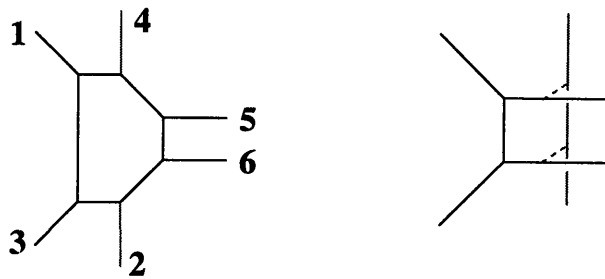
Figure 9-29: Web diagram for the cone over the non-generic blow-up of dP_2, and its deformation. The external legs have been labeled indicating their correspondence to the nodes in the quiver in Figure 9-28.

The geometric deformation of this space is shown in Figure 9-29b. Using our arguments in section 9.2.3, this corresponds to strong coupling dynamics associated with nodes 2 and 4 in the quiver diagram. In order to show this using D3-brane probes of this infrared dynamics, we consider the quiver gauge theory with rank vector

$$\vec{N} = M(0,1,0,1,0,0) + M(1,1,1,1,1,1) = M(1,2,1,2,1,1) \qquad (9.5.70)$$

In this situation, nodes 2 and 4 have $N_f = N_c$, and have a quantum deformed moduli space. Hence the above gauge theory (along the mesonic branch) describes the dynamics of D3-brane probes in the left over geometry after the complex structure deformation of the original geometry PdP_3. In the following, we follow the by now familiar arguments to determine the latter.

We introduce the meson fields

$$\mathcal{M} = \begin{bmatrix} M_{15} & M_{35} \\ M_{16} & M_{36} \end{bmatrix} = \begin{bmatrix} X_{12}X_{25} & X_{32}X_{25} \\ X_{12}X_{26} & X_{32}X_{26} \end{bmatrix}$$

$$\mathcal{N} = \begin{bmatrix} N_{51} & N_{53} \\ N_{61} & N_{63} \end{bmatrix} = \begin{bmatrix} X_{54}X_{41} & X_{54}X_{43} \\ X_{64}X_{41} & X_{64}X_{43} \end{bmatrix} \qquad (9.5.71)$$

In terms of mesons and baryons, the superpotential becomes

250

$$W = M_{15}N_{51} + M_{36}N_{63} - M_{35}X_{51}Y_{13} - N_{61}X_{13}X_{36}$$
$$+ Y_{13}X_{36}X_{61} + X_{13}X_{35}X_{51} - M_{16}X_{61} - N_{53}X_{35} \tag{9.5.72}$$
$$- X_1 \left(\det \mathcal{M} - \mathcal{B}\tilde{\mathcal{B}} - \Lambda^{4M} \right) - X_2 \left(\det \mathcal{N} - \mathcal{C}\tilde{\mathcal{C}} - \Lambda^{4M} \right)$$

The mesonic branch is given by

$$X_1 = X_2 = \Lambda^{4-4M} \quad ; \quad \mathcal{B} = \tilde{\mathcal{B}} = 0 \quad ; \quad \mathcal{C} = \tilde{\mathcal{C}} = 0 \tag{9.5.73}$$

with the mesons subject to the quantum constraints. Also, along the mesonic branch, the symmetry is broken by recombining the gauge factors 1 and 5, and 3 and 6, into their respective diagonal combinations.

Restricting now to the Abelian case, the superpotential is

$$W = M_{15}N_{51} + M_{36}N_{63} - M_{35}X_{51}Y_{13} - N_{61}X_{13}X_{36}$$
$$+ Y_{13}X_{36}X_{61} + X_{13}X_{35}X_{51} - M_{16}X_{61} - N_{53}X_{35} \tag{9.5.74}$$
$$- M_{15}M_{36} + M_{16}M_{35} - N_{51}N_{63} + N_{61}N_{53}$$

Using the equations of motion, we obtain e.g. $N_{61} = X_{35}$, $M_{16} = X_{61}$, $N_{51} = M_{36}$, $M_{15} = N_{63}$. The superpotential is

$$W = M_{35}X_{51}Y_{13} - N_{61}X_{13}X_{36} + Y_{13}X_{36}M_{16} + X_{13}N_{61}X_{51} \tag{9.5.75}$$

Relabeling the unbroken group as $SU(N)_A \times SU(N)_B$, and the fields as $Y_{13} \to X_{AB}$, $M_{35} \to X_{BA}$, $X_{51} \to \Phi_{AA}$, $X_{13} \to Y_{AB}$, $N_{61} \to Y_{BA}$, $X_{36} \to \Phi_{BB}$, the final quiver is presented in Figure 9-30.

Figure 9-30: Quiver diagram after deformation of PdP_3b. It corresponds to a $\mathbb{C}^2/\mathbb{Z}_2 \times \mathbb{C}$ geometry.

The field content and superpotential correspond to the gauge theory for a $\mathbb{C}^2/\mathbb{Z}_2 \times \mathbb{C}$ geometry. This agrees with the expected left over geometry after the complex

deformation. In addition, the theory contains massless meson degrees of freedom, subject to the quantum constraint. They describe the dynamics of the D3-brane probe in the geometry given by the complex deformation of PdP_3 to $\mathbb{C}^2/\mathbb{Z}_2 \times \mathbb{C}$.

As usual, it is possible to study the situation where the final gauge theory contains fractional branes. This theory is $\mathcal{N} = 2$ supersymmetric, hence its RG evolution could be determined from its exact solution. As usual in non-conformal $\mathcal{N} = 2$ theories, instead of a duality cascade we expect strong coupling singularities. In the dual supergravity side, they are described as enhançon configurations [107].

9.6 Conclusions

In this chapter we have centered on the gauge field theory dynamics associated with the smoothing of singularities in warped throat solutions dual to RG flows for branes at singularities in the presence of fractional branes. We have established that in a large set of examples the smoothing corresponds to a complex deformation of the cone geometries. We have described this phenomenon in the dual gauge field theory, by using D3-brane probes of the infrared dynamics. The geometric deformation arises as a quantum deformation of the moduli space of the D3-brane probes. The field theory description is in full agreement with the geometric description of the complex deformation using toric methods.

In addition, we have constructed new explicit examples of cascading RG flows for some of these theories. These duality cascades, along with the infrared deformations, are generalizations of the Klebanov-Strassler RG flow, but show a richer structure in several respects. For instance, very interestingly, several examples correspond to duality cascades with several scales of partial confinement and deformation, after each of which the remaining quiver theory continues cascading down the infrared in a different pattern. Their supergravity duals should correspond to warped throats whose warp factor and flux structure jumps at particular values of the radial coordinate. In other words, to warped throats based on a deformed geometry with several 3-cycles, which are of hierarchically different size. It would be interesting to develop a better

understanding of these throats directly from the supergravity side. Also, we expect several interesting applications of these richer throat structures to compactification and model building such as the constructions in [28].

Our work opens a set of new questions. For instance, certain geometries do admit fractional branes, and even have known KT-like warped throat solutions, but do not admit complex deformations to smooth out their singularities. It would be interesting to understand the infrared behavior of this class of models. In particular, the real cones over the recently studied $Y^{p,q}$ manifolds, of which the five-dimensional horizon of the complex cone over dP_1 is an example, fall in this class. This direction is being pursued in [51].

Finally, there is an interesting phenomenon taking place in the quiver gauge theories we have studied, which is however not involved in the nice RG flows we have centered on. Namely, some of these theories, for other choices of fractional branes (or of UV gauge couplings) exhibit duality walls [85, 56, 55, 61]. It is conceivable that a gauge theory with in principle a duality wall in its UV can actually be UV completed by regarding it as a remnant after confinement of a larger gauge theory at higher energies, with a better behaved UV regime. Thus our work may shed some light also into these more exotic RG flows.

9.7 Appendix A: A more careful look at the mesonic branch

In this appendix we present an alternative approach to the field theory analysis of the IR complex deformation of the geometry, which complements our methods in Section 9.2.4. The strategy will be to consider the dynamics of the fluctuations of the meson fields around the expectation values required by the quantum constraints. As we will see, this method has the advantage of clarifying how the relative signs of the Lagrange multipliers are determined and shows how the low energy limit with respect to the strong coupling scales is taken explicitly.

In order to illustrate these ideas, we will focus on the example of the deformation from dP_3 down to the conifold. We will reproduce the computations performed in Section 9.4.2 from a different viewpoint.

As discussed, the quantum modified constraints on the meson and baryon fields (9.2.13) are imposed via Lagrange multipliers X_i. The quiver for the phase of dP_3 we are considering is shown in Figure 9-22. The ranks are

$$\vec{N} = M(1,1,1,1,1,1) + M(1,0,0,1,0,0) \qquad (9.7.76)$$

leading to a quantum modified moduli space for nodes 1 and 4. The meson fields for these nodes are

$$\mathcal{M} = \begin{bmatrix} M_{63} & M_{62} \\ M_{53} & M_{52} \end{bmatrix} = \begin{bmatrix} X_{61}X_{13} & X_{61}X_{12} \\ X_{51}X_{13} & X_{51}X_{12} \end{bmatrix} \quad ; \quad \mathcal{N} = \begin{bmatrix} N_{36} & N_{35} \\ N_{26} & N_{25} \end{bmatrix} = \begin{bmatrix} X_{34}X_{46} & X_{34}X_{45} \\ X_{24}X_{46} & X_{24}X_{45} \end{bmatrix}$$

In terms of them and the baryonic operators, the quantum corrected superpotential is

$$\begin{aligned} W = \; & M_{62}X_{23}N_{35}X_{56} - X_{23}X_{35}X_{56}X_{62} - M_{63}N_{36} - M_{52}N_{25} + M_{53}X_{35} + N_{26}X_{62} \\ & + X_1(\det M - B\tilde{B} - \Lambda^{4M}) + X_2(\det N - C\tilde{C} - \Lambda^{4M}) \end{aligned} \qquad (9.7.77)$$

Let us focus on the mesonic branch of the moduli space, i.e. solutions with $\mathcal{B} = \tilde{\mathcal{B}} = \mathcal{C} = \tilde{\mathcal{C}} = 0$.

$$\begin{aligned} \partial_{X_1} W = 0 \quad &\Rightarrow \quad \det \mathcal{M} = \Lambda^{4M} \\ \partial_{X_2} W = 0 \quad &\Rightarrow \quad \det \mathcal{N} = \Lambda^{4M} \end{aligned} \qquad (9.7.78)$$

For simplicity, we concentrate on a particularly simple choice of vev's satisfying (9.7.78)

$$< \mathcal{M} >= \Lambda^2 \begin{bmatrix} 1_{M \times M} & 0 \\ 0 & 1_{M \times M} \end{bmatrix} \qquad < \mathcal{N} >= \Lambda^2 \begin{bmatrix} 1_{M \times M} & 0 \\ 0 & 1_{M \times M} \end{bmatrix} \quad (9.7.79)$$

Denoting η_{ij} and ξ_{ij} the fluctuations of M_{ij} and N_{ij} around their respective expectation values, and dropping a constant term, the superpotential in the Abelian case becomes

$$
\begin{aligned}
W &= \eta_{62} X_{23} \eta_{35} X_{56} - X_{23} X_{35} X_{56} X_{62} - 2\Lambda^4 - \Lambda^2(\eta_{63} + \eta_{36} + \eta_{52} + \eta_{25}) \\
&- \eta_{63}\eta_{36} - \eta_{52}\eta_{25} + \eta_{53}X_{35} + \eta_{26}X_{62} \\
&+ X_1(\Lambda^2(\eta_{63} + \eta_{52}) + \eta_{63}\eta_{52} - \eta_{53}\eta_{62}) \\
&+ X_2(\Lambda^2(\eta_{36} + \eta_{25}) + \eta_{36}\eta_{25} - \eta_{35}\eta_{26}) \qquad (9.7.80)
\end{aligned}
$$

We are interested in looking at energies much smaller than the dynamical scale Λ. This can be systematically implemented by taking the large Λ limit of the superpotential, which we will call W', and looking at the approximate equations of motion that follow. For large Λ, the superpotential becomes

$$W' = -\Lambda^2(\eta_{63}+\eta_{52}) - \Lambda^2(\eta_{36}+\eta_{25}) - \Lambda^2 X_1(\eta_{63}+\eta_{52}) - \Lambda^2 X_2(\eta_{36}+\eta_{25}) + \mathcal{O}(\Lambda^0) \quad (9.7.81)$$

This determines the value of the Lagrange multipliers through

$$
\frac{\partial W'}{\partial(\eta_{63} + \eta_{52})} = 0 \quad \rightarrow \quad X_1 = 1
$$
$$
\frac{\partial W'}{\partial(\eta_{36} + \eta_{25})} = 0 \quad \rightarrow \quad X_2 = 1 \qquad (9.7.82)
$$

Plugging this into (9.7.80), we obtain an expression identical to (9.4.51), with the mesons replaced by their corresponding fluctuations. The rest of the proof is the same

255

as the one in Section 9.4.2.

This type of discussion makes clear, for example, how the relative minus sign in the values of the Lagrange multipliers X_1 and X_2 assumed in (9.3.26) is determined.

9.8   Appendix B: Description of complex deformations

In this section we provide a precise geometric description of the complex deformation corresponding to the removal of sub-webs in the toric diagram of our geometries. For additional details and other examples see [3].

The basic process in the separation of a sub-web in a toric diagram is the separation of two lines. This basic process is already present in the complex deformation of the conifold. In order to describe it in toric language, recall the toric data for the conifold

$$
\begin{array}{ccccc}
 & a_1 & a_2 & b_1 & b_2 \\
Q & 1 & 1 & -1 & -1
\end{array}
$$

Namely, one is performing a Kähler quotient of $\mathbb{C}^4$ by the $U(1)$ action acting on it with the above charges. Physically, the conifold is the target of the 2d linear sigma model specified by the above charges for a set of four chiral multiplets. The moment map equation (equivalently the D-term equations for the linear sigma model) are

$$
|a_1|^2 + |a_2|^2 - |b_1|^2 - |b_2|^2 = s \tag{9.8.83}
$$

The geometry is toric, namely can be regarded as a fibration of circles over a base. The $U(1)$ action is simply generated by the three independent phase rotations of the chiral multiplets, up to the above $U(1)$ action (which is a gauge equivalence).

The geometry can be describe using the gauge-invariant quantities $x = a_1 a_2$, $y = b_1 b_2$, $u = a_1 b_1$, $v = a_2 b_2$, as the hypersurface in $\mathbb{C}^4$ defined by $xy = uv$. This may be equivalently described by the two equations $xy = z$, $uv = z$. The $U(1)$ actions degenerate along lines in the subspace $z = 0$. The toric projection in Figure 9-31

describes the loci in $z = 0$ where the $U(1)$ actions degenerate. Notice that s measures the size of the 2-cycle in the resolved conifold.
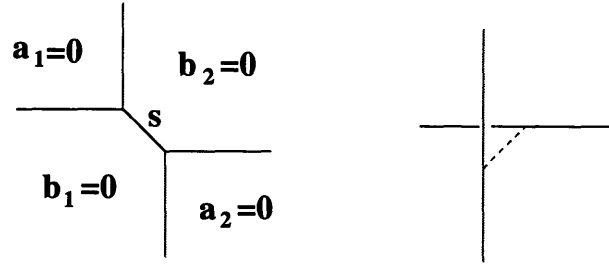
Figure 9-31: Toric projection and complex deformation for the conifold.

The complex deformation involving the separation of the two lines, Figure 9-31b, is possible when $s = 0$. To describe it, we simply use monomials invariant under the $U(1)$ gauge symmetry associated to s, namely x, y, u, v, and deform their constraint to

$$xy - uv = \epsilon \tag{9.8.84}$$

This may be recast as $xy = z + \epsilon$, $uv = z$, showing that there are two different values of z at which the toric fibers degenerate. This implies that the two lines have separated from each other.
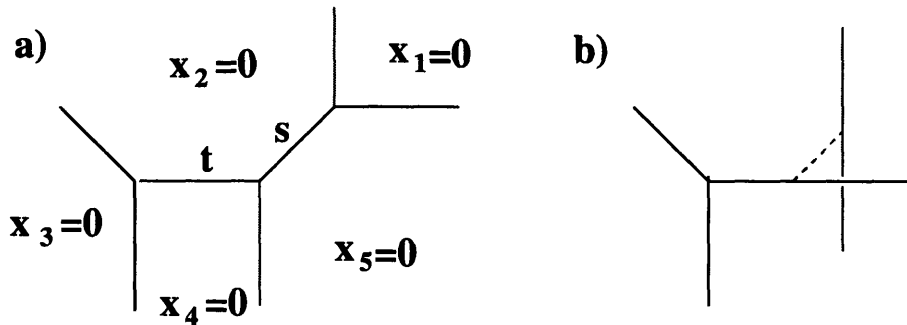
Figure 9-32: Toric projection and complex deformation for the SPP.

The procedure generalizes to more involved situations. Let us consider the SPP singularity, for which the toric data are

257

$$
\begin{array}{cccccc}
 & x_1 & x_2 & x_3 & x_4 & x_5 \\
Q_s & 1 & -1 & 0 & 1 & -1 \\
Q_t & 0 & 0 & 1 & -2 & 1
\end{array}
$$

The corresponding D-term equations are

$$
|x_1|^2 + |x_4|^2 - |x_2|^2 - |x_5|^2 = s,
$$

$$
|x_3|^2 + |x_5|^2 - 2|x_4|^2 = t \tag{9.8.85}
$$

There are two parameters s, t which control the size of two independent 2-cycles in the geometry. The toric picture, showing the degeneration loci of the toric circle actions, is shown in Figure 9-32a. The complex structure of the SPP is given by

$$
uv = xy^2, \tag{9.8.86}
$$

where x, y, u, v are gauge invariant coordinates,

$$
x = x_1 x_2, \quad y = x_3 x_4 x_5, \quad u = x_1 x_4 x_5^2, \quad v = x_2 x_3^2 x_4. \tag{9.8.87}
$$

The complex structure deformation, in Figure 9-32b, arises when $s = 0$. In order to describe it, we introduce variables invariant under $U(1)_s$

$$
x = x_1 x_2, \quad y = x_3 x_4 x_5 \quad \rho = x_1 x_5 / x_3 \quad v = x_2 x_3^2 x_4 \tag{9.8.88}
$$

(which are well-defined for $x_3 \neq 0$). They satisfy a constraint $x\tilde{y} = \rho\tilde{v}$, which we deform to

$$
xy - \rho v = \epsilon \tag{9.8.89}
$$

In the complete manifold, using that $\rho = u/y$, we obtain for the complex deformation

$$
xy^2 = (\rho v + \epsilon)\, y = uv + \epsilon y \tag{9.8.90}
$$

258

Notice that this geometric argument and the deformed geometry nicely dovetail the field theory argument at the end of section 9.3.3.

9.9 Appendix C: Cones over the $Y^{p,q}$ manifolds

Real cones over the manifolds $Y^{p,q}$ [65, 63, 66, 64, 134] provide an infinite family of 6 dimensional singular geometries on which we can place D3-branes. This leads to an infinite class of quiver gauge theories, which have been determined in [14], and whose study is a promising new direction in the gauge/gravity correspondence.

One interesting feature is that the five dimensional $Y^{p,q}$ manifolds have only one collapsing 2-cycle and thus admit a single kind of fractional brane, which triggers a cascading RG flow. Some particular cascades, as well as the KT-like supergravity solutions for the general case, have been recently constructed in [92]. The warped throat solutions contain a naked singularity at their tip. A natural question is whether a smooth solution exists, based on a complex deformation of the underlying geometry, and how to understand it from the dual field theory viewpoint.

In general these 6-dimensional manifolds correspond to spaces which do not admit complex deformations. This can be seen from the web diagrams of those spaces, see Figure 9-33.
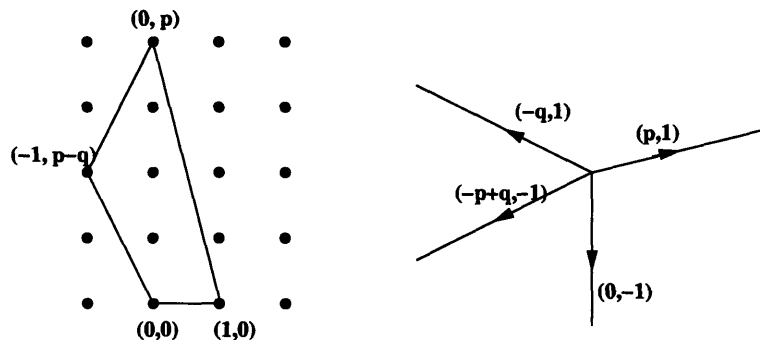
Figure 9-33: The toric and web diagram for the cone over the general $Y^{p,q}$ manifold. No leg recombination is possible except for the case $q = 0$.

Only in the case of $Y^{p,0}$ a decomposition of the web into sub-webs is possible. This case is also special, since it corresponds to a $\mathbb{Z}_p$ quotient of the conifold. More

concretely, defining the conifold by the equation

$$xy - zw = 0 \qquad (9.9.91)$$

the cone over $Y^{p,0}$ is obtained by modding out by the $\mathbb{Z}_p$ action generated by θ, which acts as

$$x \to e^{2\pi i/p}x \quad , \quad y \to e^{-2\pi i/p}y \quad , \quad z \to e^{2\pi i/p}z \quad , \quad w \to e^{-2\pi i/p}w \qquad (9.9.92)$$

which is clearly a symmetry of (9.9.91).

The complex deformation of the manifold is simply the $\mathbb{Z}_p$ quotient of the complex deformation of the conifold

$$xy - zw = \epsilon \qquad (9.9.93)$$

The 3-cycle in the deformed space is the Lens space $S^3/\mathbb{Z}_p$.

Therefore, although both warped supergravity throats and logarithmic RG duality cascades seem to exist for all the $Y^{p,q}$ cases, the class of $Y^{p,0}$ manifolds stand out as the only cases which admit a complex deformation, presumably removing the infrared singularity of their supergravity solutions. Our plan is to center on this class and indeed derive the deformation from the viewpoint of the strong dynamics of the dual gauge theory with fractional branes in general. The IR of $Y^{p,q}$ cascading RG flows for $p \geq q$ is studied in [51]

For that purpose we need the corresponding quiver gauge theories. These can be obtained using the rules in [14], but for illustration purposes we construct them using their realization as $\mathbb{Z}_p$ quotients of the conifold. This can be done following the ideas in [164]. Concretely, the conifold theory is $SU(N_1) \times SU(N_2)$ with fields A_1, A_2 in the $(\square, \overline{\square})$ and B_1, B_2 in the $(\overline{\square}, \square)$. We also have the superpotential

$$W = A_1 B_1 A_2 B_2 - A_1 B_2 A_2 B_1 \qquad (9.9.94)$$

By the realization of the conifold as the moduli space of the gauge theory, there is a relation between the fields and the coordinates x, y, z, w. Roughly

$$x \simeq A_1 B_1 \quad , \quad y \simeq A_2 B_2 \quad , \quad z \simeq A_1 B_2 \quad , \quad w \simeq A_2 B_1 \qquad (9.9.95)$$

The action (9.9.92) can thus be implemented as the action

$$A_1 \to e^{2\pi i/p} A_1 \quad , \quad A_2 \to e^{-2\pi i/p} A_2 \quad , \quad B_1 \to B_1 \quad , \quad B_2 \to B_2 \qquad (9.9.96)$$

In addition, we have to specify the action of θ on the $SU(N_1)$ and $SU(N_2)$ Chan-Paton labels. This is done by two order p discrete gauge transformations, which without loss of generality can be chosen

$$\gamma_{\theta,1} = \operatorname{diag}\left(\mathbf{1}_{n_0}, e^{2\pi i/p}\mathbf{1}_{n_1}, \ldots, e^{2\pi i(p-1)/p}\mathbf{1}_{n_{p-1}}\right)$$
$$\gamma_{\theta,2} = \operatorname{diag}\left(\mathbf{1}_{m_0}, e^{2\pi i/p}\mathbf{1}_{m_1}, \ldots, e^{2\pi i(p-1)/p}\mathbf{1}_{m_{p-1}}\right) \qquad (9.9.97)$$

with $\sum_a n_a = N_1$ and $\sum_a m_a = N_2$.

Now we have to project with respect to the combined geometric and Chan-Paton action. For vector multiplets, the geometric action is trivial, and we simply get a gauge group

$$SU(n_0) \times \ldots \times SU(n_{p-1}) \times SU(m_0) \times \ldots \times SU(m_{p-1}) \qquad (9.9.98)$$

while the projection for the chiral multiplets leads to a set of chiral multiplets in the following representations

$$(A_1)_{a,a+1} = (n_a, \overline{m}_{a+1}) \qquad (A_2)_{a,a-1} = (n_a, \overline{m}_{a-1})$$
$$(B_1)_{a,a} = (\overline{n}_a, m_a) \qquad (B_2)_{a,a} = (\overline{n}_a, m_a) \qquad (9.9.99)$$

The superpotential is directly obtained from the conifold one and reads

$$W = \sum_a \left[(A_1)_{a,a+1}(B_1)_{a+1,a+1}(A_2)_{a+1,a}(B_2)_{a,a} - (A_1)_{a,a+1}(B_2)_{a+a,a+1}(A_2)_{a+1,a}(B_1)_{a,a} \right]$$

The complete result agrees with that using the rules in [14] (by relabeling $B_\alpha \to U^\alpha$, $A_1 \to Z$, $A_2 \to Y$). It is easy to check that the quiver for e.g. $Y_{4,0}$ agrees with that in figure 8 in [14].

This gauge theory admits a single kind of fractional brane. The gauge theory corresponds to $n_a = N + M$, and $m_a = N$. The RG flow presumably leads to a cascade of Seiberg dualities with structure very similar to that of the conifold. Although we have not carried out a complete analysis, we would like to make the following natural proposal. Consider all the nodes $SU(N)$ to have equal coupling at some UV scale, and all nodes $SU(N + M)$ to have equal coupling. Namely, we consider the couplings to respect the $\mathbb{Z}_p$ symmetry of the quiver. As we run to the IR, the nodes $SU(N + M)$ get to strong coupling. Let us Seiberg dualize them simultaneously (to do it in practice, we may do it sequentially, but presumably the order is not important). After this, we obtain a similar quiver, with all ranks $N + M$ replaced by $N - M$. So next one should dualize all the nodes of rank N, etc. This just amounts to inheriting the cascade from the parent to the orbifold theory.

Let us now consider the infrared behavior of the cascade. For N a multiple of M (in which case we center in what follows) the endpoint of the cascade is a theory of p decoupled $N = 1$ SYM nodes, with equal gauge coupling (or dynamical scale) due to the $\mathbb{Z}_p$ symmetry of the flow. The unique dynamical scale should be associated with a finite-size 3-cycle in a deformed geometry.

In order to check that the geometry at the tip of the throat is the deformed geometry described above, we consider the gauge theory describing the dynamics of M D3-brane probing the IR theory. Namely, using the by now familiar technique we take the quiver theory with group

$$\prod_a SU(2M)_a \times \prod_a SU(M)_a \qquad (9.9.100)$$

The nodes $SU(2M)_a$ condense, so we introduce the mesons

$$\mathcal{M} = \begin{bmatrix} M_{a,a+1} & \tilde{M}_{a,a+1} \\ M_{a,a-1} & \tilde{M}_{a,a-1} \end{bmatrix} = \begin{bmatrix} (A_1)_{a,a+1}(B_1)_{a+1,a+1} & (A_1)_{a,a+1}(B_2)_{a+1,a+1} \\ (A_2)_{a,a-1}(B_1)_{a-1,a-1} & (A_2)_{a,a-1}(B_2)_{a-1,a-1} \end{bmatrix} \tag{9.9.101}$$

In terms of these, the superpotential reads

$$W = \sum_a \left[M_{a,a+1}\tilde{M}_{a+1,a} - \tilde{M}_{a,a+1}M_{a+1,a} \right] \tag{9.9.102}$$

We now should impose the quantum constraint, and pick the mesonic branch. Along the mesonic branch, all the $SU(M)_a$ gauge groups are broken to a single diagonal combination. Therefore all mesons transform in the adjoint representation of this gauge group. Imposing the constraint as a superpotential and centering in the Abelian case as usual, we have

$$W = \sum_a \left[M_{a,a+1}\tilde{M}_{a+1,a} - \tilde{M}_{a,a+1}M_{a+1,a} - M_{a,a+1}\tilde{M}_{a,a-1} + M_{a,a-1}\tilde{M}_{a,a+1} \right] \tag{9.9.103}$$

Notice that we have $4pM^2$ meson degrees of freedom. However, they have to satisfy the F-term equations

$$\begin{aligned} \tilde{M}_{a+1,a} &= \tilde{M}_{a,a-1} & M_{a+1,a} &= M_{a,a-1} \\ \tilde{M}_{a,a+1} &= \tilde{M}_{a-1,a} & M_{a,a+1} &= M_{a-1,a} \end{aligned} \tag{9.9.104}$$

These are apparently $4pM^2$ relations. However, they are not all independent. This can be seen by noticing that they only fix the relative vevs of the mesons for different values of a, but they do not fix the overall size of a given kind of meson. Therefore, there are four operators whose vevs are not fixed by the above conditions. They are

$$M_{11} = \prod_a M_{a,a+1} \quad , \quad M_{12} = \prod_a \tilde{M}_{a,a+1} \tag{9.9.105}$$

$$\tag{9.9.106}$$

$$M_{21} = \prod_a M_{a+1,a} \quad , \quad M_{22} = \prod_a \tilde{M}_{a+1,a}$$

Notice however that the original mesons are also constrained by the quantum constraint (which is obtained from $\partial W/\partial X_a = 0$ before going into the mesonic branch etc). This implies that the final operators have to satisfy

$$M_{11}M_{22} - M_{12}M_{21} = \Lambda^P \tag{9.9.107}$$

This moduli space indeed corresponds to a deformed space. Moreover, the fact that the fundamental mesons are related to the above fields by the order p relation (9.9.107) shows that the final space is a $\mathbb{Z}_p$ quotient of the deformed conifold.

Hence the whole family of $Y^{p,0}$ cones is closely related to the KS conifold, and a generalization of the complex cone over F_0, which is the case $p = 2$ in the above language. The field theory argument plus the geometric analysis strongly support the existence of a smooth supergravity solution describing a complete RG flow for these theories. Indeed, these exist and are given simply by the $\mathbb{Z}_p$ quotient of the KS solution.

Chapter 10

An Infinite Family of Superconformal Quiver Gauge Theories with Sasaki-Einstein Duals

In this chapter we describe an infinite family of quiver gauge theories that are AdS/CFT dual to a corresponding class of explicit horizon Sasaki–Einstein manifolds. The quivers may be obtained from a family of orbifold theories by a simple iterative procedure. A key aspect in their construction relies on the global symmetry which is dual to the isometry of the manifolds. For an arbitrary such quiver we compute the exact R–charges of the fields in the IR by applying a–maximization. The values we obtain are generically quadratic irrational numbers and agree perfectly with the central charges and baryon charges computed from the family of metrics using the AdS/CFT correspondence. These results open the way for a systematic study of the quiver gauge theories and their dual geometries. This chapter is based on our work in [14].

10.1 Introduction

Many lessons have been learned about the dynamics of supersymmetric field theories from their embedding in String Theory constructions. Similarly, many properties of the string theory constructions were revealed by studying the gauge theories embedded in them.

In this chapter we will study D3-branes probing toric singularities, which represent a relatively simple, yet extremely rich, set in the space of possible Calabi–Yau manifolds. The AdS/CFT correspondence [132] connects the strong coupling regime of gauge theories on D–branes with supergravity in a mildly curved geometry. For the case of D3–branes placed at the singularities of metric cones over five–dimensional geometries Y_5, the gravity dual is of the form $AdS_5 \times Y_5$, where Y_5 is a Sasaki–Einstein manifold [116, 121, 1, 138].

During the last year, we have witnessed considerable progress in the understanding of these gauge theories. This has been due to developments on various different fronts. A key ingredient has been the discovery of the principle of a–maximization [102], which permits the determination of R–charges of superconformal field theories. This principle is applicable to any superconformal field theory, regardless of whether or not it is possible to embed the theory in a String Theory construction. The a–maximization principle has been successively extended in a series of works [123, 104, 122, 10, 124], broadening its range of applicability outside of conformal fixed points and bringing us closer to a proof of the supersymmetric a–theorem.

Further progress has been made in the study of the non–conformal theories that are produced when, in addition to probe D3–branes, fractional D3–branes are included in the system. Fractional D3–branes are D5–branes wrapped on vanishing 2–cycles of the probed geometry and trigger cascading RG flows, *i.e.* flows in which Seiberg duality is used every time infinite coupling is reached, generating a sequence of gauge theories, each of them providing a simpler description of the theory at every scale. Duality cascades have been studied in detail, and they have been shown to exhibit a plethora of interesting phenomena, such as duality walls and chaotic RG

flows [85, 56, 55, 61]. These works were reviewed in Chapters 7 and 8. In addition, supergravity duals of cascading RG flows for D3–branes probing complex cones over del Pezzo surfaces have been constructed [61] (even without knowledge of the metric of the underlying horizon), validating the applicability of the cascade idea. Interesting cascading gauge theories dual to throat geometries with several warp factors (associated with various dynamical scales generated by the field theory) can also be studied [59]. We reviewed their construction in Chapter 9. These constructions seem to have potential phenomenological applications.

On the geometry side there has also been dramatic progress – from knowledge of only one non–trivial Sasaki–Einstein five–manifold, namely $T^{1,1}$, we now have an infinite family of non–regular metrics on $S^2 \times S^3$ [65, 63]. These manifolds are called $Y^{p,q}$, where p and q are positive integers with $0 \leq q \leq p$. The associated Type IIB supergravity solutions should be dual to 4d $\mathcal{N} = 1$ superconformal field theories. These theories are superconformal quivers, $i.e.$ all the fields trasform in representations of the gauge group with two indices. From computations using these metrics, it became clear in [63] that the dual field theories would exhibit very remarkable properties, such as irrational R–charges. The work of [134] has then provided a detailed description of these manifolds and their associated Calabi–Yau singularities in terms of toric geometry. It turns out that all the cases with $p \leq 2$ are well known and the corresponding superconformal quiver has already been found. $Y^{1,0}$ is the conifold $T^{1,1}$ [121]. $Y^{2,0}$ is associated to the $\mathbf{F}_0$ quiver [138]. The cone over $Y^{1,1}$ is simply $\mathbb{C} \times \mathbb{C}^2/\mathbb{Z}_2$ and the quiver has two gauge groups and $\mathcal{N} = 2$ supersymmetry. $Y^{2,1}$, for which the dual quiver gauge theory was computed in [45] and was also presented in [134], happens to be the first del Pezzo surface (also called $\mathbf{F}_1$). For this case, the authors of [21] have carried out an explicit check of the conformal anomaly coefficient, using a–maximization [102], finding remarkable agreement with the geometrical prediction of [134]. The cone over $Y^{2,2}$ is a $\mathbb{Z}_4$ orbifold of $\mathbb{C}^3$, or equivalently a complex cone over the Hirzebruch surface $\mathbf{F}_2$. In general $Y^{p,p}$ is an orbifold $\mathbb{Z}_{2p}$ orbifold of $\mathbb{C}^3$, and the corresponding quiver can be found easily by standard techniques.

The purpose of this chapter is to construct the field theory duals to the entire

infinite family of geometries. Section 10.2 reviews some properties of the $Y^{p,q}$ geometries. Section 10.3 is devoted to the construction of the associated superconformal quiver gauge theories. The quiver diagrams are constructed and the precise form of the superpotential is found. In general it is a–non trivial task to find the exact superpotential. In the case of the $Y^{p,q}$ manifolds, however, global symmetries and the *quiver toric condition* can be used to fix the complete form of the superpotential. This leads to a successful comparison between global $SU(2) \times U(1)$ flavor symmetries and isometries. Also the $U(1)$ baryonic global symmetry of the theories is shown to follow from the topology of the $Y^{p,q}$ manifolds. From the quiver diagram it is also possible to infer various topological properties of the supersymmetric 3–cycles of the Sasaki-Einstein manifolds, as we discuss at the end of Section 10.4. Here also agreement between gauge theory and geometry is achieved.

Once the quiver diagrams and the exact superpotentials are given, it is a simple exercise to apply the general a–maximization procedure of [102]. This leads to a successful comparison between, on the geometry side, volumes of the 5–manifolds and of some supersymmetric 3–cycles and, on the gauge theory side, gravitational central charges and R–charges of dibaryon operators.

Having an infinite set of Type IIB solutions, together with their gauge theory duals, represents a substantial advancement of our understanding of gauge/gravity duals and opens up the possibility of exciting progress in numerous directions.

10.2   The geometries

In this section we give a brief summary of the geometry of the Sasaki–Einstein $Y^{p,q}$ manifolds, focusing on those aspects which are particularly relevant for the construction of, and comparison to, the gauge theory. Further details may be found in [63, 134].

The local form of the $Y^{p,q}$ metrics may be written as

$$\begin{aligned}
ds^2 &= \frac{1-y}{6}(d\theta^2 + \sin^2\theta d\phi^2) + \frac{1}{w(y)q(y)}dy^2 + \frac{q(y)}{9}(d\psi - \cos\theta d\phi)^2 \\
&\quad + w(y)\left[d\alpha + f(y)(d\psi - \cos\theta d\phi)\right]^2 \\
&\equiv ds^2(B) + w(y)[d\alpha + A]^2
\end{aligned} \tag{10.2.1}$$

where

$$\begin{aligned}
w(y) &= \frac{2(b-y^2)}{1-y} \\
q(y) &= \frac{b - 3y^2 + 2y^3}{b - y^2} \\
f(y) &= \frac{b - 2y + y^2}{6(b-y^2)}.
\end{aligned} \tag{10.2.2}$$

Here b is, *a priori*, an arbitrary constant[1]. These local metrics are Sasaki–Einstein, meaning that the metric cone $dr^2 + r^2 ds^2$ is Calabi–Yau. For all values of b, with $0 < b < 1$, the base B can be made into a smooth manifold of topology $S^2 \times S^2$. In particular, the coordinate y ranges between the two smallest roots y_1, y_2 of the cubic $b - 3y^2 + 2y^3$, so $y_1 \le y \le y_2$. For completeness we quote the range of the other 4 coordinates: $0 \le \theta \le \pi, 0 \le \phi \le 2\pi, 0 \le \psi \le 2\pi, 0 \le \alpha \le 2\pi\ell$. Then for a countably infinite number of values of b in the interval $(0,1)$ the periods of dA over the two two–cycles in B are rationally related, and hence the metric can be made complete by periodically identifying the α coordinate with appropriate period. The ratio of the two periods of dA is then a rational number p/q, and by choosing the maximal period for α one ensures that the Chern numbers p and q for the corresponding $U(1)$ principle bundle are coprime. Moreover, the bound on b implies that $q < p$. One now has a complete manifold with the topology of a circle fibration over $S^2 \times S^2$. Applying Smale's classification of 5–manifolds, one can deduce the topology is always $S^2 \times S^3$. For $\mathrm{hcf}(p,q) = h > 1$ one has a smooth quotient of this by $\mathbb{Z}_h$. In particular, since

---

[1]In [63, 134] b was denoted "a". However, we change notation here to avoid any possible confusion with the a central charge of the quivers. Both will ultimately have rather similar, but different, expressions in terms of p and q.

$H_3(Y^{p,q}; \mathbb{Z}) \cong \mathbb{Z} \oplus \mathbb{Z}_h$, the dual field theories will possess a baryonic $U(1)_B$ flavour symmetry arising from reduction of the Type IIB four–form on the non–trivial non–torsion three–cycle. We denote the complete Sasaki–Einstein manifolds obtained in this way by $Y^{p,q}$.

For completeness we give the value of b, which crucially determines the cubic function appearing in $q(y)$, as well as the two smallest roots y_1, y_2 of this cubic in terms of p and q:

$$
\begin{aligned}
b &= \frac{1}{2} - \frac{(p^2 - 3q^2)}{4p^3}\sqrt{4p^2 - 3q^2} \\
y_1 &= \frac{1}{4p}\left(2p - 3q - \sqrt{4p^2 - 3q^2}\right) \\
y_2 &= \frac{1}{4p}\left(2p + 3q - \sqrt{4p^2 - 3q^2}\right) .
\end{aligned}
\tag{10.2.3}
$$

The period of α is $2\pi\ell$ where

$$
\ell = \frac{q}{3q^2 - 2p^2 + p\sqrt{4p^2 - 3q^2}}
\tag{10.2.4}
$$

and the volume is then easily calculated to be

$$
\mathrm{vol}(Y^{p,q}) = \frac{q^2[2p + \sqrt{4p^2 - 3q^2}]}{3p^2[3q^2 - 2p^2 + p\sqrt{4p^2 - 3q^2}]}\pi^3 .
\tag{10.2.5}
$$

Note that this is bounded by

$$
\mathrm{vol}(T^{1,1}/\mathbb{Z}_p) > \mathrm{vol}(Y^{p,q}) > \mathrm{vol}(S^5/\mathbb{Z}_2 \times \mathbb{Z}_p)
\tag{10.2.6}
$$

and is monotonic in q. In fact, it will be useful to define $Y^{p,0}$ and $Y^{p,p}$ formally as corresponding quotients of $T^{1,1}$ and $S^5/\mathbb{Z}_2$ by $\mathbb{Z}_p$. These arise naturally as limits of the toric diagrams for $Y^{p,q}$ [134], although strictly speaking the global analysis performed in [63] does not hold in these limits – for example, in the case $b = 1$ ($p = q$) the base B collapses to a weighted projective space.

It will also be important to recall that these geometries contain two supersym-

metric submanifolds [134], which are topologically Lens spaces $\Sigma_1 = S^3/\mathbb{Z}_{p+q}$ and $\Sigma_2 = S^3/\mathbb{Z}_{p-q}$. Here supersymmetric means that the metric cones $C(\Sigma_1), C(\Sigma_2)$ are calibrated submanifolds (in fact divisors) in the Calabi–Yau cone. These submanifolds are located at the two roots $y = y_1$ and $y = y_2$, respectively. In fact, the $Y^{p,q}$ manifolds are cohomogeneity one, meaning that the isometry group acts with generic orbit of codimension one. The isometry group depends on p and q: for both p and q odd it is $SO(3) \times U(1) \times U(1)$, otherwise it is $U(2) \times U(1)$. For a compact cohomogeneity one manifold there are then always precisely two special orbits of higher codimension, and in the present case these are Σ_1 and Σ_2. Note in particular that $SU(2) \sim SO(3)$ is contained in the isometry groups.

It is straightforward to compute the volumes of Σ_1, Σ_2. However, the following combination

$$R[B_i] \equiv \frac{2}{3} \cdot \left(\frac{\pi}{2\mathrm{vol}(Y^{p,q})} \right) \cdot \mathrm{vol}(\Sigma_i) \qquad i = 1, 2 \tag{10.2.7}$$

is more relevant for AdS/CFT purposes, since this formula gives the exact R–charges for baryons in the dual gauge theory, arising from D3–branes wrapped over the corresponding cycles Σ_i. These are easily calculated [134]:

$$
\begin{aligned}
R[B_1] &= \frac{1}{3q^2} \left[-4p^2 + 2pq + 3q^2 + (2p - q)\sqrt{4p^2 - 3q^2} \right] \\
R[B_2] &= \frac{1}{3q^2} \left[-4p^2 - 2pq + 3q^2 + (2p + q)\sqrt{4p^2 - 3q^2} \right] .
\end{aligned}
\tag{10.2.8}
$$

Note that this formula is homogeneous with respect to re-scaling $p \to hp, q \to hq$, implying that manifolds with equal value of the ratio p/q will have the same R–charges. Let us also note that the R–symmetry in the field theory is dual to the canonically defined Killing vector field on the Sasaki–Einstein manifolds

$$K = 3\frac{\partial}{\partial\psi} - \frac{1}{2}\frac{\partial}{\partial\alpha} . \tag{10.2.9}$$

From the point of view of the Calabi–Yau cone, K arises by contracting the Euler vector $r\partial/\partial r$ into the Kähler form. Note that K has closed orbits precisely when ℓ is a rational number, since ψ has period 2π and α has period $2\pi\ell$. In this case the

271

Sasaki–Einstein manifold $Y^{p,q}$ is said to be **quasi–regular**, and the space of leaves of the foliation defined by K is a Kähler–Einstein orbifold. This is true if and only if the following quadratic diophantine holds:

$$4p^2 - 3q^2 = n^2 \ , \tag{10.2.10}$$

for n an integer number. If ℓ is irrational the generic orbits of K do not close, but instead densely fill the orbits of the torus generated by $[\partial/\partial\psi, \ell\partial/\partial\alpha]$ and the Sasaki–Einstein manifold $Y^{p,q}$ is said to be **irregular**. Note that the orbits close over the submanifolds Σ_1, Σ_2.

The local form of the metrics is not particularly useful for constructing the dual gauge theories. However, one can make contact with the large literature on gauge theories for D3–branes placed at Calabi–Yau singularities by noting that the group $U(1)^3$ acts as a symmetry of $Y^{p,q}$. The Calabi–Yau cone $C(Y^{p,q})$ is thus toric. One can compute the toric diagram as follows [134]. The Kähler form of the Calabi–Yau may be regarded as a symplectic form, and one can then introduce a moment map for the Hamiltonian torus action by $U(1)^3$, which is a map $\mu : C(Y^{p,q}) \to \mathbb{R}^3$. The image is always a polyhedral cone, of a special type, and the moment map exhibits the Calabi–Yau as a $U(1)^3$ fibration over this polyhedral cone. The latter has four faces, where various $U(1)$ subgroups degenerate over the faces of the cone in a way determined by the normal vectors to the faces. One can now apply a Delzant theorem to this cone to obtain a gauged linear sigma model for $C(Y^{p,q})$. This is a simple algorithm that takes the combinatorial data that defines the polyhedral cone and produces the charges of the gauged linear sigma model. The result [134] is a $U(1)$ theory with 4 chiral superfields with charges $(p, p, -p + q, -p - q)$. Equivalently, because the space we start with is Calabi–Yau, the normal vectors to the four faces of the polyhedral cone lie in a plane. Projecting the four vectors onto this plane gives the vertices of the toric diagram.

10.3 The quiver theories

In this section we will present the quiver theories for the infinite class of manifolds which were presented in the previous section. We will recall the toric diagrams of each manifold, draw its corresponding (p,q)–web, extract simple information like the number of nodes and the number of fields in a given quiver theory from its corresponding toric diagram, and then present the quiver itself. Finally we write down the superpotential for the quiver theory.

The toric diagrams for $Y^{p,q}$ were found in [134] and are defined by the convex polygon over a $\mathbb{Z}^2$ lattice defined by four vertices located at

$$[0,0], \qquad [1,0], \qquad [p,p], \qquad [p-q-1, p-q] . \qquad (10.3.11)$$

See Figure 10-1 for the toric diagram of $Y^{4,2}$ and Figure 10-2 for a schematic description of the general case. Given the toric diagram, it is in principle possible to determine the gauge theory for any $Y^{p,q}$, by the process of partial resolution [45]. The starting point can be for example an abelian orbifold of the form $\mathbb{C}^3/\mathbb{Z}_m \times \mathbb{Z}_n$, with m and n sufficiently large. In particular, the toric diagrams of $Y^{p,q}$ could be obtained by partial resolutions of the $\mathbb{C}^3/\mathbb{Z}_{p+1} \times \mathbb{Z}_{p+1}$ orbifold, for any q at fixed p. Partial resolution corresponds to turning on non–generic Fayet–Illiopoulos parameters that reduce the toric diagram to the desired one. This method becomes computationally intractable even for modest values of p and q, and thus different approaches have to be developed.

We would like to get as much information as possible about the gauge theory from this toric description. Given a toric diagram, there are three steps in determining a supersymmetric quiver gauge theory with 4 supercharges that is associated with it. First we would like to get the number of gauge groups. Second we look for the number of bifundamental fields and the gauge quantum numbers. Finally we find which of the allowed gauge invariant terms appear in the superpotential. We will see now that, using very simple geometric ideas, it is possible to go far in answering the first two questions.

For a given toric diagram the number of gauge groups is a constant associated with the geometry. It is independent of any action of dualities that the gauge theory is undergoing. One way to look at the different gauge groups of the quiver is as living on the world volume of fractional branes which are given by bound states of D–branes which wrap even dimensional cycles in the geometry. These are the number of possible ways in which D–branes (3, 5, and 7–branes) can be wrapped on 0, 2 and 4–cycles, respectively. For the manifolds under study this number turns out to be particularly simple and is just the Euler characteristic of the 4d–base. In the toric diagram this number is given by the number of triangles in any possible triangulation of the corresponding diagram. Equivalently the number of triangles is given by the area of the toric diagram in units in which a single triangle has area 1. Different triangulations are related by flops, which correspond in the gauge theory to Seiberg duality transformations. Let us first notice that the vertex $(p - q - 1, p - q) = (p - q, p - q) + (-1, 0)$ sits always on a line parallel to the one joining the $(0,0)$ and (p, p) points, located one lattice spacing to the left of it. In order to count the number of triangles, we can use a uniform triangulation for every $Y^{p,q}$, given by the line that joins the points $(0,0)$ and (p, p), and the segments that connect $(1, 0)$ and $(p - q - 1, p - q)$ with the (i, i) points for $0 \leq i \leq p$. It is clear from this construction that the quiver associated to $Y^{p,q}$ has $2p$ gauge groups, namely $2p$ nodes. We illustrate this triangulation in Figure 10-1 for the example of $Y^{4,2}$.
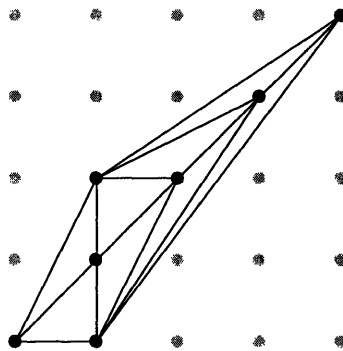
Figure 10-1: Triangulation of the toric diagram for $Y^{4,2}$. The number of gauge groups in the associated quiver theory is given by the number of triangles, which in this case is equal to eight.

Every toric diagram has an associated (p,q)-web, corresponding to the reciprocal diagram in which lines are replaced by orthogonal lines and nodes are exchanged with faces. The boundary of the toric diagram determines the charges of the external legs of the web. Figure 10-2 shows this construction for the case of $Y^{4,2}$ [2].
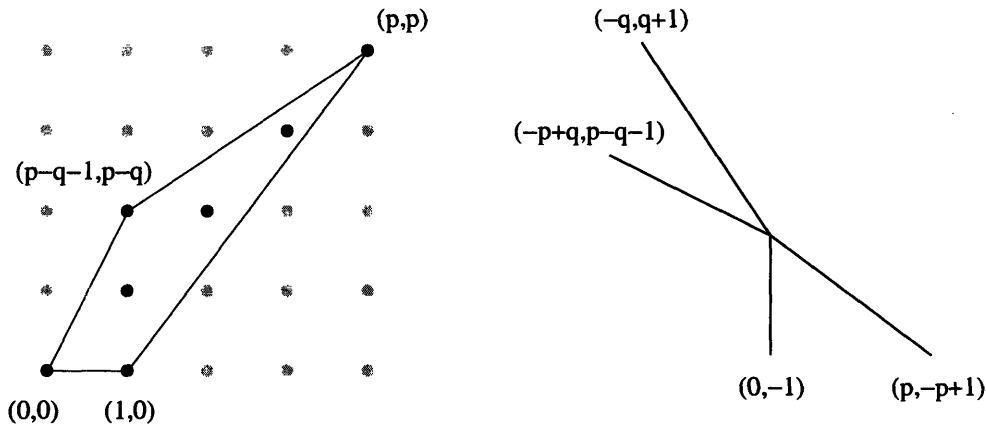
Figure 10-2: Toric diagram and external legs of the corresponding (p,q)-web for $Y^{4,2}$.

Furthermore, external legs determine the total number of bifundamental fields using the formula

$$
n_{fields} = \frac{1}{2} \sum_{i,j \in \text{legs}}^{4} \left| \det \begin{pmatrix} p_i & q_i \\ p_j & q_j \end{pmatrix} \right|.
\tag{10.3.12}
$$

This comes from the mapping of 0, 2 and 4–cycles to 3–cycles in the mirror manifold and computing their intersection, as described in [80].

For $Y^{p,q}$, the charges of the external legs of the web diagram can be computed from the toric diagram given by (10.3.11), and are

$$
\begin{aligned}
(p_1, q_1) &= (-p + q, p - q - 1) \\
(p_2, q_2) &= (-q, q + 1) \\
(p_3, q_3) &= (p, -p + 1) \\
(p_4, q_4) &= (0, -1)
\end{aligned}
\tag{10.3.13}
$$

---

[2]The cones over $Y^{p,q}$ are generically examples of geometries with more than one collapsing 4–cycle. The study of the gauge theories using (p,q)–webs was initiated in [54], in the context of quivers obtained by general Picard–Lefschetz monodromies.

from which, using (10.3.12), we can compute $n_{fields} = 4p + 2q$.

The determination of the superpotential typically is the most difficult task in completing the quiver theory and at the moment we do not have a general method of computing it for an arbitrary toric diagram. However, an important restriction for any quiver theory corresponding to an affine toric variety is that each of the fields in the quiver appears in the superpotential precisely twice (*i.e.* the F–term equations are of the form monomial equals monomial). As a result when counting the total number of fields appearing in each of the polygons contributing to the superpotential we should find $8p + 4q$ such fields.

In addition, geometric blow–downs correspond to Higgsings in the gauge theory. In such cases, the non–zero expectation value of a bifundamental field introduces a scale. When running the RG flow to scales much smaller than this vev, one encounters the gauge theory for the blown–down geometry. This approach has been implemented in [44] to derive the superpotentials of several gauge theories. Furthermore, the (p,q)–web representation of the toric singularities enables a simple identification of the bifundamental field acquiring a vev [52]. It turns out that the $Y^{p,q}$ geometries can be blow–down to the $\mathbb{C}^3/\mathbb{Z}_{p+q}$ orbifold, for which the quiver and the superpotential are known by standard methods. It is then possible to perform a further check of our construction by verifying that the proposed superpotential produces the final gauge theory after Higgsing.

In the case at hand, as explained in the previous section, the superconformal field theories we are looking for possess a $SU(2)$ global symmetry. This considerably restricts the possible choices of superpotential and, combining this requirement with the toric restrictions (each field has to appear exactly twice in the superpotential, one time with sign *plus* and one time with sign *minus*), it will turn out that in all of the cases there is precisely one superpotential satisfying all the properties, modulo an overall rescaling.

10.3.1 An iterative procedure starting with the $Y^{p,p}$ quiver

We now move on and construct the quiver for $Y^{p,q}$. That is, we will now determine how the $4p + 2q$ bifundamental fields of $Y^{p,q}$ are charged under its $2p$ gauge groups.

A convenient way to construct the quiver theories for the $Y^{p,q}$ manifolds for a fixed p is to start with the case $q = p$ and work our way down. For the case $q = p$, $Y^{p,p}$ is the base of the orbifold $\mathbb{C}^3/\mathbb{Z}_{2p}$. This orbifold group has an action on the three coordinates of $\mathbb{C}^3$, $z_i, i = 1, 2, 3$ by $z_i \to \omega^{a_i} z_i$ with ω a $2p$-th root of unity, $\omega^{2p} = 1$, and $(a_1, a_2, a_3) = (1, 1, -2)$. Since $2p$ is always even the group $\mathbb{Z}_{2p}$ with this action is actually reducible and one can write this group action as $\mathbb{Z}_2 \times \mathbb{Z}_p$. For special cases of p the group $\mathbb{Z}_p$ can be further reducible with the induced action but to keep the discussion general we will just refer to this group as $\mathbb{Z}_p$, without looking at the detailed structure, and bearing in mind that this group can be reducible.

The quiver theory for an orbifold is particularly simple and can be computed along the lines given in [79]. As stated above it has $2p$ nodes and, using the formula below equation (10.3.13) for the number of fields, we find that there are $6p$ bifundamental fields. Figure 10-3 shows the quiver theory for the $\mathbb{C}^3/\mathbb{Z}_8$ orbifold.
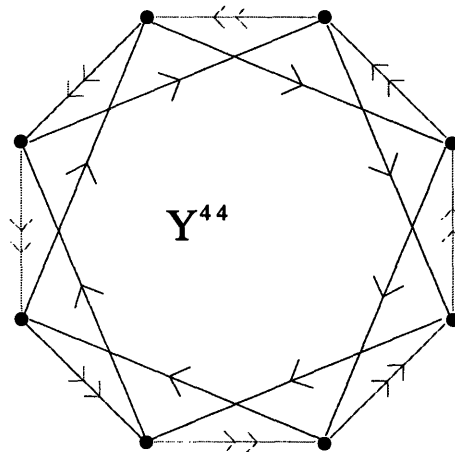
Figure 10-3: Quiver diagram for the $\mathbb{C}^3/\mathbb{Z}_8$ orbifold. We have color–coded bifundamental fields in accordance to the forthcoming discussion. Superpotential terms appear in the quiver diagram as triangles combining a green, a blue and a cyan arrow.

Since $a_1 = a_2$ there is a natural $SU(2) \times U(1)$ isometry of this space. The $SU(2)$ part acts on the coordinates z_1 and z_2 which transform as a doublet and the $U(1)$

part acts as the subgroup of $SU(3)$ which commutes with this $SU(2)$. This isometry becomes a global symmetry of the quiver gauge theory. All fields and their combinations transform in an irreducible representation of this group. As a result we can divide the $6p$ fields into $2p$ doublets that go along the edges of a polygon of $2p$ nodes. There are additional $2p$ singlet fields, which form triangles with each of two adjacent edges. There are $2p$ such triangles, all of which contribute to the superpotential. We require invariance of the theory under the global symmetry and therefore each time we have two doublets in the superpotential it should be understood that they are contracted by an epsilon symbol and therefore there will be two terms for each such polygon. We can now count the number of fields in the superpotential to be $2p \cdot 3 \cdot 2 = 12p$, as expected from the fact that this quiver corresponds to an affine toric variety. Specifically we denote the doublet fields as $X_i^\alpha, i = 1, \ldots, 2p, \alpha = 1, 2$, with i labeling the $\mathbb{Z}_{2p}$ index which takes values mod $2p$, while α labels the $SU(2)$ global symmetry index. Furthermore, we denote the singlets as $Y_i, i = 1, \ldots, 2p$. We use the convention that an arrow is labeled by the node number at which it starts. The superpotential then takes the simple form

$$W = \sum_{i=1}^{2p} \epsilon_{\alpha\beta} X_i^\alpha X_{i+1}^\beta Y_{i+2}. \qquad (10.3.14)$$

It is understood in this notation that the gauge quantum numbers are summed over in cyclic order and are therefore suppressed. In what follows, and due to the fact the the orbifold group $\mathbb{Z}_{2p}$ is reducible to at least $\mathbb{Z}_2 \times \mathbb{Z}_p$, it will be convenient to rename the X fields as follows: $U_i = X_{2i}, V_i = X_{2i+1}$. Note that the fields U are even under $\mathbb{Z}_2$ while the fields V are odd under $\mathbb{Z}_2$. From now on we will adhere to the convention, already used in Figure 10-3, of indicating V_i fields in green and U_i fields in cyan. In terms of these fields the superpotential takes the form

$$W = \sum_{i=1}^{p} \epsilon_{\alpha\beta} (U_i^\alpha V_i^\beta Y_{2i+2} + V_i^\alpha U_{i+1}^\beta Y_{2i+3}). \qquad (10.3.15)$$

The gauge theory for $Y^{p,p-1}$ results from the following set of operations, which

278

remove three fields and add one:

- Pick an edge of the polygon, say the one which has an arrow V_i starting at node $2i + 1$, and remove one arrow from the corresponding doublet to make it a singlet. Call this type of singlet Z_i.

- Remove the two diagonal singlets, Y that are connected to the two ends of this singlet Z. Since we chose the V_i arrow which is removed to start at node $2i + 1$ the Y fields which are removed are Y_{2i+2} and Y_{2i+3}. This action removes from the superpotential the corresponding two cubic terms that involve these Y fields.

- Add a new singlet Y_{2i+3} in such a way that, together with the two doublets at both sides of the singlet Z_i, they form a rectangle. Specifically this arrow starts at node $2i + 3$ and ends at node $2i$. The new rectangle thus formed contains two doublets which as before should be contracted to an $SU(2)$ singlet. This term is added to the superpotential.

By the end of this process, we get $6p - 2$ fields. There are p doublet fields U_i, $p - 1$ doublet fields $V_j, j \neq i$, one field of type Z_i and $2p - 1$ diagonal singlets of type $Y_j, j \neq 2i + 2$. We present in Figure 10-4 the $Y^{4,3}$ example, obtained from $Y^{4,4} = \mathbb{C}^3/\mathbb{Z}_8$ by the series of steps outlined above. We indicate the new Z singlet in red.

The new superpotential has $(2p - 2)$ triangles and 1 rectangle (recall that when we refer to one triangle or one rectangle, we are actually indicating the $SU(2)$ invariant combination given by two of them). The resulting superpotential is

$$W = \sum_{i \neq j = 1}^{p} \epsilon_{\alpha\beta}(U_j^\alpha V_j^\beta Y_{2j+2} + V_j^\alpha U_{j+1}^\beta Y_{2j+3}) + \epsilon_{\alpha\beta} Z_i U_{i+1}^\alpha Y_{2i+3} U_i^\beta. \qquad (10.3.16)$$

As a check we can verify that the model still satisfies the toric condition regarding the number of fields in the superpotential. There are $(p - 1) \cdot 3 \cdot 2 \cdot 2 + 4 \cdot 2 = 12p - 4$, in agreement with our expectation.

279
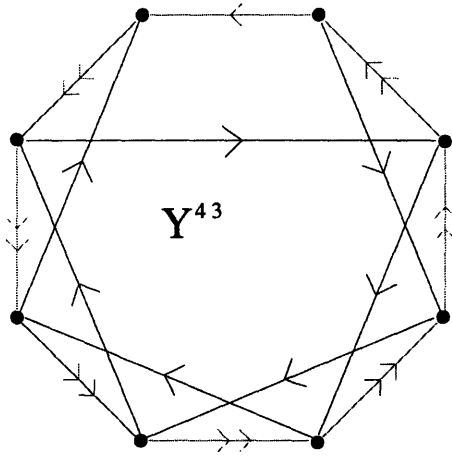
Figure 10-4: Quiver diagram for $Y^{4,3}$, obtained from $Y^{4,4} = \mathbb{C}^3/\mathbb{Z}_8$.

We now continue to construct the $Y^{p,p-2}$ model. This is an easy task and is just a repetition of the 3–step process described above. We pick an index $j \neq i$ and turn a V_j doublet into a Z_j singlet by repeating the sequence of steps previously explained. The result is a theory with $6p - 4$ fields forming p U doublets, $p - 2$ V doublets, 2 Z singlets and $2p - 2$ Y singlets. We present the $Y^{4,2}$ example in Figure 10-5.
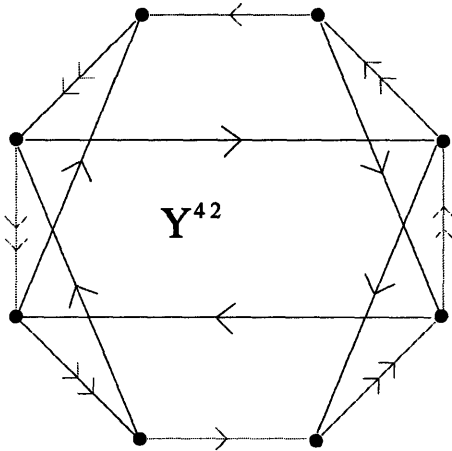
Figure 10-5: Quiver diagram for $Y^{4,2}$, obtained from $Y^{4,4} = \mathbb{C}^3/\mathbb{Z}_8$ by applying the three step sequence twice.

When one applies the procedure the second time, there is the possibility of choosing the double leg to "open up". For instance in the case of $Y^{4,2}$ there are two different choices that can be made. One is Figure 10-5, the other is Figure 10-6.

These two quivers are different, but are actually related by Seiberg duality. They
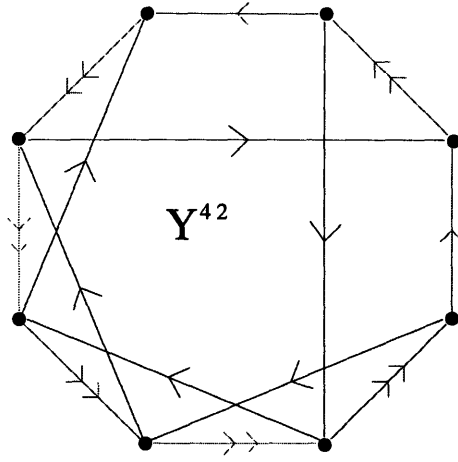
Figure 10-6: A different quiver diagram for $Y^{4,2}$, corresponding to a different toric phase.

correspond to two different "toric phases" of the same Duality Tree [56, 55].

The superpotential now has $2p - 4$ triangles and 2 rectangles and is given by

$$W = \sum_{i \neq j \neq k = 1}^{p} \epsilon_{\alpha\beta}(U_k^\alpha V_k^\beta Y_{2k+2} + V_k^\alpha U_{k+1}^\beta Y_{2k+3}) + \epsilon_{\alpha\beta} \sum_{k=i,j} Z_k U_{k+1}^\alpha Y_{2k+3} U_k^\beta \quad (10.3.17)$$

and has $(p - 2) \cdot 3 \cdot 2 \cdot 2 + 2 \cdot 4 \cdot 2 = 12p - 8$ fields, which is consistent with the fact that the probed geometry is toric.

We can keep going down in q by iterating the procedure above. Thus, for $Y^{p,q}$ there are $4p + 2q$ fields forming p U doublets, q V doublets, $(p - q)$ Z singlets and $(p+q)$ diagonal singlets Y. The superpotential has $2q$ triangles and $(p-q)$ rectangles. The general superpotential is

$$W = \sum_{k} \epsilon_{\alpha\beta}(U_k^\alpha V_k^\beta Y_{2k+2} + V_k^\alpha U_{k+1}^\beta Y_{2k+3}) + \epsilon_{\alpha\beta} \sum_{k} Z_k U_{k+1}^\alpha Y_{2k+3} U_k^\beta. \quad (10.3.18)$$

The sum k for the cubic terms is in indices in which V exists and the sum k for the quartic terms is in indices in which Z exists. Note that any of the indices 1 to p appears precisely once either in the cubic or the quartic sum. The number of fields in the superpotential is $q \cdot 3 \cdot 2 \cdot 2 + (p - q) \cdot 4 \cdot 2 = 8p + 4q$, verifying the quiver is toric.

For completeness we also give the quivers for $Y^{4,1}$ and $Y^{4,0}$.
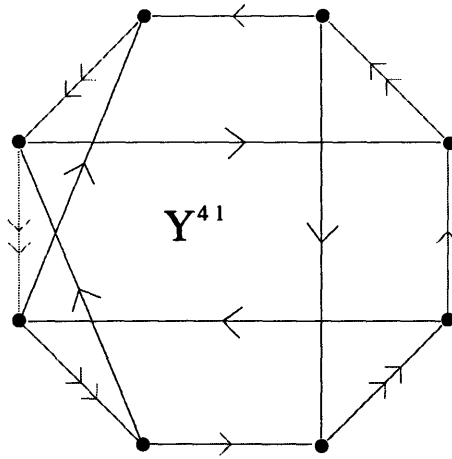
Figure 10-7: Quiver diagram for $Y^{4,1}$. In this case we just see one toric phase.
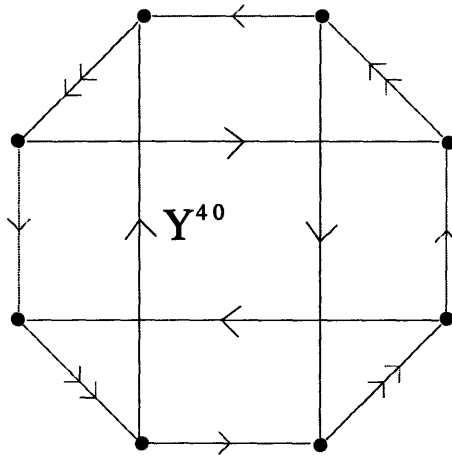
Figure 10-8: Quiver diagram for $Y^{4,0}$. Note that the superpotential terms are only quartic. Correspondingly, the nodes have precisely 2 incoming and 2 outgoing arrows. This quiver diagram is indeed a $\mathbb{Z}_4$ orbifold of the conifold.

All the different quivers constructed by our iterative procedure satisfy the following property. In the $Y^{p,p}$ models every node has precisely 3 incoming and 3 outgoing arrows. Each time the procedure is applied, for precisely two nodes of the quiver the number of incoming and outgoing arrows becomes 2. At the end of the process we are left with a quiver where all of the nodes have precisely 2 incoming and 2 outgoing arrows. A way to rephrase this fact is by saying that the "relative number of flavors" for each gauge group passes from 3 to 2. This "relative number of flavors" is discussed in detail in [15] and is useful in order to understand the structure of Seiberg dualities for any superconformal quiver. The whole set of Seiberg dual phases of the

same theory can be organized in a Duality Tree [56, 55]. Also for the models we are discussing it is generically possible to construct an infinite tower of superconformal quivers related to the ones constructed here by applying Seiberg dualities. The fact that the relative number of flavors is always greater than (or equal to) 2 implies that we are just seeing the "minimal models" of the Duality Tree [15]. We notice that a generic quiver in the Duality Tree will not satisfy the quiver toric condition, *i.e.* the equality for all the ranks of the gauge groups. In many cases it is known that the different models in the Duality Tree are classified by solutions of Diophantine equations; it would be nice to understand if this is true also here.

Closed loops in the Duality Tree can be used to engineer Duality Cascades of Klebanov–Strassler type. In the conifold case however the Duality Tree is trivial, meaning that it is composed of just one theory and there is just one closed loop of length one. Duality cascades for these theories, along with their supergravity duals, have been constructed in [92].

10.3.2 Higgsing the $Y^{p,q}$ quivers

In some special cases, the $Y^{p,q}$'s correspond to geometries whose associated gauge theories are well understood. We have already seen that $Y^{p,p}$ corresponds to $\mathbb{C}^3/\mathbb{Z}_{2p}$. In addition, $Y^{p,0}$ has no triangles at all and the R–charges for bifundamental fields are $1/2$. This agrees with the fact that, as is clear from the corresponding toric diagram, $Y^{p,0}$ corresponds to the $\mathbb{Z}_p$ orbifold of the conifold.

Another appealing observation that follows from our construction of the general quiver is that the quiver for $Y^{p,q}$ can be Higgsed to the one for the orbifold $\mathbb{C}^3/\mathbb{Z}_{p+q}$ by turning on non–zero vevs for all the $(p-q)$ Z fields. One can see this geometrically as follows. We begin with S^5, viewed as the unit sphere in $\mathbb{C}^3$ with complex coordinates (z_1, z_2, z_3). Consider the $U(1)$ action with weights $(1, 1, -2)$, so that $(z_1, z_2, z_3) \mapsto (\lambda z_1, \lambda z_2, \lambda^{-2} z_3)$ with $\lambda \in U(1)$. The quotient by this action is a form of weighted projective space, which we denote $W\mathbb{C}P^2_{[1,1,-2]}$. However, before we quotient out, we may first factor through by $\mathbb{Z}_{p+q} \subset U(1)$ to give $S^5/\mathbb{Z}_{p+q}$. This is precisely the orbifold that is dual to the Higgsing described above.

283

A useful description of $W\mathbb{C}P^2_{[1,1,-2]}$ is as follows. One takes T^*S^2, which has boundary $\mathbb{R}P^3 = S^3/\mathbb{Z}_2$, and glues onto this the A_1 singularity $\mathbb{R}^4/\mathbb{Z}_2$. In this realization the two–sphere $(z_1, z_2, 0)$ corresponds to the zero section of T^*S^2 whereas the A_1 singularity is located at the point $(0, 0, z_3)$. The idea now is to blow up the A_1 singularity in the base in the usual way, replacing it with another copy of T^*S^2. The resulting space is an S^2 bundle over S^2 in which the gluing function across the equator corresponds to $2 \in \mathbb{Z} \cong \pi_1(U(1))$, where $U(1) \subset SO(3)$ acts on the fibre two–sphere. This bundle can also be made by gluing T^*S^2 to minus itself along the common boundary $\mathbb{R}P^3$. Notice that this is precisely the topological construction of the base B of the Sasaki–Einstein manifolds $Y^{p,q}$ in [63].

Having resolved the base, we must now consider the fibre S^1. Notice that over $W\mathbb{C}P^2_{[1,1,-2]}$ minus its singular point, which gives topologically T^*S^2, the original $U(1)$ bundle has winding number $p + q$ over S^2. However, note that $H^2(\mathbb{R}P^3; \mathbb{Z}) \cong \mathbb{Z}_2$. One easily sees that the map from $\mathbb{Z}$, which determines the topology of the $U(1)$ bundle over T^*S^2, to $\mathbb{Z}_2$, which determines the topology on the boundary $\mathbb{R}P^3$, is just reduction modulo 2. To extend the $U(1)$ bundle over the blown–up copy of S^2, topologically we must specify an integer $l \in \mathbb{Z}$ which gives the winding number over the blown–up cycle. However, in order for this to glue onto the existing $U(1)$ bundle described above, it is clear that we must have $l \cong p + q$ mod 2 in order that the boundaries match. The resulting space is a $U(1)$ bundle over B with winding numbers $p + q$ and l over two S^2 zero sections. Note that these were called S_1, S_2 in [63] and [134]. Moreover, without loss of generality we may set $l = p - q$, since $l \cong p + q$ mod 2.

Notice that the final space has precisely the topology of $Y^{p,q}$. Moreover, we also have the following relation between volumes:

$$\mathrm{vol}(S^5/\mathbb{Z}_{2p}) < \mathrm{vol}(Y^{p,q}) < \mathrm{vol}(S^5/\mathbb{Z}_{p+q}) \qquad q < p . \qquad (10.3.19)$$

This process we have described is therefore consistent with an a–theorem for Higgsing.

As an example consider the model $Y^{4,3}$; giving a vev to the bifundamental field Z

284

and flowing to the infra–red there is a Higgsing mechanism. The gauge group passes from $SU(N)^8$ to $SU(N)^7$ and the quartic term in the superpotential disappears. In summary, the low energy theory becomes the known orbifold $\mathbb{C}^3/\mathbb{Z}_7$.

The same procedure can be applied to one of the phases of $Y^{4,2}$. Here new features arise. Giving a vev to both of the two Z fields one ends up with the orbifold $\mathbb{C}^3/\mathbb{Z}_6$, which is actually the model $Y^{3,3}$. This fact also relates some observations made in Section 2 about monotonic behaviour of the volumes of $Y^{p,q}$ with the supersymmetric a–theorem.

Giving instead a vev for just one of the Z fields one finds a new model, which is the orbifold $\mathbb{C}^3/\mathbb{Z}_7$ where the above described three–step operation has been applied. These types of models are not part of the $Y^{p,q}$ series, as can be seen from the fact that all the $Y^{p,q}$ models have precisely one baryonic $U(1)$ symmetry. The quivers $\mathbb{C}^3/\mathbb{Z}_{odd}$ instead cannot have precisely one $U(1)$ baryonic symmetry, since the number of baryonic symmetries is given by the number of nodes of the quiver minus the rank of the (antisymmetric part of) the quiver intersection matrix minus one. Since an antisymmetric matrix always has even rank, in a quiver with an odd number of nodes the number of baryonic $U(1)$'s is always even.

10.4   R–charges and horizon volumes

In this section we compute the exact R–charges as well as the a central charge of the $Y^{p,q}$ quivers using a–maximization, and compare with the geometrical predictions of [63] and [134]. The agreement found is perfect.

Let us first recall the logic of a–maximization. As explained in [102], in this procedure one assigns some trial R–charges to the different fields and the *exact* R–charges are then determined by those values that (locally) maximize the combination of 't Hooft anomalies found in [7, 6]:

$$a(R) = \frac{3}{32}(3\mathrm{tr}R^3 - \mathrm{tr}R) . \tag{10.4.20}$$

The maximal value of this function is then precisely the exact a central charge of the theory at the IR fixed point. As proposed in [102] the trial R–charges can be chosen by assigning a fiducial R–charge R_0, provided the latter satisfies the constraints imposed by anomaly cancellation. The fiducial R–charge is allowed to mix with the abelian global symmetries, which for all the $Y^{p,q}$ quivers is $U(1)_F \times U(1)_B$.

We find it more convenient to implement this procedure in the following equivalent fashion [56, 97]. Recall that for a supersymmetric gauge theory with gauge group G, the beta function for the gauge coupling $\alpha = g^2/4\pi$ is

$$\beta(\alpha) = -\frac{\alpha^2}{2\pi} \frac{3T(G) - \sum_i T(r_i)(1 - \gamma_i(\alpha))}{1 - \frac{\alpha}{2\pi}T(G)} \tag{10.4.21}$$

where γ_i is the anomalous dimension of a chiral superfield in the representation r_i, and for $G = SU(N)$ the Casimirs take the values $T(\text{fund}) = 1/2$ and $T(G) = T(\text{adj}) = N$.

At the IR fixed point all the numerators of the beta functions corresponding to each gauge group factor (node of the quiver) must vanish, thus imposing the relations

$$N - \frac{1}{2}N\sum_i(1 - R_i) = 0 \tag{10.4.22}$$

where we used the fact that at the fixed point the anomalous dimension is related to the R–charge as $\gamma_i = 3R_i - 2$. We have also used the fact that our quivers are always "toric", in the sense that all the ranks of the gauge groups are equal (to N in this case). We can then consider a set of arbitrary R–charges R_i which satisfy equation (10.4.22) at each node, as well as the additional requirement that each monomial in the superpotential has R–charge precisely 2.

Let us illustrate this procedure with an example, and then move on to the general $Y^{p,q}$ quivers.

10.4.1 Gauge theory analysis for $Y^{3,2}$

At the bottom of the infinite family we have $Y^{2,1}$, which is a metric on the horizon of the complex cone over dP_1 [134]. The gauge theory for this geometry was computed

in [45] and is also presented in [43]. It has recently been discussed in reference [21], resolving an apparent mismatch between gauge theory results in the literature and the geometric analysis of [134]. The next case is $Y^{3,2}$ and the corresponding quiver is presented in Figure 10-9 below.
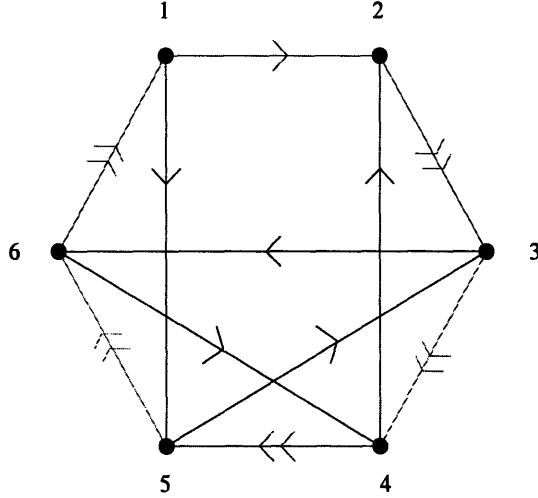
Figure 10-9: Quiver diagram for $Y^{3,2}$.

The gauge group for the theory is $SU(N)^6$. We may now determine the exact central charge of this theory using a–maximization. For the $Y^{3,2}$ quiver we have $1 + 5 + 5 = 11$ *a priori* different R–charges, subject to 6 linear relations coming from (10.4.22)

$$
\begin{aligned}
\frac{\beta_1}{N} &= 1 + \frac{1}{2}(R_{12} - 1) + \frac{1}{2}(R_{15} - 1) + \frac{1}{2}2(R_{61} - 1) = 0 \\
\frac{\beta_2}{N} &= 1 + \frac{1}{2}(R_{12} - 1) + \frac{1}{2}(R_{42} - 1) + \frac{1}{2}2(R_{23} - 1) = 0 \\
\frac{\beta_3}{N} &= 1 + \frac{1}{2}(R_{53} - 1) + \frac{1}{2}(R_{36} - 1) + \frac{1}{2}2(R_{23} - 1) + \frac{1}{2}2(R_{34} - 1) = 0 \\
\frac{\beta_4}{N} &= 1 + \frac{1}{2}(R_{64} - 1) + \frac{1}{2}(R_{42} - 1) + \frac{1}{2}2(R_{34} - 1) + \frac{1}{2}2(R_{45} - 1) = 0 \\
\frac{\beta_5}{N} &= 1 + \frac{1}{2}(R_{15} - 1) + \frac{1}{2}(R_{53} - 1) + \frac{1}{2}2(R_{45} - 1) + \frac{1}{2}2(R_{56} - 1) = 0 \\
\frac{\beta_6}{N} &= 1 + \frac{1}{2}(R_{36} - 1) + \frac{1}{2}(R_{64} - 1) + \frac{1}{2}2(R_{56} - 1) + \frac{1}{2}2(R_{61} - 1) = 0 \quad (10.4.23)
\end{aligned}
$$

and 5 conditions from the superpotential

$$R_{56} + R_{61} + R_{15} = 2$$
$$R_{45} + R_{56} + R_{64} = 2$$
$$R_{34} + R_{45} + R_{53} = 2$$
$$R_{23} + R_{34} + R_{42} = 2$$
$$R_{12} + R_{23} + R_{36} + R_{61} = 2 \ . \tag{10.4.24}$$

However, one can check that two charges remain undetermined – this is a general feature, valid for all the $Y^{p,q}$ models, and is related to the fact that the global symmetry is always $U(1) \times U(1)$. The maximization is then always performed over a two dimensional space of trial R–charges.

We can parameterize the two trial R–charges as follows:

$$R_{12} = x \qquad R_{36} = R_{15} = R_{64} = R_{53} = R_{42} = y$$
$$R_{34} = R_{56} = 1 + \frac{1}{2}(x - y) \qquad R_{61} = R_{45} = R_{23} = 1 - \frac{1}{2}(x + y) \ . \tag{10.4.25}$$

Recall the definition of a in terms of these R–charges:

$$a = \frac{3}{32}\Big(2|G| + \sum_i 3(R_i - 1)^3 - (R_i - 1)\Big) \tag{10.4.26}$$

where $|G|$ is the number of vector multiplets. Here it is straightforward to check that $\mathrm{tr}R = 0$ as shown on general grounds in [15]. One can now compute $a(x,y) = 9/32\mathrm{tr}R^3$ which reads[3]

$$\frac{32}{9}a(x,y) = 6 + (x - 1)^3 + 5(y - 1)^3 + \frac{1}{2}(x - y)^3 - \frac{3}{4}(x + y)^3 \ . \tag{10.4.27}$$

The local maximimum is found at

$$x_{max} = \frac{1}{3}(-9 + 4\sqrt{6}) \qquad y_{max} = -1 + 2\sqrt{\frac{2}{3}} \tag{10.4.28}$$

---

[3]Here, and henceforth, we suppress factors of N.

for which we find $a_{max} = \frac{27}{16}(-9 + 4\sqrt{6})$, which indeed agrees with $\pi^3/(4 \cdot \mathrm{vol}(Y^{3,2}))$.

10.4.2 a–maximization in the general case

As explained in Section 10.3, the $Y^{p,q}$ family is obtained from the $Y^{p,p} \simeq \mathbb{C}^3/\mathbb{Z}_2 \times \mathbb{Z}_p$ model by a sequence of $(p - q)$ simple modifications. Following this construction, and applying the same logic presented for $Y^{3,2}$, it is straightforward to obtain a parametrization of the R–charges in the general case. There are then $2p$ relations from imposing the vanishing of the beta functions at each node, and $p + q$ relations from requiring that each term in the superpotential (again, by each term, we mean each $SU(2)$ doublet) has R–charge 2. These are $3p + q$ linear relations in all, for $(p - q) + p + q + (p + q) = 3p + q$ a priori independent R–charges. However, two of the relations are redundant, and we can therefore parameterize the R–charges of all fields in terms of two unknowns x and y as follows:

- The $(p - q)$ singlets Z around the outer loop of the quiver have R–charge x.

- The $(p + q)$ diagonal singlets Y have R–charge y.

- The p doublets U around the outer loop have R–charge $1 - \frac{1}{2}(x + y)$.

- The q doublets V around the outer loop have R–charge $1 + \frac{1}{2}(x - y)$.

As already noted, the fact that the maximization is performed over a two dimensional space implies that there are precisely two $U(1)$ symmetries with which the R–symmetry can mix. It now follows that

$$\mathrm{tr}R(x, y) = 2p + (p - q)(x - 1) + (p + q)(y - 1) - p(x + y) + q(x - y) = 0 \quad (10.4.29)$$

where $\mathrm{tr}R$ is a fermionic trace and the first contribution of $2p$ comes from the gauginos. We thus have $\mathrm{tr}R = 0$. This fact is always true for a theory with a weakly coupled supergravity dual [91] (this corresponds to having $c = a$). In [15] a general proof is given that shows that $\mathrm{tr}R$ vanishes for any superconformal quiver. We can now

compute $\mathrm{tr}R^3(x, y)$ which reads

$$\mathrm{tr}R^3(x,y) = 2p + (p-q)(x-1)^3 + (p+q)(y-1)^3 - \frac{p}{4}(x+y)^3 + \frac{q}{4}(x-y)^3 \quad (10.4.30)$$

The maximum is found at

$$
\begin{aligned}
y_{max} &= \frac{1}{3q^2}\left[-4p^2 + 2pq + 3q^2 + (2p-q)\sqrt{4p^2 - 3q^2}\right] \\
x_{max} &= \frac{1}{3q^2}\left[-4p^2 - 2pq + 3q^2 + (2p+q)\sqrt{4p^2 - 3q^2}\right] \, . \quad (10.4.31)
\end{aligned}
$$

Notice immediately that these are precisely the same as the baryon charges $R[B_1]$, $R[B_2]$ (10.2.8) computed using the metrics. Moreover, substituting into a we also reproduce the correct volume formula (10.2.5) via the AdS/CFT formula

$$a(Y^{p,q}) = \frac{\pi^3}{4 \cdot \mathrm{vol}(Y^{p,q})} \, . \quad (10.4.32)$$

10.4.3 Continuous global symmetries

We are now in a position to summarise the results obtained so far and conclude our comparison between geometric and field theoretic results.

In section 10.3 we constructed the quivers and wrote down the explicit superpotential. This superpotential is toric and satisfies a global $SU(2)$ symmetry. All the fields are in the spin–0 representation of $SU(2)$ or in the spin–1/2 representation. We note that applying successive Seiberg Dualities one expects to find higher dimensional representations.

In this section, solving the linear beta–function constraints, we showed that there are precisely two global $U(1)$ symmetries. For any $Y^{p,q}$ quiver the rank of the (antisymmetric) quiver matrix is $2p - 2$ and the number of nodes is $2p$. This implies that there is precisely one $U(1)$ *baryonic* symmetry. The reason is that this baryonic symmetry turns out to be equal to a particular combination of the $U(1)$ factors of the original $U(N)^{2p}$ gauge groups. There are two symmetries that can be constructed by linear combinations of these $2p$ $U(1)$ factors: one is completely decoupled and the

other one is the baryonic symmetry. One way of checking that this is a baryonic symmetry is by computing the cubic 't Hooft anomaly, which has to vanish. The reason is that in the AdS dual description this global symmetry becomes a gauge symmetry, and the gauge field is given by Kaluza Klein reduction of the RR four–form of Type IIB superstrings on a 3–cycle of the transverse 5–dimensional space. The cubic 't Hooft anomalies correspond to a Chern–Simons term in AdS that does not exist for gauge fields coming from RR four–forms.

As a result of the previous discussion, we see from the gauge theory that any $Y^{p,q}$ quiver has to have precisely one $U(1)$ *flavor* symmetry. For this symmetry one does not expect the cubic anomalies to vanish. This symmetry is related to the $U(1)$ part of the isometries of the transverse 5–dimensional manifold. We summarise the final charges in table 10.1.

Field	number	$R -$ charge	$U(1)_B$	$U(1)_F$
Y	$p+q$	$(-4p^2 + 3q^2 + 2pq + (2p-q)\sqrt{4p^2-3q^2})/3q^2$	$p-q$	-1
Z	$p-q$	$(-4p^2 + 3q^2 - 2pq + (2p+q)\sqrt{4p^2-3q^2})/3q^2$	$p+q$	$+1$
U^α	p	$(2p(2p - \sqrt{4p^2-3q^2}))/3q^2$	$-p$	0
V^α	q	$(3q - 2p + \sqrt{4p^2-3q^2})/3q$	q	$+1$

Table 10.1: Charge assignments for the four different types of fields present in the general quiver diagram for $Y^{p,q}$.

From table 10.1 it is straightforward to compute

$$\mathrm{tr}U(1)_B = \mathrm{tr}U(1)_F = 0 . \tag{10.4.33}$$

These linear anomalies have to vanish, since we have resolved the mixing with the R–symmetry. A simple computation shows that also the cubic 't Hooft anomalies for $\mathrm{tr}U(1)_B^3$ and $\mathrm{tr}U(1)_F^3$ vanish, for instance

$$\mathrm{tr}U(1)_B^3 = (p+q)(p-q)^3 + (p-q)(p+q)^3 + 2p(-p)^3 + 2q(q)^3 = 0 . \tag{10.4.34}$$

The mixed 't Hooft anomalies $\mathrm{tr}U(1)_F^2 U(1)_B$ and $\mathrm{tr}U(1)_B^2 U(1)_F$ are instead non–zero. We note that the relation $\mathrm{tr}U(1)_F^3 = 0$ does not have a direct physical meaning, since one can always redefine the flavor symmetry, mixing it with the baryonic symmetry. In this case, $\mathrm{tr}U(1)_F^3$ does not necessarily have to vanish.

It is worth explaining the reason for the claim that $U(1)_B$, as given in table 10.1, corresponds to a *baryonic* symmetry, since the cubic anomalies $U(1)_B$ and $U(1)_F$ show a similar behaviour. One possible explanation is that $U(1)_B$ can be directly constructed as a linear combination of the $2p$ decoupled gauge $U(1)$s, while $U(1)_F$ cannot. In the next subsection we will give a different explanation of this fact.

10.4.4 Some properties of the baryons

In this subsection we give a simple analysis of the baryonic operators in the $Y^{p,q}$ quivers, along the lines of [19, 103, 96, 97].

Since all the $2p$ gauge groups have the same rank, N, it is possible to construct simple dibaryonic operators with one type of bifundamental field $A_\alpha{}^\beta$:

$$\mathcal{B}[A] = \varepsilon^{\alpha_1 \cdots \alpha_N} \, A_{\alpha_1}^{\beta_1} \, \cdots \, A_{\alpha_N}^{\beta_N} \, \varepsilon_{\beta_1 \cdots \beta_N} \ . \tag{10.4.35}$$

In the $Y^{p,q}$ quivers there are four classes of bifundamental fields, so there are four classes of dibaryonic operators: $\mathcal{B}[Y]$, $\mathcal{B}[Z]$, $\mathcal{B}[U]$ and $\mathcal{B}[V]$. Since the fields U^α and V^α transform in the 2–dimensional representation of the global $SU(2)$, the corresponding baryonic operators transform in the $(N+1)$–dimensional representation, as explained in [19]. This fact tells us immediately that the corresponding D3–brane (wrapping a supersymmetric 3–cycle inside the $Y^{p,q}$ manifold) can be freely moved on the round S^2 parametrized by the coordinates θ and ϕ. The corresponding 3–cycle is thus part of a family of supersymmetric cycles parametrized by an S^2.

The operators like (10.4.35) are chiral, so their scaling dimension is precisely the scaling dimension of the bifundamental A, multiplied by N. These scaling dimensions correspond holographically to the volumes of the corresponding 3–cycles. Computations of the volumes give precisely the values listed in table 10.1.

From the quiver it is also possible to derive some information about the topology of the $Y^{p,q}$ manifolds and of the supersymmetric 3–cycles. A more complete treatment would require the algebraic computation of the moduli space of vacua of the gauge theory, which should reproduce the quotient of $\mathbb{C}^4$ determined in [134] and described in section 10.3.

Taking the product of two different consecutive dibaryons it is possible to get rid of the two ε–symbols corresponding to the same gauge group [19]. For instance (for $q < p$) we can compose U–dibaryons with Z–dibaryons:

$$\mathcal{B}[U]\mathcal{B}[Z] \sim \varepsilon^{\alpha_1 \ldots \alpha_N} \, U_{\alpha_1}^{\beta_1} \, \ldots \, U_{\alpha_N}^{\beta_N} Z_{\beta_1}^{\gamma_1} \, \ldots \, Z_{\beta_N}^{\gamma_N} \, \varepsilon_{\gamma_1 \ldots \gamma_N} \sim \mathcal{B}[UZ] \, . \qquad (10.4.36)$$

It is thus possible to associate (poly–)baryonic operators to connected paths in the quiver diagram. When the path closes all the ε–symbols disappear and the operator is not baryonic anymore.

We thus look at the closed oriented paths in the quiver diagram. From the quiver diagrams we can recognize four different types of simple loops:

- One type of loop has length 3 and is made of one Y–field, one U–field and one V–field.

- One type of loop has length 4 and is made of one Z–field, two U–fields and one Y–field.

- The third type of loop instead goes all the way around the quiver and has length $2p$: it is made of p U–fields, q V–fields and $p - q$ Z–fields.

- The last type has length $2p - q$ and is made of p Y–fields and $p - q$ U–fields.

In order that the interpretation of a closed path of baryonic operators as a non-baryonic operator makes sense, it is necessary that the total baryonic charge vanishes. If we substitute the charges of table 10.1 into the four types of closed loops listed above, we find that the two "short" loops have vanishing charge both for the $U(1)_B$ and the $U(1)_F$ (as has to be the case since they enter in the superpotential), but the

293

charge of the two "long" loops is zero only for $U(1)_B$. This implies that precisely the symmetry called $U(1)_B$ in table 10.1 is the baryonic symmetry.

The fact that a closed loop of baryons is equivalent to a non–baryonic operator has an interpretation in terms of the topology of the 3–cycles wrapped by the corresponding D3–brane: the sum of the cycles associated to the dibaryons entering the loop has to be the topologically trivial 3–cycle. Denoting $\Sigma[A]$ the 3–cycle associated to the dibaryons constructed with the bifundamental A, we thus have the following four relations for the corresponding homology cycles of the $Y^{p,q}$ manifold:

$$\Sigma[Y] + \Sigma[U] + \Sigma[V] = 0 \qquad (10.4.37)$$

$$\Sigma[Z] + 2\,\Sigma[U] + \Sigma[Y] = 0 \qquad (10.4.38)$$

$$p\,\Sigma[U] + q\,\Sigma[V] + (p-q)\,\Sigma[Z] = 0 \qquad (10.4.39)$$

$$p\,\Sigma[Y] + (p-q)\,\Sigma[U] = 0 \ . \qquad (10.4.40)$$

Recall that using the results of [134] one can see that for the singlet dibaryons $\Sigma[Z] = \Sigma_2 = S^3/\mathbb{Z}_{p-q}$ and $\Sigma[Y] = \Sigma_1 = S^3/\mathbb{Z}_{p+q}$. Moreover in [134] it is shown that the representative cycles, given by $\{y = y_i\}$ respectively, are supersymmetric, meaning that the cones over these are complex divisors of the Calabi–Yau cones.

We will now show the existence of two new supersymmetric three–cycles, corresponding precisely to the two remaining dibaryons, $\Sigma[U]$ and $\Sigma[V]$. First, let us verify that we can pick a representative cycle of $\Sigma[U]$, which is supersymmetric and reproduces the correct volume/charge formula. This is again straightforward using the results of [134]. Consider the three–cycle obtained by setting $\{\theta, \phi\}$ to some constant value on the round S^2, and denote this by Σ_3. One easily computes

$$\frac{1}{2} J \wedge J|_{\{\theta,\phi\}=\text{const.}} = \frac{1}{3} r^3 \mathrm{d}r \wedge \mathrm{d}y \wedge \mathrm{d}\psi \wedge \mathrm{d}\alpha = \text{vol}_{\{\theta,\phi\}=\text{const.}}(\Sigma_3) \qquad (10.4.41)$$

where J is the Kähler two–form of the Calabi–Yau cone over $Y^{p,q}$ [134], and the induced volume form is computed using the metric (10.2.1). This shows that the cycle is supersymmetric. The topology is $S^3/\mathbb{Z}_p$, as follows from the discussion in [134],

294

with the Chern number of the $U(1)$ fibration over the $y - \psi$ two–sphere being p. The volume is trivially computed by integrating (10.4.41) and indeed reproduces exactly $R[U]$. Finally, we may simply define the remaining cycle as the sum $\Sigma_4 \equiv -\Sigma_1 - \Sigma_3$. Thus from (10.4.37) we have $\Sigma[V] = \Sigma_4$. Note that, correctly, $\mathrm{vol}(\Sigma_4) \propto R[V] = R[U] + R[Z]$. Clearly the cycle is supersymmetric.

It is fairly straightforward to verify the topological relations (10.4.38)– (10.4.40) directly from the definitions of the cycles, thus providing a non–trivial check of the gauge theory calculation above. Let us first recall that S_1, S_2 are the two copies of S^2 in the base B at $y = y_1$, $y = y_2$, respectively, and that C_1 is a copy of the fibre S^2 in B at fixed θ and ϕ. By definition, taking the α circle bundle over these submanifolds gives the 3–cycles $\Sigma[Y]$, $-\Sigma[Z]$ and $-\Sigma[U]$, respectively[4]. Recall now from [63] that

$$S_1 - S_2 = 2C_1 \qquad\qquad (10.4.42)$$

holds as a homology relation in B. Thus taking the α circle bundle over this gives (10.4.38).

Using (10.4.37) and (10.4.38) one may now show that the left hand sides of (10.4.39) and (10.4.40) are given by

$$
\begin{aligned}
p\Sigma[Y] + (p-q)\Sigma[U] &= \frac{1}{2}\left((p+q)\Sigma[Y] - (p-q)\Sigma[Z]\right) \qquad (10.4.43)\\
&= -\left(p\Sigma[U] + q\Sigma[V] + (p-q)\Sigma[Z]\right) .
\end{aligned}
$$

Consider the quotient by $U(1)_\alpha$. As a homology relation in B we have

$$
\begin{aligned}
\tfrac{1}{2}\left((p+q)\Sigma[Y] - (p-q)\Sigma[Z]\right)/U(1)_\alpha &= \tfrac{1}{2}\left((p+q)S_1 + (p-q)S_2\right)\\
&= pC_2 + qC_1
\end{aligned}
\qquad (10.4.44)
$$

where recall [63] that by definition

$$S_1 + S_2 = 2C_2 \qquad\qquad (10.4.45)$$

---

[4]For further discussion of the topology the reader might consult [134].

and C_1 and C_2 are the canonical generators of the two two–cycles in $B \cong S^2 \times S^2$. Thus we must show that the $U(1)_\alpha$ bundle over $pC_2 + qC_1$ is the trivial 3–cycle in $Y^{p,q}$.

To see this, we begin by noting that $\pi^* c_1$, the pull–back of the first Chern class of the $U(1)_\alpha$ bundle to the total space of $Y^{p,q}$, is trivial as a cohomology class. Here $\pi : Y^{p,q} \to B$ is the projection. This is a standard fact, and can be seen in a number of different ways. For example, the one–form $(d\alpha + A)/2\pi\ell$ is globally defined on $Y^{p,q}$, where here $dA/2\pi\ell$ is a representative for c_1 and α/ℓ is a periodic coordinate on the α circle direction with period 2π. The essential point is that a gauge transformation in α is cancelled by the corresponding gauge transformation in A, thus giving a globally well–defined one–form on the total space – the so–called global angular form. In particular, we note that the exterior derivative of this one–form, which represents the pull–back of c_1, is exact.

To get to the desired homology relation, we simply apply Poincaré duality to the above. Since by definition $c_1 = p\sigma_1 + q\sigma_2$, where $\int_{C_i} \sigma_j = \delta_{ij}$ for each $i, j = 1, 2$, the Poincaré dual to c_1 in B is $pC_2 + qC_1$. Following through

$$H_2(B; \mathbb{Z}) \cong H^2(B; \mathbb{Z}) \xrightarrow{\pi^*} H^2(Y^{p,q}; \mathbb{Z}) \cong H_3(Y^{p,q}; \mathbb{Z}) \qquad (10.4.46)$$

then maps the two–cycle $pC_2 + qC_1$ in B to the 3–cycle in $Y^{p,q}$ which is simply the total space of the α circle bundle over this. As we've just explained, this image is zero.

10.5 Conclusions

The results presented in this chapter change the *status quo* in AdS/CFT. Until recently, the only explicitly known non–trivial Sasaki–Einstein metric in dimension five was $T^{1,1}$, whose dual superconformal field theory – a rather simple quiver gauge theory – was given by Klebanov and Witten [121]. We now have an infinite number of explicit toric Sasaki–Einstein five–manifolds [63], their associated toric diagrams

[134], and, from the results of this chapter, we also have the whole infinite family of dual quiver gauge theories. This is remarkable.

We have applied the technique of a–maximization [102] to this infinite family of gauge theories to obtain the exact R–charges of the fields at the IR fixed point. As pointed out in [102], since one is maximizing a cubic function with rational coefficients, the charges are generically quadratic irrational numbers, rather than rational numbers, and indeed this is typically true for the field theories presented here. There are also infinite numbers of theories where the R–charges are rational, namely the $Y^{p,q}$ quivers with $4p^2 - 3q^2$ an integer square. The central charges of these theories, computed using field theory techniques, precisely match with the volumes computed using the explicit metrics found in [63]. Furthermore, the R–charges of the gauge–invariant baryonic operators remarkably match the R–charges computed geometrically as volumes of supersymmetric cycles in the $Y^{p,q}$ geometries.

In order to have a more complete picture it would be interesting to determine the moduli space of vacua of the $Y^{p,q}$ gauge theories, and reproduce the algebro–geometric results of [134]. In fact, it is possible to do so using a novel procedure involving dimers that is the subject of Chapter 11.

Clearly this work opens the door to very interesting applications, and generalizations, in many different directions. First let us note that the construction of the Sasaki–Einstein metrics in [63] was immediately generalised to all (odd) dimensions in [66]. In particular, in dimension seven there are similar (p, q) families of Sasaki–Einstein metrics which are based on any positive Kähler–Einstein metric in dimension four. These are classified, and consist of $\mathbb{C}P^2$, $S^2 \times S^2$ and the del Pezzo surfaces $dP_3, \ldots, dP_8$. These will therefore serve as supersymmetric M–theory backgrounds of the form $AdS_4 \times Y_7$, which are expected to be dual to $\mathcal{N} = 2$ superconformal field theories arising on M2–branes that probe the corresponding Calabi–Yau four–fold singularities. When the Kähler–Einstein is toric, the Calabi–Yau singularities are again toric. It would be interesting to try to develop methods to analyse the gauge theory duals of these Sasaki–Einstein manifolds.

Let us also recall that the entire family of solutions explored in this chapter has a

dual description in M–theory, where it uplifts to supersymmetric $AdS_5 \times M_6$ solutions, with M_6 a complex S^2 bundle over $T^2 \times S^2$ [65]. However, there are many more solutions presented in [65], with M_6 replaced by more general manifolds. It will be very interesting to investigate if, guided by our results, one could explicitly construct the dual four–dimensional superconformal field theories for these also. If so, this could shed considerable light on the corresponding M5–brane theory, it least in a conformal regime.

Another interesting avenue of research is to understand what the geometric dual of a–maximization is. It is remarkable that such a simple field theory calculation reproduces not only the volumes of the metrics, but also the volumes of supersymmetric cycles. This geometric procedure has recently been constructed in [133].

Chapter 11

Brane Dimers and Quiver Gauge Theories

In this chapter we describe a technique which enables one to quickly compute an infinite number of toric geometries and their dual quiver gauge theories. The central object in this construction is a "brane tiling," which is a collection of D5-branes ending on an NS5-brane wrapping a holomorphic curve that can be represented as a periodic tiling of the plane. This construction solves the longstanding problem of computing superpotentials for D-branes probing a singular non-compact toric Calabi-Yau manifold, and overcomes many difficulties which were encountered in previous work. The brane tilings give the largest class of $\mathcal{N} = 1$ quiver gauge theories yet studied. A central feature of this work is the relation of these tilings to dimer constructions previously studied in a variety of contexts. We do many examples of computations with dimers, which give new results as well as confirm previous computations. Using our methods we explicitly derive the moduli space of the entire $Y^{p,q}$ family of quiver theories, verifying that they correspond to the appropriate geometries. Our results may be interpreted as a generalization of the McKay correspondence to non-compact 3-dimensional toric Calabi-Yau manifolds. The material in this chapter is based on [58].

11.1 Introduction

Shortly after the discovery of the importance of D-branes in string theory, it became clear that they provide a deep connection between algebra and geometry. This is realized in string theory in the following way: the D-brane, a physical object in spacetime, probes the geometry in which it lives, and the properties of spacetime fields are reflected in its worldvolume gauge theory. On the other hand, the D-brane has fundamental strings ending on it, thus giving rise to gauge quantum numbers which enumerate the possible ways strings can end on the brane when it is embedded in the given singular geometry. This fact leads to a pattern of algebraic relations, which are conveniently encoded in terms of algebraic quantities like Dynkin diagrams and, more generally, quiver gauge theories.

One simple example is given by a collection of N parallel D-branes; these have fundamental strings stretching between them and are in one-to-one correspondence with Dynkin diagrams of type A_{N-1}. Branes are mapped to nodes in the Dynkin diagrams and fundamental strings are mapped to lines. Placing this configuration on a circle leads to an affine Dynkin diagram $\hat{A}_{N-1}$, where the imaginary root is mapped to a fundamental string encircling the compact direction. Many more examples of this type lead to a beautiful relationship between branes and Lie algebras.

When D-branes in Type II string theory are placed on an ALE singularity of ADE type, the gauge theory living on them is encoded by an affine ADE Dynkin diagram. Here, fractional branes are mapped to nodes in the Dynkin diagram while strings stretching between the fractional branes are mapped to lines in the Dynkin diagram. The gauge theory living on the branes has 8 supercharges, since the ALE singularity breaks one half of the supersymmetry while the D-branes break a further half. With this amount of supersymmetry ($\mathcal{N} = 2$ in four dimensions), it is enough to specify the gauge group and the matter content in order to fix the Lagrangian of the theory uniquely. As above, we see that this gauge theory also realizes the relationship between algebra and geometry: on the algebra side, we have the Dynkin diagram, and on the geometry side there is a moduli space of vacua which is the ADE

type singularity. This connection between the Lie algebras of affine Dynkin diagrams and the geometry of ALE spaces is known as the McKay correspondence [136]. This relation was first derived in the mathematics literature and later – with the help of D-branes – became an important relation in string theory.

The McKay correspondence can be realized in other ways in string theory. One example which will be important to us in this chapter is the configuration of NS5-branes and D-branes stretching between them which was studied in [86]. A collection of N NS5-branes with D-branes stretching between them results in a gauge theory on the D-branes which turns out to be encoded by an A_{N-1} Dynkin diagram. Here, NS5-branes are mapped to lines while D-branes stretching between NS5-branes are mapped to nodes in the quiver gauge theory. Putting this configuration on a circle leads to an affine version of this correspondence $\hat{A}_{N-1}$; the imaginary root now corresponds to a D-brane which wraps the circle. This correspondence is very similar to the D-brane picture which was presented above and indeed, using a chain of S- and T-dualities, one can get from one configuration of branes to the other, while keeping the algebraic structure the same. Furthermore, the gauge theory living on a D-brane stretched between NS5-branes is very similar to the gauge theory living on a D-brane that probes an A_{N-1} singularity. Indeed, as first observed in [145], the collection of N NS5-branes on a circle is T-dual to an ALE singularity of type A_{N-1} with one circular direction. A detailed study of this correspondence was performed in [112].

Many attempts at generalizing the McKay correspondence from a 2 complex dimensional space to a 3 complex dimensional space have been made in the literature. From the point of view of branes in string theory it is natural to extend the 2-dimensional correspondence stated above from D-branes probing a 2-dimensional singular manifold to a collection of D-branes probing a 3 dimensional singular Calabi-Yau (CY) manifold. A few qualitative features are different in this case. First, the supersymmetry of the gauge theory living on the D-brane is now reduced to 4 supercharges. This implies that gauge fields and matter fields are not enough to uniquely determine the Lagrangian of the theory, and one must also specify a superpotential which encodes the interactions between the matter fields.

This is an important observation: any attempt at stating the 3-dimensional McKay correspondence must incorporate the superpotential, which was uniquely constrained in the 2-dimensional case. Second, the matter multiplets in theories with 4 supercharges are chiral and therefore have a natural orientation. In the theories with 8 supercharges, for every chiral multiplet there is another chiral multiplet with an opposite orientation, transforming together in a hypermultiplet. Therefore, an overall orientation is not present in a theory with 8 supercharges. We conclude that the 3-dimensional McKay correspondence requires information about these orientations, absent in the 2-dimensional case.

Studying the first few examples for the 3-dimensional McKay correspondence (the simplest of which is the orbifold $\mathbb{C}^3/\mathbb{Z}_3$), it became clear that the objects which replace the Dynkin diagrams are quivers with oriented arrows [39]. For these objects, nodes represent gauge groups, oriented arrows between two nodes represent bifundamental chiral multiplets, and certain closed paths in the quiver (which represent gauge-invariant operators) represent terms in the superpotential. It is important to note that only a subset of all closed paths on the quiver appears in the superpotential, and finding which particular subset is selected for the quiver associated to a given toric singularity is a difficult task. This difficulty will be greatly simplified with the results presented in this chapter.

In previous chapters, we have discussed in detail the construction of quivers via string theory. Let us make a briefly summary of what is known about them in order to put the forthcoming discussion into context. The first known examples of quiver theories obtained from string theory were those dual to $\mathbb{C}^3/\Gamma$, where Γ is any discrete subgroup of $SU(3)$ [125, 79]. The most common examples of this type take $\Gamma = \mathbb{Z}_n$ or $\Gamma = \mathbb{Z}_n \times \mathbb{Z}_m$. These theories are easy to construct, since it is straightforward to write down an orbifold action on the coordinates of $\mathbb{C}^3$. If $|\Gamma| = k$, then there are k nodes in the dual quiver and a bifundamental for each orbifold action on $\mathbb{C}^3$ that connects different regions of the covering space. These orbifold theories may be described torically in a straightforward manner. It was then realized that partial resolution of these orbifold spaces corresponds to Higgsing the quivers; in this manner, people

302

were able to obtain many different quiver theories and their dual toric geometries [45, 46, 12].

It was not long before a general algorithm for deriving toric data from a given quiver was found; this procedure is usually called "The Forward Algorithm" [45]. Although the procedure is well-understood, it is computationally prohibitive for quivers with more than approximately ten nodes. As discussed in detail in Chapter 5, the Forward Algorithm, in addition to providing the toric data for a given quiver theory, also gives the relative **multiplicities** of the gauged linear sigma model (GLSM) fields in the related sigma model [43]. However, the same problem applies here as well: the toric diagrams and their associated multiplicities are difficult to derive for large quivers.

Recently, there has been much progress in the arena of gauge theories dual to toric geometries. Gauntlett, Martelli, Sparks, and Waldram [63] found an infinite class of Sasaki-Einstein (SE) metrics; previous to their work, only two explicit SE metrics were known. These metrics are denoted $Y^{p,q}$ and depend only on two integers p and q, where $0 < q < p$. In related work, Martelli and Sparks [134] found the toric descriptions of the $Y^{p,q}$ theories, and noted that some of these spaces were already familiar, although their metrics had not previously been known. One of the simplest examples is $Y^{2,1}$, which turns out to be the SE manifold which is the base of the complex cone over the first del Pezzo surface. More progress was made when the gauge theory duals of the $Y^{p,q}$ spaces were found [14], providing an infinite class of AdS/CFT dual pairs. This piece of work was the subject of Chapter 10. These theories have survived many nontrivial checks of the AdS/CFT correspondence, such as central charge and R-charge computations from volume calculations on the string side and a-maximization [102] on the gauge theory side. Inspired by these gauge theories, there have since been many new and startling checks of AdS/CFT, such as the construction of gravity duals for cascading RG flows [92]. Thus, there has been remarkable progress recently in the study of toric Calabi-Yau manifolds and their dual gauge theories; however, a general procedure for constructing the dual to a given CY is still unknown. In this work, we will shed some light on this problem.

One of the results of the present work is that the ingredients required to uniquely define an $\mathcal{N} = 1$ quiver gauge theory – gauge groups, chiral matter fields, and superpotential terms – may be represented in terms of nodes, lines and faces of a *single object*, which is the quiver redrawn as a planar graph on the torus (for the quiver theories corresponding to toric singularities). This point will be crucial in the construction of the quiver gauge theory using dimers, as will be discussed in detail in section 11.3.

One may also ask how these theories may be constructed in string theory by using branes, as explained above for the case of theories with 8 supercharges. A key observation is that if a collection of m NS5-branes is T-dual to an orbifold $\mathbb{C}^3/\mathbb{Z}_m$, then a collection of m NS5-branes intersecting with n NS5'-branes with both sets of NS5-branes sharing 3+1 space-time directions, is equivalent under two T-dualities to an orbifold singularity of type $\mathbb{C}^3/(\mathbb{Z}_m \times \mathbb{Z}_n)$. When D3-brane probes are added over the orbifold, they are mapped to D5-branes suspended between the NS5-branes on the T-dual configuration. Indeed, a study of these theories using the Brane Box Models of [87] was done in [84]. Another important development in the brane construction of quiver gauge theories with 4 supercharges was made in [2] where it was realized that the quiver gauge theories which live on D-branes probing the conifold and its various orbifolds are constructed by "Brane Diamonds." Brane diamonds were also applied to the study of gauge theories for D-branes probing complex cones over del Pezzo surfaces [48].

In the present chapter, we consider a more intricate configuration of branes. First, we take an NS5-brane which extends in the 0123 directions and wraps a complex curve $f(x, y) = 0$, where x and y are holomorphic coordinates in the 45 and 67 directions, respectively. We typically depict this by drawing this curve in the 4 and 6 directions, where it looks like a network that separates the plane into different regions, i.e. a tiling. We do not explicitly write down the equation for this curve, but do note that a requirement of our construction is that the tiling of the 46 plane is such that all polygons have an even number of sides. The 4 and 6 directions are compact, forming a torus, and we take the D5 branes to be finite in these directions (but extended

in the 0123 directions) and bounded by the curve which is wrapped by the NS5-brane. As above, this brane configuration results in a quiver gauge theory living on the D5-branes. The rules for computing this quiver theory turn out to follow similar guidelines to those in the constructions mentioned above: gauge groups are faces of the intersecting brane configuration, bifundamental fields arise across NS5-branes which are lines in the brane configuration, and superpotential terms show up as vertices.

It is important to note that the Brane Box Models were formulated using periodic square graphs for encoding the rules of the quiver gauge theory, but it will become clear in this chapter that the correct objects to use to recover that construction are hexagonal graphs, and in fact the brane boxes are recovered in a degenerate limit in which two opposite edges of the hexagons are reduced to zero length.

We observe that in both the brane box and diamond constructions, the brane configurations are related to the quiver gauge theory in the following sense: faces in the brane configuration are mapped to nodes in the quiver, lines are mapped to orthogonal lines and nodes are mapped to faces. The statement of this duality will be formulated precisely in Section 11.2.1, and will prove to be a very powerful tool in generalizing these constructions to a larger class of quiver gauge theories (those whose moduli space describe non-compact toric CY 3-folds).

Thus, we find that it is possible to encode **all the data** necessary to uniquely specify an $\mathcal{N} = 1$ quiver gauge theory in a tiling of the plane. The dual graph is then essentially the quiver theory, written in such a way as to encode the superpotential data as well. As we will now see, however, this tiling encodes much more than just the quiver theory – it also encodes the dual toric geometry! The central object for deriving the toric geometry is the **dimer**, which we now explain.

Since we have taken our brane tiling to consist of polygons with an even number of sides, and all cycles of our periodic graph have even length, it is always possible to color the nodes of the graph with two different colors (say, black and white) in such a way that any given black node is adjacent only to white nodes, and vice versa. Such graphs are well-known in condensed matter physics, where the links between black

nodes and white nodes are called dimers; one may think of a substance formed out of two different type of atoms (e.g. a salt), where a dimer is just an edge of the lattice with a different atom at each end. One can allow bonds between adjacent atoms to break and then re-form in a possibly different configuration; the statistical mechanics of such systems has been extensively studied.

Recently, dimers have shown up in the context of string theory on toric Calabi-Yau manifolds. In [144], the authors propose a relationship between the statistical mechanics of dimer models and topological strings on a toric non-compact Calabi-Yau. The relationship between toric geometry and dimer models was developed further in [82], where it was shown how it is possible to obtain toric diagrams and GLSM multiplicities via dimer techniques. In general, however, we expect that one should be able to derive the quiver gauge theory dual to any given toric geometry. This is the purpose of the present work, to describe how dimer technology may be used to efficiently derive both the quiver theory and the toric geometry, thus giving a fast and straightforward way of deriving AdS/CFT dual pairs.

We can now state that the 3-dimensional McKay correspondence is represented in string theory as a physical brane configuration of an NS5-brane spanning four dimensions and wrapping an holomorphic curve on four other dimensions, and D5-branes. Alternatively, we can use a twice T-dual (along the 4 and 6 directions) description: the McKay correspondence is realized by the quiver gauge theory that lives on D-branes probing toric CY 3-folds. As a byproduct of these two equivalent representations we can argue that it is possible to find NS5-brane configurations that are twice T-dual to these toric singular CY manifolds. One removes the D-branes and ends up with NS5-branes on one side and singular geometries on the other.

The outline of this chapter is as follows. In Section 11.2, we summarize the basic features of our construction, and establish the relationship between brane tilings and quiver gauge theories. We explain the brane construction that leads to the quiver theory, and detail how it is possible to read off all relevant data about the quiver theory from the brane tiling. We derive an interesting identity for which the brane tiling perspective provides a simple proof. We illustrate these ideas with a simple

example, Model I of del Pezzo 3. Additionally, we describe a new object, the "periodic quiver," which is the dual graph to the brane tiling and neatly summarizes the quiver and superpotential data for a given gauge theory.

In Section 11.3, we describe the utility of the dimer model and review the relationship between dimers and toric geometries. We begin by summarizing relevant facts about dimer models which we will use repeatedly throughout the chapter. The central object in any computation is the Kasteleyn matrix, which is a weighted adjacency matrix that is easy to derive. We do a simple computation as an example, which illustrates the basic techniques required to compute the toric geometry related to any given brane tiling.

Section 11.4 provides the relationship between dimers and fields in the related gauged linear sigma model. We review the relationship of toric geometries to GLSMs, and describe how the dimer model allows one to compute multiplicities of GLSM. These techniques are illustrated with an example, that of the Suspended Pinch Point (SPP) [138].

Section 11.5 briefly describes how massive fields arise via the brane tiling description, and comments on the process of integrating out these fields from the perspective of both the brane tiling and the Kasteleyn matrix. Section 11.6 talks about Seiberg duality from three complementary perspectives: the brane tiling, the quiver, and the Kasteleyn matrix. We illustrate these viewpoints with F_0 as an example.

Section 11.7 gives two descriptions of the process of partial resolution of orbifold singularities, both from the brane tiling and quiver perspectives. In Section 11.8, we describe how one may construct brane tilings which produce identical quivers but different superpotentials; this is illustrated via the quiver from Model II of dP_3. In Section 11.9, we present many different examples of brane tilings, and compute the Kasteleyn matrix and dual toric geometry in each example. These computations duplicate known results, as well as generate new ones. Most notably, we find that toric diagrams with specified GLSM multiplicities are not in one-to-one correspondence with toric phases of quiver gauge theories, as had previously been suspected. This computation is done for Pseudo del Pezzo 5, where we find two toric phases with

identical GLSM multiplicities. Finally, in Section 11.10, we briefly conclude and present some suggestions for further study.

11.2   Brane tilings and quivers

In this section we introduce the concept of **brane tilings**. They are Type IIB configurations of NS5 and D5-branes that generalize the brane box [84] and brane diamond [2] constructions and are dual to gauge theories on D3-branes transverse to arbitrary **toric** singularities. From now on, we proceed assuming that the dual geometry is toric and introduce the relevant brane configurations. The reason for the requirement that the corresponding singularities are toric will become clear in this and subsequent sections.

In our construction, the NS5-brane extends in the 0123 directions and wraps a holomorphic curve embedded in the 4567 directions (the 46 directions are taken to be compact). D5-branes span the 012346 directions and stretch inside the holes in the NS5 skeleton like soap bubbles. The D5-branes are bounded by NS5-branes in the 46 directions, leading to a 3+1 dimensional theory in their world-volume at low energies. The branes break supersymmetry to 1/8 of the original value, leading to 4 supercharges, i.e. $\mathcal{N} = 1$ in four dimensions. In principle, there can be a different number of D5-branes N_I in each stack. This would lead to a product gauge group $\prod_I SU(N_I)$. Strings stretching between D5-branes in a given stack give rise to the gauge bosons of $SU(N_I)$ while strings connecting D5-branes in adjacent stacks I and J correspond to states in the bifundamental of $SU(N_I) \times SU(N_J)$. We will restrict ourselves to the case $N_I = N$ for all I. Theories satisfying this restriction on the ranks were dubbed **toric phases** in [43], We should emphasize though, that there are quivers that are dual to toric geometries but that do not satisfy this condition.

It is worthwhile here to note a few properties of NS5-branes that are relevant for this construction. As is well-known, an NS5-brane backreacts on its surrounding spacetime to create a throat geometry. When we have two sets of D5-branes ending on different sides of the NS5-brane, the throat separates the two sets of branes. The

D-branes may then only interact via fundamental strings stretching between them; these are the bifundamentals in the quiver gauge theory. Initially it might seem like there are two conjugate bifundamentals which pair up to form hypermultiplets, but in this case, where the NS5-brane wraps a holomorphic curve, the orientation of the NS5-brane projects one of these out of the massless spectrum [42]. Thus the resulting quiver theory will generically have arrows pointing in only one direction (it is easy to get quivers with bidirectional arrows as well, but these will instead come from strings stretching across different NS5-branes rather than both orientations across the same NS5-brane).

The important physics is captured by drawing the brane tiling in the 46 plane. The NS5-branes wrap a holomorphic curve, the real section of which is a graph G in the 46 plane, which we will later show must be **bipartite**. A graph is bipartite when its nodes can be colored in white and black, such that edges only connect black nodes to white nodes and vice versa. By construction, G is $\mathbb{Z}^2$-periodic under translations in the 46 plane since these directions are taken to be compact.

We will see in the next section that the existence of G is associated to the duality between quiver gauge theories and dimer models. Given a brane tiling, it is straightforward to derive its associated quiver gauge theory. The brane tiling encodes both the quiver diagram and the superpotential, which can be constructed using the following dictionary (see the following section):

Brane tiling	String theory	Gauge theory
$2n$-sided face	D5-branes	Gauge group with n flavors
Edge between two polygons I and J	String stretched between D5-branes through NS5 brane.	Bifundamental chiral multiplet between gauge groups I and J; We orient the arrow such that the white node is to the right.
k-valent vertex	Region where k strings interact locally.	Interaction between k chiral multiplets, i.e. order k term in the superpotential. The signs for the superpotential terms are assigned such that white and black nodes correspond to plus and minus signs respectively.

Conversely, we can use this set of rules to construct a brane tiling from a given quiver with a superpotential. In the following section we will make this correspondence precise.

Several interesting consequences follow naturally from this simple set of rules. Some of them are well known, while others are new. The fact that the graphs under consideration are bipartite implies that each edge has a black and a white endpoint. Edges correspond to bifundamental fields while nodes indicate superpotential terms, with their sign determined by the color of the node. Thus, we conclude that each bifundamental field appears exactly twice in the superpotential, once with a plus and once with a minus sign. We refer to this as the **toric condition** and it follows from the underlying geometry being an affine toric variety [43].

The total number of nodes inside a unit cell is even (there are equal numbers of black and white nodes). Thus, we conclude that the total number of terms in the superpotential of a quiver theory for a toric singularity is even. Although this condition is reminiscent of the toric condition, it is different. It is comforting to see that it is satisfied by all the examples in the literature (orbifolds, del Pezzos, $\mathbf{F_0}$,

pseudo-del Pezzos, SPP, $Y^{p,q}$, $X^{p,q}$, etc).

Bidirectional arrows and even adjoint fields in the quiver can be simply implemented in this construction, by suitably choosing the adjacency of polygons. We will present an example containing both situations in section 11.4.1.

Let us define

Brane tiling	Gauge theory
F: number of faces	N_g: number of gauge groups
E: number of edges	N_f: number of fields
N: number of nodes	N_W: number of superpotential terms

According to the dictionary above, $F = N_g$, $E = N_f$ and $N = N_W$. Applying Euler's formula to a unit cell in the graph, we see that $F + N - E = 2g - 2 = 0$ (where we have used that the graph lives on the torus), which translates into the following identity for quiver theories[1]:

$$N_g + N_W - N_f = 0. \tag{11.2.1}$$

The geometric intuition we gain when using brane tilings make the derivation of this remarkable identity straightforward.

It is interesting to point out here that the Euler formula has another interpretation. Let us assign an R-charge to each bifundamental field in the quiver, i.e. to each edge in the brane tiling. At the IR superconformal fixed point, we know that each term in the superpotential must satisfy

$$\sum_{i \in edges\ around\ node} R_i = 2 \qquad \text{for each node} \tag{11.2.2}$$

where the sum is over all edges surrounding a given node. We can sum over all the nodes in the tiling, each of which corresponds to a superpotential term, to get $\sum_{edges,nodes} R = 2N$. Additionally, the beta function for each gauge coupling must

---

[1]This identity was derived empirically with Barak Kol using the known examples. The brane tiling gives a proof for a generic $\mathcal{N} = 1$ toric theory.

vanish,

$$2 + \sum_{i \in edges\ around\ face} (R_i - 1) = 0 \qquad \text{for each face} \qquad (11.2.3)$$

where the sum is over all edges surrounding a given face. But we can now sum this over all the faces in the tiling to get $2F + 2N - 2E = 0$, where we have used the fact that the double sum hits every edge twice, and (11.2.2). The sums $\sum_{edges,nodes} R$ and $\sum_{edges,faces} R$ are equal because each double sum has the R-charge of each bifundamental contributing twice. Thus we see that the requirements that the superpotential have $R(W) = 2$ and the beta functions vanish (i.e. that the theory is superconformal in the IR) imply that the Euler characteristic of the tiling is zero. This condition is the analog of a similar condition for superconformal quivers discussed in [103, 15]. Conversely we see that, in the case in which the ranks of all gauge groups are equal, the construction of tilings over Riemann surfaces different from a torus leads to non-conformal gauge theories.

Let us illustrate the concepts introduced in this section with a simple example, one of the toric phases of dP_3, denoted Model I in [43]. Its corresponding quiver diagram is presented in Figure 11-1 and its superpotential is

$$\begin{aligned} W &= X_{12}X_{23}X_{34}X_{45}X_{56}X_{61} - (X_{23}X_{35}X_{56}X_{62} + X_{13}X_{34}X_{46}X_{61} + X_{12}X_{24}X_{45}X_{51}) \\ &\quad + (X_{13}X_{35}X_{51} + X_{24}X_{46}X_{62}). \end{aligned}$$

$$(11.2.4)$$

The quiver diagram has 6 gauge groups and 12 bifundamental fields. Hence, the brane configuration will have 6 faces and 12 edges in a unit cell. The superpotential (11.2.4) has 1 order six, 3 quartic and 2 cubic terms. According to (11.2.1) we thus have 1 6-valent, 3 4-valent and 2 3-valent nodes. The final brane tiling is shown in Figure 11-1.

11.2.1 Unification of quiver and superpotential data

An $\mathcal{N} = 1$ quiver gauge theory is described by the following data: a directed graph representing the gauge groups and matter content, and a set of closed paths on
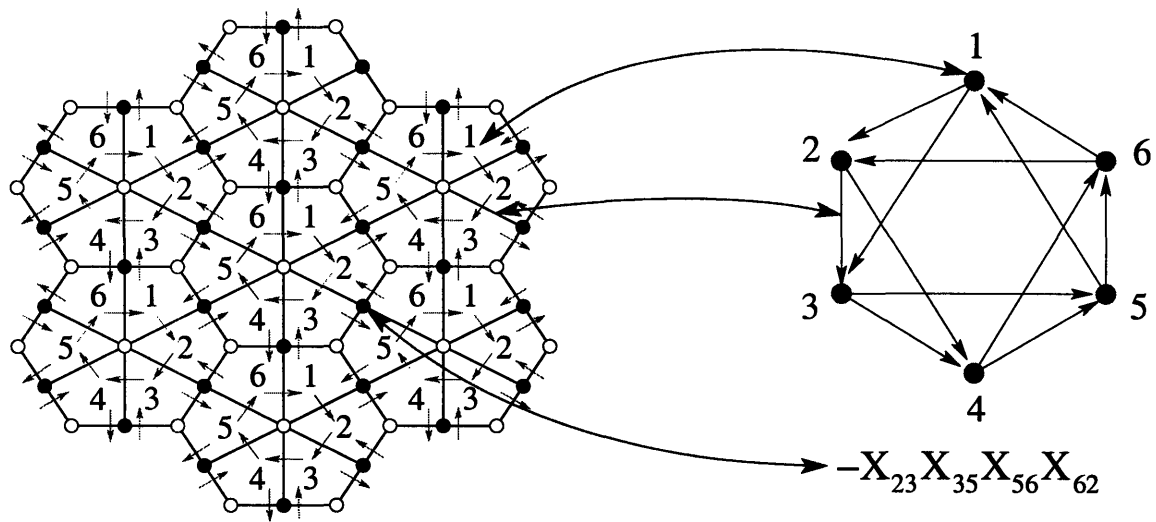
Figure 11-1: A finite region in the infinite brane tiling and quiver diagram for Model I of dP_3. We indicate the correspondence between: gauge groups $\leftrightarrow$ faces, bifundamental fields $\leftrightarrow$ edges and superpotential terms $\leftrightarrow$ nodes.

the graph representing the gauge invariant interactions in the superpotential. An equivalent way to characterise this data is to view it as defining a CW-complex; in other words, we may take the superpotential terms to define the 2-dimensional faces of the complex bounded by a given set of edges and vertices (the 1-skeleton and 0-skeleton of the complex). Thus, the quiver and superpotential may be combined into a single object, a planar tiling of a 2-dimensional (possibly singular) space. Toric quiver theories, as we will see, are defined by planar tilings of the 2-dimensional torus.

This is a key observation. Given the presentation of the quiver data (quiver graph and superpotential) as a planar graph tiling the torus, the bipartite graph appearing in the dimer model (the brane construction of the previous section) is nothing but the planar dual of this graph! Moreover, as we have argued, this dual presentation of the quiver data is *physical*, in that it appears directly in string theory as a way to construct the 3 + 1-dimensional quiver gauge theory in terms of intersecting NS5 and D5-branes. The logical flow of these ideas is shown in Figure 11-2. Some of the concepts in this diagram have not yet been discussed in this chapter, but will be addressed shortly.

Let us see how the properties of the brane tiling arise from those of the quiver
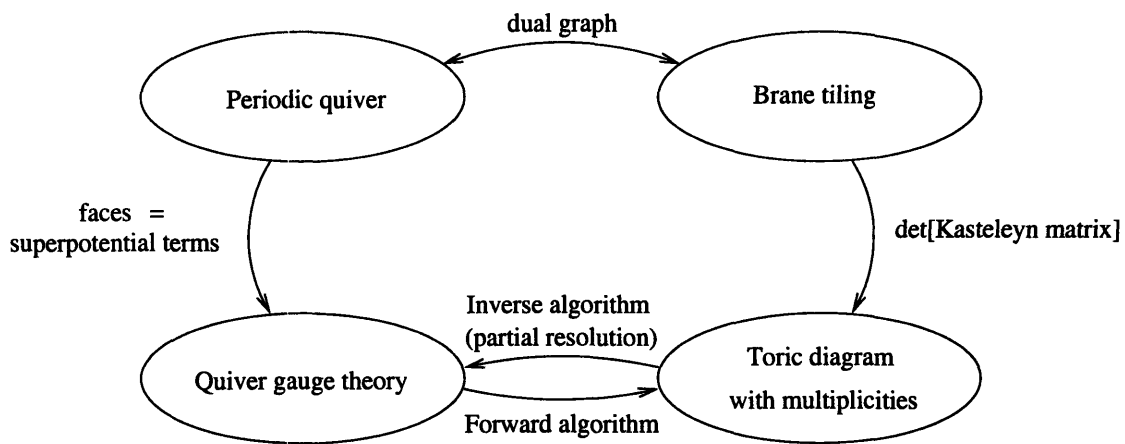
Figure 11-2: The logical flowchart.

theory. We will show that we can think of the superpotential and quiver together as a tiling of a two-dimensional surface, where bifundamentals are edges, superpotential terms are faces, and gauge groups are nodes. We refer to this as the "periodic quiver" representation. The toric condition, which states that each matter field appears in precisely two superpotential terms of opposite sign, means that the faces all glue together in pairs along the common edges. Since every field is represented exactly twice in the superpotential, this tiling has no boundaries. Thus, the quiver and its superpotential may be combined to give a tiling of a Riemann surface without boundary; this periodic quiver gives a discretization of the torus. Since the Euler characteristic of the quiver is zero for toric theories (as discussed in the previous section), the quiver and superpotential data are equivalent to a planar tiling of the two-dimensional torus. See Figure 5 of [45] for an early example of a periodic quiver.

This tiling has additional structure. The toric condition implies that adjacent faces of the tiling may be labelled with opposite signs according to the sign of the corresponding term in the superpotential. Thus, under the planar duality the *vertices* of the dual graph may be labelled with opposite signs; this is the bipartite property of the dimer model. Since the periodic quiver is defined on the torus, the dual bipartite graph also lives on the torus.

Anomaly cancellation of the quiver gauge theory is represented by the balancing of all incoming and outgoing arrows at every node of the quiver. In the dual graph,

314

bipartiteness means that the edges carry a natural orientation (e.g. from black to white). This induces an orientation for the dual edges, which transition between adjacent faces of the brane tiling (vertices of the planar quiver). For example, these dual arrows point in a direction such that, looking at an arrow from its tail to its head, the black node is to the left and the white node is to the right (this is just a convention and the opposite choice is equivalent by charge conjugation). Arrows around a face in G alternate between incoming and outcoming arrows of the quiver; this is how anomaly cancellation is manifested in the brane tiling picture. Alternatively, we can say that arrows "circulate" clockwise around white nodes and counterclockwise around black nodes.
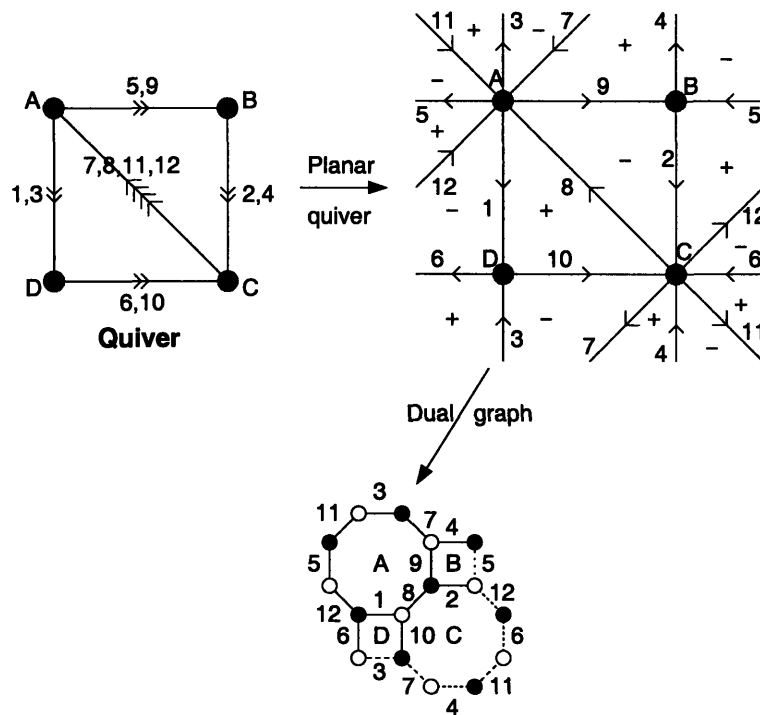
Figure 11-3: The quiver gauge theory associated to one of the toric phases of the cone over F_0. In the upper right the quiver and superpotential (11.2.6) are combined into the periodic quiver defined on T^2. The terms in the superpotential bound the faces of the periodic quiver, and the signs are indicated and have the dual-bipartite property that all adjacent faces have opposite sign. To get the bottom picture, we take the planar dual graph and indicate the bipartite property of this graph by coloring the vertices alternately. The dashed lines indicate edges of the graph that are duplicated by the periodicity of the torus. This defines the brane tiling associated to this $\mathcal{N} = 1$ gauge theory.

Figure 11-3 shows an example of the periodic quiver construction for the quiver gauge theory associated to one of the toric phases of the Calabi-Yau cone over F_0. The superpotential for this theory is [46]

$$W = X_1 X_{10} X_8 - X_3 X_{10} X_7 - X_2 X_8 X_9 - X_1 X_6 X_{12} \qquad (11.2.5)$$
$$+ X_3 X_6 X_{11} + X_4 X_7 X_9 + X_2 X_{12} X_5 - X_4 X_{11} X_5.$$

11.3 Dimer model technology

Given a bipartite graph, a problem of interest to physicists and mathematicians is to count the number of perfect matchings of the graph. A **perfect matching** of a bipartite graph is a subset of edges ("dimers") such that every vertex in the graph is an endpoint of precisely one edge in the set. A **dimer model** is the statistical mechanics of such a system, i.e. of random perfect matchings of the graph with assigned edge weights. As discussed in the previous section, we are interested in dimer models associated to doubly-periodic graphs, i.e. graphs defined on the torus T^2. We will now review some basic properties of dimers; for additional review, see [82, 117].

Many important properties of the dimer model are governed by the **Kasteleyn matrix** $K(z, w)$, a weighted, signed adjacency matrix of the graph with (in our conventions) the rows indexed by the white nodes, and the columns indexed by the black nodes. It is constructed as follows:

To each edge in the graph, multiply the edge weight by ± 1 so that around every face of the graph the product of the edge weights over edges bounding the face has the following sign

$$\mathrm{sign}\Big(\prod_i e_i\Big) = \begin{cases} +1 & \mathit{if}\ (\#\ \mathrm{edges}) = 2 \mod 4 \\ -1 & \mathit{if}\ (\#\ \mathrm{edges}) = 0 \mod 4 \end{cases} \qquad (11.3.6)$$

It is always possible to arrange this [113].

The coloring of vertices in the graph induces an orientation to the edges, for

example the orientation "black" to "white". This orientation corresponds to the orientation of the chiral multiplets of the quiver theory, as discussed in the previous section. Now construct paths γ_w, γ_z in the dual graph (i.e. the periodic quiver) that wind once around the $(0,1)$ and $(1,0)$ cycles of the torus, respectively. We will refer to these fundamental paths as **flux lines**. In terms of the periodic quiver, the paths γ pick out a subset of the chiral multiplets whose product is gauge-invariant and forms a closed path that winds around one of the fundamental cycles of the torus. For every such edge (chiral multiplet) in G crossed by γ, multiply the edge weight by a factor of w or $1/w$ (respectively z, $1/z$) according to the relative orientation of the edges in G crossed by γ.

The adjacency matrix of the graph G weighted by the above factors is the Kasteleyn matrix $K(z, w)$ of the graph. The determinant of this matrix $P(z, w) = \det K$ is a Laurent polynomial (i.e. negative powers may appear) called the characteristic polynomial of the dimer model

$$P(z, w) = \sum_{i,j} c_{ij} z^i w^j. \tag{11.3.7}$$

This polynomial provides the link between dimer models and toric geometry [82].

Given an arbitrary "reference" matching M_0 on the graph, for any matching M the difference $M - M_0$ defines a set of closed curves on the graph in T^2. This in turn defines a height function on the faces of the graph: when a path in the dual graph crosses a curve, the height is increased or decreased by 1 according to the orientation of the crossing. A different choice of reference matching M_0 shifts the height function by a constant. Thus, only differences in height are physically significant.

In terms of the height function, the characteristic polynomial takes the following form:

$$P(z, w) = z^{h_{x0}} w^{h_{y0}} \sum c_{h_x, h_y} (-1)^{h_x + h_y + h_x h_y} z^{h_x} w^{h_y} \tag{11.3.8}$$

where c_{h_x, h_y} are integer coefficients that count the number of perfect matchings corresponding to a height change (h_x, h_y) around the two fundamental cycles of the

torus.

The overall normalization of $P(z, w)$ is not physically meaningful: since the graph does not come with a prescribed embedding into the torus (only a choice of periodicity), the paths $\gamma_{z,w}$ winding around the primitive cycles of the torus may be taken to cross any edges en route. Different choices of paths γ multiply the characteristic polynomial by an overall power $z^i w^j$, and by an appropriate choice of path $P(z, w)$ can always be normalized to contain only non-negative powers of z and w.

The **Newton polygon** $N(P)$ is a convex polygon in $\mathbb{Z}^2$ generated by the set of integer exponents of the monomials in P. In [82], it was conjectured that the Newton polygon can be interpreted as the toric diagram associated to the moduli space of the quiver gauge theory, which by assumption is a non-compact toric Calabi-Yau 3-fold. In the following section, we will prove that the perfect matchings of the dimer model are in 1-1 correspondence with the fields of the gauged linear sigma model that describes the probed toric geometry.

The connection between dimer models and toric geometry was explored in [82]. In that paper the action of orbifolding the toric singularity was understood in terms of the dimer model: the orbifold action by $\mathbb{Z}_m \times \mathbb{Z}_n$ corresponds to enlarging the fundamental domain of the graph by $m \times n$ copies, and non-diagonal orbifold actions correspond to a choice of periodicity of the torus, i.e. an offset in how the neighboring domains are adjoined. Furthermore, results analogous to the Inverse Algorithm were developed for studying arbitrary toric singularities and their associated quiver theories. In this chapter we derive and significantly extend the results of [82], and place them into the context of string theory.

Let us illustrate how the computation of the Kasteleyn matrix and the toric diagram works for the case of Model I of dP_3. The brane configuration is shown in Figure 11-4a. The corresponding unit cell is presented in Figure 11-4b. As expected, it contains one valence 6, three valence 4 and two valence 3 nodes. It also contains twelve edges, corresponding to the twelve bifundamental fields in the quiver.

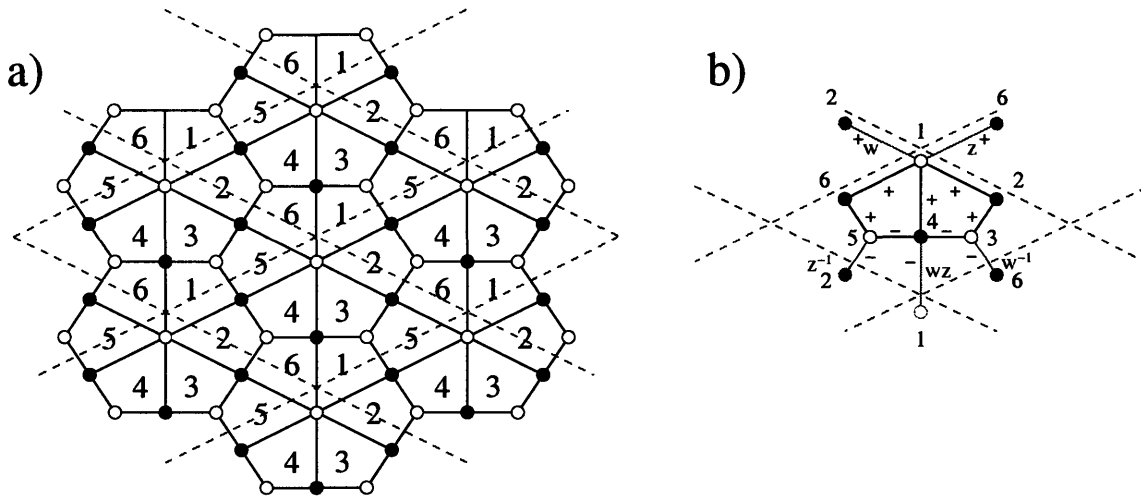From the unit cell, we derive the following Kasteleyn matrix

318

Figure 11-4: a) Brane tiling for Model I of dP_3 with flux lines indicated in red. b) Unit cell for Model I of dP_3. We show the edges connecting to images of the fundamental nodes in green. We also indicate the signs associated to each edge as well as the powers of w and z corresponding to crossing flux lines.

$$K = \begin{pmatrix} & 2 & 4 & 6 \\ \hline 1 & 1+w & 1-zw & 1+z \\ 3 & 1 & -1 & -w^{-1} \\ 5 & -z^{-1} & -1 & 1 \end{pmatrix}$$

(11.3.9)

We observe that it has twelve monomials, associated with the twelve bifundamental fields. This matrix leads to the characteristic polynomial

$$P(z,w) = w^{-1}z^{-1} - z^{-1} - w^{-1} - 6 - w - z + wz.$$

(11.3.10)

The toric data corresponding to this gauge theory can be read from this polynomial, and is shown in Figure 11-5.

The Kasteleyn matrix is a square matrix whose size is equal to half the total number of points in the unit cell. Thus, for a given toric quiver K is a $N_W/2 \times N_W/2$ matrix. This is remarkable, since this size can be very modest even for very complicated gauge theories. The simplicity of computing the toric data using this procedure should be contrasted with the difficulty of the Forward Algorithm.

This procedure has a profound impact on the study of quiver theories for arbi-
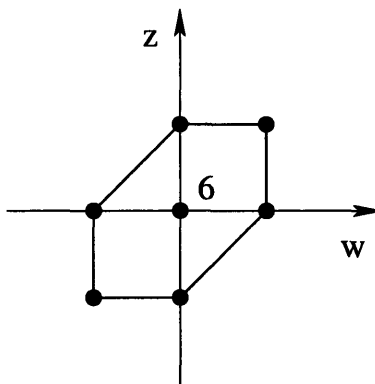
319

Figure 11-5: Toric diagram for Model I of dP_3 derived from the characteristic polynomial in (11.3.10).

trary toric singularities. Given a candidate quiver theory for D3-branes over some geometry, instead of running the lengthy Forward Algorithm, one simply constructs the associated brane tiling using the rules of Section 11.2 and computes the corresponding characteristic polynomial. We can thus refer to the determination of toric data from brane tilings as the **Fast Forward Algorithm**[2]. This simplification will become clear when we present explicit results for infinite families of arbitrarily large quivers in Sections 11.9.3.

11.4 An explicit correspondence between dimers and GLSMs

Following [82], we have argued in the previous section that the characteristic polynomial encodes the toric data of the probed geometry. We now explore the reason for this connection, establishing a correspondence between fields in the gauged linear sigma model description of the singularity and perfect matchings in the brane tiling.

Given a toric Calabi-Yau 3-fold, the principles of determining the gauge theory on the world-volume of a stack of D3-brane probes are well established. Conversely, the determination of the toric data of the singularity from the gauge theory is also clear. This procedure has been algorithmized in [45] and dubbed the **Forward Algo-**

---

[2]A name coined by Pavlos Kazakopoulous.

rithm. Nevertheless, although a general prescription exists, its applicability beyond the simplest cases is limited due to the computational complexity of the algorithm.

Let us review the main ideas underlying the Forward Algorithm (for a detailed description and explicit examples, we refer the reader to [45]). The starting point is a quiver with r $SU(N)$ gauge groups and bifundamentals X_i, $i = 1, \ldots, m$, together with a superpotential. The toric data that describes the probed geometry is computed using the following steps:

- Use F-term equations to express all bifundamental fields X_i in terms of $r + 2$ independent variables v_j. The v_j's can be simply equal to a subset of the bifundamentals. The connection between these variables and the original bifundamental fields is encoded in an $m \times (r + 2)$ matrix K (this matrix should not be confused with the Kasteleyn matrix; which of them we are talking about will be clear from the context), such that

$$X_i = \prod_j v_j^{K_{ij}}, \quad i = 1, 2, \ldots, m, \quad j = 1, 2, \ldots, r + 2. \tag{11.4.11}$$

Since the F-term equations take the form of a monomial equated to another monomial, it is clear that generically K_{ij} has negative entries (i.e. negative powers of the v_j can appear in the expressions for the X_i).

- In order to avoid the use of negative powers, a new set of variables p_α, $\alpha = 1, \ldots, c$, is introduced. The number c is not known *a priori* in this approach, and must be determined as part of the algorithm. We will later see that it corresponds to the number of perfect matchings of G, the periodic bipartite graph dual to the quiver.

- The reduction of the c p_α's to the $r + 2$ independent variables v_i is achieved by introducing a $U(1)^{c-(r+2)}$ gauge group. The action of this group is encoded in a $(c - r - 2) \times c$ charge matrix Q.

- The original $U(1)^{r-1}$ action (one of the r $U(1)$'s is redundant) determining the D-terms is recast in terms of the p_α by means of a $(r - 1) \times c$ charge matrix Q_D.

- Q and Q_D are combined in the total matrix of charges Q_t. The $U(1)$ actions of the symplectic quotient defining the toric variety correspond to a basis of linear relations among the vectors in the toric diagram. Thus, the toric diagram corresponds to the columns in a matrix G_t such that $G_t = (\ker Q_t)^T$.

At this stage, it is important to stress some points. The main difficulty in the Forward Algorithm is the computation of T, which is used to map the intermediate variables v_i to the GLSM fields p_α. Its determination involves the computation of a dual cone, consisting of vectors such that $\vec{K} \cdot \vec{T} \geq 0$. The number of operations involved grows drastically with the "size" (i.e. the number of nodes and bifundamental fields) of the quiver. The computation becomes prohibitive even for quivers of moderate complexity. Thus, one is forced to appeal to alternative approaches such as (un-)Higgsing [44]. Perhaps the most dramatic examples of this limitation are provided by recently discovered infinite families of gauge theories for the $Y^{p,q}$ [14] and $X^{p,q}$ [81] singularities. The methods presented in this section will enable us to treat such geometries. This also represents a significant improvement over the brute force methods of [82], since the relevant brane tiling may essentially be written down directly from the data of the quiver theory.

It is natural to ask whether the possibility of associating dimer configurations to a gauge theory, made possible due to the introduction of brane tilings, can be exploited to find a natural set of variables playing the role of the p_α's, overcoming the main intricacies of the Forward Algorithm. This is indeed the case, and we now elaborate on the details of the **dimer/GLSM correspondence**. The fact that the GLSM multiplicities are counted by the c_{ij} coefficients in the characteristic polynomial provides some motivation for the correspondence.

We denote the perfect matchings as $\tilde{p}_\alpha$. Every perfect matching corresponds to a collection of edges in the tiling. Hence, we can define a natural product between an edge e_i, corresponding to a bifundamental field X_i, and a perfect matching $\tilde{p}_\alpha$

$$< e_i, \tilde{p}_\alpha > = \begin{cases} 1 \text{ if } e_i \in \tilde{p}_\alpha \\ 0 \text{ if } e_i \notin \tilde{p}_\alpha \end{cases} \tag{11.4.12}$$

Given this product, we propose the following mapping between bifundamental fields and the perfect matching variables $\tilde{p}_\alpha$

$$X_i = \prod_\alpha \tilde{p}_\alpha^{<e_i, \tilde{p}_\alpha>}. \tag{11.4.13}$$

According to (11.4.12), the X_i involve only possitive powers of the $\tilde{p}_\alpha$. We will now show that F-term equations are trivially satisfied when the bifundamental fields are expressed in terms of perfect matchings variables according to (11.4.13). For any given bifundamental field X_0, we have

$$W = X_0 P_1(X_i) - X_0 P_2(X_i) + \ldots \tag{11.4.14}$$

where we have singled out the two terms in the superpotential that involve X_0. $P_1(X_i)$ and $P_2(X_i)$ represent products of bifundamental fields. The F-term equation associated to X_0 becomes

$$\partial_{X_0} W = 0 \quad \Leftrightarrow \quad P_1(X_i) = P_2(X_i). \tag{11.4.15}$$

This condition has a simple interpretation in terms of the bipartite graph, as shown in Figure 11-6.
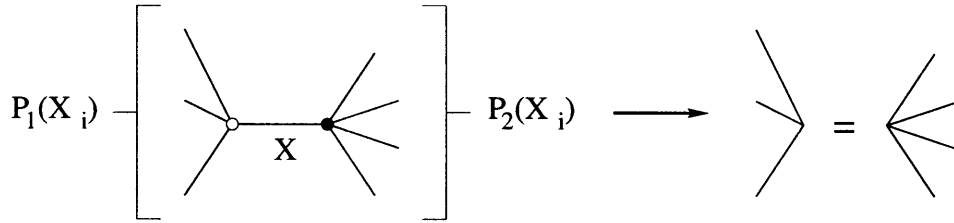
Figure 11-6: F-term equations from the brane tiling perspective.

After excluding the edge associated to X_0, the product of edges connected to node 1 has to be equal to the product of edges connected to node 2. In terms of perfect matchings, (11.4.15) becomes

$$\prod_{i \in P_1} \prod_\alpha \tilde{p}_\alpha^{<e_i, \tilde{p}_\alpha>} = \prod_{i \in P_2} \prod_\alpha \tilde{p}_\alpha^{<e_i, \tilde{p}_\alpha>}. \tag{11.4.16}$$

323

Every time that a given $\tilde{p}_\alpha$ appears on the L.H.S. of (11.4.16), it has to appear on the R.H.S. Here is where the fact that the $\tilde{p}_\alpha$'s are perfect matchings becomes important: since nodes 1 and 2 are separated exactly by one edge (the one corresponding to X_0) every time a perfect matching contains any of the edges in P_1, it contains one of the edges in P_2. This is necessary for the p_α to be a perfect matching (nodes 1 and 2 have to be covered exactly once). Thus, perfect matchings are the appropriate choice of variables that satisfy F-term conditions automatically. We conclude that the perfect matchings can be identified with the GLSM fields $\tilde{p}_\alpha = p_\alpha$. Then, the matrix that maps the bifundamental fields to the GLSM fields is

$$(KT)_{i\alpha} = < e_i, \tilde{p}_\alpha > . \qquad (11.4.17)$$

11.4.1 A detailed example: the Suspended Pinch Point

Let us illustrate the simplifications achieved by identifying GLSM fields with perfect matchings with an explicit example. To do so, we choose the Suspended Pinch Point (SPP) [138]. The SPP has a quiver shown in Figure 11-7 with superpotential

$$W = X_{21}X_{12}X_{23}X_{32} - X_{32}X_{23}X_{31}X_{13} + X_{13}X_{31}X_{11} - X_{12}X_{21}X_{11}. \qquad (11.4.18)$$
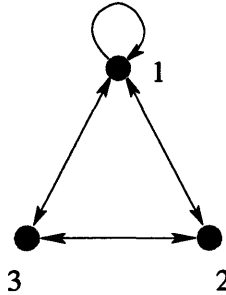

Figure 11-7: Quiver diagram for the SPP.

It is interesting to see how our methods apply to this example, since it has both adjoint fields and bidirectional arrows. Figure 11-8 shows the brane tiling for the

SPP. The adjoint field in the quiver corresponds to an edge between two faces in the tiling representing the first gauge group. The Kasteleyn matrix is
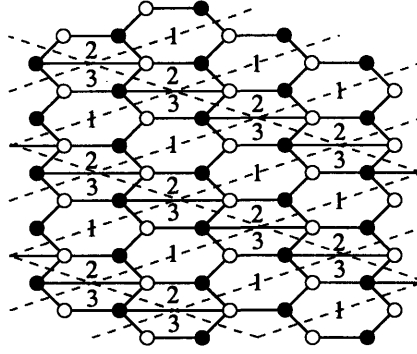
Figure 11-8: Brane tiling for the SPP.

$$K = \begin{pmatrix} & 2 & 4 \\ \hline 1 & 1 + w^{-1} & z + w^{-1}z \\ 3 & 1 & 1 + w^{-1} \end{pmatrix}$$

(11.4.19)

from which we determine the characteristic polynomial

$$P(z, w) = w^{-2} + 2w^{-1} + 1 - w^{-1}z - z.$$

(11.4.20)

From it, we construct the toric diagram shown in Figure 11-9.

Figure 11-9: Toric diagram for the *SPP*. We indicate the perfect matchings corresponding to each node in the toric diagram.

There are six perfect matchings of the *SPP* tiling. We show them in Figure 11-10. Setting a reference perfect matching, we can compute the slope (h_w, h_z) for each of them, i.e. the height change when moving around the two fundamental cycles of the torus.

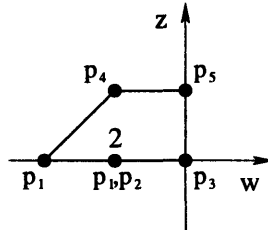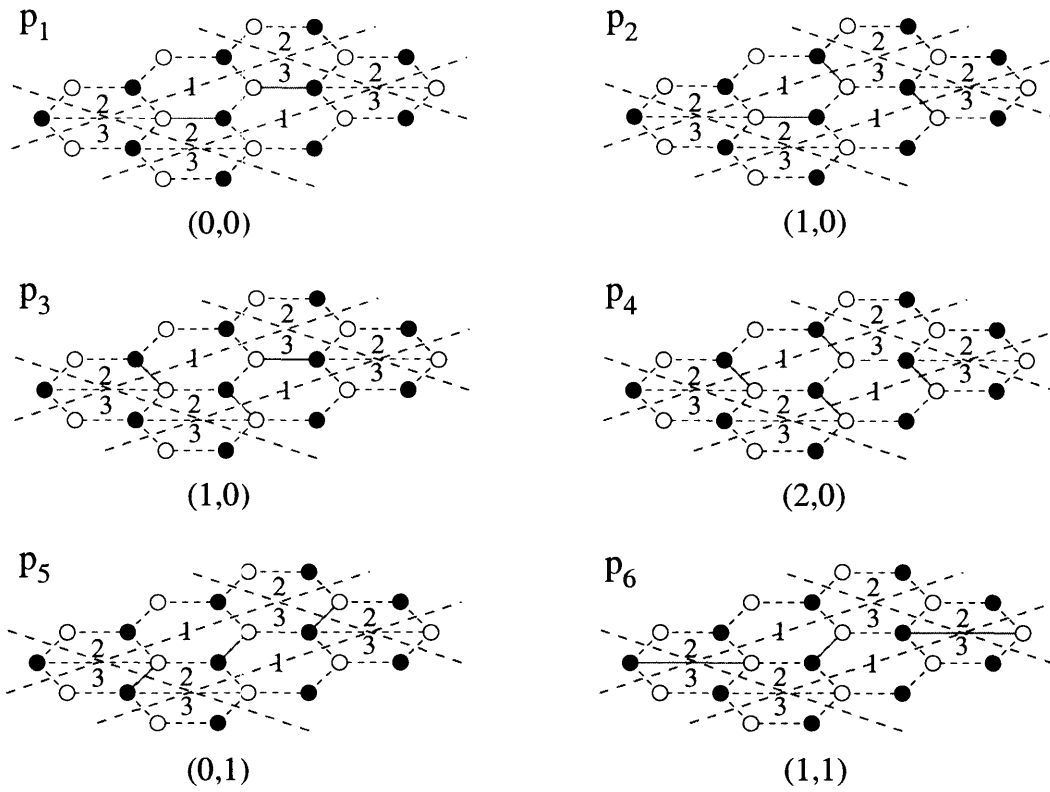Figure 11-10: Perfect matchings for the SPP. We indicate the slopes (h_w, h_z), which allow the identification of the corresponding node in the toric diagram as shown in Figure 11-9.

Using (11.4.12) and (11.4.17), it is straightforward to determine the KT matrix.

$$
KT = \begin{pmatrix}
 & p_1 & p_2 & p_3 & p_4 & p_5 & p_6 \\
\hline
X_{11} & 0 & 0 & 0 & 0 & 1 & 1 \\
X_{12} & 1 & 1 & 0 & 0 & 0 & 0 \\
X_{21} & 0 & 0 & 1 & 1 & 0 & 0 \\
X_{31} & 1 & 0 & 1 & 0 & 0 & 0 \\
X_{13} & 0 & 1 & 0 & 1 & 0 & 0 \\
X_{23} & 0 & 0 & 0 & 0 & 1 & 0 \\
X_{32} & 0 & 0 & 0 & 0 & 0 & 1
\end{pmatrix} \qquad (11.4.21)
$$

This agrees with the computation of this matrix done in Section 3.2 of [45].

326

11.5 Massive fields

By definition, massive fields appear in the superpotential as quadratic terms. Therefore they appear in the brane tiling as bivalent vertices. In the IR limit of the gauge theory, these massive fields become non-dynamical and should be integrated out using their equations of motion. We now show how to perform this procedure on the brane tiling and Kasteleyn matrix.

By performing a suitable relabelling of fields, one can always write the superpotential as follows (up to an overall minus sign if the quadratic term comes with opposite sign):

$$W(\Phi_i) = \Phi_1 \Phi_2 - \Phi_1 P_1(\Phi_i) - \Phi_2 P_2(\Phi_i) + \dots \tag{11.5.22}$$

where the omitted terms do not involve Φ_1, Φ_2, and P_1, P_2 are products of two disjoint subsets of the remaining Φ that do not include Φ_1 or Φ_2. This structure follows from the toric condition, which specifies that each field appears exactly twice in the superpotential, with terms of opposite signs.

Integrating out Φ_1 and Φ_2 by their equations of motion gives

$$W(\Phi) = -P_1(\Phi_i)P_2(\Phi_i) + \dots \tag{11.5.23}$$

This operation takes the form shown in Figure 11-11 and collapses two nodes separated by a bivalent node of the opposite color into a single node of valence equal to the sum of the valences of the original nodes.

The operation of integrating out a massive field can also be implemented in terms of the Kasteleyn matrix. From this perspective, it is simply row or column reduction of the matrix on rows or columns with two non-zero entries (or a single entry containing two summands, if both neighboring vertices to the bivalent vertex are identified in the graph). In the example of figure 11-11, if the bivalent white node has label 1 and the adjacent black nodes are $1'$ and $2'$ (this can always be arranged by a reordering of rows or columns, with the corresponding action of (-1) to preserve the determinant),
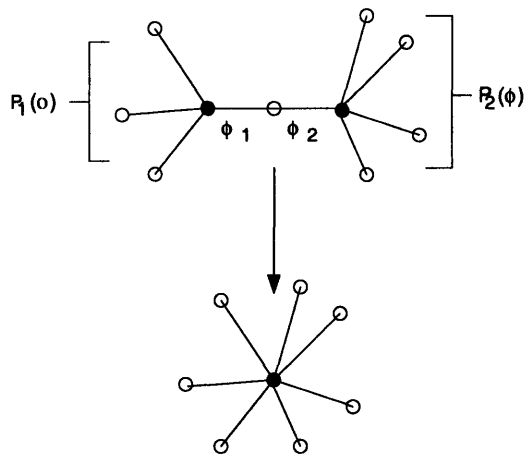
Figure 11-11: Integrating out a massive field corresponds to collapsing the two vertices adjacent to a bivalent vertex into a single vertex of higher valence.

the Kasteleyn matrix (or its transpose) has the following structure:

$$K = \begin{pmatrix} v_1^{(1)} & v_1^{(2)} & 0 & \dots & 0 \\ v_2^{(1)} & v_2^{(2)} & & & \\ \vdots & \vdots & & \star & \\ v_n^{(1)} & v_n^{(2)} & & & \end{pmatrix} \tag{11.5.24}$$

where $v^{(1)}$ and $v^{(2)}$ index the adjacent nodes to $1'$ and $2'$, i.e. contain $\deg(P_{1,2}(\Phi)) + 1$ non-zero entries.

Performing elementary column operations, the matrix can be brought to the following form[3]:

$$K = \begin{pmatrix} 1 & 0 & 0 & \dots & 0 \\ v_2^{(1)}/v_1^{(1)} & v_2^{(2)}v_1^{(1)} - v_2^{(1)}v_1^{(2)} & & & \\ \vdots & \vdots & & \star & \\ v_n^{(1)}/v_1^{(1)} & v_n^{(2)}v_1^{(1)} - v_n^{(1)}v_1^{(2)} & & & \end{pmatrix} \tag{11.5.25}$$

---

[3]If the sets of vertices $v^{(1)}$, $v^{(2)}$ adjacent to vertices $1'$ and $2'$ (excluding the common neighbor 1) are not disjoint, then after integrating out there will be two or more edges between the same pairs of vertices. In such cases, these multiple edges may be replaced by a single edge carrying the sum of the weights of the individual edges, since this reproduces the correct counting of matchings of the graph. This is indeed what happens in the column reduction process, which may produce entries that are the sum or difference of two non-zero entries.

and therefore can be reduced in rank without changing the determinant, by deleting the first row and column, giving the reduced Kasteleyn matrix

$$
K = \begin{pmatrix} v_2^{(2)} v_1^{(1)} - v_2^{(1)} v_1^{(2)} & \star & \star & \dots \\ \vdots & \star & \star & \dots \\ v_n^{(2)} v_1^{(1)} - v_n^{(1)} v_1^{(2)} & \star & \star & \dots \end{pmatrix}
\tag{11.5.26}
$$

corresponding to the graph with bivalent vertex deleted.

11.6 Seiberg duality

11.6.1 Seiberg duality as a transformation of the quiver

We now discuss how one can understand Seiberg duality from the perspective of the brane tilings. To motivate our construction, let us first recall what happens to a quiver theory when performing Seiberg duality at a single node. This was first done for orbifold quivers in [153]. Recall first that since Seiberg duality takes a given gauge group $SU(N_c)$ with N_f fundamentals and N_f anti-fundamentals to $SU(N_f - N_c)$, if we want the dual quiver to remain in a toric phase, we are only allowed to dualize on nodes with $N_f = 2N_c$. Dualizing on such a node (call it I) is straightforward, and is done as follows:

- To decouple the dynamics of node I from the rest of the theory, the gauge couplings of the other gauge groups and superpotential should be scaled to zero. The fields corresponding to edges in the quiver that are not adjacent to I decouple, and the edges between I and other nodes reduce from bifundamental matter to fundamental matter transforming under a global flavor symmetry group. This reduces the theory to the SQCD-like theory with $2N_c$ flavors and additional gauge singlets, to which Seiberg duality may be applied.

- Next, reverse the direction of all arrows entering or exiting the dualized node. This is because Seiberg duality requires that the dual quarks transform in the

conjugate flavor representations to the originals, and the other end of each bifundamental transforms under a gauge group which acts as an effective flavor symmetry group. Because we want to describe our theory with a quiver, we perform charge conjugation on the dualized node to get back bifundamentals. This is exactly the same as reversing the arrows in the quiver.

- Next, draw in N_f bifundamentals which correspond to composite (mesonic) operators that are singlets at the dualized node I and carry flavor indices in the pairs nodes connected to I. This is just the usual $Q_i \widetilde{Q}^j \to M_i^j$ "electric quark $\to$ meson" map of Seiberg duality, but since each flavor group becomes gauged in the full quiver theory, the Seiberg mesons are promoted to fields in the bifundamental representation of the gauge groups.

- In the superpotential, replace any composite singlet operators with the new mesons, and write down new terms corresponding to any new triangles formed by the operators above. It is possible that this will make some fields massive (e.g. if a cubic term becomes quadratic), in which case the appropriate fields should then be integrated out.

11.6.2 Seiberg duality as a transformation of the brane tiling

By writing the action of Seiberg duality in the periodic quiver picture, one may derive the corresponding transformation on the dual brane tiling. This operation may be encoded in a transformation on the Kasteleyn matrix of the graph, and the recursive application of Seiberg duality may be implemented by computer to traverse the Seiberg duality tree [56, 55] and enumerate all toric phases [4].

Consider a node in the periodic quiver. For the toric phases of the quiver all nodes in the quiver correspond to gauge groups of equal rank. If the node has 2 incoming

---

[4]Assuming this graph is connected. In fact, this is not allways the case and it is possible for the toric phases to appear in disconnected (i.e. connected by non-toric phases) regions of the duality tree. A simple example of this situation is given by the duality tree of dP$_1$. This tree is presented in [56], where the connected toric components where denoted "toric islands". In addition, it is interesting to see that if the theory is taken out of the conformal point by the addition of fractional branes, the cascading RG flow can actually "migrate" among these islands [61].

arrows (and therefore 2 outgoing arrows by anomaly cancellation, for a total of 4 arrows), then for this gauge group $N_f = 2N_c$, and Seiberg duality maps

$$N_c \mapsto \hat{N}_c = N_f - N_c = N_c \qquad (11.6.27)$$

so after the duality the theory remains in a toric phase.

At such a node V, a generic quiver can be represented as in Figure 11-12. The 4 faces F_i adjacent to V share an edge with their adjacent faces, and contain some number of additional edges.
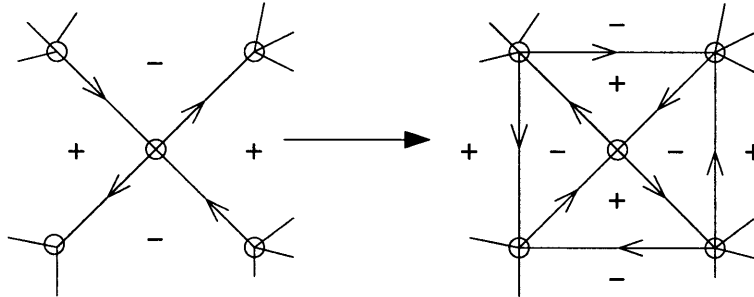

Figure 11-12: The action of Seiberg duality on a periodic quiver to produce another toric phase of the quiver. Also marked are the signs of superpotential terms, showing that the new terms (faces) are consistent with the pre-existing 2-coloring of the global graph.

The neighboring vertices to V are not necessarily all distinct (they may be identified by the periodicity of the torus on which the quiver lives). However by the periodic quiver construction, if there are multiple fields in the quiver connecting the same two vertices, these appear as distinct edges in the periodic quiver.

Note that the new mesons can only appear between adjacent vertices in the planar quiver, because the edges connecting opposing vertices do not have a compatible orientation, so they cannot form a holomorphic, gauge-invariant combination. There are indeed 4 such arrows that can be drawn on the quiver corresponding to the $2 \times 2 = 4$ Seiberg mesons.

It is easy to translate this operation to the dual brane tiling. Gauge groups with $N_f = 2N_c$ correspond to quadrilaterals in the tiling. Performing Seiberg duality on

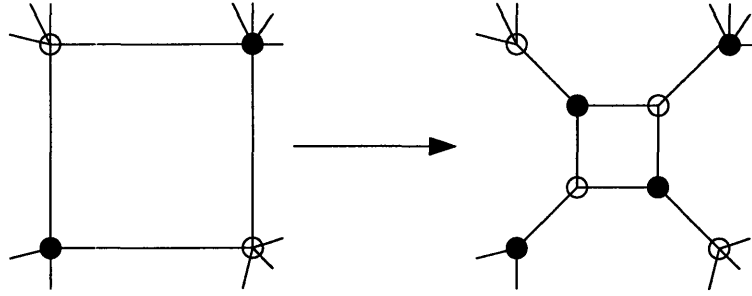such a face corresponds to the operation depicted in Figure 11-13[5].

Figure 11-13: Seiberg duality acting on a brane tiling to produce another toric phase. This is the planar dual to the operation depicted in Figure 11-12. Whenever 2-valent nodes are generated by this transformation, the corresponding massive fields can be integrated out as explained in Section 11.5.

Note that this operation (and the dual operation on the quiver) are local operations on the graph, in that they only affect a face and its neighbors, and the global structure of the graph is unaffected[6].

As a simple example, consider F_0. This is a $\mathbb{Z}_2$ orbifold of the conifold, and as such one can simply take the two-cell fundamental domain of the conifold and double its area to get the F_0 fundamental domain; this phase of this theory is given by a square graph with four different cells. In Figure 11-14, we have drawn this phase of the theory as well as the phase obtained by dualizing on face 1. The blue dotted lines are the lines of magnetic flux delineating the fundamental region, which do not change during Seiberg duality. It is straightforward to see that these regions give the correct Kasteleyn matrices, and reproduce the known multiplicities of sigma model fields [82].

It is useful to see how this action of Seiberg duality can be understood from the brane perspective. Since the area of each cell (volume of the D-brane) is related to the gauge coupling of the corresponding group [83], one would expect that Seiberg duality

---

[5]The extension to non-toric Seiberg dualities appears obvious on the periodic quiver, although there are subtleties involved in the precise operation on the Kasteleyn matrix.

[6]The transformation that we have identified with the action of Seiberg duality on the bipartite graph was discussed in [151], where it was referred to as "urban renewal". This work used a different assignment of weights in the transformed graph in order to keep the determinant (i.e. the GLSM field multiplicities, in our language) invariant across the operation. This is not what we want for Seiberg duality, which maps a toric diagram with one set of multiplicities to the same toric diagram with (in general) *different* multiplicities.
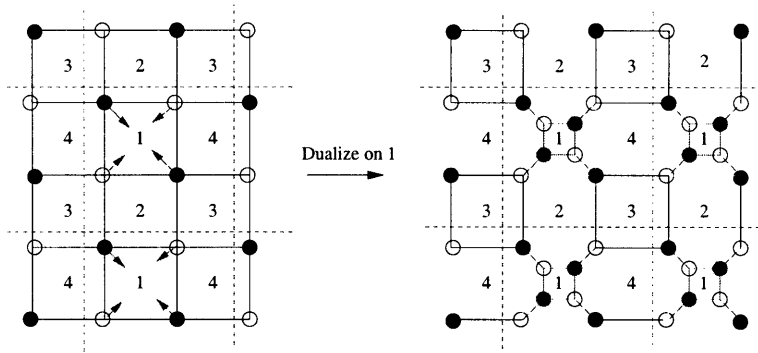
Figure 11-14: The operation of Seiberg duality on a phase of F_0.

could be viewed as a cell shrinking and then growing with the opposite orientation, e.g. as branes move through one another. It is possible to see this from Figure 11-14: we can simply take the NS5-branes at the sides of region 1 and pull them through one another. In doing this, we generate the diagonal lines. Since we are in a toric phase with $N_f = 2N_c$, the ranks of the gauge groups do not change in this crossing operation and no new branes are created.

11.6.3   Seiberg duality acting on the Kasteleyn matrix

Since the Kasteleyn matrix encodes all of the information about the graph, it is possible to implement the transformation of Seiberg duality directly in terms of the matrix. The first step is to identify the candidate (quadrilateral) faces to be dualized. These form a square in the Kasteleyn matrix, e.g. :

$$
K = \begin{pmatrix}
\star & a & \star & \ldots & b \\
\star & \star & \star & \ldots & \star \\
\vdots & \vdots & \vdots & & \vdots \\
\star & c & \star & \ldots & d \\
\star & \star & \star & \ldots & \star
\end{pmatrix}
\tag{11.6.28}
$$

However not all such squares represent the boundary of a face, e.g. on small enough graphs there can be a closed path of 4 edges which winds around the torus (for a closed cycle of 4 edges there are no other possibilities, as there is no room for additional

333

"internal" edges that would allow the cycle to have zero winding but not bound a face of the graph). The way to distinguish these cases is to use the magnetic flux through the cycle; if the cycle has no net winding around the torus then the flux lines γ_z, γ_w must each cross the cycle twice: once to enter and once to leave. Depending on the orientation with which they cross the edges (which depends on the choice of paths γ and is therefore not invariant), they may each contribute z or $1/z$ (similarly w or $1/w$), but it is invariantly true that the product of the edges must have even degree in both z and w. Conversely, a path with net winding around the torus will have odd degree in one or both of z and w.

Having identified the four edges forming the quadrilateral to be dualized, we wish to implement the transformation on the underlying graph depicted in Figure 11-13. This requires the addition of 2 white and 2 black nodes to the graph, increasing the rank of the adjacency matrix by 2. The large square is removed from the graph by setting to zero the four edges a, b, c, d found previously, the smaller square is added in by setting to non-zero the weights in the new 2×2 diagonal block, and the new smaller square is connected to the rest of the graph by adding non-zero elements to the $2 \times n$ and $n \times 2$ blocks in the rows and columns corresponding to the removed entries.

Since the new square has opposite orientation with respect to the large square, the power of z and w along the edges must be inverted. This may change the normalization of the determinant, so to correct this we can rescale a row by z^{d_z} and a column by w^{d_w}, where $d_{w,z} = \deg_{w,z} abcd$. Finally, since the graph transformation adds 2 additional edges to each of the 4 faces adjacent to the square, each of these faces must gain an additional minus sign on one of the new edges bounding it, in order to satisfy the sign rules discussed in section 11.3.

Explicitly, the new Kasteleyn matrix corresponding to the Seiberg dual graph can be written in the following form (where for convenience we have relabeled the rows and columns to bring the 4 entries corresponding to edges of the quadrilateral into the bottom-right position):

334

$$K = \begin{pmatrix} \begin{array}{c|c} A_{(n-2)\times(n-2)} & B_{(n-2)\times 2} \\ \hline C_{2\times(n-2)} & \begin{array}{cc} a & b \\ c & d \end{array} \end{array} \end{pmatrix} \mapsto K' = \begin{pmatrix} \begin{array}{c|c|c} A_{(n-2)\times(n-2)} & B_{(n-2)\times 2} & 0_{2\times 2} \\ \hline C_{2\times(n-2)} & 0_{2\times 2} & \begin{array}{cc} z^{d_z} & 0 \\ 0 & 1 \end{array} \\ \hline 0_{2\times(n-2)} & \begin{array}{cc} 0 & -1 \\ -w^{d_w} & 0 \end{array} & \begin{array}{cc} \frac{1}{b}z^{d_z} & \frac{1}{d} \\ \frac{1}{a}w^{d_w}z^{d_z} & \frac{1}{c}w^{d_w} \end{array} \end{array} \end{pmatrix}$$

$$(11.6.29)$$

As discussed above, after Seiberg duality there may be massive fields in the theory which should be integrated out; we described in section 11.5 how to implement this on the Kasteleyn matrix.

This form of Seiberg duality is amenable to efficient implementation on computer. For example, the enumeration of 17 of the toric phases of the $Y^{6,0}$ quiver took several days using the algorithm of [82] (which was itself much more efficient than the previous Inverse Algorithm). Since $Y^{6,0}$ is a $\mathbb{Z}_6$ orbifold of the conifold, it is possible to use the orbifold formulæ in [82] and immediately write down the Kasteleyn matrix for two of these phases; either one is a suitable starting point for iteration of Seiberg duality, which produces these 17 phases within a few seconds.

However, this raises an important subtlety: it is possible for two distinct quiver theories to have the same set of multiplicities of points in the toric diagram. It had previously been conjectured, based on the results presented in Chapter 5, that the multiplicities of GLSM fields uniquely characterized the possible toric phases of the quiver gauge theory, i.e. in dimer language that the characteristic polynomial was an invariant of the dimer graph up to graph isomorphism (relabelling of fields). In the example of $Y^{6,0}$, only 17 distinct sets of multiplicities are produced, compared with an expectation of 18 toric phases [81]; this mismatch was noted already in [82][7]. Furthermore, extending the set of data considered to include the set of orders of terms in the superpotential (which can be read off from the Kasteleyn matrix

---

[7]A simpler example manifesting this collision of multiplicities is that of pseudo-del Pezzo 5: two of the four toric phases of this theory have the same multiplicities, as we discuss in section 11.9.

independently of the field labelling), and the set of neighboring toric phases that are reachable under Seiberg duality, still only distinguishes 17 distinct phases. By writing down the brane tilings explicitly and reconstructing the quivers[8], we were able to isolate the "missing" 18th phase and confirm that it indeed has the same toric diagram with multiplicities as one of the remaining 17, but is nonetheless a distinct quiver theory that is not equivalent under field redefinition. In addition, these two phases have the same superpotential orders and Seiberg duality neighbors. In Section 11.9.2, we will present a similar example in which two gauge theories produce the same toric diagram and multiplicities, although in that case the superpotentials will have different orders and numbers of terms.

How can we understand this situation? It is a known result in mathematics that the characteristic polynomial (in the usual linear algebra sense) of the adjacency matrix of a graph does not uniquely characterize the graph up to isomorphism: there may be two distinct graphs with the same characteristic polynomial. The determinant of the Kasteleyn matrix of the graph is essentially a double characteristic polynomial (due to the block structure of the matrix, as explained in [82]), so the result explains the observed non-uniqueness of GLSM multiplicities of the toric quivers. Similarly, it is believed that there exists *no* invariant of a graph up to isomorphism that distinguishes between all non-isomorphic graphs. In other words, the only invariant of a graph that characterizes it uniquely is the graph itself, and in order to distinguish between the pathological cases where the would-be-invariants fail, one must resort to explicit testing of graph isomorphism, which is an expensive (non-polynomial) operation. Thus, the enumeration of toric phases by testing graph invariants such as the characteristic polynomial can only produce a lower bound on the number of phases, and in general there may be phases (or even entire regions of the toric duality graph) that are missed by this counting.

---

[8]This work was done in conjunction with P. Kazakopoulos.

11.7 Partial resolution

Many of the first known examples of gauge theories dual to toric geometries were described by embedding them in orbifolds [45, 46, 12]. For example, partial resolutions of $\mathbb{C}^3/\mathbb{Z}_3 \times \mathbb{Z}_3$ give the first three del Pezzo theories and F_0, among others. Partially resolving the orbifold singularity corresponds to turning on Fayet-Iliopoulos terms in the dual gauge theory, which by the D-flatness conditions gives vacuum expectation values to bifundamental fields. These vevs then reduce the rank of the gauge group via the Higgs mechanism. From the standpoint of the toric diagram, this is simply removing an external point. Doing so decreases the area of the toric diagram, and consequently decreases the number of gauge groups in the dual superconformal theory.

It is straightforward to see how Higgsing operates from the perspective of the dimer models. We give a non-zero vev to a bifundamental field, which reduces the two gauge group factors under which the bifundamental is charged to the diagonal combination. Hence, Higgsing is nothing more than the removal of an edge from the fundamental region of the graph, which causes two faces of the graph to become one.

This method was used in [82] to obtain the bipartite graphs corresponding to an arbitrary toric singularity, but the algorithm presented was computationally expensive since it was unknown how to identify the desired Higgsing in the quiver side. Using the duality between the quivers and brane tilings, it is straightforward to identify the edge of the bipartite graph to be removed that corresponds to the Higgsing of any given field in the quiver. Thus, the relations between quiver theories under Higgsing may be easily followed on the dual brane tiling, avoiding any computational difficulties.

Let us begin with Model I of dP_3, since we have already studied this tiling in a previous section. Since this model is perfectly symmetric and contains only single bifundamental field between any two gauge groups, giving a vev to any field should result in the same theory. This theory is dP_2, which has five nodes in its quiver. One can easily check that removing any edge from this tiling for dP_3 results in the expected gauge theory. Figure 11-15 illustrates this process: removing the edge between regions 5 and 6 is equivalent to removing the bifundamental between the corresponding nodes.
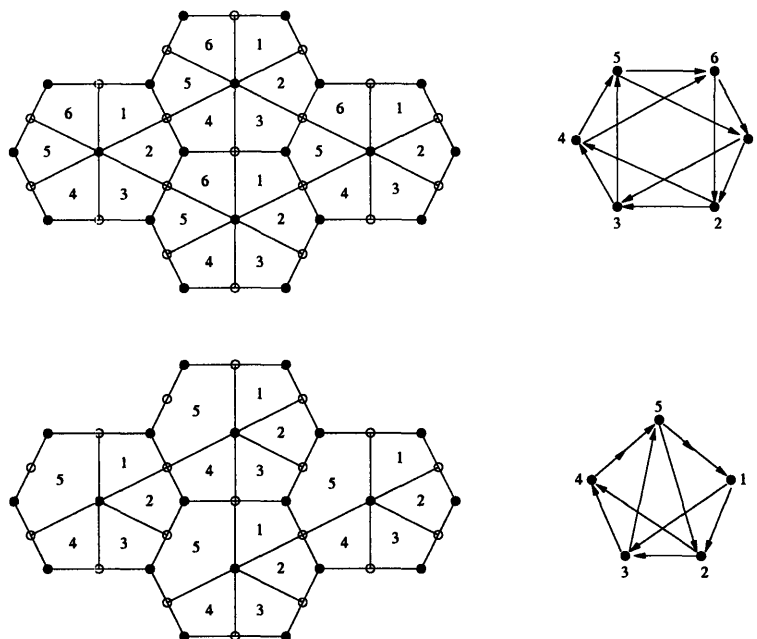
337

Figure 11-15: Removing the edge from between faces 5 and 6 Higgses Model I of dP_3 (top) to one of the two toric phases of dP_2 (bottom).

The example of taking Model I of dP_3 to one of the two toric phases of dP_2 (called Model II in [43]) is particularly simple, since no fields acquire a mass when X_{56} gets a vev. It is not any more difficult to see what happens when bifundamentals do become massive, as we can see by considering the dP_2 example. We know that the dP_2 theory can be Higgsed to either dP_1 or F_0; this corresponds to giving a vev to X_{34} (or equivalently X_{12} by the symmetry of the quiver) or X_{23}, respectively. In the brane tiling, we delete the edge between regions 2 and 3 of the tiling. This puts an isolated node between the two regions. As per our discussion in Section 11.5, we then simply collapse those two edges to a point, which corresponds to integrating out the fields X_{35} and X_{52}. See Figure 11-16.

We expect from string theory that we may embed any toric quiver in an appropriately large Abelian orbifold theory of the form $\mathbb{C}^3/\mathbb{Z}_m \times \mathbb{Z}_n$. The tiling for $\mathbb{C}^3/\mathbb{Z}_m \times \mathbb{Z}_n$ is hexagonal, so one expects that we can reach **any** tiling by removing edges from hexagons. This is indeed the case, as noted by [118] and used extensively in [82].
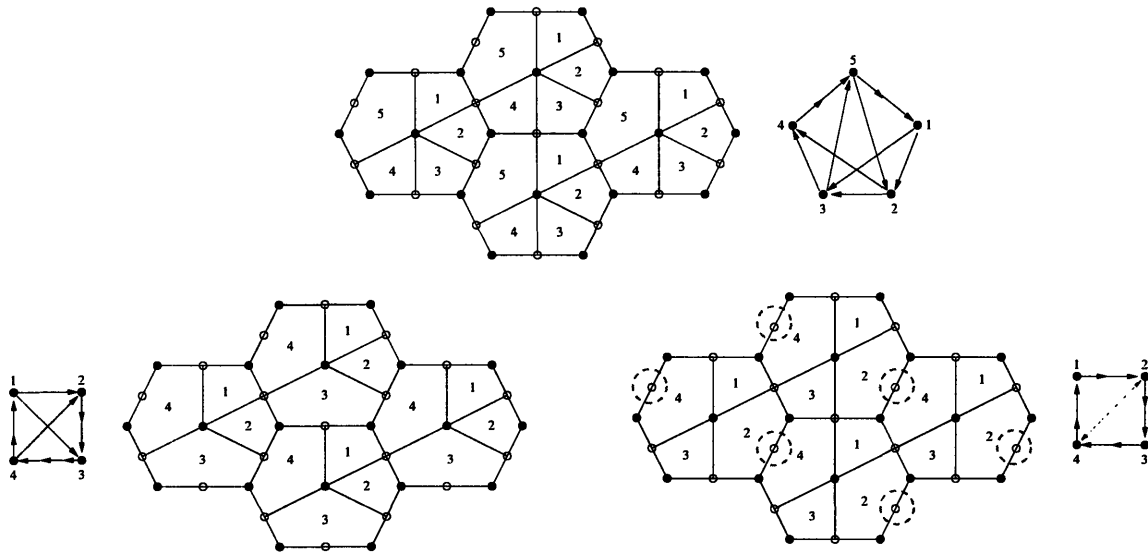
Figure 11-16: The dP_2 tiling (top) can be taken to either dP_1 (bottom left) or F_0 (bottom right), depending on which edge gets removed. In the F_0 tiling, one should collapse the edge between regions 2 and 4 to a point; this corresponds to the bifundamentals on the diagonal of the quiver.

11.8   Different toric superpotentials for a given quiver

Dimer methods can be used to tackle another interesting problem. Given a quiver diagram, it is sometimes possible to construct more than one consistent toric superpotential. Constructing the corresponding tilings shows immediately how these theories differ and enables a straightforward computation of their toric data.

Let us consider a concrete example, given by the quiver diagram shown in Figure 11-17. This is the quiver for Model II of dP_3 [43]. This quiver has 6 gauge groups and 14 bifundamental fields. From (11.2.1), we see that the number of superpotential terms is $N_W = 14 - 6 = 8$. There are two possible toric superpotentials consistent with the node symmetry group of the quiver. They have been considered in [43] and [49] and are

$$
\begin{aligned}
W_A \;=\; & [X_{12}X_{26}X_{61} - X_{12}X_{25}X_{51} + X_{36}X_{64}X_{43} - X_{35}X_{54}X_{43}] \\
& +[-X_{61}X_{13}X_{36} + X_{51}Y_{13}X_{35}] + [-X_{26}X_{64}X_{41}Y_{13}X_{32} + X_{25}X_{54}X_{41}X_{13}X_{32}]
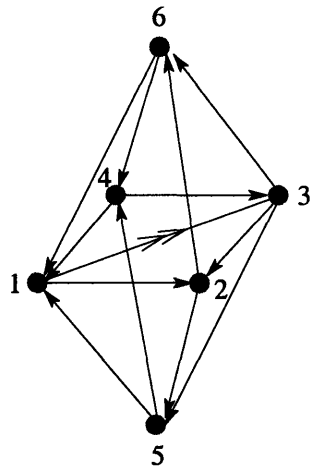\end{aligned}
$$

$$(11.8.30)$$

339

Figure 11-17: Quiver diagram admitting two toric superpotentials.

$$W_B = Y_{13}X_{36}X_{61} + X_{13}X_{35}X_{51} - X_{61}X_{12}X_{26} - X_{43}X_{35}X_{54}$$
$$+ X_{12}X_{25}X_{54}X_{41} + X_{26}X_{64}X_{43}X_{32} - X_{25}X_{51}Y_{13}X_{32} - X_{64}X_{41}X_{13}X_{36}$$
$$\tag{11.8.31}$$

W_A corresponds to a brane tiling with six valence-3 and two valence-5 nodes. This brane tiling is shown in Figure 11-18. For W_B the brane tiling has four valence-3 and four valence-4 nodes and it is shown in Figure 11-19. The Kasteleyn matrices for
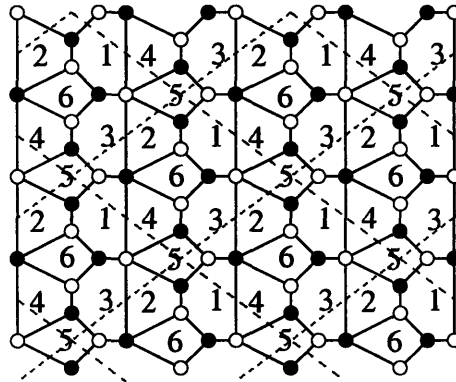

Figure 11-18: Brane tiling corresponding to the quiver diagram in Figure 11-17 and the superpotential in (11.8.30).
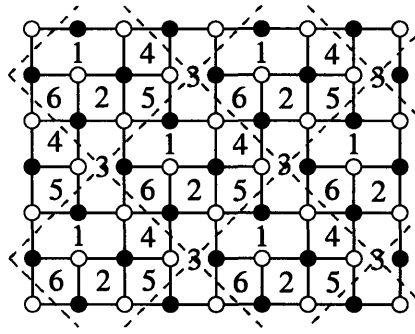
these tilings are

340

Figure 11-19: Brane tiling corresponding to the quiver diagram in Figure 11-17 and the superpotential in (11.8.31).

$$K_A = \begin{pmatrix} & 2 & 4 & 6 & 8 \\ \hline 1 & 1 & z^{-1} & 0 & w \\ 3 & -1 & 1 & 1 & 0 \\ 5 & z + w^{-1} & w^{-1} & 1 & -z \\ 7 & 1 & 0 & 1 & 1 \end{pmatrix} \qquad K_B = \begin{pmatrix} & 2 & 4 & 6 & 8 \\ \hline 1 & 1 & 0 & w^{-1} & w^{-1} \\ 3 & z & 1 & 0 & w^{-1} \\ 5 & 1 & 1 & -1 & 1 \\ 7 & z & -1 & z & 1 \end{pmatrix}$$

$$(11.8.32)$$

The corresponding characteristic polynomials are

$$P_A(z, w) = w^{-1}z^{-1} + z^{-1} - w^{-1} + 7 - w + z + wz \qquad (11.8.33)$$

$$P_B(z, w) = -w^{-2} - 2w^{-1} - 1 - w^{-2}z + 7w^{-1}z - z - w^{-1}z^2 \qquad (11.8.34)$$

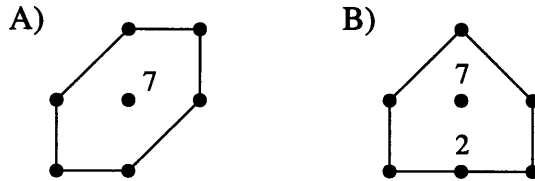From (11.8.33) and (11.8.34), we extract the toric diagrams shown in Figure 11-20.

Figure 11-20: Toric diagram for the quiver in Figure 11-17 and superpotentials W_A and W_B

Thus we see that W_A leads to Model II of dP_3 (the multiplicities of GLSM fields are

341

in agreement with the ones derived in [43]) while W_B leads to a non-generic blow-up of $\mathbb{CP}^2$ at three points, denoted PdP_{3b} in [49].

11.9 Examples

Here we present the brane tiling configurations for several interesting gauge theories. Many of them can be obtained using the Seiberg duality and partial resolution ideas discussed in previous sections. When doing so, we generate data on GLSM multiplicities for all these models.

11.9.1 Del Pezzo 2

There are two toric phases for dP_2. Their corresponding quivers and superpotentials can be found in [43]. We now construct their corresponding brane tilings.

Model I

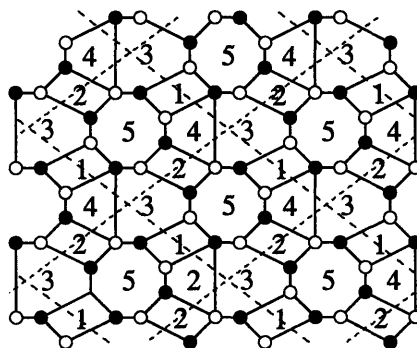The brane tiling for this model is shown in Figure 11-21. The Kasteleyn matrix is

Figure 11-21: Brane tiling for Model I of dP_2.

$$K = \begin{pmatrix} 1 & w^{-1} & w^{-1}z^{-1} & 1 \\ 1 & 1 & -z^{-1} & 0 \\ 0 & 1 & -1 & -w \\ z & 0 & 1 & 1 \end{pmatrix} \qquad (11.9.35)$$

leading to

$$P(z, w) = w^{-1}z^{-1} + z^{-1} + w^{-1} - 6 + w + z \qquad (11.9.36)$$

Model II

The tiling for this model was obtained in Section 11.7 by means of partial resolution. We show it again in Figure 11-22. The corresponding Kasteleyn matrix is
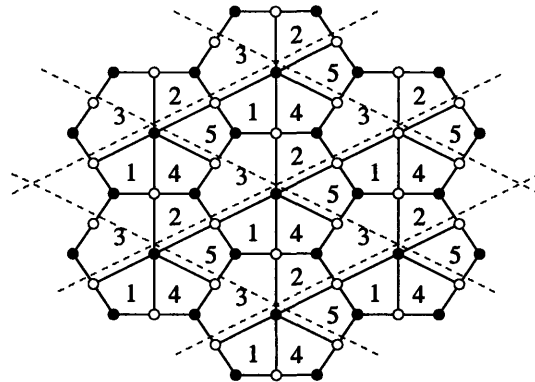

Figure 11-22: Brane tiling for Model II of dP_2.

$$K = \begin{pmatrix} 1 - z^{-1} & w & 1 \\ 1 & 1 & z \\ -1 + w^{-1}z^{-1} & 1 & 1 \end{pmatrix} \qquad (11.9.37)$$

which leads to the following characteristic polynomial

$$P(z, w) = w^{-1}z^{-1} - z^{-1} + 5 - w - z - wz \qquad (11.9.38)$$

From (11.9.36) and (11.9.38) we can determine the toric diagrams along with the GLSM multiplicities, which are in agreement with the results in [43].

Del Pezzo 3

There are four toric phases for dP_3. We refer the reader to [43] for their quivers and superpotentials. We have already presented the tiling for Model I in Figure 11-1. Its

343

Kasteleyn matrix and characteristic polynomial are written in (11.3.9) and (11.3.10). Figure 11-18 shows the tiling for Model II. Its Kasteleyn matrix and characteristic polynomial are presented in (11.8.32) and (11.8.33). We now proceed with the construction of the brane tilings for Models III and IV.

Model III

We show the brane tiling in Figure 11-23. The Kasteleyn matrix is
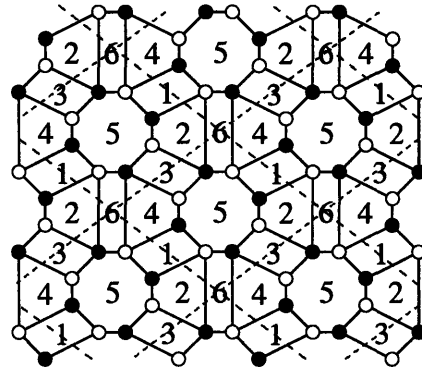
Figure 11-23: Brane tiling for Model III of dP_3.

$$K = \begin{pmatrix} & 2 & 4 & 6 & 8 \\ \hline 1 & 1 & w^{-1} & w^{-1}z^{-1} & 1 \\ 3 & 1 & 1 & -z^{-1} & 0 \\ 5 & wz & 1 & -1 & -w \\ 7 & z & 0 & 1 & 1 \end{pmatrix} \tag{11.9.39}$$

from which we compute the determinant

$$P(z,w) = w^{-1}z^{-1} + z^{-1} - w^{-1} - 8 + w + z + wz \tag{11.9.40}$$

This corresponds to the toric diagram of dP_3 with multiplicity 8 for the central point. This result agrees with the Forward Algorithm computations in [43].

344

Model IV

Figure 11-24 shows the brane tiling for this theory.
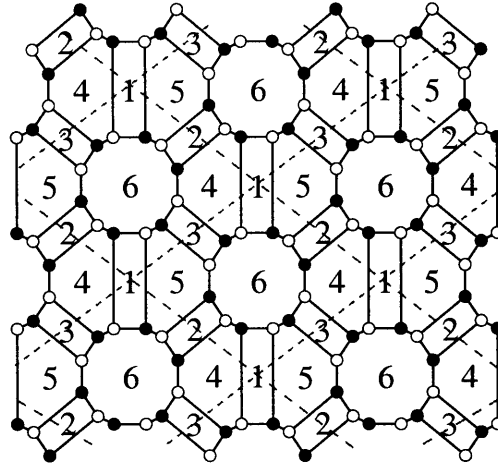
Figure 11-24: Brane tiling for Model IV of dP_3.

The Kasteleyn matrix is given by

$$K = \begin{pmatrix}
 & 2 & 4 & 6 & 8 & 10 & 12 \\
\hline
1 & 1 & 0 & 0 & -wz & 0 & -1 \\
3 & 1 & 1 & 0 & 0 & z & 0 \\
5 & 0 & -1 & 1 & 0 & 0 & -w^{-1} \\
7 & w^{-1}z^{-1} & 0 & 1 & 1 & 0 & 0 \\
9 & 0 & -z^{-1} & 0 & -1 & 1 & 0 \\
11 & 0 & 0 & w & 0 & 1 & 1
\end{pmatrix} \qquad (11.9.41)$$

and the characteristic polynomial is

$$P(z,w) = -w^{-1}z^{-1} - z^{-1} - w^{-1} + 11 - w - z - wz \qquad (11.9.42)$$

Once again, this corresponds to the toric diagram of dP_3. In this case, the multiplicity of the central point is 11, in agreement with the computations in [43].

345

11.9.2 Pseudo del Pezzo 5

We now consider a complex cone over non-generic, toric blow-up of $\mathbb{CP}^2$ at five points. The geometry corresponds to a $\mathbb{Z}_2 \times \mathbb{Z}_2$ orbifold of the conifold and was dubbed PdP_5 in [44], where the corresponding gauge theories were studied. There are four toric phases for this geometry. We refer the reader to [44] for the quivers and superpotentials. The brane tilings for these four phases are shown in Figure 11-25
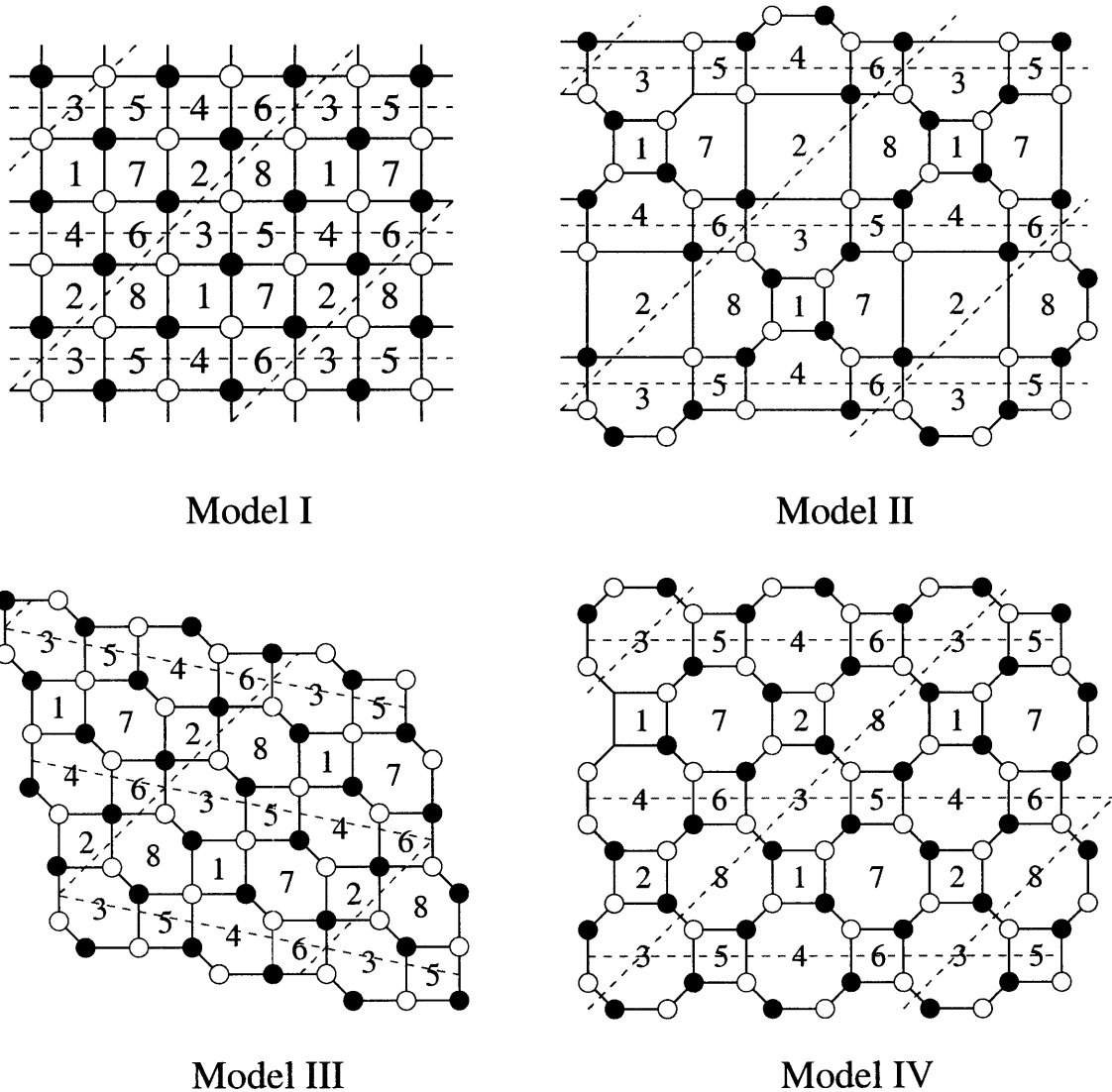

Model I

Model II

Model III

Model IV

Figure 11-25: Brane tilings for the four toric phases of PdP_5.

$$K_I = \begin{pmatrix} & 2 & 4 & 6 & 8 \\ \hline 1 & -1 & -w & 1 & wz \\ 3 & -1 & -1 & z & 1 \\ 5 & z^{-1} & w & 1 & w \\ 7 & 1 & z^{-1} & 1 & 1 \end{pmatrix}$$

$$K_{II} = \begin{pmatrix} & 2 & 4 & 6 & 8 & 10 & 12 \\ \hline 1 & -1 & 0 & -w & 0 & 0 & wz \\ 3 & -1 & 1 & 0 & 0 & 1 & 0 \\ 5 & 0 & -1 & -1 & z & 0 & 1 \\ 7 & 0 & z^{-1} & w & 1 & 0 & w \\ 9 & 1 & 0 & 0 & 1 & 1 & 0 \\ 11 & 0 & 0 & z^{-1} & 0 & -1 & 1 \end{pmatrix}$$

$$K_{III} = \begin{pmatrix} & 2 & 4 & 6 & 8 & 10 & 12 \\ \hline 1 & 1 & 0 & w & 0 & 0 & -wz \\ 3 & 1 & 1 & 0 & -z & -1 & 0 \\ 5 & 0 & -1 & 1 & 0 & 0 & -1 \\ 7 & 0 & 0 & -w & -1 & 0 & -w \\ 9 & -1 & -z^{-1} & 0 & -1 & -1 & 0 \\ 11 & 0 & 0 & -z^{-1} & 0 & 1 & -1 \end{pmatrix}$$

$$K_{IV} = \begin{pmatrix} & 2 & 4 & 6 & 8 & 10 & 12 & 14 & 16 \\ \hline 1 & 1 & 0 & 0 & w & 0 & 0 & wz & 0 \\ 3 & -1 & 1 & 0 & 0 & 0 & 1 & 0 & 0 \\ 5 & 0 & 1 & 1 & 0 & z & 0 & 0 & 0 \\ 7 & 0 & 0 & -1 & 1 & 0 & 0 & 0 & 1 \\ 9 & 0 & z^{-1} & 0 & 0 & -1 & 0 & 0 & w \\ 11 & 1 & 0 & 0 & 0 & 1 & 1 & 0 & 0 \\ 13 & 0 & 0 & 0 & z^{-1} & 0 & 1 & -1 & 0 \\ 15 & 0 & 0 & 1 & 0 & 0 & 0 & 1 & 1 \end{pmatrix}$$

$$(11.9.43)$$

From these matrices, we compute the corresponding characteristic polynomials

$$P_I(z,w) = P_{III}(z,w) = \quad z^{-2} + 2z^{-1} + 2wz^{-1} + 1 - 12w + w^2 + 2wz + 2w^2z + w^2z^2$$

$$P_{II}(z,w) = \quad z^{-2} + 2z^{-1} + 2wz^{-1} + 1 - 14w + w^2 + 2wz + 2w^2z + w^2z^2$$

$$P_{IV}(z,w) = \quad z^{-2} - 2z^{-1} - 2wz^{-1} + 1 - 21w + w^2 - 2wz - 2w^2z + w^2z^2$$

$$(11.9.44)$$

Remarkably, although K_I and K_{III} are different matrices with different dimensions, their characteristic polynomials turn out to be identical. This is a counterexample to the conjecture that GLSM multiplicities are in one to one correspondence with the dual phases of the gauge theory. Different phases can indeed lead to exactly the same multiplicities. We present the toric diagrams with multiplicities in Figure 11-26.
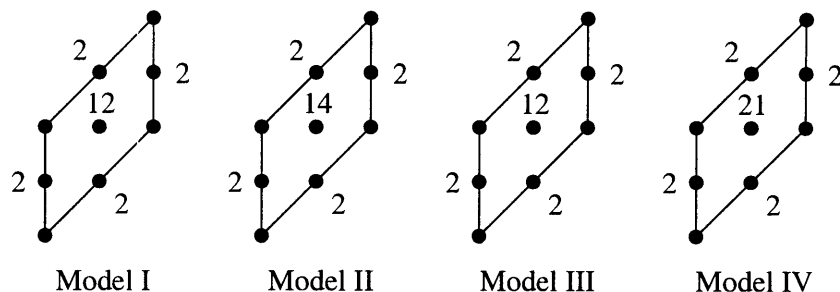
Figure 11-26: Toric diagrams with multiplicities for the four toric phases of PdP_5. We observe that the GLSM multiplicities are the same for Models I and III.

11.9.3 Tilings for infinite families of gauge theories

One of the problems for which dimer methods show their full power is in the determination of dual geometries for infinite families of gauge theories. Infinite sets of quiver theories have recently been constructed in [14] (see Chapter 10) and [81]. On one hand, we have already discussed that the application of the Forward Algorithm to large quivers becomes computationally prohibitive. In addition, it is obviously impossible to apply the Forward Algorithm to an infinite number of theories. Hence, the determination of gauge theories dual to an infinite number of geometries usually involve indirect evidence such as: (un)higgsing, global symmetries, computation of R-charges and central charges and comparison to volumes in the underlying geometry [14, 81].

$Y^{p,q}$ tilings

Let us discuss now how the $Y^{p,q}$ theories [14] appear in the brane tiling picture. A simple way to construct the $Y^{p,q}$'s is to start with $Y^{p,q=p}$ and decrease q by introducing "impurities" into the quiver [16]. This procedure can be similarly carried out with tilings. Since $Y^{p,p}$ is the base of the orbifold $\mathbb{C}^3/\mathbb{Z}_{2p}$, it corresponds to the hexagonal graph with a fundamental cell containing $2 \times p$ hexagons. This is shown in Figure 11-27 for $Y^{3,3}$.

Let us put now a single impurity into the tiling. The impurity covers four hexagons, and is indicated in blue in Figure 11-28. Two disjoint single impurities can be generated by adding an identical shaded region into the tiling, separated from

348
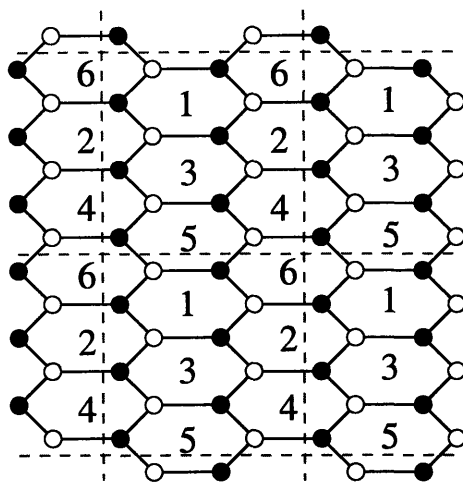
Figure 11-27: Brane tiling for $Y^{3,3}$
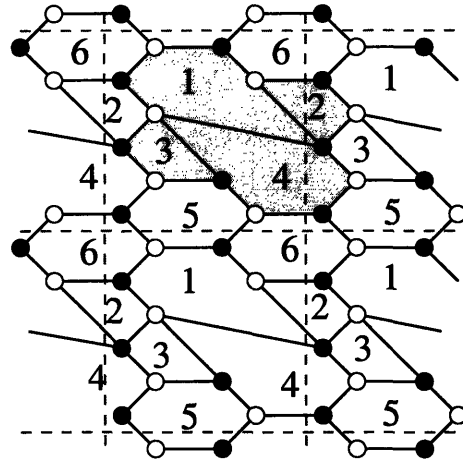
Figure 11-28: Brane tiling for $Y^{3,2}$. The impurity is the blue area.

the first one by some hexagonal faces. For $Y^{3,1}$ this is not possible because the fundamental cell consists of only six hexagons, whereas two separated single impurities would cover eight of them. Instead, we can consider the case in which the two impurities are adjacent. This corresponds to a similar impurity graph, which is shown in Figure 11-29.

One can continue adding impurities and discover the simplicity of the Kasteleyn matrix for $Y^{p,q}$. It contains elements only in the diagonal and its neighbors and in the corners. It can be written down immediately, without actually drawing the corresponding brane tiling. One starts with the following $2p \times 2p$ Kasteleyn matrix for $Y^{p,p}$.
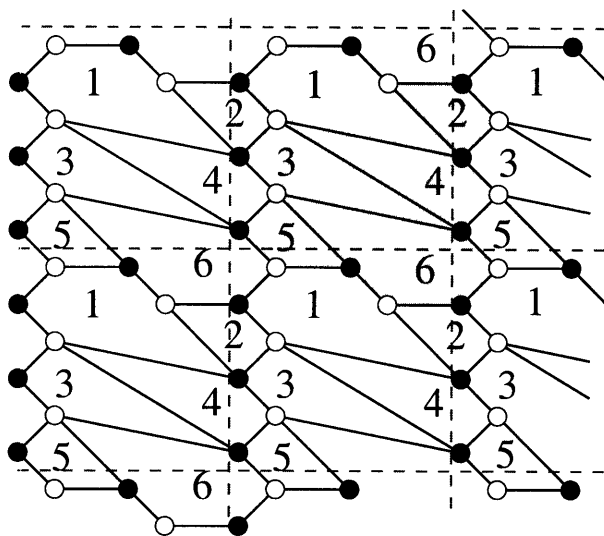
Figure 11-29: Brane tiling for $Y^{3,1}$.

$$K = \begin{pmatrix} 1 & 1 & 0 & 0 & \ldots\ldots & 0 & z^{-1} \\ 1 & w & 1 & 0 & \ldots\ldots\ldots & & 0 \\ 0 & 1 & 1 & 1 & 0 & \ldots\ldots & 0 \\ 0 & 0 & 1 & w & 1 & 0 & \ldots & 0 \\ & \vdots & & & & \ddots & \\ 0 & \ldots\ldots\ldots & & 0 & 1 & 1 & 1 \\ z & 0 & \ldots\ldots\ldots & & 0 & 1 & w \end{pmatrix} \qquad (11.9.45)$$

We see that the elements around the diagonal consist of the alternating "codons":

$$A_1 := (1,1,1) \qquad (11.9.46)$$

$$A_2 := (1,w,1) \qquad (11.9.47)$$

We define three other codons

$$S := (1,w,w) \qquad (11.9.48)$$

$$I := (1,-1+w,w) \qquad (11.9.49)$$

$$E := (1,-1+w,1) \qquad (11.9.50)$$

350

Placing impurities into the quiver means changing the $A_1, A_2, A_1, A_2, \ldots$ sequence in the matrix. For n single impurities we get $Y^{p,p-n}$ and the Kasteleyn matrix gets smaller, it is now a $(2p-n) \times (2p-n)$ matrix. We change the sequence of the codons as the following. In the second row we put S (start codon), then $n-1$ times the I (iteration codon), and we close it with E (end codon). Then we continue the series with $A_1, A_2, A_1, A_2, \ldots$ until the end of the matrix. As an example, we present the Kasteleyn matrix for $Y^{5,3}$ (i.e. $n = 2$)

$$K = \begin{pmatrix} A_1 & 1 & 1 & 0 & 0 & 0 & 0 & 0 & z^{-1} \\ S & 1 & w & w & 0 & 0 & 0 & 0 & 0 \\ I & 0 & 1 & -1+w & w & 0 & 0 & 0 & 0 \\ E & 0 & 0 & 1 & -1+w & 1 & 0 & 0 & 0 \\ A_1 & 0 & 0 & 0 & 1 & 1 & 1 & 0 & 0 \\ A_2 & 0 & 0 & 0 & 0 & 1 & w & 1 & 0 \\ A_1 & 0 & 0 & 0 & 0 & 0 & 1 & 1 & 1 \\ A_2 & z & 0 & 0 & 0 & 0 & 0 & 1 & w \end{pmatrix} \qquad (11.9.51)$$

The determinant of the Kasteleyn matrix is then

$$P(w,z) = -1 + 16w - 41w^2 + 33w^3 - 10w^4 + w^5 - z^{-1} - w^2 z, \qquad (11.9.52)$$

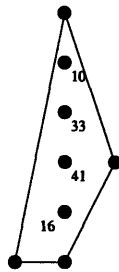and the toric diagam (with GLSM multiplicities) is given in Figure 11-30.

Figure 11-30: Toric diagram of a phase of $Y^{5,3}$

We note that the above rules for constructing the Kasteleyn matrix produce the toric diagrams for all $Y^{p,q}$ with $p > q > 0$. To check this, we can see that the correct

monomials appear in the determinant. First, the only powers of z that appear in $\det K$ are -1,0, and 1. Terms of the form $z^0 w^k$ appear for all $k = 0, \ldots, p$; these come from the diagonal. Second, there is a term $z^{-1} w^0$ that comes from the lower off-diagonal. Finally, the term $z w^n$, where $n = p - q$ is the number of single impurities, comes from the upper off-diagonal and gets contributions from only the S and I codons. Thus, we have shown that the moduli spaces of the $Y^{p,q}$ quivers reproduce the correct toric geometries.

For $Y^{p,0}$ the matrix gets too small and there is not enough space for A_1 and A_2. The Kasteleyn matrix consists of only I codons:

$$
K = \begin{pmatrix}
-1+w & w & 0 & 0 & \ldots\ldots\ldots\ldots & z^{-1} \\
1 & -1+w & w & 0 & \ldots\ldots\ldots\ldots & 0 \\
0 & 1 & -1+w & w & 0 \;\;\ldots\ldots\ldots & 0 \\
0 & 0 & 1 & -1+w & w \;\; 0 \quad \ldots & 0 \\
& \vdots & & & \ddots & \\
0 & \ldots\ldots\ldots\ldots\ldots\ldots\ldots & 0 \;\; 1 \;\; -1+w & w \\
wz & 0 & \ldots\ldots\ldots\ldots\ldots & 0 \;\; 1 & -1+w
\end{pmatrix}
$$

$$(11.9.53)$$

For example, the Kasteleyn matrix of $Y^{3,0}$ is:

$$
K = \begin{pmatrix}
-1+w & w & z^{-1} \\
1 & -1+w & w \\
wz & 1 & -1+w
\end{pmatrix}
\tag{11.9.54}
$$

with determinant

$$
P(w, z) = -1 + 6w - 6w^2 + w^3 + z^{-1} + w^3 z
\tag{11.9.55}
$$

and the toric diagram of Figure 11-31.

These Kasteleyn matrices give the toric diagrams of a certain phase of the theories (the one with only single impurities, all of them together). Other phases can be obtained by performing Seiberg duality transformations. As discussed in section 11.6
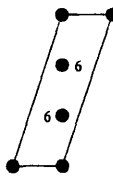
Figure 11-31: Toric diagram of a phase of $Y^{3,0}$ with three single impurities.

this may be efficiently implemented on a computer and used to enumerate the toric phases of the theory, together with the duality graph showing the interconnections between phases.

$Y^{3,1}$ with double impurity

In [16], it was shown that all toric phases of $Y^{p,q}$ theories can be constructed by adding single and double impurities to the $\mathbb{C}^3/\mathbb{Z}_{2p}$ quiver. Double impurities arise when Seiberg duality makes two single impurities "collide". As an example of Seiberg duality, we now study the double impurity phase of $Y^{3,1}$. This phase can be obtained by dualizing face 3 (see Figure 11-32). The resulting graph can be deformed to the more symmetric form which is shown in Figure 11-33. The determinant of the Kasteleyn matrix again gives the $P(w,z)$ polynomial, from which we get the toric diagram (Figure 11-34).
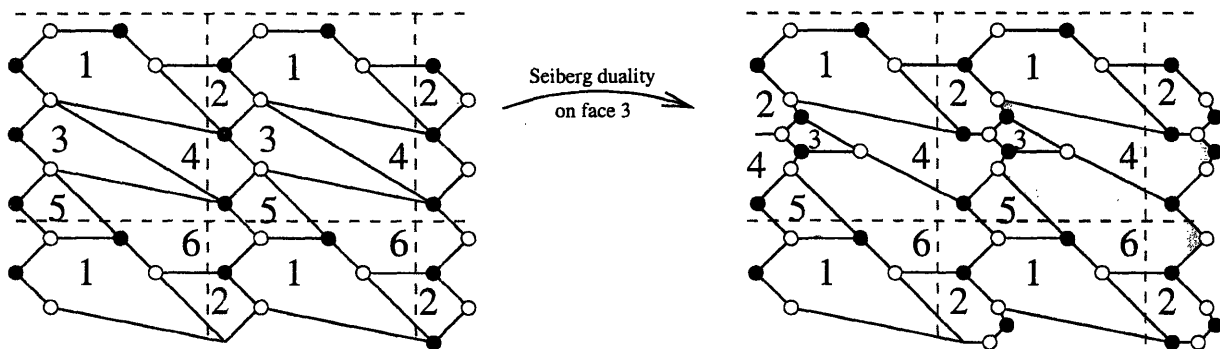
Figure 11-32: Dualizing face 3 in $Y^{3,1}$ with two single impurities. In the resulting tiling, we indicate the double impurity in pink.
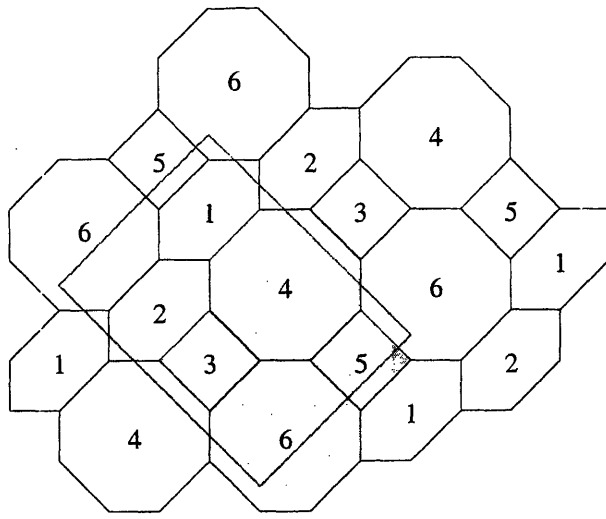
Figure 11-33: The double impurity in $Y^{3,1}$

$$K = \begin{pmatrix} 1 & 1 & 0 & 0 & 0 & z^{-1} \\ w^{-1} & 1 & w^{-1} & 0 & 0 & 0 \\ 0 & 1 & 1 & 1 & 0 & 0 \\ 0 & 0 & w^{-1} & 1 & 1 & 0 \\ 0 & 0 & 0 & 1 & -1 & -1 \\ z^{-1} & 0 & 0 & 0 & w & 1 \end{pmatrix} \qquad (11.9.56)$$

$$P(w,z) = -7 - w^{-2} + 9w^{-1} + w + w^{-1}z^{-1} + zw^{-1} \qquad (11.9.57)$$
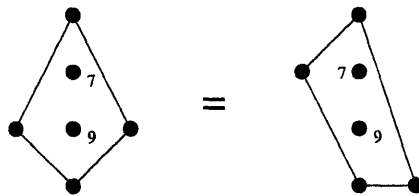
Figure 11-34: Toric diagram for $Y^{3,1}$ in the double impurity phase

All the multiplicity results in this and previous section agree with the ones derived using the Forward Algorithm in [40].

354

We now describe the brane tilings for the $X^{p,q}$ spaces constructed in [81]. Recall that these spaces are defined by the property that an $X^{p,q}$ theory can be Higgsed to both $Y^{p,q}$ and $Y^{p,q-1}$. Constructing the brane tilings for the $X^{p,q}$ is quite straightforward, but it will be convenient for our purposes to use a slightly modified (but entirely equivalent) description of the $Y^{p,q}$ spaces from the one used in the previous section.

We use the following description of $Y^{p,q}$, with $p - q$ single impurities. For this tiling, we need $2(p - q)$ quadrilaterals and $2q$ hexagons. We build the quadrilaterals by starting with a hexagonal grid, and drawing lines through the center of a given hexagon, connecting opposite vertices. This divides the hexagon into two quadrilaterals. A given $Y^{p,q}$ is then given by placing these hexagons and divided hexagons along a single diagonal such that the divided hexagons are separated from each other by an even number of non-divided hexagons; this is simply the requirement that the single impurities be separated from each other by an odd number of doublets. For examples of this construction, see Figure 11-35.

$$Y^{3,0} \qquad Y^{3,1} \qquad Y^{3,2}$$
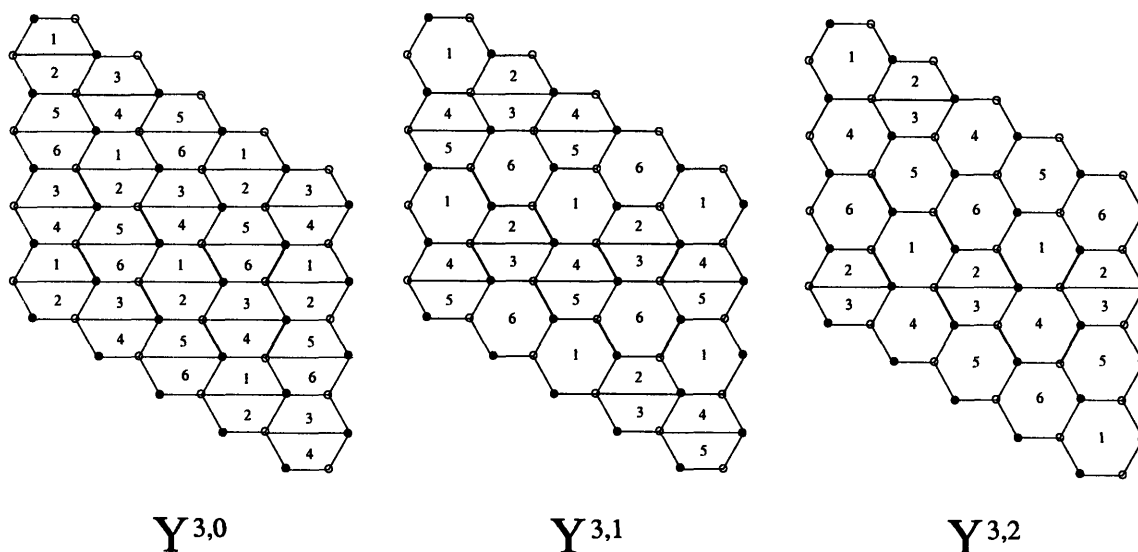
Figure 11-35: Brane tilings for $Y^{3,q}$.

Constructing the $X^{p,q}$ brane tilings is now straightforward. We give the example of $X^{3,1}$ below; the other $X^{p,q}$ tilings work similarly. To build the tilings, simply insert diagonal lines in hexagons such that removing the line from the $X^{p,q}$ tiling gives the

$Y^{p,q}$ to which it descends. This diagonal line should always share a node with one of the horizontal lines subdividing a hexagon in two; this is what allows one to blow down to $Y^{p,q-1}$ as well as $Y^{p,q}$. In Figure 11-36, one may remove the line between regions 6 and 7 or the line between regions 5 and 6 to yield $Y^{3,1}$ and $Y^{3,0}$, respectively.
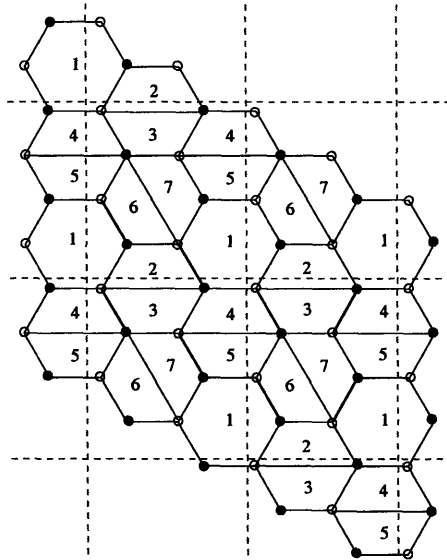
Figure 11-36: A brane tiling for $X^{3,1}$.

The Kasteleyn matrix for this tiling is

$$
K = \begin{pmatrix}
 & 2 & 4 & 6 & 8 \\
\hline
1 & 1+w^{-1} & 1 & 0 & z \\
3 & 1 & -1-w & 1 & 0 \\
5 & 0 & 1 & w^{-1} & 1 \\
7 & z^{-1} & 1 & 1 & -1
\end{pmatrix}
\tag{11.9.58}
$$

which has determinant $\det K = 7w^{-1} + w^{-2} + 8 + w - z^{-1} - z + w^{-1}z$. This yields the proper toric diagram and multiplicities for this phase of $X^{3,1}$ [40].

11.10 Conclusions

In this chapter, we have presented a piece of technology which not only simplifies previously difficult calculations, but also establishes new connections to other inter-

esting areas of study. In this section, we present some concluding remarks about brane tilings and dimers, and suggest some arenas for further study.

First, we note the computational power of our construction. The correspondence between toric singularities, brane tilings, and dimers presented in the present work goes well beyond any other correspondence yet proposed. We established a precise connection between toric diagrams, GLSM multiplicities, and dimer quantities. This connection enables us to explore toric singularities other than only the simplest ones, and promises to be extremely useful for the future study of toric geometries. We further emphasize here that the central object in our construction, the brane tiling, is a **physical** object constructed out of NS5-branes and D5-branes in Type IIB string theory, and not just a mathematical tool.

Prior to this work, it had been suspected that there was a one-to-one correspondence between toric geometries with specified GLSM multiplicites and toric phases of the quiver gauge theory. The increased computational power provided by the brane tiling has enabled us to show that there is a relatively simple counterexample to this conjecture, that of Pseudo del Pezzo 5. We find that in fact there are examples where the only way of distinguishing two phases is by checking graph isomorphism, i.e. there exists no simpler characterisation of the graph other than the graph itself.

The operation of Seiberg duality on a quiver theory is straightforward, although it becomes extremely cumbersome to implement it many times. The dimer model allows us to encode Seiberg duality as an operation on the Kasteleyn matrix. In many cases this provides an extremely efficient way of enumerating all toric phases of a quiver theory, as long as one has at least one phase of the quiver theory to start with. It is an interesting question whether or not one can explore even non-toric theories via Seiberg duality.

In [133], a geometrical method was given for performing a-maximization [102] purely in terms of toric data, without needing to know the explicit Calabi-Yau metric on the toric space. This method involved the use of a Monge-Ampere equation to extremise a certain function. It is interesting to note that the solution to a Monge-Ampere equation also appears in the dimer model literature [118], where it is related

to the extremization of the surface tension functional that determines the asymptotic shape (limit curve) of a random matching of many copies of the fundamental domain of a bipartite graph. It would be fascinating to determine whether or not these two extremization problems are related.

In general, there are many different properties of dimer models that have been studied in the mathematics literature. It is undoubtedly worth exploring this literature in depth, since there are surely many additional connections one can draw between the mathematics and physics of dimers. In particular, the mathematical literature has different examples of partition functions that can be defined on a dimer model. Could some of these quantities be related to e.g. a central charge for the quiver gauge theory, and is it possible to prove the a-theorem for even the simple example of Higgsing?

The limit curve of the dimer model is related to the geometry that is mirror to the toric Calabi-Yau cone. This mirror geometry encodes the quantum corrections from worldsheet instantons to the classical geometry of the toric CY, and provides a point of contact between dimer models and topological string theory [144]. It would be interesting to investigate this connection in more detail.

Finally, we note that in this chapter, we do not discuss at all the problem of starting with a given toric geometry and deriving the brane tiling from that. Ideally, one would like to be able to do this, since there would then be a direct link to the dual SCFT from any given toric geometry.

Bibliography

[1] Bobby S. Acharya, J. M. Figueroa-O'Farrill, C. M. Hull, and B. Spence. Branes at conical singularities and holography. *Adv. Theor. Math. Phys.*, 2:1249–1286, 1999.

[2] Mina Aganagic, Andreas Karch, Dieter Lust, and Andre Miemiec. Mirror symmetries for brane configurations and branes at singularities. *Nucl. Phys.*, B569:277–302, 2000.

[3] Mina Aganagic and Cumrun Vafa. G(2) manifolds, mirror symmetry and geometric engineering. 2001.

[4] Ofer Aharony and Amihay Hanany. Branes, superpotentials and superconformal fixed points. *Nucl. Phys.*, B504:239–271, 1997.

[5] Ofer Aharony, Amihay Hanany, and Barak Kol. Webs of (p,q) 5-branes, five dimensional field theories and grid diagrams. *JHEP*, 01:002, 1998.

[6] D. Anselmi, J. Erlich, D. Z. Freedman, and A. A. Johansen. Positivity constraints on anomalies in supersymmetric gauge theories. *Phys. Rev.*, D57:7570–7588, 1998.

[7] D. Anselmi, D. Z. Freedman, Marcus T. Grisaru, and A. A. Johansen. Non-perturbative formulas for central functions of supersymmetric gauge theories. *Nucl. Phys.*, B526:543–571, 1998.

[8] Paul S. Aspinwall. Resolution of orbifold singularities in string theory. 1994.

[9] Paul S. Aspinwall, Brian R. Greene, and David R. Morrison. Calabi-yau moduli space, mirror manifolds and spacetime topology change in string theory. *Nucl. Phys.*, B416:414–480, 1994.

[10] Edwin Barnes, Ken Intriligator, Brian Wecht, and Jason Wright. Evidence for the strongest version of the 4d a-theorem, via a-maximization along rg flows. *Nucl. Phys.*, B702:131–162, 2004.

[11] Chris Beasley, Brian R. Greene, C. I. Lazaroiu, and M. R. Plesser. D3-branes on partial resolutions of abelian quotient singularities of calabi-yau threefolds. *Nucl. Phys.*, B566:599–640, 2000.

[12] Chris E. Beasley and M. Ronen Plesser. Toric duality is seiberg duality. *JHEP*, 12:001, 2001.

[13] Katrin Becker and Melanie Becker. M-theory on eight-manifolds. *Nucl. Phys.*, B477:155–167, 1996.

[14] Sergio Benvenuti, Sebastian Franco, Amihay Hanany, Dario Martelli, and James Sparks. An infinite family of superconformal quiver gauge theories with sasaki-einstein duals. 2004.

[15] Sergio Benvenuti and Amihay Hanany. New results on superconformal quivers. 2004.

[16] Sergio Benvenuti, Amihay Hanany, and Pavlos Kazakopoulos. The toric phases of the y(p,q) quivers. 2004.

[17] David Berenstein. Reverse geometric engineering of singularities. *JHEP*, 04:052, 2002.

[18] David Berenstein and Michael R. Douglas. Seiberg duality for quiver gauge theories. 2002.

[19] David Berenstein, Christopher P. Herzog, and Igor R. Klebanov. Baryon spectra and ads/cft correspondence. *JHEP*, 06:047, 2002.

[20] Aaron Bergman and Christopher P. Herzog. The volume of some non-spherical horizons and the ads/cft correspondence. *JHEP*, 01:030, 2002.

[21] M. Bertolini, F. Bigazzi, and A. L. Cotrone. New checks and subtleties for ads/cft and a-maximization. *JHEP*, 12:024, 2004.

[22] Volker Braun. On berenstein-douglas-seiberg duality. *JHEP*, 01:082, 2003.

[23] Agostino Butti, Mariana Grana, Ruben Minasian, Michela Petrini, and Alberto Zaffaroni. The baryonic branch of klebanov-strassler solution: A supersymmetric family of su(3) structure backgrounds. *JHEP*, 03:069, 2005.

[24] F. Cachazo, B. Fiol, K. A. Intriligator, S. Katz, and C. Vafa. A geometric unification of dualities. *Nucl. Phys.*, B628:3–78, 2002.

[25] F. Cachazo, Kenneth A. Intriligator, and Cumrun Vafa. A large n duality via a geometric transition. *Nucl. Phys.*, B603:3–41, 2001.

[26] F. Cachazo, S. Katz, and C. Vafa. Geometric transitions and n = 1 quiver theories. 2001.

[27] J. F. G. Cascales, M. P. Garcia del Moral, F. Quevedo, and A. M. Uranga. Realistic d-brane models on warped throats: Fluxes, hierarchies and moduli stabilization. *JHEP*, 02:031, 2004.

[28] Juan F. G. Cascales, Fouad Saad, and Angel M. Uranga. Holographic dual of the standard model on the throat. 2005.

[29] Sergio Cecotti and Cumrun Vafa. On classification of n=2 supersymmetric theories. *Commun. Math. Phys.*, 158:569–644, 1993.

[30] David A. Cox. The homogeneous coordinate ring of a toric variety, revised version. 1993.

[31] Jin Dai, R. G. Leigh, and Joseph Polchinski. New connections between string theories. *Mod. Phys. Lett.*, A4:2073–2083, 1989.

[32] Keshav Dasgupta, Kyungho Oh, and Radu Tatar. Geometric transition, large n dualities and mqcd dynamics. *Nucl. Phys.*, B610:331–346, 2001.

[33] Keshav Dasgupta, Govindan Rajesh, and Savdeep Sethi. M theory, orientifolds and g-flux. *JHEP*, 08:023, 1999.

[34] Xenia De la Ossa, Bogdan Florea, and Harald Skarke. D-branes on noncompact calabi-yau manifolds: K-theory and monodromy. *Nucl. Phys.*, B644:170–200, 2002.

[35] Frederik Denef and Michael R. Douglas. Distributions of flux vacua. *JHEP*, 05:072, 2004.

[36] Oliver DeWolfe, Tamas Hauer, Amer Iqbal, and Barton Zwiebach. Uncovering the symmetries on (p,q) 7-branes: Beyond the kodaira classification. *Adv. Theor. Math. Phys.*, 3:1785–1833, 1999.

[37] Duiliu-Emanuel Diaconescu and Michael R. Douglas. D-branes on stringy calabi-yau manifolds. 2000.

[38] Michael R. Douglas, Brian R. Greene, and David R. Morrison. Orbifold resolution by d-branes. *Nucl. Phys.*, B506:84–106, 1997.

[39] Michael R. Douglas and Gregory W. Moore. D-branes, quivers, and ale instantons. 1996.

[40] A. Dunn and A. Hanany. Work in progress.

[41] S. Elitzur, A. Giveon, D. Kutasov, and E. Rabinovici. Algebraic aspects of matrix theory on t**d. *Nucl. Phys.*, B509:122–144, 1998.

[42] S. Elitzur, A. Giveon, D. Kutasov, E. Rabinovici, and G. Sarkisian. D-branes in the background of ns fivebranes. *Int. J. Mod. Phys.*, A16:880–890, 2001.

[43] Bo Feng, Sebastian Franco, Amihay Hanany, and Yang-Hui He. Symmetries of toric duality. *JHEP*, 12:076, 2002.

[44] Bo Feng, Sebastian Franco, Amihay Hanany, and Yang-Hui He. Unhiggsing the del pezzo. *JHEP*, 08:058, 2003.

[45] Bo Feng, Amihay Hanany, and Yang-Hui He. D-brane gauge theories from toric singularities and toric duality. *Nucl. Phys.*, B595:165–200, 2001.

[46] Bo Feng, Amihay Hanany, and Yang-Hui He. Phase structure of d-brane gauge theories and toric duality. *JHEP*, 08:040, 2001.

[47] Bo Feng, Amihay Hanany, Yang Hui He, and Amer Iqbal. Quiver theories, soliton spectra and picard-lefschetz transformations. *JHEP*, 02:056, 2003.

[48] Bo Feng, Amihay Hanany, Yang-Hui He, and Angel M. Uranga. Toric duality as seiberg duality and brane diamonds. *JHEP*, 12:035, 2001.

[49] Bo Feng, Yang-Hui He, and Francis Lam. On correspondences between toric singularities and (p,q)- webs. *Nucl. Phys.*, B701:334–356, 2004.

[50] Bartomeu Fiol. Duality cascades and duality walls. *JHEP*, 07:058, 2002.

[51] Hanany A. Saad F. Franco, S. and A. Uranga. Fractional branes and dynamical supersymmetry breaking. *Work in progress.*

[52] Sebastian Franco and Amihay Hanany. Geometric dualities in 4d field theories and their 5d interpretation. *JHEP*, 04:043, 2003.

[53] Sebastian Franco and Amihay Hanany. Toric duality, seiberg duality and picard-lefschetz transformations. *Fortsch. Phys.*, 51:738–744, 2003.

[54] Sebastian Franco and Amihay Hanany. On the fate of tachyonic quivers. *JHEP*, 03:031, 2005.

[55] Sebastian Franco, Amihay Hanany, and Yang-Hui He. A trio of dualities: Walls, trees and cascades. *Fortsch. Phys.*, 52:540–547, 2004.

[56] Sebastian Franco, Amihay Hanany, Yang-Hui He, and Pavlos Kazakopoulos. Duality walls, duality trees and fractional branes. 2003.

[57] Sebastian Franco, Amihay Hanany, and Pavlos Kazakopoulos. Hidden exceptional global symmetries in 4d cfts. *JHEP*, 07:060, 2004.

[58] Sebastian Franco, Amihay Hanany, Kristian D. Kennaway, David Vegh, and Brian Wecht. Brane dimers and quiver gauge theories. 2005.

[59] Sebastian Franco, Amihay Hanany, and Angel M. Uranga. Multi-flux warped throats and cascading gauge theories. 2005.

[60] Sebastian Franco, Yang-Hui He, Christopher Herzog, and Johannes Walcher. Chaotic cascades for d-branes on singularities. 2004.

[61] Sebastian Franco, Yang-Hui He, Christopher Herzog, and Johannes Walcher. Chaotic duality in string theory. *Phys. Rev.*, D70, 2004.

[62] W. Fulton. Introduction to toric varieties. *Princeton University Press*, 1993.

[63] Jerome P. Gauntlett, Dario Martelli, James Sparks, and Daniel Waldram. Sasaki-einstein metrics on s(2) x s(3). 2004.

[64] Jerome P. Gauntlett, Dario Martelli, James Sparks, and Daniel Waldram. Supersymmetric ads backgrounds in string and m-theory. 2004.

[65] Jerome P. Gauntlett, Dario Martelli, James Sparks, and Daniel Waldram. Supersymmetric ads(5) solutions of m-theory. *Class. Quant. Grav.*, 21:4335–4366, 2004.

[66] Jerome P. Gauntlett, Dario Martelli, James F. Sparks, and Daniel Waldram. A new infinite class of sasaki-einstein manifolds. 2004.

[67] Steven B. Giddings, Shamit Kachru, and Joseph Polchinski. Hierarchies from fluxes in string compactifications. *Phys. Rev.*, D66:106006, 2002.

[68] Eric G. Gimon and Joseph Polchinski. Consistency conditions for orientifolds and d-manifolds. *Phys. Rev.*, D54:1667–1676, 1996.

[69] Amit Giveon and David Kutasov. Brane dynamics and gauge theory. *Rev. Mod. Phys.*, 71:983–1084, 1999.

[70] Amit Giveon, Massimo Porrati, and Eliezer Rabinovici. Target space duality in string theory. *Phys. Rept.*, 244:77–202, 1994.

[71] Suresh Govindarajan and T. Jayaraman. D-branes, exceptional sheaves and quivers on calabi-yau manifolds: From mukai to mckay. *Nucl. Phys.*, B600:457–486, 2001.

[72] Mariana Grana and Joseph Polchinski. Supersymmetric three-form flux perturbations on ads(5). *Phys. Rev.*, D63:026001, 2001.

[73] Michael B. Green, J. H. Schwarz, and Edward Witten. Superstring theory. vol. 1: Introduction, vol. 2: Loop amplitudes, anomalies and phenomenology. Cambridge, Uk: Univ. Pr. (1987) (Cambridge Monographs On Mathematical Physics).

[74] Brian R. Greene. D-brane topology changing transitions. *Nucl. Phys.*, B525:284–296, 1998.

[75] Steven S. Gubser. Einstein manifolds and conformal field theories. *Phys. Rev.*, D59:025006, 1999.

[76] Steven S. Gubser. Supersymmetry and f-theory realization of the deformed conifold with three-form flux. 2000.

[77] Steven S. Gubser, Christopher P. Herzog, and Igor R. Klebanov. Symmetry breaking and axionic strings in the warped deformed conifold. *JHEP*, 09:036, 2004.

[78] Sergei Gukov, Cumrun Vafa, and Edward Witten. Cft's from calabi-yau four-folds. *Nucl. Phys.*, B584:69–108, 2000.

[79] Amihay Hanany and Yang-Hui He. Non-abelian finite gauge theories. *JHEP*, 02:013, 1999.

[80] Amihay Hanany and Amer Iqbal. Quiver theories from d6-branes via mirror symmetry. *JHEP*, 04:009, 2002.

[81] Amihay Hanany, Pavlos Kazakopoulos, and Brian Wecht. A new infinite class of quiver gauge theories. 2005.

[82] Amihay Hanany and Kristian D. Kennaway. Dimer models and toric diagrams. 2005.

[83] Amihay Hanany, Matthew J. Strassler, and Angel M. Uranga. Finite theories and marginal operators on the brane. *JHEP*, 06:011, 1998.

[84] Amihay Hanany and Angel M. Uranga. Brane boxes and branes on singularities. *JHEP*, 05:013, 1998.

[85] Amihay Hanany and Johannes Walcher. On duality walls in string theory. *JHEP*, 06:055, 2003.

[86] Amihay Hanany and Edward Witten. Type iib superstrings, bps monopoles, and three-dimensional gauge dynamics. *Nucl. Phys.*, B492:152–190, 1997.

[87] Amihay Hanany and Alberto Zaffaroni. On the realization of chiral four-dimensional gauge theories using branes. *JHEP*, 05:001, 1998.

[88] Yang-Hui He. Some remarks on the finitude of quiver theories. 1999.

[89] Yang-Hui He. On algebraic singularities, finite graphs and d-brane gauge theories: A string theoretic perspective. 2002.

[90] Yang-Hui He and Jun S. Song. Of mckay correspondence, non-linear sigma-model and conformal field theory. *Adv. Theor. Math. Phys.*, 4:747–790, 2000.

[91] M. Henningson and K. Skenderis. The holographic weyl anomaly. *JHEP*, 07:023, 1998.

[92] C. P. Herzog, Q. J. Ejaz, and I. R. Klebanov. Cascading rg flows from new sasaki-einstein manifolds. *JHEP*, 02:009, 2005.

[93] Christopher P. Herzog. Exceptional collections and del pezzo gauge theories. *JHEP*, 04:069, 2004.

[94] Christopher P. Herzog, Igor R. Klebanov, and Peter Ouyang. Remarks on the warped deformed conifold. 2001.

[95] Christopher P. Herzog, Igor R. Klebanov, and Peter Ouyang. D-branes on the conifold and n = 1 gauge / gravity dualities. 2002.

[96] Christopher P. Herzog and James McKernan. Dibaryon spectroscopy. *JHEP*, 08:054, 2003.

[97] Christopher P. Herzog and Johannes Walcher. Dibaryons from exceptional collections. *JHEP*, 09:060, 2003.

[98] Petr Horava. Strings on world sheet orbifolds. *Nucl. Phys.*, B327:461, 1989.

[99] Kentaro Hori, Amer Iqbal, and Cumrun Vafa. D-branes and mirror symmetry. 2000.

[100] Kentaro Hori and Cumrun Vafa. Mirror symmetry. 2000.

[101] C. M. Hull and P. K. Townsend. Unity of superstring dualities. *Nucl. Phys.*, B438:109–137, 1995.

[102] Ken Intriligator and Brian Wecht. The exact superconformal r-symmetry maximizes a. *Nucl. Phys.*, B667:183–200, 2003.

[103] Ken Intriligator and Brian Wecht. Baryon charges in 4d superconformal field theories and their ads duals. *Commun. Math. Phys.*, 245:407–424, 2004.

[104] Ken Intriligator and Brian Wecht. Rg fixed points and flows in sqcd with adjoints. *Nucl. Phys.*, B677:223–272, 2004.

[105] Kenneth A. Intriligator and N. Seiberg. Mirror symmetry in three dimensional gauge theories. *Phys. Lett.*, B387:513–519, 1996.

367

[106] Yukari Ito and Kiraku Nakajima. Mckay correspondence and hilbert schemes in dimension three.

[107] Clifford V. Johnson, Amanda W. Peet, and Joseph Polchinski. Gauge theory and the excision of repulson singularities. *Phys. Rev.*, D61:086001, 2000.

[108] V. G. Kac. Infinite root systems, representations of graphs and invariant theory. *Inv. Math.*, 56, 1980.

[109] Shamit Kachru et al. Towards inflation in string theory. *JCAP*, 0310:013, 2003.

[110] Shamit Kachru and Eva Silverstein. 4d conformal theories and strings on orbifolds. *Phys. Rev. Lett.*, 80:4855–4858, 1998.

[111] M. Kaku. Introduction to superstrings. NEW YORK, USA: SPRINGER (1988) 568 P. (GRADUATE TEXTES IN CONTEMPORARY PHYSICS).

[112] Andreas Karch, Dieter Lust, and Douglas J. Smith. Equivalence of geometric engineering and hanany-witten via fractional branes. *Nucl. Phys.*, B533:348–372, 1998.

[113] P. Kasteleyn. Graph theory and crystal physics. 1967.

[114] Sheldon Katz, Albrecht Klemm, and Cumrun Vafa. Geometric engineering of quantum field theories. *Nucl. Phys.*, B497:173–195, 1997.

[115] Sheldon Katz and Cumrun Vafa. Geometric engineering of n = 1 quantum field theories. *Nucl. Phys.*, B497:196–204, 1997.

[116] A. Kehagias. New type iib vacua and their f-theory interpretation. *Phys. Lett.*, B435:337–342, 1998.

[117] R. Kenyon. An introduction to the dimer model. 2003.

[118] Richard Kenyon, Andrei Okounkov, and Scott Sheffield. Dimers and amoebae. 2003.

[119] Igor R. Klebanov and Matthew J. Strassler. Supergravity and a confining gauge theory: Duality cascades and chisb-resolution of naked singularities. *JHEP*, 08:052, 2000.

[120] Igor R. Klebanov and Arkady A. Tseytlin. Gravity duals of supersymmetric su(n) x su(n+m) gauge theories. *Nucl. Phys.*, B578:123–138, 2000.

[121] Igor R. Klebanov and Edward Witten. Superconformal field theory on three-branes at a calabi-yau singularity. *Nucl. Phys.*, B536:199–218, 1998.

[122] D. Kutasov. New results on the 'a-theorem' in four dimensional supersymmetric field theory. 2003.

[123] David Kutasov, Andrei Parnachev, and David A. Sahakyan. Central charges and u(1)r symmetries in n = 1 super yang- mills. *JHEP*, 11:013, 2003.

[124] David Kutasov and Adam Schwimmer. Lagrange multipliers and couplings in supersymmetric field theory. *Nucl. Phys.*, B702:369–379, 2004.

[125] Albion E. Lawrence, Nikita Nekrasov, and Cumrun Vafa. On conformal field theories in four dimensions. *Nucl. Phys.*, B533:199–209, 1998.

[126] Andre Leclair, Jose Maria Roman, and German Sierra. Russian doll renormalization group, kosterlitz-thouless flows, and the cyclic sine-gordon model. *Nucl. Phys.*, B675:584–606, 2003.

[127] R. G. Leigh. Dirac-born-infeld action from dirichlet sigma model. *Mod. Phys. Lett.*, A4:2767, 1989.

[128] Robert G. Leigh and Matthew J. Strassler. Exactly marginal operators and duality in four-dimensional n=1 supersymmetric gauge theory. *Nucl. Phys.*, B447:95–136, 1995.

[129] W. Lerche, P. Mayr, and J. Walcher. A new kind of mckay correspondence from non-abelian gauge theories. 2001.

[130] Naichung Conan Leung and Cumrun Vafa. Branes and toric geometry. *Adv. Theor. Math. Phys.*, 2:91–118, 1998.

[131] D. Lust and S. Theisen. Lectures on string theory. *Lect. Notes Phys.*, 346:1–346, 1989.

[132] Juan M. Maldacena. The large n limit of superconformal field theories and supergravity. *Adv. Theor. Math. Phys.*, 2:231–252, 1998.

[133] D. Martelli, J. Sparks, and S. T. Yau. The geometric dual of a-maximisation for toric sasaki- einstein manifolds. 2005.

[134] Dario Martelli and James Sparks. Toric geometry, sasaki-einstein manifolds and a new infinite class of ads/cft duals. 2004.

[135] P. Mayr. Phases of supersymmetric d-branes on kaehler manifolds and the mckay correspondence. *JHEP*, 01:018, 2001.

[136] J McKay. Graphs, singularities, and finite groups. *Proc. Symp.Pure Math.*, 47, 1980.

[137] Alexei Morozov and Antti J. Niemi. Can renormalization group flow end in a big mess? *Nucl. Phys.*, B666:311–336, 2003.

[138] David R. Morrison and M. Ronen Plesser. Non-spherical horizons. i. *Adv. Theor. Math. Phys.*, 3:1–81, 1999.

[139] David R. Morrison and M. Ronen Plesser. Summing the instantons: Quantum cohomology and mirror symmetry in toric varieties. *Nucl. Phys.*, B440:279–354, 1995.

[140] David R. Morrison and Nathan Seiberg. Extremal transitions and five-dimensional supersymmetric field theories. *Nucl. Phys.*, B483:229–247, 1997.

[141] Tomomi Muto and Taro Tani. Stability of quiver representations and topology change. *JHEP*, 09:008, 2001.

[142] V. A. Novikov, Mikhail A. Shifman, A. I. Vainshtein, and Valentin I. Zakharov. Exact gell-mann-low function of supersymmetric yang-mills theories from instanton calculus. *Nucl. Phys.*, B229:381, 1983.

[143] Kyung-ho Oh and Radu Tatar. Duality and confinement in n = 1 supersymmetric theories from geometric transitions. *Adv. Theor. Math. Phys.*, 6:141–196, 2003.

[144] Andrei Okounkov, Nikolai Reshetikhin, and Cumrun Vafa. Quantum calabi-yau and classical crystals. 2003.

[145] Hirosi Ooguri and Cumrun Vafa. Two-dimensional black hole and singularities of cy manifolds. *Nucl. Phys.*, B463:55–72, 1996.

[146] J. Park, R. Rabadan, and A. M. Uranga. Orientifolding the conifold. *Nucl. Phys.*, B570:38–80, 2000.

[147] J. Polchinski. String theory. vols. 1 and 2. Cambridge, UK: Univ. Pr. (1998).

[148] Joseph Polchinski. Dirichlet-branes and ramond-ramond charges. *Phys. Rev. Lett.*, 75:4724–4727, 1995.

[149] Joseph Polchinski. Lectures on d-branes. 1996.

[150] Joseph Polchinski, Shyamoli Chaudhuri, and Clifford V. Johnson. Notes on d-branes. 1996.

[151] J Propp. Generalized domino-shuffling. 2001.

[152] Augusto Sagnotti. Open strings and their symmetry groups. 1987.

[153] Martin Schmaltz. Duality of non-supersymmetric large n gauge theories. *Phys. Rev.*, D59:105018, 1999.

[154] Martin Schvellinger. Glueballs, symmetry breaking and axionic strings in non-supersymmetric deformations of the klebanov-strassler background. *JHEP*, 09:057, 2004.

[155] John H. Schwarz. Lectures on superstring and m theory dualities. *Nucl. Phys. Proc. Suppl.*, 55B:1–32, 1997.

[156] N. Seiberg. Electric - magnetic duality in supersymmetric nonabelian gauge theories. *Nucl. Phys.*, B435:129–146, 1995.

[157] Nathan Seiberg. Five dimensional susy field theories, non-trivial fixed points and string dynamics. *Phys. Lett.*, B388:753–760, 1996.

[158] Jun S. Song. Three-dimensional gorenstein singularities and su(3)-hat modular invariants. *Adv. Theor. Math. Phys.*, 4:791–822, 2000.

[159] M. J.H Strassler. Duality in supersymmetric field theory and an application to real particle physics. *International Workshop on Perspectives of Strong Coupling Gauge Theories (SCGT 96), Nagoya, Japan.*, 1996.

[160] Chien-Hao Liu Ti Hu and Shing-Tung Yau. Toric morphisms and fibrations of toric calabi-yau hypersurfaces.

[161] G Tian. Kaehler-einstein metrics with positive scalar curvature. *Inv. Math.*, 137, 1997.

[162] Alessandro Tomasiello. D-branes on calabi-yau manifolds and helices. *JHEP*, 02:008, 2001.

[163] P. K. Townsend. Four lectures on m-theory. 1996.

[164] Angel M. Uranga. Brane configurations for branes at conifolds. *JHEP*, 01:022, 1999.

[165] Cumrun Vafa. Lectures on strings and dualities. 1997.

[166] Cumrun Vafa. Superstrings and topological strings at large n. *J. Math. Phys.*, 42:2798–2817, 2001.

[167] Edward Witten. Phases of n = 2 theories in two dimensions. *Nucl. Phys.*, B403:159–222, 1993.

[168] Edward Witten. String theory dynamics in various dimensions. *Nucl. Phys.*, B443:85–126, 1995.

[169] Edward Witten. Bound states of strings and p-branes. *Nucl. Phys.*, B460:335–350, 1996.

[170] B. Zwiebach. A first course in string theory. Cambridge, UK: Univ. Pr. (2004) 558 p.